Transport des polluants et variabilité atmosphérique du CO2 en Sibérie : Apport des mesures in situ aéroportées

Jean-Daniel Paris

UNIVERSITE DE VERSAILLES SAINT QUENTIN EN YVELINES
UFR DES SCIENCES

Thèse de doctorat, spécialité Météorologie et Océanographie
Ecole doctorale Sciences de l'Environnement d'Ile de France

Transport des polluants et variabilité atmosphérique du CO_2 en Sibérie : Apport des mesures in situ aéroportées

Jean-Daniel Paris

Soutenue publiquement le 2 décembre 2008

Membres du jury :

Philippe Bousquet	Président du jury
Vincent-Henri Peuch	Rapporteur
Andreas Stohl	Rapporteur
Kathy Law	Examinatrice
Patrick Monfray	Examinateur
Philippe Nédélec	Examinateur
Philippe Ciais	Directeur de thèse
Boris Belan	Invité

Laboratoire des Sciences du Climat et de l'Environnement, IPSL, UMR CNRS-CEA-UVSQ,
CEA Saclay, Orme des Merisiers, 91191 Gif sur Yvette

Remerciements

Je tiens à remercier tout d'abord Philippe Ciais pour avoir accepté de diriger cette thèse, ainsi que Laurent Turpin et Robert Vautard pour m'avoir accueilli au LSCE durant ces trois années. Je remercie également Michel Ramonet pour son encadrement.

Je remercie MM Vincent-Henri Peuch et Andreas Stohl et tous les membres du jury pour avoir accepté de juger cette thèse.

Les campagnes en Sibérie se sont toujours effectuées dans une ambiance chaleureuse et amicale en plus d'être professionnelle, et je tiens ici à remercier notamment Philippe Nédélec, Michel Ramonet, Mikhail Arshinov, Jean-Marc Cousin, Boris Belan, Mikhail Panchenko, Dmitry Pestunov, Grégoire Cayez, Adrien Royer, Frédéric Boumard, Sasha, Artem, et tous les autres, ainsi que les équipes de pilotage pour leur travail extrêmement professionnel. J'espère que Philippe aura d'autres occasions de montrer ses talents de pilote de jumbo-jet.

Merci à Jean-Luc Teffo, Patrick Le Fort, Philippe Galdemard, Dominique Filippi, Stéphanie Rebelo, Sabrina Formuso et toutes les personnes ayant rendu possible la réalisation de ce projet.

Je remercie également les personnes avec lesquelles j'ai étroitement collaboré pour le travail d'interprétation des mesures, et notamment les modélisateurs : Andreas Stohl, Robert Vautard, Philippe Bousquet, Claire Carouge, Jocelyn Turnbull, François Delage et Philippe Peylin.

Merci à l'équipe RAMCES et tous les collègues du LSCE pour leur présence et leur amitié, et en particulier le clan de Courcelles (Rémi le savoyard, Adrien et François), Cyril, Yannick, Thomas et tant d'autres.

Merci aux amis et à la famille pour leur soutien (bravo à Erwan).

Merci à Anna (et bon courage).

Résumé

Le travail de thèse présenté ici a pour objectif de caractériser et d'analyser les variations de concentration atmosphérique en CO_2, CO et O_3 et en aérosols ultrafins, au dessus de la Sibérie, lors de trois campagnes intensives de mesures aéroportées YAK-AEROSIB. Ces campagnes ont eu lieu en avril 2006, septembre 2006 et en août 2007. La composition de la troposphère sibérienne, éloignée des grandes sources de pollution de l'hémisphère nord, est mal connue. Mais la connaissance de la distribution de polluants et de gaz à effet de serre dans cette région est cruciale pour améliorer la représentation du transport à grande échelle de ces polluants au dessus de l'Eurasie, et plus généralement de l'hémisphère nord. Plusieurs études de modélisation ont principalement conclu à une faible pollution de l'atmosphère sibérienne par les polluants européens exportés dans la basse troposphère. Les mesures obtenues lors des campagnes aéroportées YAK-AEROSIB ont permis de mettre en évidence que la concentration en CO peut être largement affectée par un ensemble de processus de transport et d'émissions parmi lesquels l'advection de polluants chinois dans des perturbations baroclines, l'advection diffuse ou non de polluants européen à diverses altitudes, des feux de biomasse en Asie Centrale. Cet ensemble de facteurs est étudié à travers une nouvelle technique d'analyse en cluster du rétro-transport simulé par le modèle lagrangien FLEXPART. Des gradients importants de CO_2 ont été observés durant les campagnes d'été. J'utilise ces gradients pour analyser le mélange vertical du modèle de circulation globale LMDZ à travers la distribution simulée du CO_2. Enfin je mets en évidence un possible maximum de nucléation dans la moyenne troposphère continentale propre en été à partir de mesures de particules ultrafines.

Abstract

The work presented here intends to characterize the variations of atmospheric concentrations of CO_2, CO, O_3 and ultrafine particles, over a large scale aircraft transect above Siberia, during three intensive YAK-AEROSIB campaigns in April 2006, September 2006 and August 2007, respectively. The Siberian tropospheric composition, far from the main northern hemisphere emission regions, remains poorly sampled. But knowledge of pollutant and greenhouse gases distribution in this region is needed to improve the representation of atmospheric long range transport of these species above Eurasia, and more generally above the Northern Hemisphere. Modelling studies have concluded that the Siberian atmosphere is weakly polluted, mostly by European pollutants exported through the boundary layer and lower troposphere. I show here that CO concentrations at the time of the campaigns is broadly affected by an ensemble of transport and emissions processes among which advection of Chinese pollutants through baroclinic perturbations, advection (diffuse or not) of European pollutants at various altitudes, of biomass burning in Central Asia. This set of factors is analyzed through a novel statistical technique based on clustering of backward transport simulated by a Lagrangian model. Large CO_2 gradients have been observed during the summer campaigns. I use these gradients to analyze the vertical mixing of the model through the simulated CO_2 distribution. At last I present ultrafine particle measurements, and show a possible nucleation summer maximum in the clean, continental mid-troposphere.

Acronymes et abréviations

ADB	Automated diffusion battery
BL	Boundary layer, couche limite atmosphérique
C	Carbone
CH_4	Méthane
CO	Monoxyde de carbone
CO_2	Dioxyde de carbone
COV	Composés organiques volatils
COVNM	Composés organiques volatils non méthaniques
EDGAR	Inventaire d'émissions
FT	Free troposphere, troposphère libre
GCM	General circulation model
GES	Gaz à effet de serre
GFED	Global Fire Emissions Database
Gt	Gigatonne, 10^9 t
HTAP	Hemispheric transport of air pollution consortium
IASI	Interféromètre atmosphérique de sondage dans l'infrarouge
IPCC	International panel on climate change
LMDZ	Modèle du Laboratoire de Météorologie Dynamique Zoomé
LPDM	Lagrangian particle dispersion model
MAPS	Measurement of Air Pollution from Satellites
MOPITT	Measurement Of Pollution In The Troposphere
NDIR	Non-dispersive infrared
NDVI	Normalized difference vegetation index
NO	Monoxyde d'azote
NO_2	Dioxyde d'azote
NOx	Oxydes nitreux réactifs
O_3	Ozone
PAN	Peroxyacétylnitrate

PES	Potential emission sensitivity
Pg	Pétagramme, 10^{15} g
ppb	Part per billion, partie par milliard
ppm	Part per million, partie par million
SO_2	Dioxyde de soufre
SRR	Source receptor relationship
Tg	Téragramme, 10^{12} g
TRACE-P	TRAnsport & Chemical Evolution over the Pacific
UTC	Universal Time, Coordinated
YAK-AEROSIB	Airborne Extensive Regional Observations in Siberia
WCB	Warm conveyor belt

Table des matières

Chapitre 1.
Introduction

Au cours des dernières centaines d'années, l'impact humain est devenu la principale force d'altération de l'atmosphère à travers la combustion sans cesse croissante de charbon puis de combustibles fossiles supplémentaires. Dans les années 1950, on a commencé à mesurer le dioxyde de carbone, principal gaz à effet de serre d'origine humaine, dans l'atmosphère à grande distance des sources de pollution. La découverte essentielle fût une augmentation des concentrations d'année en année, attribuable aux émissions humaines globales. Dans les années 1960 et 1970, il a été établi que des espèces chimiques polluantes étaient en mesure de gagner des régions éloignées de toute source de pollution. Des réseaux de mesure, dédiés à la qualité de l'air, à l'ozone stratosphérique ou à la mesure des gaz à effet de serre, se sont ainsi développés pour surveiller les concentrations atmosphériques associées aux émissions humaines. Ces réseaux ont un maillage dense dans les zones telles que l'Europe et l'Amérique du Nord, mais restent aveugles à de vastes régions, comme par exemple, la Sibérie dans l'hémisphère nord.

Indépendamment des émissions humaines, la composition chimique de l'atmosphère naturelle est régie par une dynamique complexe. Elle résulte d'échanges de matière entre les différentes sphères de l'environnement. La végétation régule la composition atmosphérique et émet chaque année des millions de tonnes de nombreux composés organiques. Elle assimile le dioxyde de carbone. Elle a un impact sur la circulation atmosphérique en générant un flux de chaleur qui maintient un mélange important dans la basse atmosphère.

La Sibérie est le seul endroit de l'hémisphère nord suffisamment éloigné des grandes sources de pollution permettant éventuellement d'observer, dans des circonstances qui restent à déterminer, un état « naturel » de l'atmosphère. Immense étendue boréale de 13 millions d'hectares, la Sibérie rassemble une grande variété de biomes terrestres peu touchés par les activités humaines. La densité de population sibérienne est faible et l'activité industrielle dispersée.

Mais l'advection à grande distance de concentrations importantes de polluants n'est pas négligeable et constitue une perturbation anthropique mal connue. L'atmosphère sibérienne est également affectée par des perturbations naturelles comme les feux de forêts. L'isolement particulier de la Sibérie se traduit par un manque de données sur les conditions non-perturbées autant que sur les perturbations.

La zone boréale subit actuellement un réchauffement climatique régional de 0,3 à 0,4 °C par décade (Chapin et al., 2005). Un certain nombre de mécanismes de rétroaction biophysique et biogéochimique entre ces régions et le climat global sont déviés de leur trajectoire par ce changement climatique (Bonan, 2008). Les émissions biogéniques de composés organiques volatils et de gaz à effet de serre ont une dépendance forte et souvent non-linéaire à la température et aux autres variables climatiques. Or les forêts boréales, aux avant-postes du réchauffement climatique, sont une source importante de ces composés volatils. La productivité de la végétation sibérienne est limitée par les conditions climatiques qui y règnent. La capacité des forêts sibériennes à agir comme un puits de carbone n'est pas assurée (Gurney et al., 2002). Avec une température annuelle variant selon les régions entre 0 et -10°C environ, une large partie des sols y est gelée tout au long de l'année (pergélisol). Dans des conditions froides et humides, le sol des forêts boréales stockent d'importantes réserves de carbone qui s'avèrent vulnérables au réchauffement climatique en cours, et risquent ainsi d'être transférées rapidement à l'atmosphère (Gruber et al., 2004). Le réchauffement climatique pourrait affecter la fréquence des feux de forêts, qui entraîne une augmentation de polluants « naturels » dans l'atmosphère à l'échelle intercontinentale

Les régions boréales, et parmi elles la Sibérie, sont ainsi un sous-système critique et vulnérable du système Terre. La connaissance de la composition atmosphérique sibérienne et des mécanismes qui la modifient devient dès lors un premier pas nécessaire au regard des enjeux du changement global. Les travaux présentés ici s'attachent à caractériser la variabilité des concentrations de dioxyde de carbone (CO_2), du monoxyde de carbone (CO) et de l'ozone (O_3 ; CO et O_3 étant tous deux des polluants importants), ainsi que les aérosols ultrafins. Le transport atmosphérique est décrit comme un mécanisme important contrôlant la variabilité de ces espèces.

Dans les sections qui suivent je présente successivement les puits et sources de l'ozone et du CO, les facteurs affectant les concentrations de CO_2 et enfin le transport atmosphérique, replacé dans le contexte de l'hémisphère nord afin de mieux illustrer en quoi les résultats obtenus en Sibérie, présentés dans cette thèse, sont reliés à l'atmosphère globale.

1.1. Traceurs de la pollution atmosphérique : ozone et CO

Le monoxyde de carbone et l'ozone sont à la fois des espèces déterminantes pour la chimie atmosphérique et des traceurs de prédilections dans l'étude du transport intercontinental. Leurs caractéristiques essentielles sont présentées ci-dessous.

1.1.1. L'ozone, acteur central de la chimie atmosphérique

L'ozone est un gaz nuisible pour la vie animale et végétale. Il est toxique pour l'homme au-delà d'un certain seuil. Il se dépose sur la végétation à travers les stomates avec un impact néfaste pour la plante. L'ozone est également un gaz à effet de serre (GES), et il a une forte influence sur la composition atmosphérique. Il en résulte un impact radiatif non négligeable, l'ozone troposphérique contribuant au réchauffement (IPCC, 2007) contrairement à l'ozone stratosphérique qui participe d'un refroidissement net.

La troposphère contient 340 ± 40 Tg d'ozone. Les concentrations au sol sont généralement comprises entre 20 et 80 ppb, avec une forte variabilité diurne. Dans la troposphère libre, les concentrations varient entre 40 et 80 ppb environ, avec une variabilité synoptique importante. Les concentrations stratosphériques sont de l'ordre du ppm. Le bilan de l'ozone troposphérique est donné par la Table 1.1 (HTAP, 2007).

Dans la troposphère, 5100 ± 600 Tg O_3 an^{-1} sont formés in situ par l'oxydation de composés organiques volatils non méthaniques (COVNM) et de monoxyde de carbone (CO) en présence d'oxydes nitreux (NOx = NO_2 + NO, dans une proportion de 90%-10%) par réaction photochimique (Chameides et al., 1992).

Elément déterminant du bilan local de l'ozone troposphérique, les NOx sont un polluant émis par la combustion. En effet la production d'ozone est limitée d'une part par la quantité de radiation solaire et d'autre part par la concentration de NOx. Les NOx participent également à la production d'ozone à distance. Ils sont en effet rapidement convertis en peroxyacétylnitrate (PAN) selon la réaction $C_xH_yO_3 + NO_2 \rightarrow C_xH_yO_3NO_2$. Ces derniers sont stables dans la troposphère libre et peuvent donc y être transportés (Moxim et al., 1996). Ils libèrent ensuite le NO_2 en se décomposant lors d'une redescente dans la couche limite loin de la source et favorisent ainsi la formation d'ozone loin des sources de pollution.

Une seconde source de l'ozone troposphérique est le transfert d'ozone stratosphérique, avec un flux de 550 ± 170 Tg O_3 an^{-1} vers la troposphère. L'ozone est présent en concentrations bien supérieures dans la stratosphère, entre 10^3 et 10^4 ppb (Delmas et al., 2005). L'échange stratosphère-troposphère se produit de manière épisodique (Holton et al., 1995, Stohl et al., 2003), avec un maximum au printemps (Appenzeller et al., 1996). La dynamique stratosphérique force une subsidence vers les pôles (circulation de Brewer-Dobson), ce qui se traduit par des intrusions stratosphériques dans la troposphère au sein des *cut-off* cycloniques (déformation isolée de la tropopause), des blocages anticyclonique et des foliations de tropopause dans les régions extratropicales. La contribution stratosphérique est dominante dans les régions éloignées des sources de pollution anthropique (Lelieveld et Dentener 2000).

Table 1.1. Budget global de l'ozone (HTAP, 2007).

Sources (Tg O_3 an^{-1})		**Puits** (Tg O_3 an^{-1})	
Production chimique	5100 ± 600	Destruction chimique	4670 ± 730
Influx stratosphérique	550 ± 170	Dépôt au sol	1000 ± 200
Total	5650 ± 770	Total	5670 ± 930

1.1.2. CO : un traceur de la combustion dans l'hémisphère nord

Le CO est un précurseur de l'O_3 d'origine troposphérique. Sa ré action avec le radical hydroxyle a un impact important sur la chimie troposphérique (Crutzen & Fishman, 1977). La répartition des sources de CO était mal déterminée dans les années 1970, notamment entre la combustion et l'oxydation de composés organiques volatils. L'instrument MAPS embarqué à quatre reprises à bord de la navette spatiale américaine *Columbia* entre 1981 et 1994 a permis de constater que le CO était présent en plus fortes concentrations près des zones de forte activité anthropique, confirmant la thèse de la combustion comme source dominante dans l'hémisphère nord (Reichle et al., 1999). L'oxydation d'hydrocarbures est la source dominante dans les zones éloignées de l'hémisphère sud (Granier et al., 1999 ; Table 1.2). L'instrument MOPITT sur le satellite *Terra* de la NASA a ensuite fourni une couverture spatiale et temporelle plus dense avec une sensibilité aux concentrations dans la troposhère moyenne. Cet instrument est complété plus récemment par *Aura*/TES et *MetOp*/IASI. Les mesures actuelles restent très limitées en résolution verticale et ont généralement une sensibilité aux concentrations plus importante dans la haute ou moyenne troposphère.

Le budget global annuel du CO est donné par la Table 1.2 (Delmas et al., 2005). A périmètre égal Duncan et al. (2007) ont compilé des émissions sensiblement inférieures pour la période 1988-1997 pour les émissions anthropiques liées à la combustion, entre 550 et 600 Tg CO an^{-1}. La Table 1.2 montre que les sources liées à l'oxidation de composés carbonés et celles liées à la combustion sont du même ordre à l'échelle globale. L'incertitude sur les sources est de l'ordre de ± 50%. La répartition géographique des sources anthropiques est donnée par la Figure 1.1.

Aux moyennes et hautes latitudes la durée de vie du CO dans la basse troposphère varie entre 20-40 jours en été et 100 jours et plus en hiver (Duncan et al., 2007). Ces valeurs diminuent sensiblement avec l'altitude.

La mesure atmosphérique du CO a montré une tendance baissière marquée entre 1991 et 2001 dans l'hémisphère nord, de 0.5 ± 0.1 ppb an^{-1} (Novelli et al., 1994, 2003) après une tendance haussière de l'ordre de 1-2 ppb an^{-1}. Cette tendance est liée à l'amélioration des procédés de combustion notamment dans les automobiles (Novelli et al 2003). Une forte tendance à la hausse a été tout de même observée récemment pour l'Asie, et notamment la Chine (Ohara et al., 2007). Les émissions anthropiques de CO autour de la Sibérie sont montrées dans la Figure 1.1 (inventaire EDGAR 3.2 FT 2000 ; Olivier et al., 2005). L'échelle de couleur est logarithmique. On constate que les sources anthropiques sont particulièrement faibles en Sibérie, mais les émissions importantes

sont répertoriées pour la Chine, l'Inde et l'Europe. Des émissions également importantes ont lieu en Amérique du Nord.

Table 1.2. Budget global du CO (Delmas et al., 2005).

Sources (Tg CO an^{-1})		**Puits** (Tg CO an^{-1})	
Sources anthropiques		Oxydation par OH	2000 ± 750
Combustion de biomasse	1000 ± 600	Dépôt au sol	390 ± 140
Combustibles fossiles	640 ± 200	Flux vers la stratosphère	110 ± 30
Sources naturelles			
Océan	100 ± 90		
Végétation	75 ± 25		
Emissions des sols	17 ± 15		
Mixtes			
Oxydation du CH4	600 ± 300		
Oxydation des COV	900 ± 500		
Total	3300 ± 1700	Total	2500 ± 750

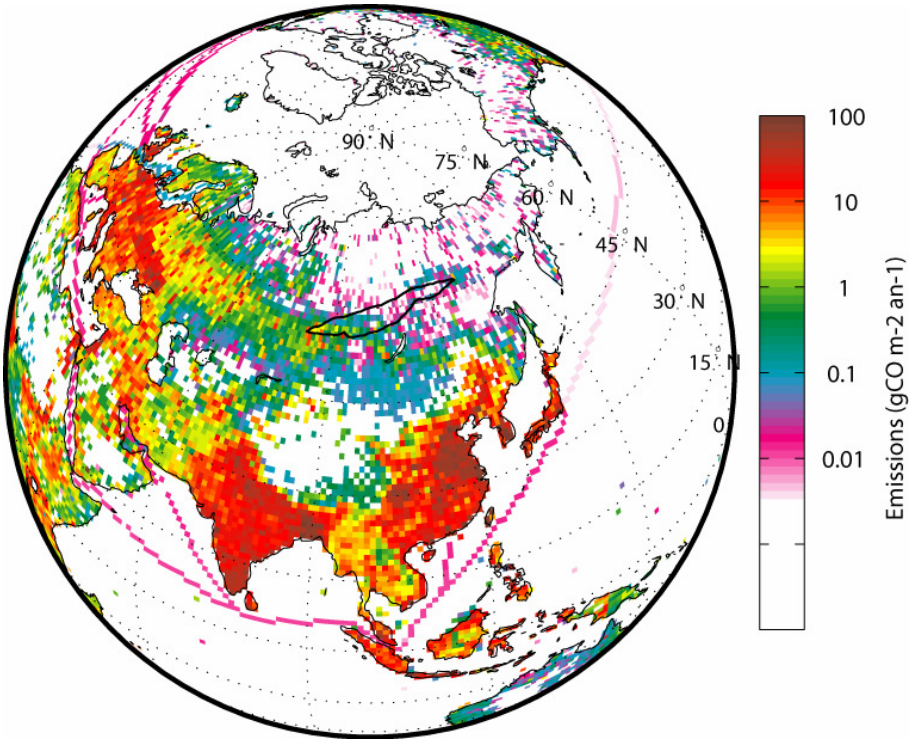

Figure 1.1. Emissions de CO anthropiques (excepté les feux de forêts) autour de la Sibérie en 2000 selon EDGAR 3.2 FT 2000 (Olivier et al., 2005).

La tendance haussière est visible malgré une variabilité interannuelle forte liée à la variabilité des feux de forêt (Wotawa et al., 2001, Novelli et al., 2003). Les concentrations de CO sont

dominées par un gradient global nord-sud lié à la concentration des processus de combustion de combustible fossile et de biomasse dans l'hémisphère nord (voir Figure 1.2).

Le puits principal du CO est l'oxydation par OH, ce qui représente un mécanisme considérable de diminution de la capacité oxydante de l'atmosphère. Une élévation des concentrations en CO diminue donc la quantité de radicaux OH disponibles pour oxyder le méthane et l'ozone. Cette oxydation du CO est une source de CO_2 estimée à environ 1 PgC an^{-1} par Folberth et al. (2005).

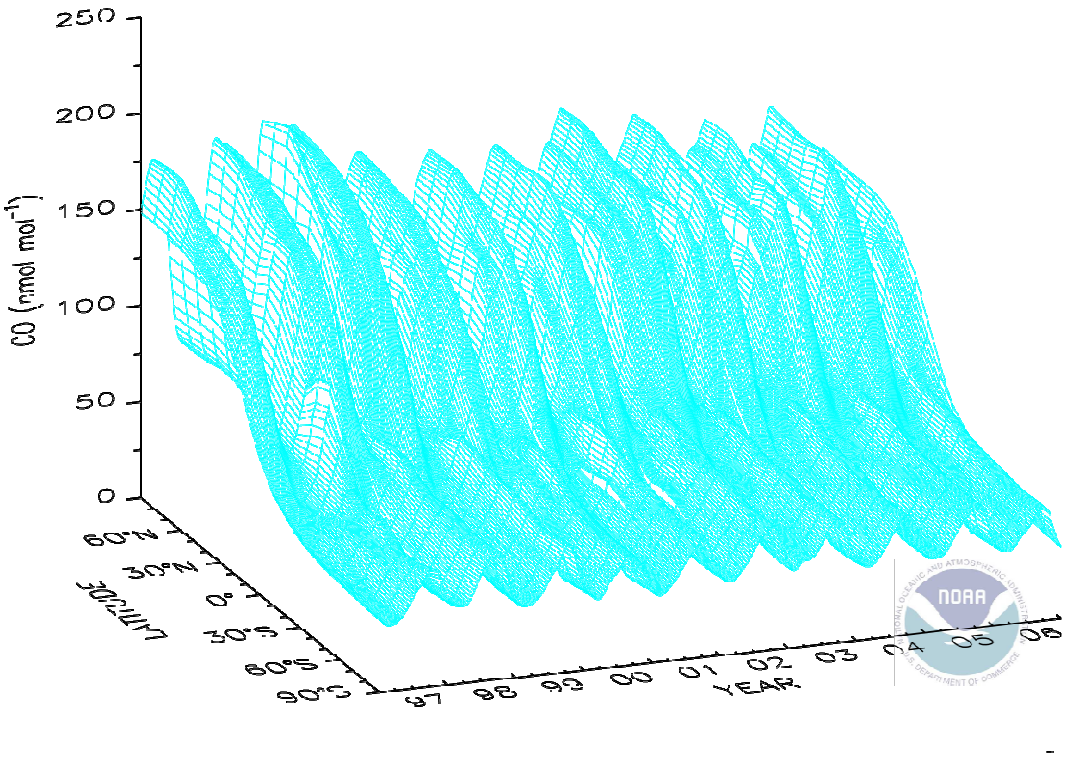

Figure 1.2. Distribution zonale et variabilité temporelle lissée du CO dans la couche limite marine. (P. Novelli, http://www.esrl.noaa.gov/gmd/)

1.1.3. Impact atmosphérique global des feux de forêt

La Sibérie contribue significativement au bilan du CO à travers les émissions gazeuses des feux de forêts. Avec les régions tropicales, les feux de forêt à l'échelle globale perturbent de manière significative la composition atmosphérique. La combustion de la biomasse constitue un flux net vers l'atmosphère de gaz à effet de serre (CO_2, CH_4) et de précurseurs de l'ozone (p.ex. CO ; Andreae et Merlet, 2001). Des particules de carbone organique ainsi que de nombreuses espèces réactives sont émises en grande quantité lors des feux (oxydes nitreux, composés soufrés, composés organiques volatils ; Andreae et Merlet, 2001). Les incendies modifient la dynamique des écosystèmes et ont un impact climatique non négligeable. Randerson et al. (2006) ont établi que l'albedo des surfaces brûlées augmentait suite à l'incendie, notamment l'albédo de printemps (la

surface est enneigée au printemps), durant 50 ans avant de revenir à la normale. Même avec un forçage radiatif positif net très important la première année (dû aux émissions cumulées de GES, aérosols, et à l'albédo modifié des suies déposées sur les surfaces gelées), l'effet climatique (80 ans) net de ce feu boréal est un forçage radiatif négatif dû à l'augmentation de l'albedo moyen les années suivant l'incendie.

Les mesures satellites de MOPITT ont permis de comprendre l'impact des feux de forêts sur les concentrations atmosphériques de CO à l'échelle hémisphérique (Lamarque et al., 2003 ; Yurganov et al., 2005 ; Pfister et al., 2005 ; Turquety et al., 2007). Une estimation des émissions à l'échelle globale est montrée par les Figures 1.3 et 1.4. La répartition géographique des sources de CO entre avril et septembre est moyennée sur la période 1997-2007 (Fig. 1.3). Les émissions sont calculées à partir de la base de données Global Fire Emissions Database (GFED) version 2 (van der Werf et al., 2006 ; http://www.geo.vu.nl/users/gwerf/GFED/index.html) basée sur des mesures d'aire brûlée obtenues par imagerie satellite. La Figure 1.4 montre la variabilité saisonnière et interannuelle des émissions de CO respectivement par les feux de forêt, sur la période 1997-2007 (GFED v2 ; van der Werf et al., 2006). Les feux de forêts sibériens dominent largement les émissions extratropicales dans l'hémisphère nord. Sur les années 1990, Wotawa et al. (2001) ont déterminé que les feux sibériens expliquaient plus de 50% de la variabilité du CO dans l'hémisphère nord extratropical. Les feux de forêts sibériens de 2003, particulièrement importants (Fig. 1.4), ont émis 130 Tg CO (Yurganov et al., 2005) rapidement transportés à travers l'hémisphère nord (Damoah et al., 2004). Ils ont ainsi provoqué une augmentation de la teneur en ozone entre 5 et 9 ppb en Amérique du Nord (Jaffe et al., 2004).

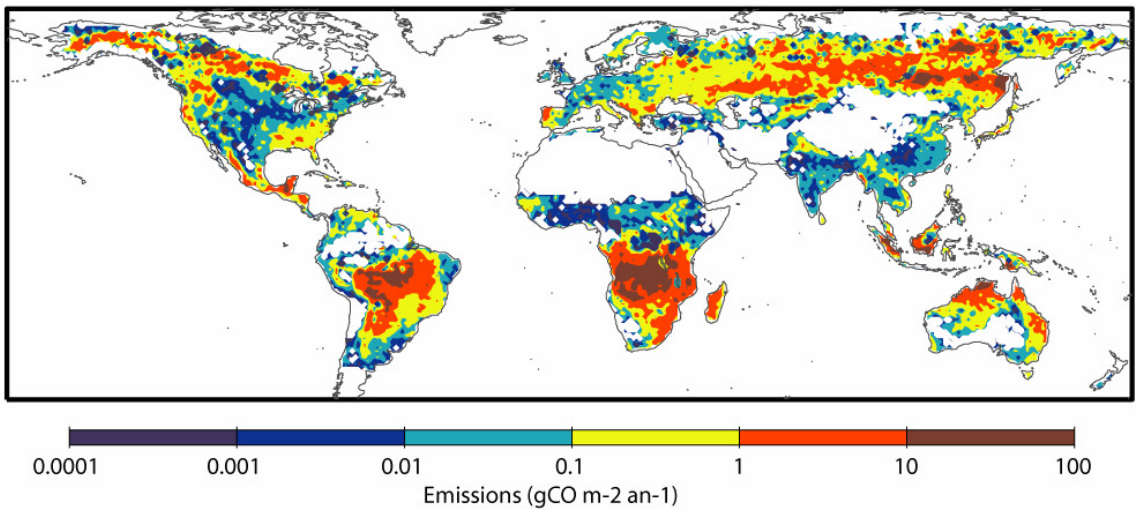

Figure 1.3. Carte des émissions de CO par les feux de forêts cumulées de mai à septembre moyennées entre 1997 et 2007 (GFED v2 ; van der Werf et al., 2006).

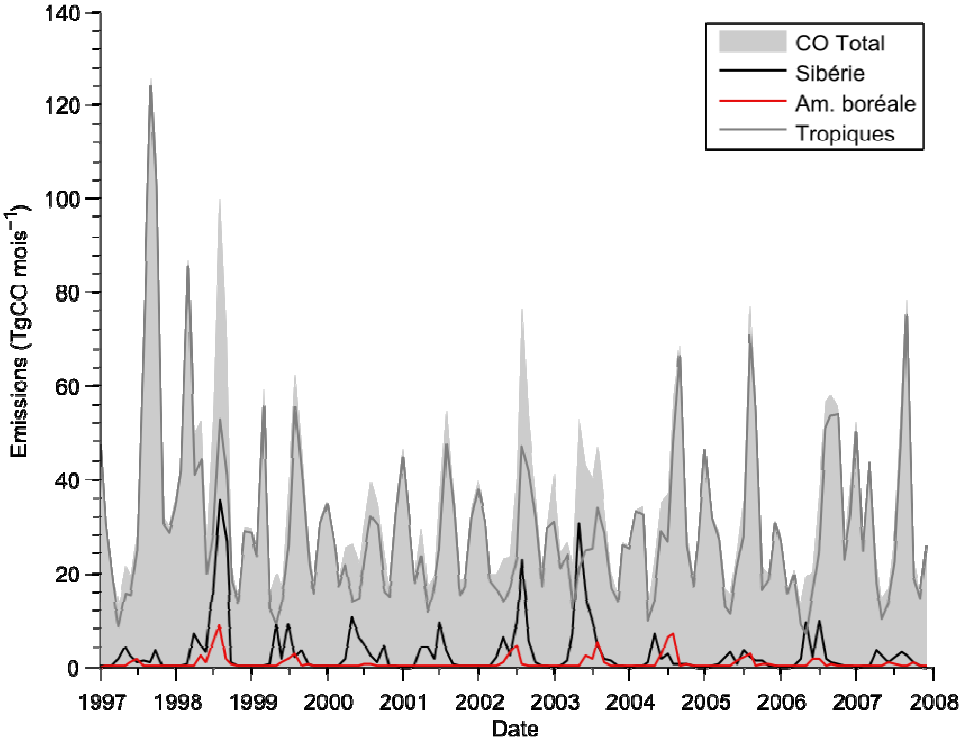

Figure 1.4. Emissions de CO par les feux de forêts boréaux et comparaison avec les régions tropicales et le total global (GFED v2 ; van der Werf et al., 2006). Sibérie : noir, Amérique du nord boréale : rouge, tropiques : gris foncé, total : gris clair

La Figure 1.5 montre la distribution saisonnière des émissions de CO dues aux feux de forêt en Sibérie selon la base de données GFED. On observe ainsi deux modes en mai et en juillet-aout qui reflètent l'activité des feux. Les feux sont moins intenses en mai car les températures après la fonte des neiges sont bien inférieures à celles d'été. Par contre, environ 60% des précipitations annuelles tombent entre juin et août, augmentant l'humidité du combustible mais n'empêchant pas la combustion durant le deuxième pic d'activité (Soja et al., 2004). Les années 1998 et 2003 ont connu une activité importante jusqu'en septembre-octobre.

Les panaches de feux de forêt dans les régions boréales peuvent être injectés en altitude par pyroconvection, parfois jusqu'à la stratosphère (Fromm & Servranckx, 2003, Trentmann et al., 2006 ; la généralité de cette conclusion ayant été contestée par Labonne et al., 2007). Ceci augmente leur capacité à être transporté rapidement sur de longues distances (Bertschi et al., 2004 ; Damoah et al., 2004) et modifie leurs propriétés chimiques.

La réaction chimique des précurseurs dans les panaches provoque une pollution régionale à l'ozone (McKeen et al., 2002). Des augmentations significatives d'ozone observées au dessus de l'océan Atlantique ont pu être reliées à des feux de forêt boréaux (Honrath et al., 2004 ; Lapina et al., 2006; Val Martin et al., 2006). Selon un mécanisme similaire à la pollution urbaine, Mauzerall et al. (1998) et Real et al. (2007) ont ainsi observé que l'injection en altitude, non seulement accélère le transport du panache, mais favorise également la formation d'ozone à grande distance sous le vent de par la conversion de NOx en PAN. La formation d'O_3 dans les panaches de feux de forêt

boréales génère des concentrations maximales après 3—5 jours de transport (Real et al., 2007), ce qui correspond à une échelle de temps de transport intercontinental (Lapina et al., 2006).

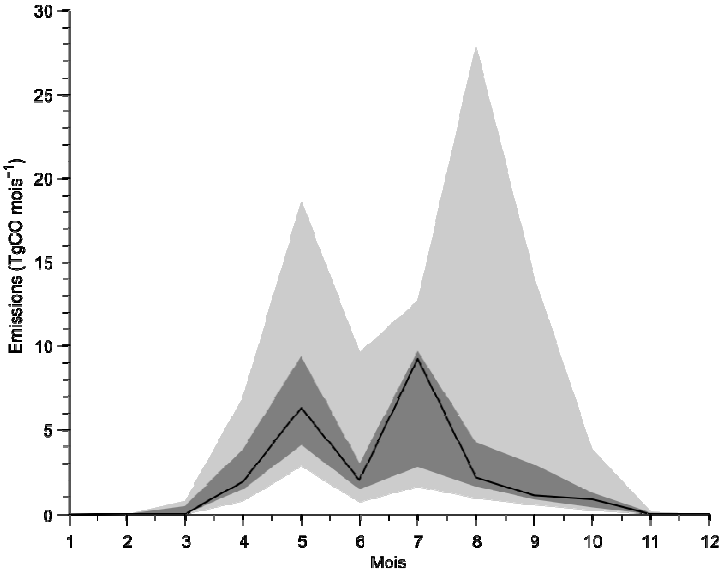

Figure 1.5. Emissions de CO mensuelles médianes dues aux feux de forêt en Sibérie, entre 1997 et 2007 (GFED). En gris clair, entre le 10^{e} et le 90^{e} percentile, en gris sombre, interquartile.

1.1.4. Caractérisation des émissions de CO

Les émissions anthropiques de CO peuvent être évaluées par des méthodes dites *bottom-up*, qui rassemblent des statistiques sur les processus émetteurs de CO et modélisent par agrégation les émissions associées. Dans le cas des émissions anthropiques, cette méthode est utilisée par exemple par Olivier et al. (2005), Streets et al. (2003, 2006) et Ohara (2007). L'application de cette méthode aux émissions de feux de forêt correspond à l'approche utilisée par exemple par van der Werf (2004, 2006), qui calcule les émissions sur une aire brûlée mesurée par imagerie satellite à partir de facteurs établis par Andreae et Merlet (2001) et d'un modèle biogéochimique.

Une approche *top-down* utilisant le comportement « intégrateur » de l'atmosphère consiste à utiliser des mesures atmosphériques, qu'elle soient obtenues par un réseau de stations de surface (Bergamaschi et al., 2000 ; Kasibhatla et al., 2002 ; Pétron et al., 2002) ou par satellite (Pétron et al., 2004). Ces études ont indiqué une sous-estimation systématique des émissions anthropiques asiatiques calculées par les méthodes *bottom-up*. Cette approche assure une homogénéité entre les émissions calculées et les concentrations atmosphériques observées, mais la séparation entre différents processus colocalisés est plus incertaine. A partir de mesures satellites de CO réalisées par l'instrument MOPITT, Pfister et al. (2005) ont pu estimer à 30 ± 5 Tg CO les émissions des feux de forêts d'Alaska en été 2004. Avec l'hypothèse que les conditions aux limites sont simples, les sources isolées géographiquement et que l'écoulement atmosphérique est correctement modélisé, des mesures directement sous le vent des régions émettrices (et notamment des campagnes aéroportées) peuvent contraindre les émissions de CO (Palmer et al., 2003).

1.2. Le CO_2 comme traceur du transport et des échanges surface continentale-atmosphère

1.2.1. CO_2 : caractéristiques, sources et puits

Le CO_2 est le principal gaz à effet de serre d'origine humaine. C'est un élément très stable et en concentration relativement homogène dans l'atmosphère. La végétation échange avec l'atmosphère une quantité importante de CO_2 lors des processus de respirations et de la photosynthèse. L'océan dissous également une quantité importante de CO_2. Ces flux bruts sont dépendants de la quantité présente dans le réservoir atmosphérique, hors la concentration atmosphérique de CO_2 n'est pas à l'équilibre.

Les émissions anthropiques ont porté les concentrations atmosphériques de 280 ± 5 ppm à l'ère « préindustrielle » à 379 ± 0,65 ppm en 2005 (IPCC, 2007), avec une croissance de 2,0 ppm an^{-1} sur la période 2000-2007 (GCP, 2008). Actuellement, le bilan du CO_2 est dominé par les émissions anthropiques associées à l'utilisation de combustibles fossiles, qui injectent 8,5 GtC an^{-1} dans l'atmosphère (en 2007 ; GCP, 2008 ; Table 1.3). La déforestation tropicale constitue également un apport de CO_2 atmosphérique. Cette modification de l'utilisation des sols contribue ainsi entre 0,5 et 2,7 GtC an^{-1} supplémentaires (1,5 GtC an^{-1} entre 2000 et 2007 ; GCP 2008). La quantité de CO_2 atmosphérique augmente néanmoins d'une valeur inférieure aux apports décrits ci-dessus. Depuis 2000, la quantité de carbone dans l'atmosphère a crû de 4,1 ± 0,1 GtC an^{-1} en moyenne. Les deux autres réservoirs capables d'échanges « rapides » avec l'atmosphère, la végétation terrestre et les océans, absorbent environ 55% de ces émissions. Ceci représente sur les 5 dernières années 2,6 GtC an^{-1} pour les écosystèmes terrestres et 2,3 GtC an^{-1} pour l'océan (GCP, 2008). Ces deux puits sont toutefois sensibles au réchauffement climatique, et pourraient montrer des signes de ralentissement significatif.

Table 1.3. Bilan atmosphérique du CO_2 sur la période 2000-2007

Sources (GtC an^{-1})		Puits (GtC an^{-1})	
Combustibles fossiles (2007)	8,5	Terrestre[a]	2,6
Déforestation	1,5	Océanique	2,3

[a] Résultat de la différence photosynthèse (~62 GtC an^{-1}) - respiration (~60 GtC an^{-1})

La variabilité interannuelle du puits terrestre (Bousquet et al., 2000) est partiellement expliquée par les feux de forêts (Langenfelds et al., 2001 ; van der Werf et al., 2004) prépondérants durant les périodes sèches associées aux variations d'El Niño. Ainsi, durant la période 1997/1998, Langenfelds et al. (2001) estime que les feux ont émis entre 0,8 et 3,7 GtC en CO_2. Avec une méthodologie différente, la base de données GFED (van der Werf et al., 2006) indique que les feux à l'échelle globale ont émis 2,4 ± 0,4 GtC an^{-1} (moyenne ± écart type), dont 0,16 ± 0,11 GtC an^{-1} pour la Sibérie. La variabilité intra et interannuelle du CO_2 lié aux feux de forêts peut etre déduite

de celle du CO (Fig. 1.6) à un facteur près. Le puits de carbone océanique a une variabilité interannuelle moindre (p. ex. Gruber et al., 2002, Bousquet et al., 2000).

1.2.2. Estimation des flux

La connaissance des flux de CO_2 entre la surface et l'atmosphère à grande échelle peut s'obtenir selon deux approches. L'approche *top-down* implique l'inversion de mesures globales des concentrations atmosphériques et permet une attribution géographique des puits de surface à partie de mesures atmosphériques. Les approches dites *bottom-up* consistent en la généralisation spatiale et temporelle d'observations localisées.

La modélisation inverse relie les concentrations atmosphériques mesurées aux flux de surface par le transport atmosphérique des anomalies de CO_2 (p. ex. Tans et al., 1990, Fan et al., 1998, Bousquet et al., 1999, Gurney et al., 2002). Les mesures de CO_2 sont effectuées à des stations de surface opérées par divers laboratoires à travers le monde. Le transport est évalué par des modèles atmosphériques. Cette méthode opère généralement à partir de flux prescrits, qui sont ensuite optimisés pour que le champ de CO_2 simulé soit en accord avec les mesures dans la limite des incertitudes. Cette méthode permet d'une part d'évaluer robustement la variabilité interannuelle (p. ex. Bousquet et al., 2000 ; Rayner et al., 2008) et d'autre part d'estimer la valeur moyenne des flux (p. ex. Gurney et al., 2002 ; IPCC, 2007).

La répartition géographique des flux terrestres de carbone est plus difficile à établir. La distribution latitudinale a été déterminée par Tans et al. (1990) et Denning et al. (1995), selon lesquels un puits important dans l'hémisphère nord est requis pour expliquer le fort gradient interhémisphérique. Par contre, déterminer la distribution longitudinale est limité par de faibles gradients est-ouest de CO_2. Fan et al. (1998) attribuent principalement le puits terrestre principal de l'hémisphère nord au continent nord-américain, alors que Bousquet et al. (1999) l'attribuent plutôt à l'Eurasie. Cette incertitude reflète également le manque de mesures : l'erreur dans la détermination de la répartition est-ouest des flux à une latitude donnée est fortement dépendante de la densité et de la disposition du réseau de mesure, en plus des erreurs de transport. Selon l'IPCC (2007, p. 523), les puits terrestres de l'hémisphère nord se répartissent pour entre -0,9 et +0,2 GtC an^{-1} en Europe, entre -1,2 et +0,3 GtC an^{-1} en Asie du nord et entre -0,6 et -1,1 GtC an^{-1} en Amérique du Nord. Il convient de noter ici l'importance des incertitudes sur l'Eurasie, et notamment sur l'Asie du Nord, en grande partie dûes au manque de mesures dans ces régions.

L'approche *bottom-up* consiste en l'extrapolation de mesures locales intégrées dans un modèle. Goodale et al. (2002) a ainsi compilé différents inventaires forestiers étendus statistiquement pour estimer les flux de C d'un grand nombre de pays de l'hémisphère nord. Les tours de flux utilisant la technique d'*eddy covariance* (Wofsy et al., 1993, Baldocchi et al., 2001) fournissent un bilan détaillé sur une zone très limitée (~1 km^2) et peuvent être intégrées dans les modèles de processus biosphériques (Reichstein et al., 2005, Santaren et al., 2007). La modélisation des flux de biosphère est toutefois difficile à réconcilier avec les flux estimés par approche *top-down* (Peylin et al., 2005a).

1.2.3. Vers l'échelle régionale

Ces estimations sont susceptibles de servir de base à des décisions liées à la maîtrise des émissions dans le cadre de la lutte contre le réchauffement climatique, et notamment du protocole de Kyoto. Il devient donc nécessaire de fournir des estimations précises à l'échelle nationale ou subcontinentale. A ce titre la modélisation inverse à de plus hautes résolutions spatiales (à l'échelle de la grille de modèle) et temporelles (journalières) est nécessaire. Par exemple Peylin et al. (2005b) estime des flux journaliers résolus spatialement à l'échelle du modèle pendant un mois ; cette méthode reste toutefois dépendante des conditions aux limites et donc d'une estimation correcte des flux à l'échelle globale. Les expériences lagrangiennes, dites aussi bilan de couche limite, proposées par Raupach et al. (1991) représentent une possibilité intéressante pour mesurer ponctuellement les flux (essentiellement diurnes ; Lloyd et al., 2001, Schmitgen et al., 2004 ; Lloyd et al., 2007). Une autre approche, similaire, de suivi lagrangien a été appliquée par Chou et al. (2002) sur la forêt Amazonienne. La précision de ces méthodes restent toutefois à améliorer et sont limitées à des périodes de temps réduites.

1.2.4. Le CO_2 comme traceur du transport ?

Le CO_2 peut également être utilisé comme traceur de transport et de mélange. C'est le principe sous-jacent de l'étude de Stephens et al. (2007) qui utilise le gradient vertical de CO_2 comme une contrainte sur la représentation du mélange vertical à grande échelle dans les modèles.

Le CO_2 peut également bénéficier d'une analyse conjointe avec le CO. Il a été établi que les concentrations de ces deux gaz sont fortement corrélées quand leurs puits respectifs (photochimique et biosphérique) sont faibles (Rivier et al., 2006 ; Suntharalingam et al., 2004). Le rapport de leur concentration peut être suffisamment conservatif pour permettre de prédire la concentration de CO_2 due à la combustion (par exemple de combustible fossile) à partir de la concentration de CO (Potosnak et al., 1999).

L'étude de l'anomalie (négative ou positive) liée aux sources et puits de CO_2 comme traceur de transport pur a été réalisée par exemple à méso-échelle par Perez-Landa et al. (2006) pour étudier l'alternance entre brise de mer et brise de terre sur la côte espagnole. Boering et al. (1996) ont utilisé la propagation verticale du CO_2 comme un traceur de transport dans la stratosphère, en combinaison avec des mesures de NOx. A plus grande échelle, Wada et al. (2007) ont pu observer, au niveau de la mer dans le Pacifique nord occidental, le transport dans le Pacifique d'anomalies négatives de CO_2 dues à l'assimilation par la végétation sibérienne et en Asie du sud-ouest. Ainsi le CO_2 s'avère être un traceur potentiel du mélange et du transport atmosphérique à différentes échelles.

1.3. Mécanismes extratropicaux de transport et de mélange atmosphérique

1.3.1. Circulation extratropicale

Le transport atmosphérique en Sibérie se caractérise par une situation à l'interface entre la circulation extratropicale (de 30°N à 60°N), relativement bien comprise, et le vortex arctique. Le transport atmosphérique extratropical associé à l'export des polluants (HTAP, 2007) est essentiellement limité à la troposphère. La circulation y est largement découplée de la circulation tropicale (matérialisé par les cellules de Hadley avec convection profonde à la zone de convergence intertropicale et subsidence dans les régions subtropicales), ainsi que du vortex polaire (Fig. 1.6). La circulation moyenne zonale suit un mouvement d'est en ouest, le vent augmentant avec l'altitude. Sa composante méridienne est négligeable par rapport à sa composante zonale. Des perturbations baroclines imposent toutefois un mélange méridien tout au long de l'année. En été la convection joue un rôle important dans la ventilation de la couche limite au dessus des surfaces terrestres.

Le transport dans la troposphère tend à se maintenir sur une surface de température potentielle constante. Une stratification stable des masses d'air transportées est ainsi possible. Ces surfaces de température potentielle constante tendent à prendre de l'altitude lorsqu'on se déplace vers les pôles. Ainsi un transport vers le pôle aura tendance à subir une ascendance. Plusieurs types de circulation viennent se superposer à la circulation moyenne décrite ci-dessus.

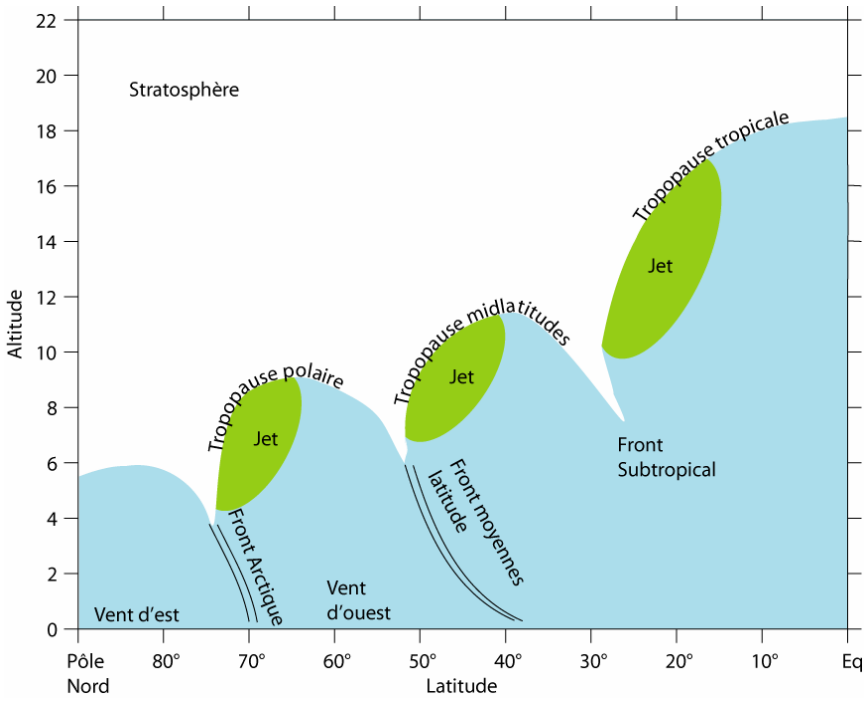

Figure 1.6. Structure de la tropopause et localisation des principaux courants de jets et positions moyenne des fronts, d'après Shapiro et al. (1986).

1.3.2. Cyclones extratropicaux

Les cyclones extratropicaux sont associés à des perturbations baroclines. Ces dernières modulent la distribution de la vitesse du courant de jet en altitude (Malardel, 2005) et favorisent l'injection en altitude de l'air présent dans la couche limite (Keyser, 1999). Les cyclones extratropicaux sont ainsi un mécanisme d'export dominant pour l'air de la couche limite des côtes est-asiatiques et est-américaines (Stohl, 2001). Ce type de transport sporadique est responsable de la majeure partie du transport trans-Pacifique de polluants (Yienger et al., 2000).

Quatre types de circulation s'établissent dans un cyclone extratropical : la *warm conveyor belt* (WCB) ascendante en avant du front froid due au fort gradient de température potentielle, la *cold conveyor belt* (CCB) légèrement ascendante, le *dry airstream* (DA) qui est typiquement associé à une intrusion stratosphérique, et la circulation de traîne post-front froid (Cotton et al., 1995 ; Cooper et al., 2002 ; Figure 1.7).

L'injection verticale due à la WCB est la plus significative pour le transport longue distance des polluants (flèche rouge dans la Figure 1.7 ; Banic et al., 1986, Bethan et al., 1998 ; Stohl, 2001) de par sa capacité à balayer la couche limite chargée en polluants et à injecter cet air à proximité du courant de jet. Le transport vertical peut être accéléré par une convection importante associée au front froid (Purvis et al., 2003). Selon Stohl (2002), les WCB permettent aux émissions nord-américaines d'atteindre l'Europe en 3 à 4 jours.

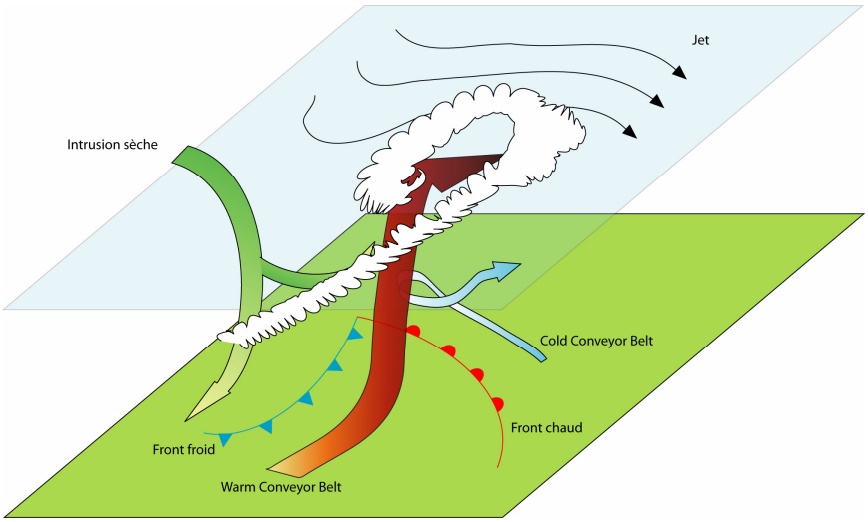

Figure 1.7. Schéma des circulations associées aux amas en virgule dans un cyclone extratropical, d'après Cotton et al. (1995) et Cooper et al. (2002).

1.3.3. Mélange vertical par convection

La convection est un autre type de mélange atmosphérique se superposant à la circulation moyenne et couplée avec le transport longue distance des polluants. La Table 1.4 montre que les différents types de convection et les cyclones extratropicaux ont une capacité de transport vertical

comparable, bien qu'associés à des quantités de précipitations différentes. L'ascension dans la convection profonde est beaucoup plus rapide (quelques minutes) que dans les cyclones extratropicaux, ce qui permet l'injection en altitude de composés plus réactifs. La ventilation de la couche limite par la succession entre croissance diurne de la couche limite et constitution d'une couche résiduelle nocturne soumise à des vents plus importants permet également d'accélérer le transport atmosphérique.

Table 1.4. Flux de masse verticaux et précipitations associées dans les systèmes nuageux

Système nuageux	Flux de masse global (10^9 kg s^{-1})	Précipitation annuelles (10^{15} kg)
Tempêtes orageuses simples [a]	211	56
Systèmes & complexes convectifs méso [a]	580	283
Cyclones extratropicaux (dont WCB) [a]	750	130
WCB atteignant 40% tropopause [b]	86	26
WCB atteignant 60% tropopause [b]	30	10
WCB atteignant 80% tropopause [b]	6.6	2.6

[a] Flux de masse vertical d'air de la couche limite à travers l'isobare 900 hPa (Cotton et al.,1995)

[b] Trajectoires de WCB identifiée comme ayant une ascension jusqu'à au moins 40%, 60% et 80% de l'altitude de la tropopause (Eckhardt et al., 2003)

Enfin, l'advection dans la couche limite est également significative bien que plus lente que dans la troposphère libre. Quand la couche limite atteint la même hauteur que le jour précédent et ré-entraîne ainsi les polluants de la couche nocturne résiduelle (Stull, 1988), le transport intercontinental peut s'effectuer intégralement dans la couche limite. Ce type de transport domine en Europe, où la convection est peu profonde et l'activité cyclonique limitée (Duncan et Bey, 2004), et entraîne la pollution européenne vers la Sibérie qui reste la région de l'hémisphère nord la moins bien caractérisée en termes de transport.

1.4. Transport des polluants dans l'hémisphère nord

Le transport à longue distance n'a été véritablement intégré que récemment dans l'étude de la pollution atmosphérique. Dans les années 1960, un lien fût trouvé entre les émissions soufrées en Europe centrale et l'acidification des lacs en Scandinavie. Ceci aboutit à la signature en 1979 de la Convention sur la pollution atmosphérique transfrontalière à longue distance, sous l'égide de la Commission économique des Nations Unies pour l'Europe (http://www.unece.org/env/lrtap/), suivi en 1984 par la mise en place du protocole EMEP de collecte de données sur les émissions européennes. Au-delà des substances acidifiantes, le transport à longue distance est également responsable de concentrations élevées de polluants à grande distance des zones d'émission.

1.4.1. Brume arctique

Les efforts de recherche ont été initialement portés sur des cas où le transport intercontinental est la seule source d'explication plausible. C'est le cas du *Arctic Haze*, ou brume arctique, une brume marron ayant une concentration élevée en polluants observée dans l'Arctique par les pilotes de l'U.S. Air Force dans les années 1950. L'explorateur Adolf Erik Nordenskiöld, dans les années 1870, avait le premier émis une hypothèse sur ce phénomène (Nordenskiöld, 1883 ; Garrett, 2008) en l'attribuant à la chute imperceptible et continue d'une poussière cosmique. Il fut également étudié par l'équipe de Frijdthof Nansen en 1894 (Nansen, 1897) qui l'attribue également à un dépôt atmosphérique. Dans les années 1970, des études plus détaillées de géochimie isotopique ont permis à Rahn et al. (1977) et Shaw et al. (1982) d'attribuer la source de la brume arctique à des émissions asiatiques ou européennes. Par la suite, Hong et al. (1994) ont même déterminé à partir de carottages au Groenland que la teneur en plomb était supérieur d'un facteur quatre à ses taux naturels sur une période concordant avec celle de l'empire Romain. Un paléo-transport intercontinental de la pollution atmosphérique par les métaux lourds a ainsi été documenté pour la période de l'Antiquité. La recherche actuelle sur le réchauffement climatique, dont l'Arctique est un avant-poste de par les nombreuses transformations qui s'y déroulent, a permis d'approfondir cette question (p. ex. Law & Stohl, 2007) et de mieux identifier le transport atmosphérique vecteur de polluants précurseurs. La brume arctique illustre un cas limite de l'isolement entre les circulations atmosphériques aux moyennes latitudes et arctiques, la Sibérie et la Scandinavie étant suffisamment froides pour exporter facilement des polluants vers l'Arctique (HTAP, 2007). Le transport associé à ce phénomène s'effectue donc principalement dans la couche limite (Stohl, 2006).

La troisième Année Polaire Internationale a ainsi permis de développer des projets tels que POLARCAT (Stohl & Law, 2006 ; www.polarcat.no) dédiés à l'étude de la chimie et du transport atmosphérique en environnement Arctique.

1.4.2. Transport trans-Pacifique

Duce et al. (1980) ont suggéré que le dépôt de poussières éoliennes dans le Pacifique, à 5000 km au sud-est des côtes asiatiques, était lié à l'activité accrue des tempêtes en avril au dessus des déserts asiatiques. Ces travaux précurseurs ont attiré l'attention de la communauté scientifique sur le transport trans-Pacifique. Depuis 10 ans de très nombreuses études sont dédiées à ce phénomène, notamment celles de Jaffe et al. (1999) et Liang et al. (1998). La pollution à distance se superpose souvent à une pollution locale ou régionale et en amplifie les effets néfastes. Ainsi le transport trans-Pacifique affecte largement les concentrations continentales d'O_3 (entre +1 et +6 ppb) aux Etats-Unis entre avril et juin (Jacob et al., 1999). L'importance du transport synoptique, et notamment les mouvements redistributifs associés aux cyclones extratropicaux (Banic et al., 1986 ; Liang et al., 1998 ; Bey, 2001), a ainsi été mis en exergue pour sa capacité à conférer un « rayon d'action » intercontinental aux polluants asiatiques mélangés dans l'atmosphère.

1.4.3. Hémisphère nord

Plus récemment, diverses équipes se sont intéressées aux polluants exportés de la couche limite nord américaine vers l'Europe (Auvray et Bey, 2005), où les perturbations baroclines à l'échelle synoptique jouent également un rôle prépondérant (Cooper et al 2001), ou encore de l'Europe vers les régions avoisinantes. Il a ainsi été observé que les polluants européens étaient régulièrement transportés, dans des proportions liées notamment à la saison et à l'indice de l'oscillation nord-atlantique, vers l'Arctique (Eckhardt et al., 2003), l'Atlantique tropical (Duncan et Bey 2004), ou le bassin Méditerranéen (Lelieveld et al., 2002). Ces études de modélisation prédisent un export significatif des polluants vers la Sibérie. Ce transport résulterait essentiellement d'un acheminement dans ou immédiatement au dessus de la couche limite (Wild et al., 2003 ; Stohl, 2001, Duncan et Bey, 2004), avec la possibilité d'un déplacement vertical dans des régions généralement convective : Allemagne et Russie européenne (Duncan et Bey 2004). Ces différents acheminements de la pollution sont synthétisés dans la Figure 1.8 pour l'hiver et l'été.

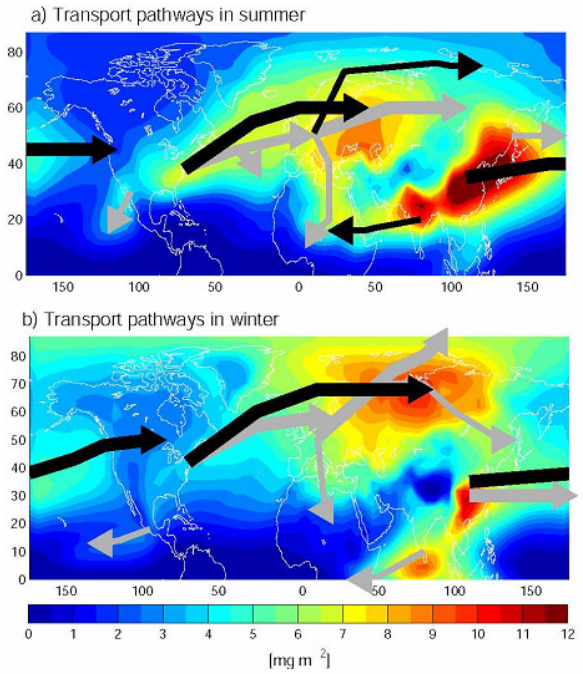

Figure 1.8. Illustration du transport intercontinental (HTAP, 2007) pour le cas d'un traceur CO inerte après 8 à 10 jours de transport (colonne totale). Les flèches grises montrent le transport dans la basse troposphère (< 3 km), dominé par l'advection dans et juste au dessus de la couche limite, les flèches noires montrent le transport dans la troposphère moyenne et haute (> 3 km), où les cyclones extratropicaux et la convection profonde jouent un rôle dominant.

L'arrivée de moyens d'observation spatiale, introduite avec les mesures de la colonne de CO et d'O_3 sur la navette spatiale (Reichle et al., 1999) ont permis d'évaluer la portée globale du transport des polluants (Edwards et al., 2004 ; Fishman et al., 2008). Notamment, l'observation de panaches de CO intercontinentaux a permis de généraliser la portée du transport de la pollution.

L'application des instruments spatiaux est toutefois limitée par la difficulté d'obtenir des mesures précises sensibles aux concentrations dans la basse ou moyenne troposphère.

1.4.4. Sibérie

La Sibérie est essentiellement la dernière région « inexplorée » en termes de transport atmosphérique. Des études de modélisation prédisent que l'influence de la pollution européenne est plus importante en hiver et au printemps quand la pollution est transportée autour de l'anticyclone sibérien ; et que cette masse d'air est généralement transportée dans la couche limite (Newell & Evans, 2000 ; Stohl et al., 2002 ; Liu et al., 2002 ; Fig. 1.8). Dans certain cas les polluants européens transportés peuvent être mélangés en concentrations significatives avec l'export asiatique vers le Pacifique (Liu et al., 2003). Basé sur des mesures dans le Sud de la Sibérie, Pochanart et al. (2003) constatent une concentration en CO supérieure et en O_3 légèrement supérieure dans les masses d'air associées à des origines européennes (+24 ppb CO et +3 ppb O3 comparés aux masses d'air très propres d'origine arctique). Le manque d'observations in situ empêche généralement de confirmer les études de modélisation. Il convient de citer les campagnes de trains instrumentés TROICA (Crutzen et al., 1998). Celles-ci n'ont pas apporté de nouvelles contraintes sur le transport intercontinental, même si elles ont permis d'observer du transport à l'échelle régionale à l'intérieur de la Russie (Bergamaschi et al., 1998 ; Röckmann et al., 1999).

Or la modélisation du CO en Asie de l'est, par exemple, ne dispose pas de contrainte observationnelle sur les concentrations en Sibérie (Akimoto, 2003), qui constituent une condition limite latérale importante et mal connue. Ceci peut fausser les conclusions quantitatives sur l'excès de CO associé aux émissions asiatiques dans des études comme celle de Liu et al. (2003). D'autres études de modélisation similaires considèrent à tort les émissions européennes comme négligeables. Dans une intercomparaison de modèles (Kiley et al., 2003), un modèle ayant intégré les mesures de Pochanart et al. (2003) dans ses conditions latérales d'import du CO se retrouve systématiquement moins biaisé dans les concentrations simulées. Des mesures permettant de valider les modèles de transport sur la Sibérie, et notamment les spécificités de l'export européen, sont donc nécessaires pour améliorer la pertinence de ces études.

1.5. Aérosols : particles nanométriques et nucléation

Les aérosols constituent la phase solide, particulaire de l'atmosphère. Ils affectent la santé humaine, modifient la visibilité et ont une influence encore mal comprise sur le climat (Charlson 1991, Ramanathan et Carmichael, 2008). En effet, ils affectent la formation et les caractéristiques de nuages et modifient l'établissement de précipitation dans ces nuages (Ramanathan et Carmichael, 2008 ; Rosenfeld et al 2008). Leur interaction avec le rayonnement solaire modifie le forçage radiatif et peut ainsi modifier la structure thermale de l'atmosphère. L'impact radiatif total (direct et à

travers l'albedo des nuages) est comparable à celui du CO_2, mais dans le sens opposé, bien que sur une échelle de temps moindre.

La taille des aérosols varie de l'échelle nanométrique pour les clusters de molécules, jusqu'au millimètre pour les poussières. Les aérosols dits primaires, souvent de taille supérieure au micron, sont des particules émises depuis la surface. La poussière et les particules de sel marin représentent un flux de masse de matière vers l'atmosphère considérable, entre 2 et 13 Gt an^{-1}, la poussière pouvant être transportée d'un bord à l'autre des bassins océaniques. La définition des aérosols est vaste et inclut suies, pollens, etc. Les aérosols dits secondaires sont formés par conversion de gaz en particules.

La conversion de gaz en particules, ou nucléation, se produit soit de manière homogène, lorsque la phase gazeuse est sursaturée, soit de manière hétérogène avec l'intervention d'une phase solide. Ceci se produit généralement sur des aérosols ou des clusters (assemblages de molécules ou « proto »-aérosols) préexistant par une combinaison de condensation (de vapeurs sur un noyau). La taille moyenne d'une population d'aérosols peut ainsi croitre soit par nucléation hétérogène soit par coagulation entre aerosols. Les processus de nucléation les plus importants dans le contexte des aérosols atmosphériques sont la nucléation binaire de l'acide sulfurique et de la vapeur d'eau (exemple de la Fig. 1.9), la nucléation ternaire de l'acide sulfurique, de l'eau et de l'ammoniac, et enfin la nucléation induite par les ions (Kulmala et al., 2004 ; Curtius, 2006). La nucléation a été observée notamment dans la couche limite dans la forêt boréale (en Finlande ; Kulmala et al., 2004, Tunved et al., 2006). Ces observations au sol ont été reproduites dans la forêt sibérienne par Dal Maso et al. (2008) qui ont trouvé des vitesses de formation de nouvelles particles et des vitesses de croissances similaires à celles observées en Finlande.

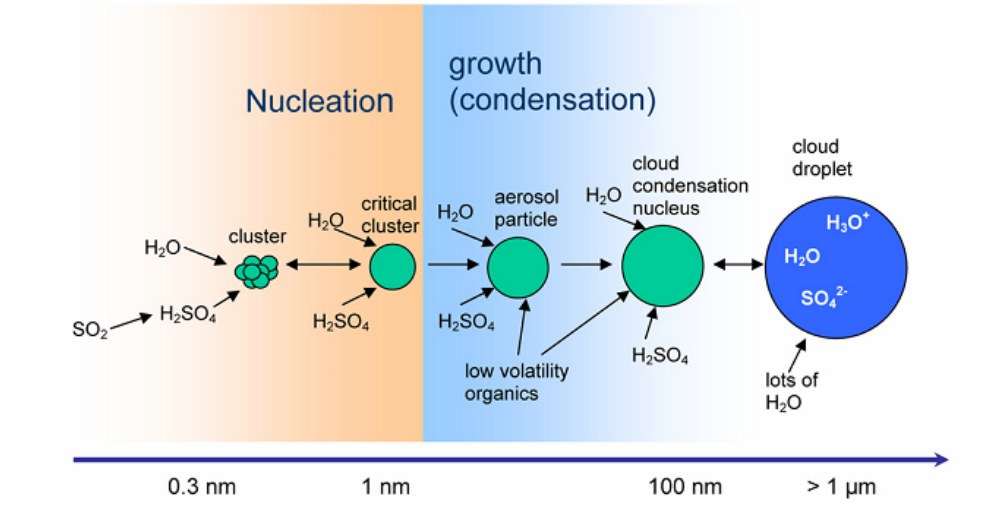

Figure 1.9. Formation et croissance des aérosols sulfatés secondaires (Curtius, 2006)

Des concentrations de particules de l'ordre de 10^4—10^6 cm^{-3} sont observées en environnement urbain, contre 10^4 cm^{-3} en environnement rural et 10^2 cm^{-3} dans la troposphere libre. L'acide sulfurique domine la nucléation dans l'atmosphère polluée. Le flux d'aérosols à base

de sulfate représente entre 80 et 90% du flux total d'aérosols secondaires. Le flux anthropique d'aérosols sulfatés est évalué entre 70 et 220 Mt an^{-1}, comparable au flux biogénique d'aérosols sulfatés valant entre 90 et 200 Mt an^{-1} (Delmas et al., 2005 et références citées, p. 180). En environnement forestier « propre », et notamment dans les forêts boréales, des précurseurs biogéniques peuvent contribuer significativement à la nucléation (Kavouras et al., 1999 ; O'Dowd et al., 2002). L'oxydation de composés organiques volatils, essentiellement biogéniques, génère également un flux vers l'atmosphère évalué entre 8 et 40 Mt an^{-1}.

1.6. Objectif général

Cette thèse a pour objectif de caractériser les variations de teneur atmosphérique en CO_2, CO et O_3, ainsi que les aérosols ultrafins, au dessus de la Sibérie, lors de campagnes intensives à l'échelle continentale. Ce jeu de données, unique de par la région couverte, a été obtenu dans le cadre du programme franco-russe YAK-AEROSIB dont l'objectif général est d'étudier le bilan des gaz à effet de serre et le transport des polluants en Sibérie avec une instrumentation *ad hoc*.

Les mesures in situ du CO_2, CO et O_3 sont interprétées en termes de transport atmosphérique, ainsi que de sources et puits, que ce soient les émissions anthropiques de CO_2 ou de CO, l'assimilation du CO_2 par la végétation, ou le CO émis par la combustion de biomasse durant les feux.

Après avoir testé le comportement des instruments en vol, cinq campagnes aéroportées ont été réalisées entre 2006 et 2008, en été pour la plupart. Les campagnes de 2006 et 2007 sont étudiées ici. Durant ces campagnes de mesures, l'avion a survolé une étendue importante de Sibérie et collecté le plus de profils verticaux (ascensions et descentes) possible. Les mesures de gaz trace ainsi obtenues sont ensuite comparées à des résultats de modélisations, afin d'interpréter les mesures et d'établir des relations source-récepteur.

La modélisation atmosphérique permet d'interpréter les mesures, celles-ci étant ponctuelles et portant sur un nombre limité d'espèces chimiques. L'origine de l'air mesuré n'est pas triviale à déterminer, particulièrement durant une campagne aéroportée, et l'utilisation de modèles de transport permet d'expliquer les observations par une relation source-récepteur. Les modèles utilisés dans cette étude sont FLEXPART, un modèle lagrangien de dispersion de particules (Stohl & Thomson, 1999, Seibert & Frank 2004, Stohl et al 2005) et LMDZ-INCA (Laboratoire de Météorologie Dynamique - Zoom et Interaction Chimie – Aérosols), un modèle eulérien global de chimie et de transport (Sadourny et Laval, 1984 ; Le Treut et al., 1994 ; Hauglustaine et al., 2004). Un second objectif est d'apporter de nouvelles contraintes sur le mélange vertical représenté par le modèle.

1.7. Plan de l'étude

Dans le chapitre 2, je présenterai le projet YAK-AEROSIB qui a permis d'obtenir ce jeu de données. Les cinq campagnes, les instruments et l'avion seront présentés, ainsi que le traitement des données de CO_2.

Dans le chapitre 3, la caractérisation de la variabilité des concentrations en CO_2, CO et O_3 sera présentée pour les campagnes d'avril et septembre 2006, ainsi qu'une étude de cas sur des concentrations élevées de CO rencontrées en altitude et attribuées à du transport depuis la couche limite chinoise.

Dans le chapitre 4 je décrirai l'application d'une technique statistique de *clustering* pour l'interprétation globale des campagnes basée sur la modélisation lagrangienne de rétrotransport. La base de cette étude inclut également la troisième campagne d'aout 2007 non traitée dans le chapitre 3. Ceci permet de caractériser le transport à grande échelle pour chaque campagne et de décrire des différences saisonnières.

Le chapitre 5 décrira les mesures d'aérosol ultra fins effectuées durant les campagnes d'avril et septembre 2006, ainsi que celles effectuées sous forme de profils verticaux réguliers au dessus de Novossibirsk. Ces données sont utilisées pour tenter d'informer sur la formation de nouvelles particules dans la troposphère libre.

Le chapitre 6 rassemble ces résultats dans une synthèse et compare les mesures de CO_2 avec un modèle eulérien, afin de proposer une nouvelle contrainte sur le mélange vertical dans les modèles utilisés pour les inversions de CO_2.

Enfin nous conclurons sur les perspectives de telles mesures en Sibérie et les applications possibles du jeu de données existant.

Les annexes en fin de volume concernent les moyens expérimentaux (Annexe 1), les mesures complètes obtenues durant les trois premières campagnes (Annexe 2) et enfin un article dédié à l'étude des inventaires d'émission pour l'Europe (Annexe 3).

Chapitre 2.
Le projet YAK-AEROSIB : objectifs et réalisation

Cinq campagnes aéroportées de mesure du CO_2, CO, O_3 et particules ultrafines ont été menées dans le cadre du projet YAK-AEROSIB. Les campagnes sont présentées dans ce chapitre, et notamment les conditions ayant prévalu durant les trois premières campagnes, sur lesquelles se focalisera l'analyse dans les chapitres suivants.

2.1. Implémentation du projet YAK-AEROSIB

2.1.1. Etudier la troposphère sibérienne in-situ

Le projet YAK-AEROSIB (Airborne Extensive Regional Observations in Siberia) a démarré en 2004 sous la forme d'une collaboration franco-russe avec l'objectif d'« établir des observations systématiques des composés atmosphériques CO, O_3 et CO_2 en moyenne et basse troposphère en Eurasie. Ces mesures ont pour objectif de décrire la variabilité saisonnière et interannuelle des sources et du transport de CO_2, ainsi que les processus de chimie-transport qui conduisent à la production d'ozone en Sibérie. » Le projet s'est structuré sous la forme d'un groupement de recherches européen (GDRE+) avec la contribution de la direction des relations internationales du CNRS. Les partenaires principaux du projet sont le Laboratoire des Sciences du Climat et de l'Environnement (LSCE) de Saclay, le Laboratoire d'Aérologie de Toulouse, l'Institut d'Optique Atmosphérique de Tomsk, l'Institut de Physique Atmosphérique de Moscou. D'autres partenaires du projet sont le Laboratoire de Physique Moléculaire pour l'Aéronomie et l'Astronomie (LPMAA)

de Paris, en charge du développement d'un instrument de mesures isotopiques in situ et l'Institut Max Planck pour la Biogéochimie (MPI-BGC) en charge du prélèvement de flacons. Ces deux instruments n'ont pas été embarqués dans l'avion. La durée du projet a été étendue jusqu'en 2011. Le projet est financé, côté français, par le Ministère de la recherche via l'Agence Nationale de la Recherche (ancien financement FNS-ACI), par la direction des relations internationales du Centre National de la Recherche Scientifique, et par le Ministère des Affaires étrangères, avec un support indirect du Commissariat à l'Energie Atomique. Le projet est également financé par la Fondation Russe pour la Recherche Fondamentale et par l'Académie des Sciences de Russie. Le projet s'est ainsi vu doté d'un budget d'environ un million d'euros pour un objectif ambitieux.

Le cahier des charge originel comprends la mesure de nombreuses espèces in situ et par prélèvements. Les mesures in situ à effectuer et exigeant un développement instrumental spécifique sont : CO_2, CO, O_3, CH4, δ13C-CO_2. L'instrument CO_2 a été développé au LSCE (voir annexes). Les instruments CO et O_3 ont été développés par le Laboratoire d'Aérologie de Toulouse. L'instrument de mesure isotopique in-situ a été développé au Laboratoire de physique moléculaire pour l'atmosphère et l'astrophysique de Paris ; l'instrument dédié au méthane a été développé au Laboratoire de spectrométrie physique de Grenoble. Les prélèvements d'air en flacons permettent de mesurer en laboratoire les concentrations d'espèces suffisamment peu réactives et utilisent un automate mis au point au Max-Planck-Institut für Biogeochemie de Iéna, en Allemagne. Durant les campagnes effectuées, il a été possible d'exploiter les instruments in situ de CO_2, CO et O_3. Les autorisations requises n'ont pas été obtenues pour les autres instruments, et en particulier le prélèvement flacon qui s'est heurté à des restrictions administratives relevant de la sécurité intérieure.

Ce projet a permis la tenue d'ateliers scientifiques internationaux, à Paris en 2006 et à Irkoutsk (Russie) en 2007.

2.2. Organisation des campagnes

2.2.1. Région survolée par les campagnes

Les campagnes YAK-AEROSIB suivent un transect qui va de Novossibirsk (55°00'N 82°54'E) à Iakoutsk (62°10'N 129°50'E), sur un domaine approximativement compris entre les parallèles 55°N et 63 °N et entre les méridiens 80°E et 130°E (Fig. 2.1).

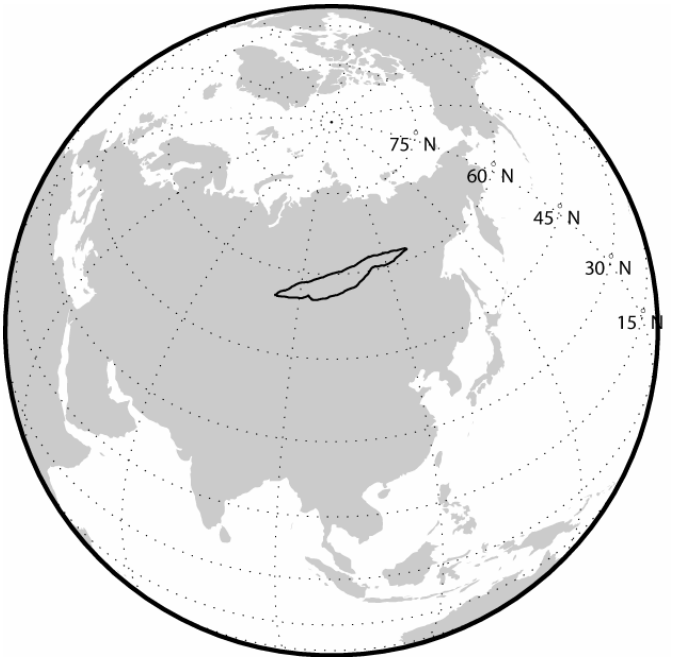

Figure 2.1. Vue générale de l'itinéraire des campagnes YAK-AEROSIB

Le domaine survolé est représentatif des forêts boréales sibériennes (Fig. 2.2), et des écosystèmes arctiques dans le cas de la campagne YAK-4 de juillet 2008. Le type dominant de végétation correspond aux espèces de taïga : principalement des mélèzes (conifère à feuilles caduques) particulièrement adaptés aux conditions sibériennes, mais aussi d'autres feuillus (bouleaux) et résineux (pins sylvestre) avec des taillis et des marais saisonniers (pergélisol) dans la région de Iakoutsk. On rencontre des terres agricoles ainsi que des steppes au sud et au sud ouest du domaine (notamment autour de Krasnoyarsk et Novosibirsk). La région a un réseau important de rivières et de petits lacs dont les fleuves Yenissei et Lena ainsi que leurs affluents. Quelques villes et centres industriels ou miniers relativement importants se trouvent sur le trajet : Novossibirsk, Tomsk, Myrni, Ieniseisk, Irkutsk, Bratsk, Krasnoyarsk et Kemerovo.

2.2.2. Plan de vol

Des profils verticaux entre 0 et 7 km sont effectuées tous les 200 km environ (Fig. 2.3). Les campagnes 1, 2 et 3 sont composées chacune de 4 vols (une couleur par vol dans la Figure 2.3), avec durant chaque vols de 4 à 10 profils verticaux, pour un total d'environ 26 profils par campagne. Chaque profil prend environ 30 minutes, avec des plateaux de vol horizontal au plus bas niveau du profil, puis à 5 km (2 km durant la campagne 2) durant la descente, puis au plus haut niveau (environ 7 km). Les informations concernant chaque vol des campagnes 1 à 3 (dates, destination, heures de vol, nombre de profils collectés) sont données dans la Table 2.1 ci-dessous.

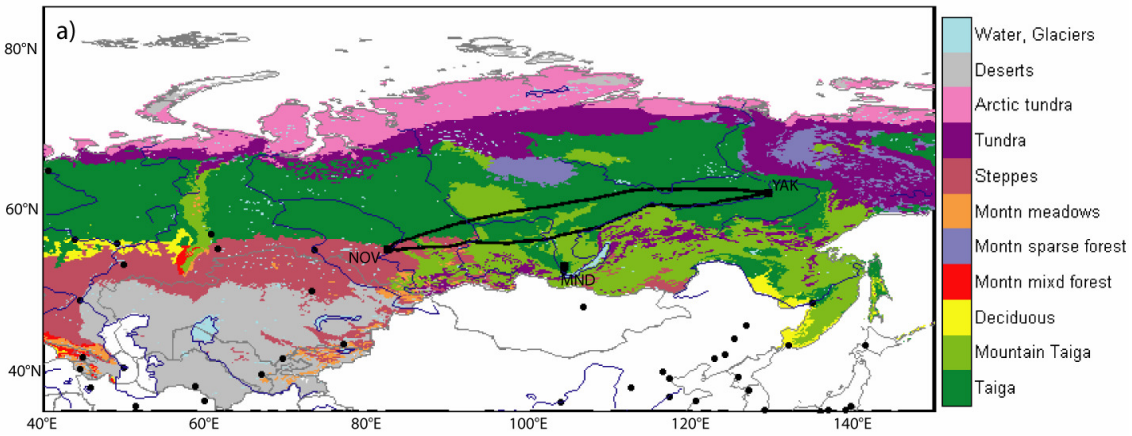

Figure 2.2. Types de végétations en Sibérie autour de l'itinéraire des campagnes YAK-AEROSIB. Les villes de Novosibirsk et Iakoutsk sont indiquées (NOV et YAK), ainsi que la station de Mondy (MND) utilisée par Pochanart et al. (2003 ; voir chapitre précédent)

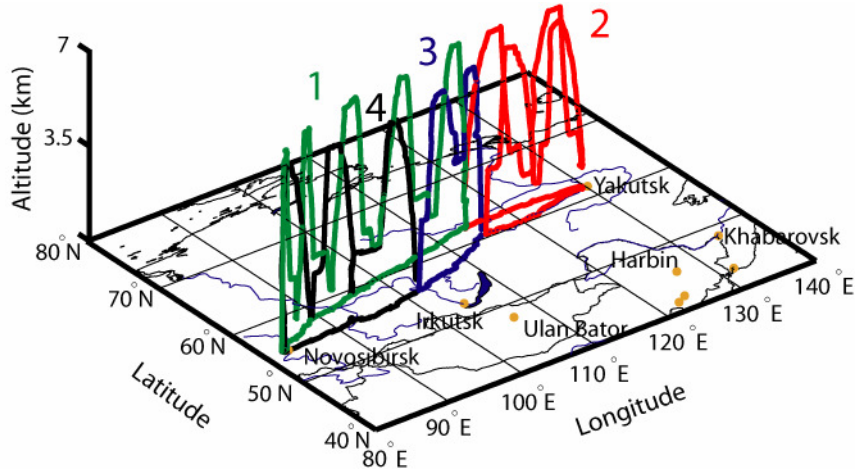

Figure 2.3. Itinéraire de la campagne YAK-1. Le plan de vol comprend de nombreuses ascension et descentes. Vol 1 (vert), 2 (rouge), 3 (bleu) et 4 (noir). Les vols 5 à 8 (YAK-2) et 9 à 12 (YAK-3) ont suivi le même itinéraire avec des plateaux à 5 km au lieu de 2 km d'altitude.

Les trois campagnes de 2006 et 2007 ont eu un plan de vol très similaire. Par contre les campagnes de 2008 ont eu un itinéraire modifié. En collaboration avec le programme POLARCAT, les deux campagnes de Juillet 2008 ont été réalisées en coordination avec d'autres campagnes aéroportées dédiées à l'étude de la chimie et du transport atmosphérique dans les régions Arctiques. Le rôle supplémentaire dévolu aux campagnes en Sibérie, dans ce cadre particulier, était d'échantillonner des panaches de feux de forêt. L'itinéraire de la campagne de début juillet (vols 13-19) était largement axé sur les régions arctiques.

Table 2.1. Informations de chaque vol sur les cinq campagnes.

Vol n°	date	heures LT	heures UTC	Nb profils	Itinéraire
1	11 Avr 06	1200-2100	0600-1200	8	Novossibirsk - Myrni
2	12 Avr 06	1100-1530	0200-0630	8	Myrni-Iakutsk-Lensk
3	12 Avr 06	1730-1900	0830-1100	4	Lensk-Bratsk
4	14 Avr 06	0830-1030	0030-0430	6	Bratsk-Novossibirsk
5	07 Sept 06	0900-1900	0300-1000	10	Novossibirsk-Myrni
6	08 Sept 06	0945-1430	0045-0530	8	Myrni-Iakutsk-Lensk
7	08 Sept 06	1600-1730	0700-0930	2	Lensk-Bratsk
8	10 Sept 06	0900-1115	0100-0515	6	Bratsk-Novossibirsk
9	17 Aou 07	0930-1815	0330-0915	10	Novossibirsk-Myrni
10[a]	18 Aou 07	0725-1200	2225-0300	8	Myrni-Iakutsk-Lensk
11	18 Aou 07	1315-1445	0415-0645	4	Lensk-Bratsk
12	20 Aou 07	0830-1000	0030-0400	6	Bratsk-Novossibirsk
13	07 Jui 08	0640-1515	0400-0915	8	Novossibirsk-Salekh.
14	07 Jui 08	1810-0115	1210-1615	4	Salekhard-Khatanga
15	08 Jui 08	1045-1515	0145-0615	6	Khatang.-Chokurdakh
16[b]	09 Jui 08	0630-1150	2130-0250	8	Chok.-Pewek- Chok.
17	11 Jui 08	0920-1240	0020-0340	6	Chokurdakh-Iakutsk
18	11 Jui 08	1455-1535	0555-0835	4	Iakutsk-Myrni
19	12 Jui 08	0850-1240	0150-0740	8	Myrni-Novossibirsk
20	21 Jui 08	1125-2050	0525-1150	8	Novossibirsk-Myrni
21	23 Jui 08	1030-1530	0130-0630	8	Myrni-Iakutsk-Lensk
22	23 Jui 08	1720-1915	0820-1115	4	Lensk-Bratsk
23	25 Jui 08	0910-1410	0110-0610	-	Lac Baïkal
24[c]	28 Jui 08	0745-1325	2345-0525	-	Lac Baïkal
25	29 Jui 08	0855-1345	0055-0745	6	Bratsk-Novossibirsk

[a] décollage le 17 aout 07 à 2225 UTC, l'essentiel du vol le 18 aout en heures UTC dates.

[b] décollage le 09 juillet en heure UTC et atterrissage le 10 juillet.

[c] décollage le 27 juillet en heures UTC.

2.3. Campagne d'avril 2006

Cette section et les suivantes donnent certaines informations nécessaires à une interprétation des résultats obtenus durant les campagnes et présentés dans les chapitres suivants.

La campagne d'Avril 2006 est marquée par une circulation zonale sur l'ouest de la Sibérie, et un blocage transitoire dans la moyenne troposphère. La circulation de surface est marquée par des

hautes pressions dans l'arctique et le nord-ouest sibérien, et un anticyclone sibérien relativement faible (Fig. 2.4).

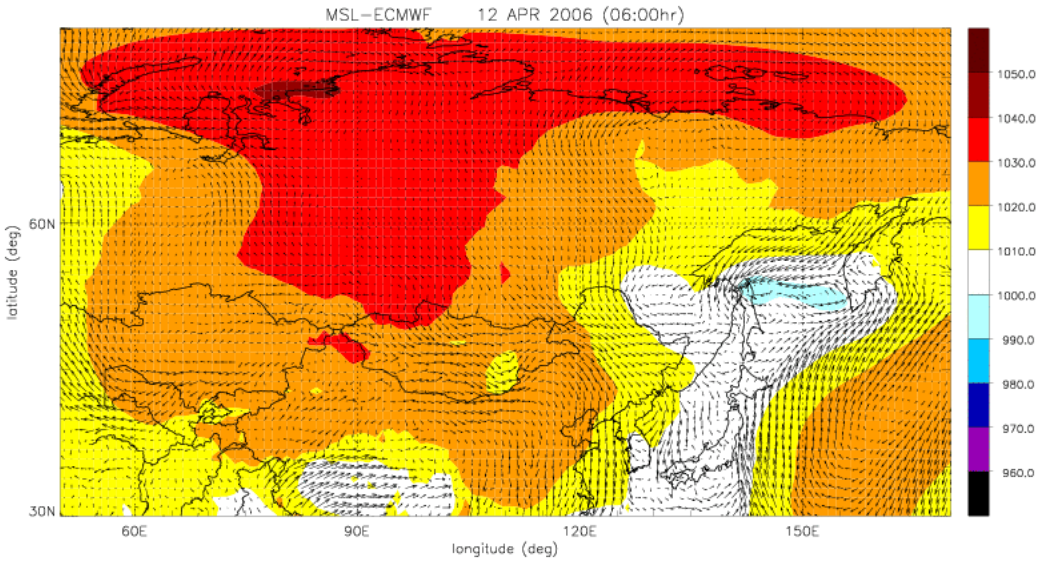

Figure 2.4. Vent et pression réduite au niveau de la mer pour le 12 avril 2006 à 0600 TU

Durant la période de cette campagne les émissions liées aux feux sont nulles en Sibérie étant donné la couverture neigeuse encore largement présente à cette période. De faibles émissions sont indiquées par l'inventaire GFED (van der Werf et al., 2006) dans les régions périphériques comme la Chine du Nord Est ou l'Ukraine (Fig. 2.5)

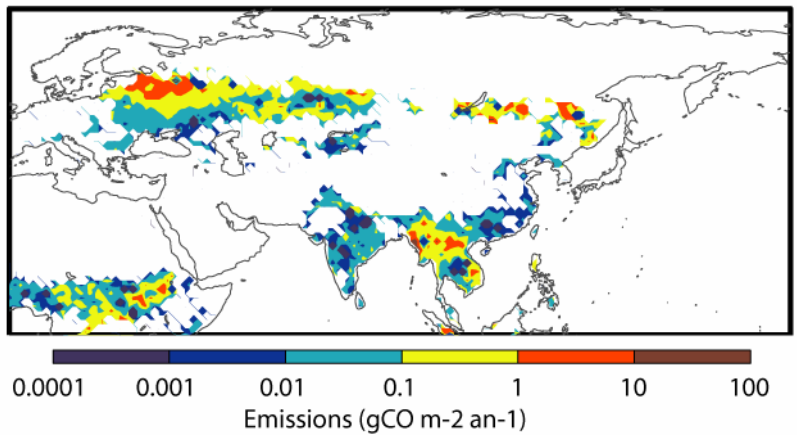

Figure 2.5. Emissions de feux de biomasse pour avril 2006

Le mois d'avril est en général le mois durant lequel les tempêtes sont les plus actives sur la façade Pacifique de l'Asie. Ceci amène d'importants épisodes de pollution qui peut être transportée à distance (Yienger et al., 2000). Immédiatement avant la campagne (7-11 avril), une série de cyclones extratropicaux a balayé la côte de Chine du nord-est (Fig. 2.6). Ce type d'événement

implique la présence de mécanismes de transport de type WCB à l'œuvre, ce qui provoque un soulèvement de la masse d'air de la couche limite vers la troposphère libre. Cette masse d'air semble avoir ensuite été partiellement advectée vers la Sibérie. La Figure 2.7 montre une image de l'indice aérosols de l'instrument OMI durant cette période (8 avril). Cet instrument est essentiellement sensible aux particules micrométriques. La figure montre très nettement une langue d'air chargée en aérosols transportée vers le nord depuis la Chine du nord est et la Corée. L'observation in situ de ce type de transport vers la Sibérie n'a jamais été rapportée dans la littérature. Ceci est pourtant très probablement connecté au phénomène de neige jaune parfois observé en cette saison en Sibérie du nord est (S. A. Zimov, communication personnelle). La Figure 2.8 montre une série d'images infrarouge de l'Asie du nord-est prises le 10 avril entre 19h00 UTC et 23h30 UTC montrant l'amas en virgule typiquement associé aux WCB, confirmant la nature de cet épisode de transport. Le chapitre 3 détaillera l'implication de ce phénomène pour les concentrations de polluants observées au dessus de Sibérie ainsi que l'altitude du panache.

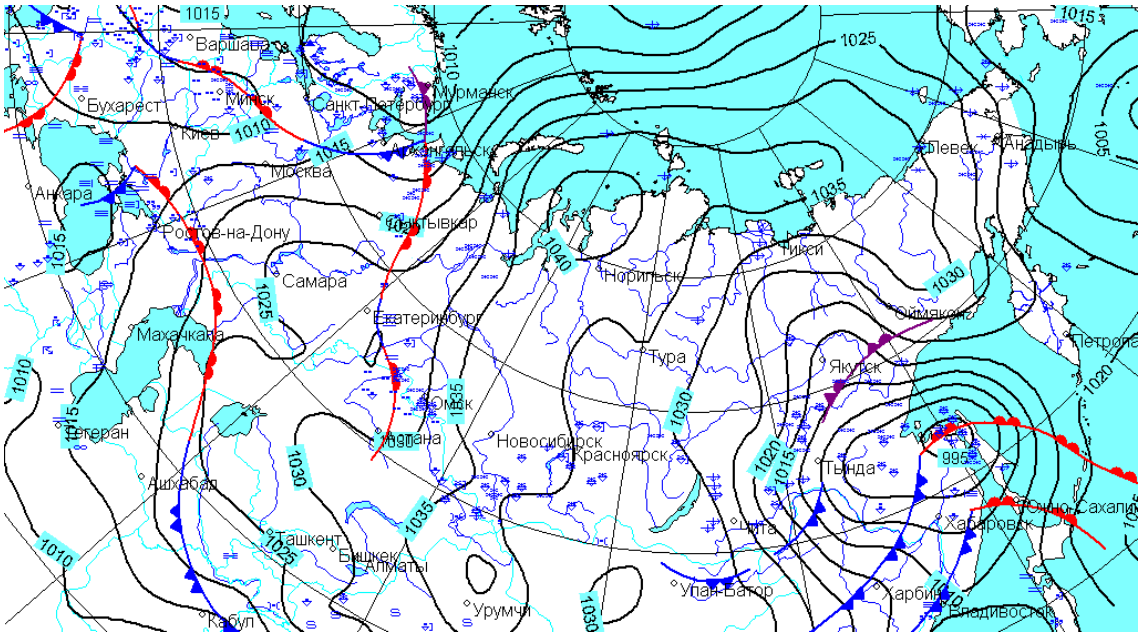

Figure 2.6. Fronts le 11 septembre 2006 à 12h UTC durant la campagne YAK-1

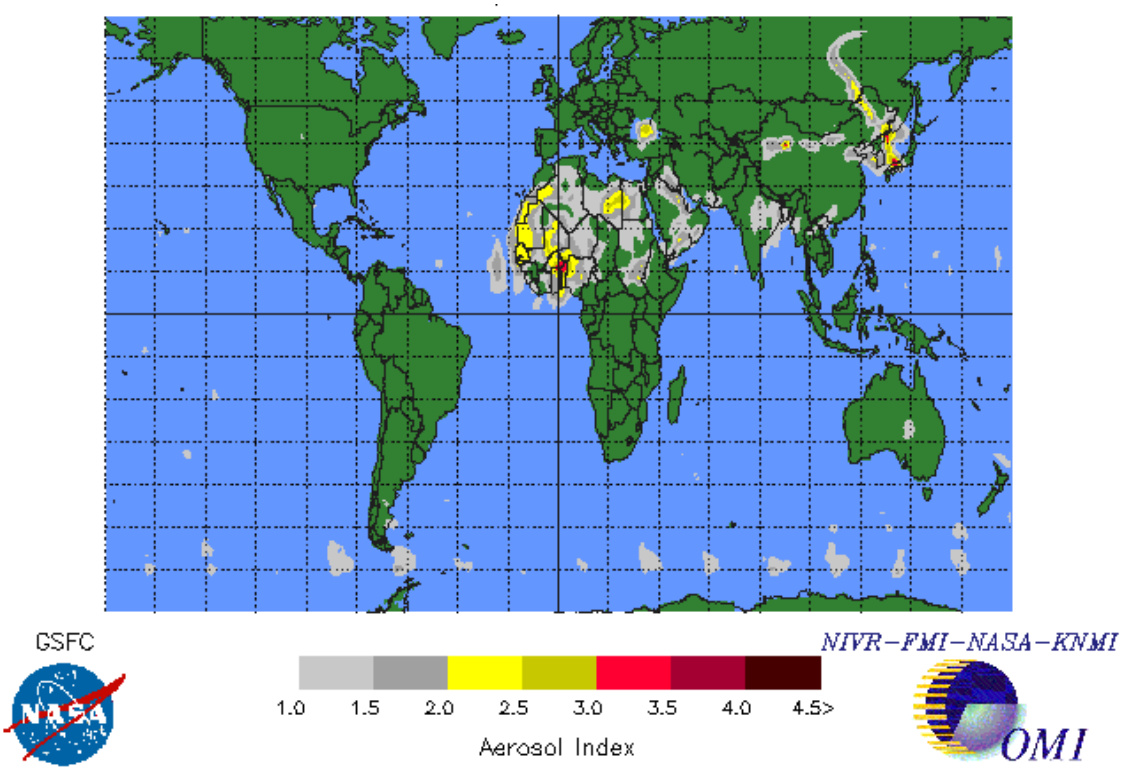

Figure 2.7. Image OMI de l'index d'aérosol le 8 Avril 2006

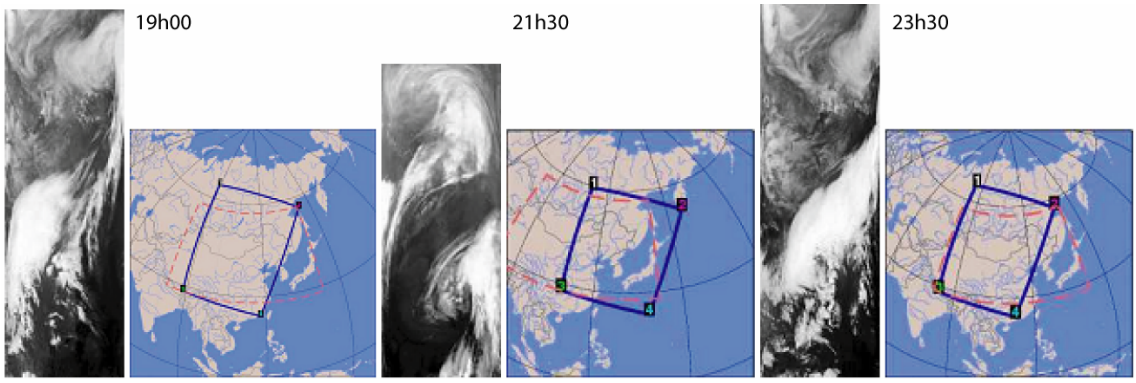

Figure 2.8. Imagerie infrarouge d'Asie du nord est le 10 avril 2006 (G. Cayez).

La végétation est peu active en Sibérie en cette saison, sauf dans la région de Krasnoïarsk sur les rives du fleuve Ienisseï, tel qu'indiqué par l'indice NDVI (*normalized difference vegetation index*) (Fig. 2.9). L'indice NDVI est calculé à partir d'imagerie spectrale, ici par l'instrument Végétation sur le satellite *Spot*. Il capture le contraste entre les canaux rouges et infrarouge proche de la réflexion de la radiation solaire par la végétation (Myneni et al., 1995). Cet indice lié à l'aire totale de feuilles vertes permet donc d'estimer la fraction de rayonnement solaire absorbée par les plantes dans le domaine spectral permettant la photosynthèse.

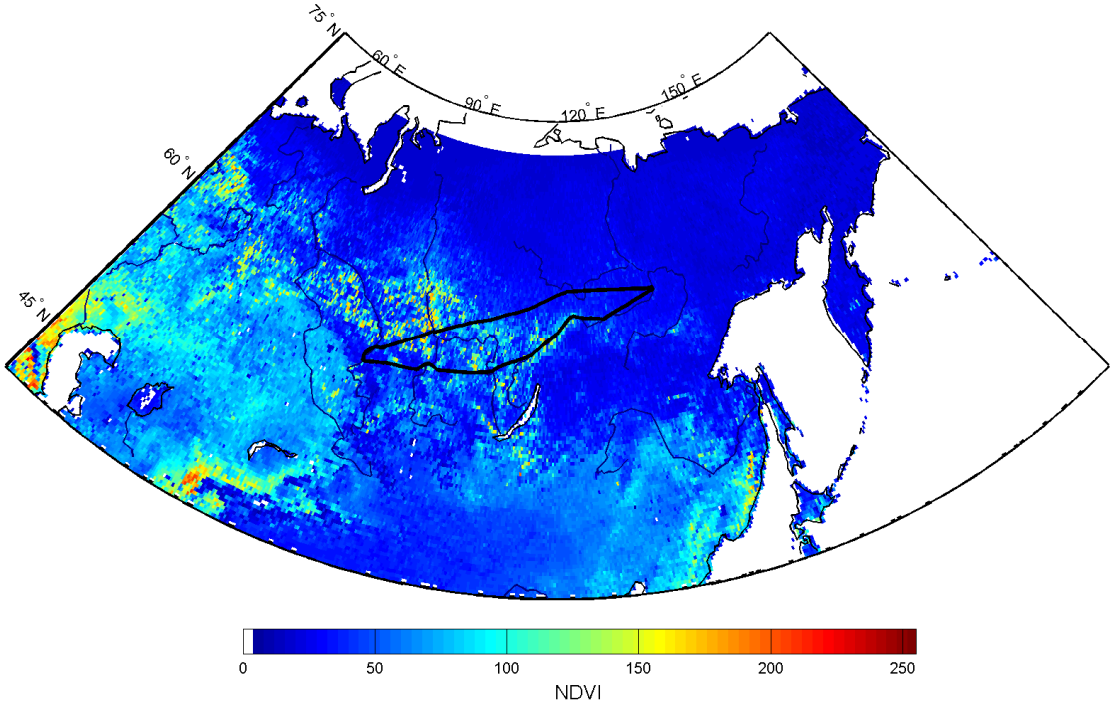

Figure 2.9. Indice NDVI moyen du 11 au 20 avril 2006 en Asie du Nord. La plage de valeur (sans unité) est transposée entre 0 et 255. L'itinéraire de la campagne est marqué par la courbe noire.

2.4. Campagne de Septembre 2006

La campagne de septembre 2006 est marquée par une circulation zonale importante dans la troposphère libre, avec une circulation en oméga. La pression au niveau de la mer et le vent de surface durant septembre 2006 sont données par la Figure 2.10. Un certain nombre de fronts a été croisé durant cette campagne, et notamment un front chaud durant le trajet Novossibirsk-Myrni du 7 septembre (Fig. 2.11). L'analyse de la distribution des masses d'air montre qu'une descente d'air arctique était présente sur l'est de la Sibérie durant la campagne, ce qui a fortement diminué les températures.

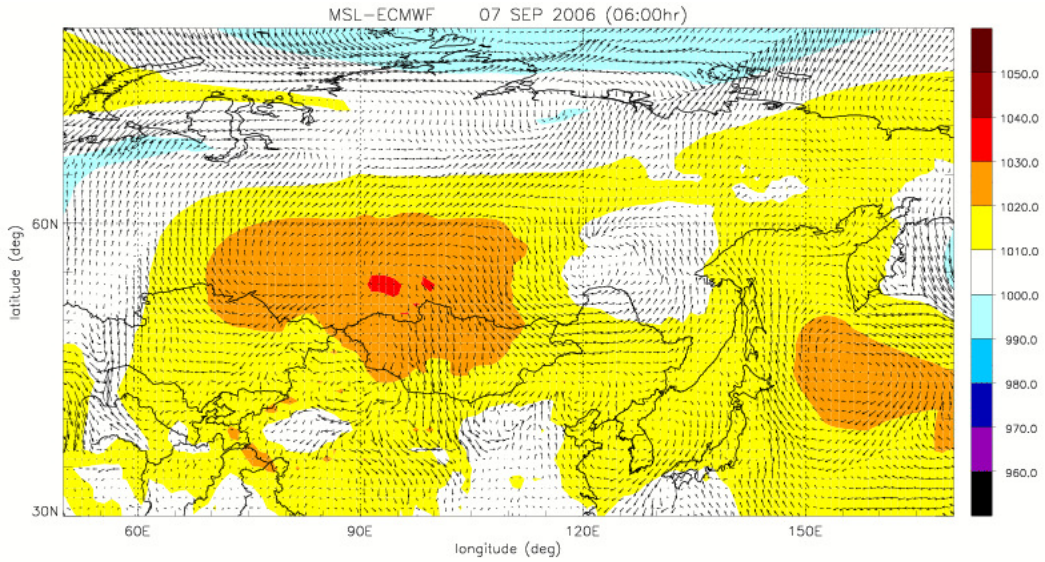

Figure 2.10. Pression réduite au niveau de la mer pour Septembre 2006

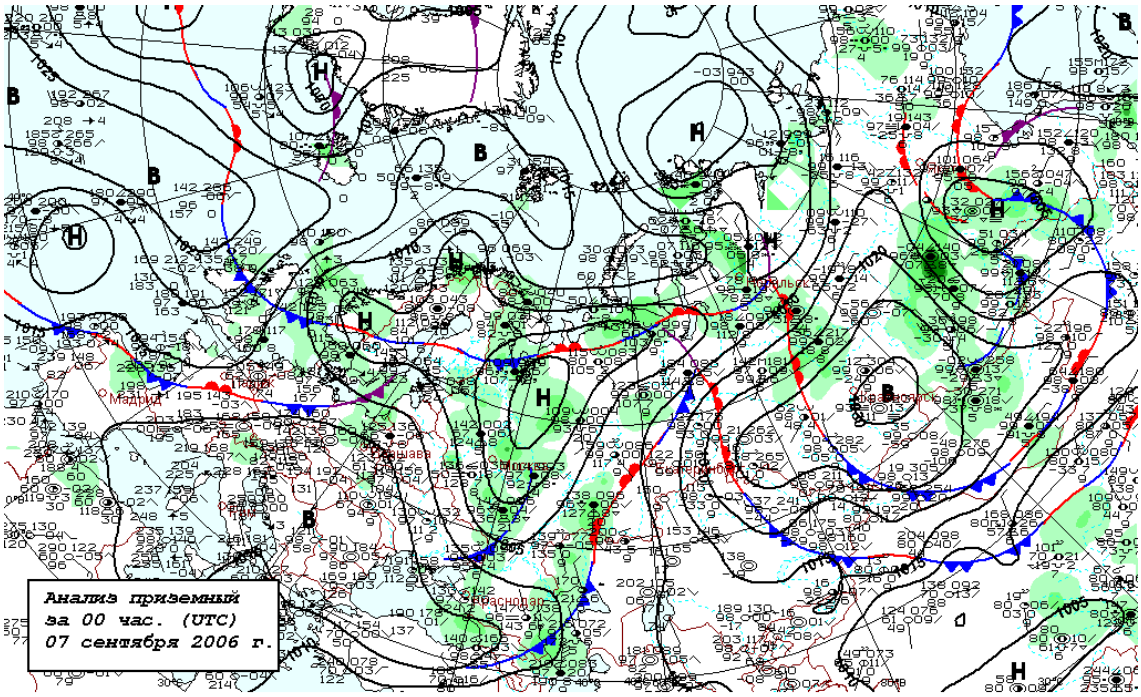

Figure 2.11. Fronts le 7 septembre 2006 à 00h UTC durant la campagne YAK-2

Pour cette campagne les émissions liées aux feux de biomasse sont essentiellement localisées dans une bande située au nord de la mer Caspienne, surtout au Kazakhstan (Fig. 2.12). Les feux en Sibérie sont très limités, au sud-est du lac Baïkal.

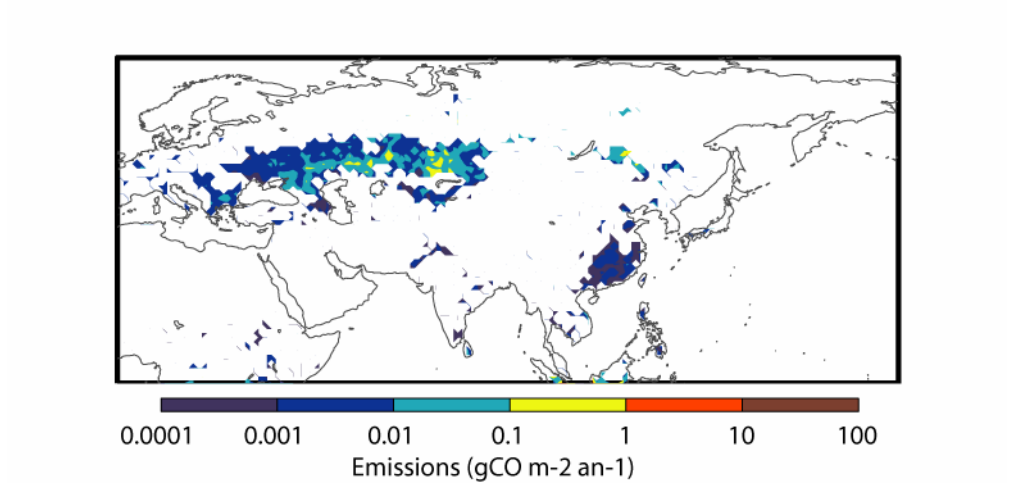

Figure 2.12. Emissions de feux de biomasse pour septembre 2006

L'examen de la carte de l'indice NDVI en septembre 2006 (Fig. 2.13) montre une activité photosynthétique forte sur la moitié ouest du trajet. La fin de la saison de croissance est marquée pour les région subarctiques. Les hautes terres de Sibérie centrale (environ 110°E, 55°N) connaissent un faible NDVI, ce qui correspond bien à la situation observée durant la campagne, à savoir un temps froid et des précipitations importantes.

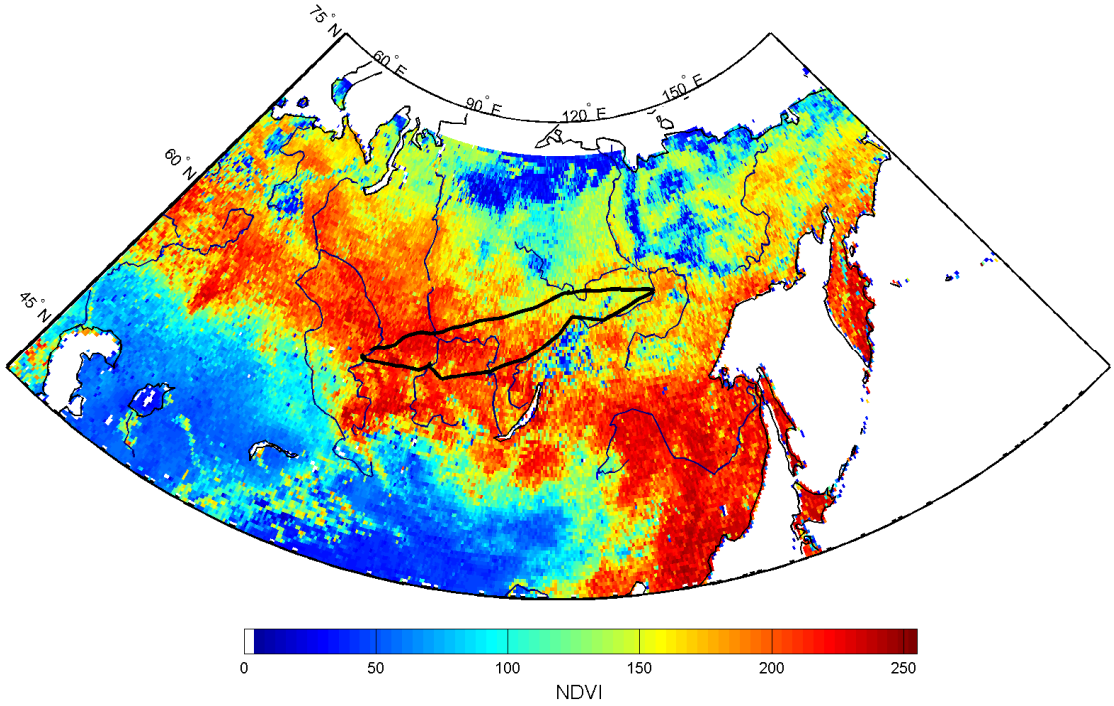

Figure 2.13. Indice NDVI moyen du 1 au 10 septembre 2006.

2.5. Campagne d'Aout 2007

La campagne d'aout 2007 était marquée par une activité frontale réduite, de faibles précipitations et des hautes pressions sur la Sibérie (Fig. 2.14). La circulation zonale était plus lente que lors des autres campagnes. Les émissions de feux de forêt étaient faibles en Sibérie (Fig. 2.15) et une grande partie des feux de forêt a eu lieu trop longtemps avant la campagne pour être échantillonnée. Les régions concernées sont centrées autour du Lac Baïkal. L'activité photosynthétique indiquée par l'indice NDVI (Fig. 2.16) est particulièrement forte en août, notamment sur l'est du trajet (Iakoutie) ce qui n'était pas le cas lors de la campagne précédente. Cette campagne constitue donc la première véritable opportunité d'échantillonner la variabilité du CO_2 durant la saison de croissance de la végétation en Sibérie.

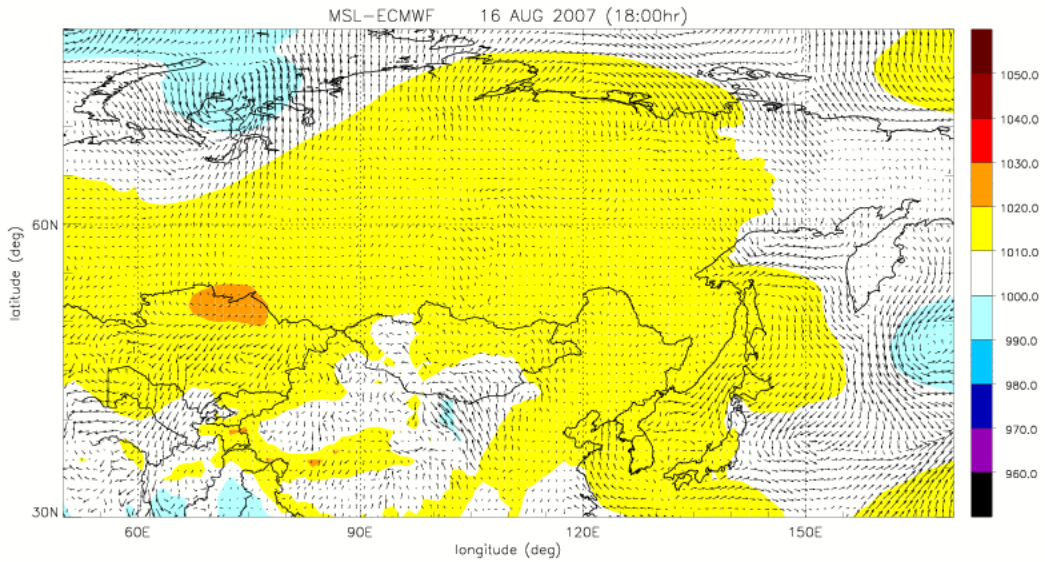

Figure 2.14. Pression réduite au niveau de la mer pour Aout 2007

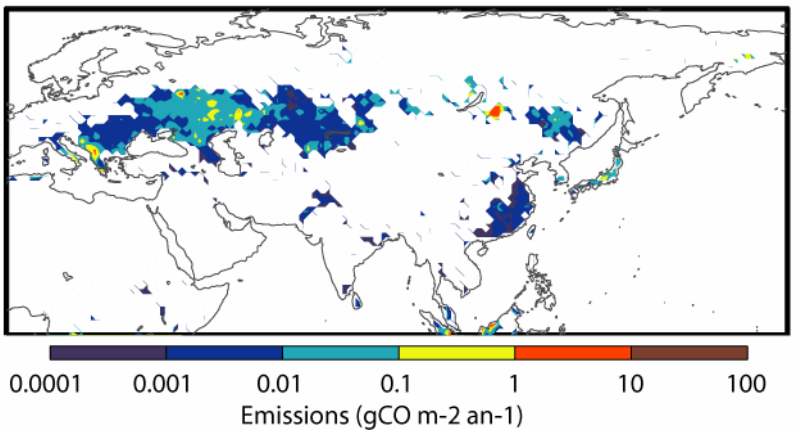

Figure 2.15. Emissions de feux de biomasse pour Aout 2007

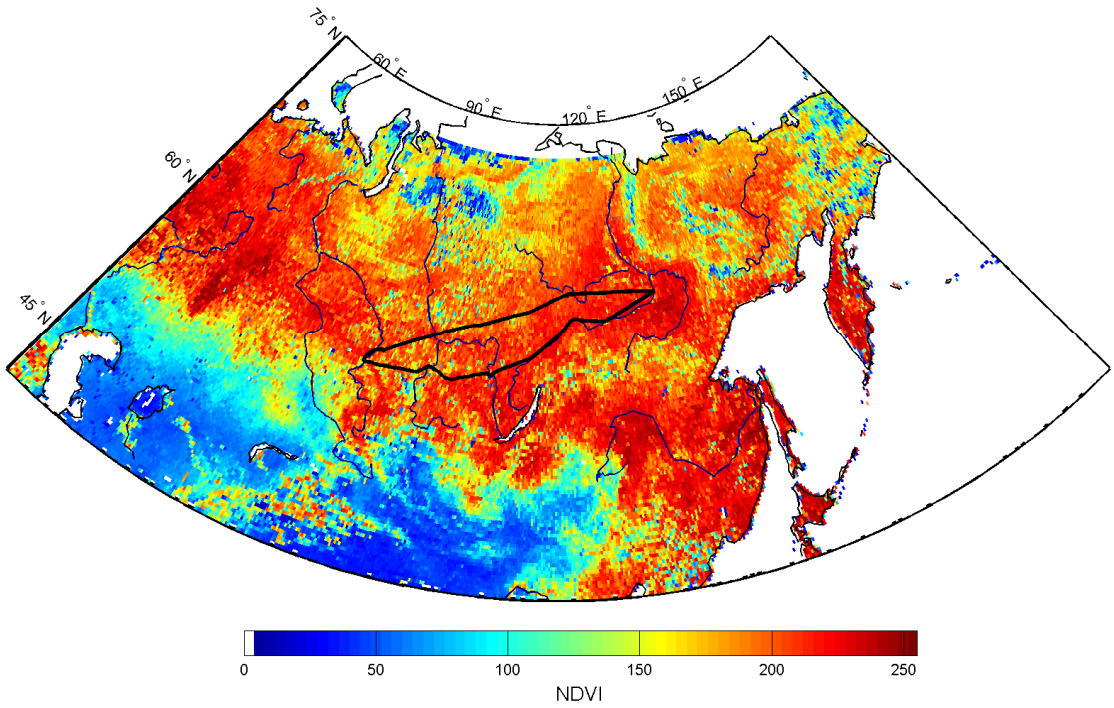

Figure 2.16. Indice NDVI moyen du 11 au 20 août 2007 en Asie du Nord.

2.6. Campagnes YAK/POLARCAT en Juillet 08

Deux campagnes se sont déroulées en Juillet 2008, en collaboration avec le projet international POLARCAT. Une de ces campagnes a suivi un itinéraire différent (Fig. 2.17) et beaucoup plus long, afin de mieux documenter la partie Arctique de la Sibérie.

Les panaches associés aux émissions des feux de forêt étaient clairement visibles en couches fines dans l'atmosphère durant ces campagnes (Fig. 2.18), et ont été échantillonnés avec des valeurs de CO et O_3 très élevées. Le panache riche en CO et pauvre en O_3 est probablement émis par un feu de forêt récemment (Fig. 2.19), avec des valeurs de CO atteignant 700 ppb à 3000 m du sol.

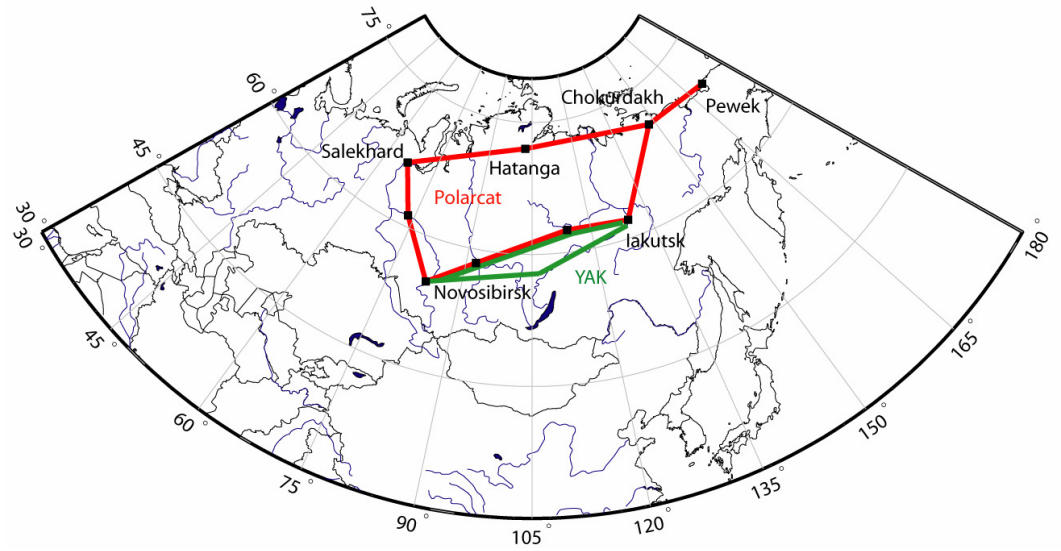

Figure 2.17. Itinéraire suivi par la grande campagne de Juillet 2008 (en rouge) et les campagnes YAK-AEROSIB « classiques » (en vert).

Figure 2.18. Atmosphère au dessus d'Iakutsk le 23 juillet 2007. La flèche indique une double couche sombre en dessous d'un léger couvert nuageux qui correspond à un panache d'émissions de feu de forêt. Des concentrations de l'ordre de 500 ppb ont été observées dans ces panaches.

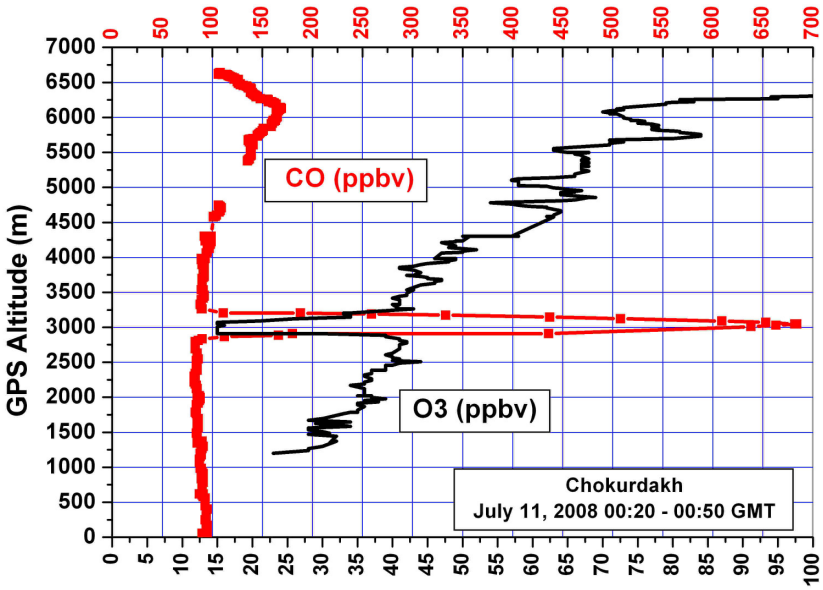

Figure 2.19. Concentration de CO et O_3 observées au dessus de Chokurdakh le 11 juillet 2008

Chapitre 3.
Campagnes transcontinentales et transport du CO_2, CO et O_3 en Sibérie

Le chapitre précédent a présenté, à partir de données extérieures aux campagnes elles-mêmes, les conditions durant les vols. Ce cadre permet de mieux comprendre les données qui vont être présentées et autorise les comparaisons entre les résultats issus des différentes campagnes dans une perspective de variabilité saisonnière. Dans ce chapitre j'aborde les mesures réalisées durant les deux premières campagnes. La variabilité des espèces (CO_2, CO, O_3) est présentée. Un cas de transport de pollution à longue distance, issu de la campagne d'avril, est analysé plus en détail et sert de base à une discussion sur l'analyse des rapports d'émissions entre CO et CO_2.

3.1. Problématique de la variabilité des composés atmosphériques

3.1.1. Variabilité troposphérique des polluants en Sibérie

Connaître la variabilité des polluants en Sibérie est important à plusieurs titres. D'une part, les nombreuses études de transport de la pollution est-asiatique à travers le Pacifique font généralement l'hypothèse d'une région amont « propre ». Ces études étudient l'apport des émissions est-asiatiques à un air supposé non préalablement enrichi en polluants. Hors ces masses d'air ont généralement résidé un temps significatif au dessus de la Sibérie. Peu d'études ont permis de confirmer ou d'infirmer l'hypothèse d'une faible variabilité des compositions atmosphérique en Sibérie. Ainsi la séparation d'une contribution « asiatique » dans les mesures effectuées dans le

bassin Pacifique n'est pas appuyée par une connaissance précise des conditions « amont ». D'autre part, la Sibérie est aussi une des régions réceptacle majeure des émissions européennes et asiatiques de polluants. Là aussi, peu de mesures ont permis de confirmer cette hypothèse.

3.1.2. Variabilité du CO_2 dans la troposphère continentale

Connaître la variabilité du CO_2 est important à plusieurs titres. L'anomalie de CO_2 intégrant les flux de surface est diluée par le mélange atmosphérique lorsqu'elle atteint les observatoires éloignés (Gloor et al., 2000). Les mesures aéroportées régionales du CO_2 peuvent aider à pallier à la difficulté d'intégrer ces mesures dans les modèles. Par ailleurs la variabilité horizontale du CO_2 renseigne l'erreur commise en comparant une mesure de surface spatialement ponctuelle à une grille de modèle (Gerbig et al., 2003 ; Lin et al., 2004).

3.1.3. Transport dans la première campagne YAK

Dans ce chapitre, j'analyse la distribution de la concentration des gaz traces obtenus durant les deux premières campagnes et utilise un modèles de dispersion lagrangien afin d'expliquer leur variabilité.

La campagne d'avril en particulier a montré une atmosphère stable et stratifiée. Plusieurs couches d'épaisseur d'environ 500 à 1000 m ont été échantillonnées lors de plusieurs profils consécutifs, ce qui correspond à environ 500 km en étendue horizontale.

Deux régimes de concentrations de CO différents ont été observés à l'ouest et à l'est de l'itinéraire en avril 2006. Dans la moyenne troposphère, l'est était marqué par de plus fortes concentrations de CO, en moyenne 200 ppb, contre 160 ppb à l'ouest. Ce gradient est interprété à l'aide de deux outils différents : la modélisation du transport atmosphérique, et l'analyse des corrélations entre CO et CO_2 comme signature des régions sources.

Le modèle lagrangien de dispersion de particules (FLEXPART) indique que les hautes concentrations observées à l'est sont essentiellement liées aux fortes émissions anthropiques et de combustion de biomasse dans le nord-est de la Chine. En particulier, le passage d'une série de fronts froids sur cette région chinoise a provoqué le soulèvement de l'air pollué de la couche limite vers la moyenne troposphère, avec une advection vers le nord, correspondant ainsi au transport associé aux *warm conveyor belts* (WCB). Le modèle indique une contribution européenne dominante pour le CO à l'ouest de l'itinéraire.

L'étude des corrélations entre CO et CO_2 indique que la pente de régression entre ces deux traceurs est significativement plus élevée à l'est qu'à l'ouest de l'itinéraire. Le rapport entre émissions de CO et CO_2 dans l'inventaire EDGAR est également plus fort en Chine du nord est qu'en Europe (incluant la Russie occidentale), ce qui permet de confirmer d'une part l'attribution du gradient de CO aux émissions chinoises et d'autre part de vérifier que les pentes de régressions peuvent être des informations conservatives après plusieurs jours de transport. Toutefois ceci n'est vrai que dans certaines conditions observées durant la campagne d'avril : l'assimilation du CO_2 par

la végétation et l'oxydation du CO sont des éléments de décorrélation. Il convient également de noter la barre d'erreur importante associée au rapport CO/CO_2 des émissions chinoises.

3.2. Résumé

Les deux campagnes d'avril et septembre 2006 ont mesuré les concentrations troposphériques et la variabilité du CO_2, du CO et de l'O_3 au dessus de la Sibérie. Afin de quantifier l'influence des sources régionales et distantes, naturelles ou anthropiques, 52 profils verticaux de ces composés ont été collectés tout les 200 km environ et jusqu'à 7 km d'altitude. Les concentrations de CO_2 et de CO étaient hautes en avril 2006 (respectivement 385-390 ppm CO_2 et 160-200 ppb CO) comparées aux valeurs de fond (telles que mesurées en moyenne mensuelle dans la station d'altitude de Sary Taukum au Kazakhstan et par rapport aux valeurs de couche limite marine de la base de données GLOBALVIEW). Des concentrations de CO jusqu'à 220 ppb ont été enregistrées au dessus de 3.5 km d'altitude en Sibérie orientale, avec des excès concentration présents sur des couches de 500 à 1000 m d'épaisseur. La présence de cet air enrichi en CO est attribuée au soulèvement frontal rapide d'une masse d'air exposée aux émissions anthropiques de Chine du Nord et à des émissions de feux en Mongolie du nord. Une origine asiatique dominante pour le CO au dessus de 4 km (71.0%) contrastant avec une origine européenne dominante (70.9%) en dessous de cette altitude est déduite à la fois de l'analyse d'un modèle de transport, et des rapports $\Delta CO/\Delta CO_2$ ayant une distribution contrastée sur la verticale. En septembre 2006, une forte anomalie négative d'O_3 (~-30ppb) est observe dans la couche limite comparé à la troposphère libre au dessus, suggérant une forte déposition d'O_3 sur les forêts Sibériennes. La hauteur de couche limite est diagnostiquée à partir des gradients de température virtuelle potentielle et de CO_2,

3.3. Article

The YAK-AEROSIB transcontinental aircraft campaigns: new insights on the transport of CO_2, CO and O_3 across Siberia and in the Northern Hemisphere. Tellus, 60B(4), 2008, p. 551-568, par J.-D. Paris, P. Ciais, P. Nédélec, M. Ramonet, B. D. Belan, M. Yu. Arshinov, G. S. Golitsyn, I. Granberg, A. Stohl, G. Cayez, G. Athier, F. Boumard, J.-M. Cousin.

Two airborne campaigns were carried out to measure the tropospheric concentrations and variability of CO_2, CO and O_3 over Siberia. In order to quantify the influence of remote and regional natural and anthropogenic sources, we analysed a total of 52 vertical profiles of these species collected in April and September 2006, every ~200 km and up to 7 km altitude. CO_2 and CO concentrations were high in April 2006 (respectively 385-390 ppm CO_2 and 160-200 ppb CO) compared to background values. CO concentrations up to 220 ppb were recorded above 3.5 km over eastern Siberia, with enhancements in 500-1000 m thick layers. The presence of CO enriched air masses resulted from a quick frontal uplift of a polluted air mass exposed to northern China anthropogenic emissions and to fire emissions in northern Mongolia. A dominant Asian origin for CO above 4 km (71.0%) contrasted with a dominant European origin below this altitude (70.9%) was deduced both from a transport model analysis, and from the contrasted $\Delta CO/\Delta CO_2$ ratio vertical distribution. In September 2006, a significant O_3 depletion (~-30 ppb) was repeatedly observed in the boundary layer, as diagnosed from virtual potential temperature profiles and CO_2 gradients, compared to the free troposphere aloft, suggestive of a strong O_3 deposition over Siberian forests.

3.4. Introduction

The purpose of the YAK-AEROSIB aircraft campaigns is to document the composition and the large-scale synoptic transport of CO_2, CO and O_3 into the Siberian air shed. The data resulting from 2 campaigns in April and September 2006 are presented.

CO_2 is the main anthropogenic greenhouse gas in the atmosphere. Also a significant greenhouse gas, tropospheric O_3 is a pollutant harmful to human and vegetation. O_3 and CO are important components of the atmospheric chemical system. Tropospheric O_3 sources are photochemical production from precursors such as CO and volatile organic compounds (VOCs), and stratospheric input. It is removed by ground deposition and photodissociation. The main net sources of CO_2 and CO are combustion processes. CO_2 sinks are terrestrial photosynthesis and oceanic uptake.

Siberia is a key region for the global carbon cycle with a CO_2 sink of 0.5 ± 0.5 GtC yr^{-1} (Gurney et al., 2002), but its magnitude is not constrained by any surface stations inside Siberia. In

addition, Siberia is a region where atmospheric transport models fail to represent the vertical profiles of atmospheric CO_2, due to covariations between ecosystem fluxes and vertical transport on seasonal time scales (Gurney et al., 2002; Stephens et al., 2007). Both the transport and the surface fluxes of CO_2 over Siberia (e.g. van der Molen and Dolman, 2007) are poorly known.

The seasonal cycle of CO_2 over the Eurasian continent has only been measured at sparse locations by means of tall tower (e.g. Maksyutov et al., 2006), or occasional or monthly vertical profiles in the lower troposphere (Machida et al., 2001; Hiyama et al, 2003; Levin et al., 2002; Lloyd et al., 2002; Ramonet et al., 2002). Snapshot boundary layer (BL) budget studies were executed in Siberia (Lloyd et al., 2002; Ramonet et al., 2002) but the inference of sources and sinks from these data using 1-D models suffers from ignoring the true 3-D complexity of regional circulations (van der Molen and Dolman, 2007). The YAK-AEROSIB data bridge this gap of scales by taking dense measurements across the entire Siberian air shed. Dense CO_2 vertical profiles are needed to better understand how ecosystem CO_2 fluxes are coupled to atmospheric transport.

In addition to large-scale transport of natural and anthropogenic fluxes, the variability of CO_2 over continents is also driven by synoptic frontal passages (Chan et al., 2004; Wang et al., 2007), meso-scale regional circulations and BL dynamics (Nakazawa et al., 1997; Sarrat et al., 2007, Nicholls et al., 2004, Wang et al., 2007). Dense vertical profiles and horizontal gradients of CO_2 over continents obtained with airborne campaigns provide unique insights to better quantify and understand the variability of the underlying CO_2 sources and sinks. For instance, Gerbig et al. (2003) and Lin et al. (2003) provided a new measure of the spatial coherence scale of CO_2 in the BL, showing that transport models should have a resolution of at least 30 km to capture it.

Like for CO_2, in addition to natural processes, the tropospheric composition over Siberia for CO and O_3 reflects also long-range transport (LRT) (e.g. Bey et al., 2001; Eckhardt et al., 2004; Newell and Evans, 2000; Stohl, 2001; Stohl et al., 2007a, 2007b; Wild et al., 2004). Wild et al. (2004) found for instance a net ozone enhancement over Siberia due to European precursor emissions. Transport of pollutants across Eurasia, and into Siberia, have received little attention (Akimoto, 2003). Data from the Mondy station in the Baikal area (Pochanart et al., 2003), and from the TROICA train transects (Crutzen et al., 1998; Bergamaschi et al., 1998; Oberlander et al., 2002) have provided a ground-based view of the gradients and origin of CO and O_3 in Siberia. Pochanart et al. (2003) documented a spring maximum and summer minimum of both CO and O_3 concentrations. They found that the most enhanced concentration levels of CO and O_3 in Baikal Lake region were observed in air masses transported from Europe. In the upper troposphere, high CO levels of 150 ppb (30% above the hemispheric background) caused by widespread forest fires have been measured over eastern Siberia during summer (Nédélec et al., 2005), indicating that fire emissions can be uplifted at high altitude over the region. Large gaps remain in understanding pollutant transport and chemistry across Eurasia.

The two YAK-AEROSIB campaigns presented here sampled the tropospheric concentrations of CO_2, CO, O_3 and of fine aerosols across a large horizontal transect between Novosibirsk (central Siberia) and Yakutsk (eastern Siberia) during 7-10 April and 11-14 September, 2006. We first describe the in-situ instrumentation for continuous measurements of CO_2, CO and

O_3 (section 2), the synoptic weather conditions during each campaign (section 3), and the associated trace gas distribution (section 4). In section 5, the fast upwards transport of Chinese pollution through a frontal event in April 2006 is analyzed. In section 6, the correlation between CO and CO_2 variations in the profiles and their potential use to trace the fossil component of CO_2 is studied. Throughout this manuscript "BL" refers to boundary layer and "FT" to free troposphere.

3.5. Campaign and instrumentation description

3.5.1. Study Area

The flight pattern of the YAK-AEROSIB campaigns is shown in Fig. 3.1. It covers the lowermost 7 km of the troposphere from 55°N to 63°N between 80°E and 130°E. The region under study is mainly forested by coniferous trees and partly covered by agricultural regions further south and west (Bartalev et al., 2003). The north-western quarter of the YAK-AEROSIB area lies in zones of continuous permafrost (100-500m thick), and discontinuous permafrost in the South. The region has an extensive network of rivers and lakes, including the Yenissei and Lena rivers and their contributors. Forested bogs are also present near the track.

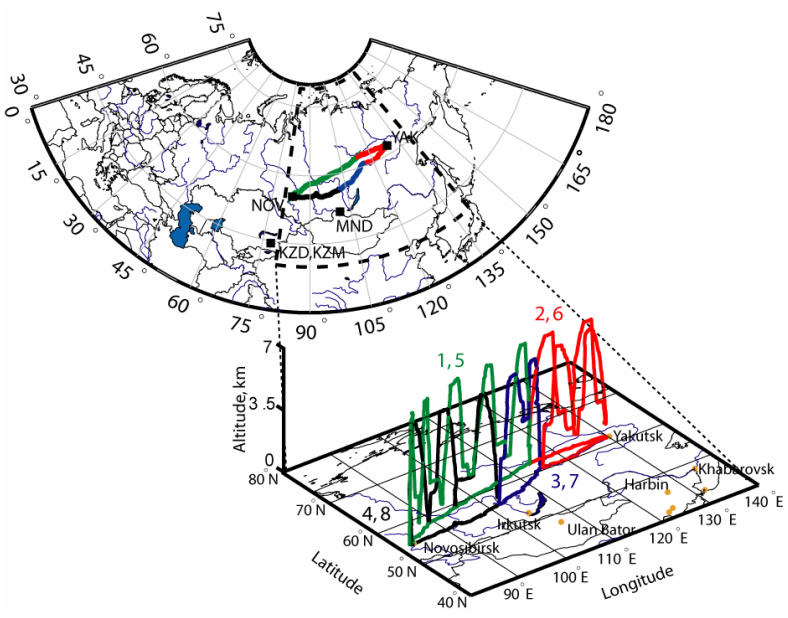

Figure 3.1. Campaign flight plan: general view and detailed 3D view with flight pattern designed to optimize vertical soundings. The actual flights shown are Flights 1 (green), 2 (red), 3 (blue) and 4 (black). Flights 5-8 follow similar routes, with plateaux at 5 km instead of 2 km. The squares labelled NOV and YAK indicate the cities of Novosibirsk and Yakutsk, respectively. MND, KZD and KZM indicate the stations of Mondy, Sary Taukum and Plateau Assy respectively.

A number of cities are crossed: Novosibirsk, Tomsk, Mirny, Yenisseisk, Irkutsk, Bratsk, Krasnoyarsk and Kemerovo. Most of them are industrial or mining centres. The areas surrounding Krasnoyarsk and Novosibirsk are also covered by agriculture. Figure 3.1 shows the YAK-AEROSIB route with the starting point Novosibirsk (NOV) and the easternmost pivot point Yakutsk (YAK). Fig. 3.1 also indicates the location of ground-based atmospheric mountain stations Mondy (MND ; 51°39N, 100°55E, 2006 m a.s.l.) in Russia, near the Baikal Lake, and of Sary Taukum in Kazakhstan (KZD, 43°15N, 77°53E, 412 m a.s.l.) and Plateau Assy, Kazakhstan (KZM, 43°13N 77°53E, 2519 m a.s.l.) which are part of the global ESRL air sampling network. Other stations of interest for this study are Barrow in Alaska (BRW), 71°19N 156°36E, 11m a.s.l.) and Pallas in Northern Finland (PAL, 67°58N, 24°07E, 560m a.s.l.). Data from these stations are compared to the aircraft profiles in section 4.

3.5.2. Campaigns description

The two YAK-AEROSIB campaigns followed the same route. Each campaign consists of 4 flights shown with different colours in Fig. 3.1. Each flight contains a series of vertical profiles. The YAK-1 campaign was conducted in April 2006. 26 vertical profiles were collected. Each profile takes about 30 minutes, including horizontal plateaus at 0.5 and 7 km, and at 5 km on descents. The YAK-2 campaign was conducted in September 2006 and included 26 vertical profiles, with plateaus at 0.5 and 7 km, and 2 km on descents (see table 3.1 for a summary). The chartered aircraft is a two-propeller Antonov-30 (see Fig. 3.2 for a picture of the aircraft and a representation of the inside instrumental setup) operated by the Institute of Atmospheric Optics of Tomsk (Zuev et al., 1992) and is equipped with meteorological instrumentation. The maximum range of the aircraft is 3400 km and its airspeed during measurement is about 85 m s^{-1}. Vertical speed during vertical profiles is about 3.5 m s^{-1} on ascent and 7 m s^{-1} on descent.

Table 3.1. Summary of flights during the YAK-AEROSIB campaigns in 2006

Flight nb	Day	Time (Local)	Time (UTC)	Nb profiles	Itinerary
1	11 Apr 06	1200-2100	0600-1200	8	Novosibirsk-Myrni
2	12 Apr 06	1100-1530	0200-0630	8	Myrni-Yakutsk-Lensk
3	12 Apr 06	1730-1900	0830-1100	4	Lensk-Bratsk
4	14 Apr 06	0830-1030	0030-0430	6	Bratsk-Novosibirsk
5	07 Sept 06	0900-1900	0300-1000	10	Novosibirsk-Myrni
6	08 Sept 06	0945-1430	0045-0530	8	Myrni-Yakutsk-Lensk
7	08 Sept 06	1600-1730	0700-0930	2	Lensk-Bratsk
8	10 Sept 06	0900-1115	0100-0515	6	Bratsk-Novosibirsk

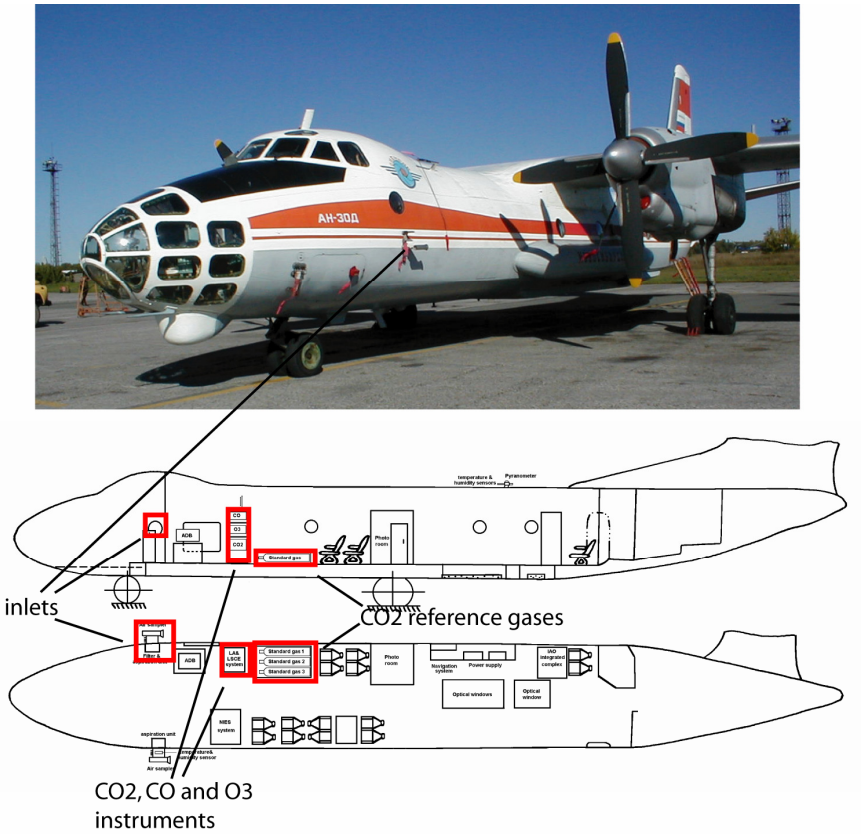

Figure 3.2. The Antonov-30 "Optik-E" aircraft operated by IAO. a) picture from outside, inlet are signalled by red tissues and b) schematics of the interior of the aircraft. The instruments giving the data studied in this paper are highlighted in red.

The flights were performed in all-weather conditions. During Flight 1 (11 April 2006) at 1030 UTC and in Flight 7 (8 September 2006) at 0800 UTC the profiles have not been completed down to the ground because of excessive cloudiness. The times of flights were dependent on logistical constraints. The April flights were carried mostly in the local afternoon, whereas the September flights started at 0900 LT (Table 3.1). The long duration of the flights allowed sampling a large diversity of combinations of air masses, cloudiness conditions, solar zenith angles and vegetation cover types. Diurnal variations of the BL height are expected to affect the comparability of individual profiles, but these differences tend to compensate over a whole flight, when making composite profiles. Synoptic variations are discussed in latter sections. In April, the sunrise occurs at about 0530 LT-Novossibirsk (GMT+0600), and sunset at 1945 LT-Novossibirsk, i.e. a photoperiod length of 14.3 hours. In September, the sunrise was at 0550 LT and sunset at 1930, i.e. a photoperiod of 13.7 hours.

3.6. Onboard instruments

3.6.1. CO_2

The CO_2 analyser is a Li-Cor 6262 modified non-dispersive infrared (NDIR) analyser modified at the LSCE. The Li-Cor is embedded in a system which regulates the temperature, flow and pressure of incoming air. Sampled air is dried upstream using magnesium perchlorate. Pressure fluctuations within 0.5 mbar around target value pressure are allowed in the data processing. Acquisition frequency is 0.5 Hz. In-flight calibrations are performed at 30 minutes intervals using three calibration gases. These gases are carried in high-pressure cylinders that are used sequentially ("high", "low", and "reference" value). Their values were determined at the LSCE laboratory prior to shipment and are traceable to a suite of primary WMO-CO_2 standards from NOAA/ESRL. The concentrations used are 370.60±0.01, 380.47±0.01 and 409.76±0.01 ppm respectively. The three calibration gases are analyzed during the flight at ~30min intervals. The drift is corrected for based on errors in estimation of reference gas. During the April 2006 campaign, the precision was 0.4 ppm and accuracy 0.15 ppm. Improvements in the electronics yielded a precision of 0.15 ppm for the September 2006 campaign. The CO_2 instrument precision is estimated from the standard deviation of the stabilized concentration signal during 1 minute after injecting the reference gas, allowing 2 minutes for stabilization in the measurement cell. The accuracy is estimated as the offset of the instrument when measuring a 'target' reference gas cylinder during 1-min in the pressure-stabilized cell. The CO_2 data are processed using a semi-automatic filter based on pressure, flow and temperature in the measurement and reference cells of the Li-Cor.

3.6.2. O_3

The O_3 analyser is developed from a commercial fast response ozone analyser (Thermo Instruments Model 49), with modifications for internal calibration and aircraft operation safety. The instrument is based on classic UV absorption in two parallel cells (zero, sample), with a precision of 2 ppb, 2% for an integration time of 4 sec. It is compensated for aircraft pressure and temperature variations. Prior to detection, air is pressurised to cabin pressure, using a Teflon KNF Neuberger pump model N735 also used for the CO instrument. Electrical improvements has been brought by Laboratoire d'Aérologie, including a 27VDC supplied power provided also to the CO instrument. For the YAK-AEROSIB project, the ozone instrument includes a specially designed computer for data acquisition and for instrument control, powered in aircraft 27VDC. Before shipping to Russia, the O_3 analyser has been calibrated against a NIST related reference calibrator Model49PS. A calibration box with an O_3 generator is used for laboratory verifications of the ozone analyser before and after the campaigns.

3.6.3. CO

The CO analyser has been described in Nédélec et al. (2003). It is a fully automated instrument designed to reach an accuracy of 5 ppb or 5%. The instrument is based on a commercial infrared absorption correlation gas analyser (Model 48C, TEI Thermo Environment Instruments, USA). The model 48CTL is qualified by U.S. EPA designated method EQSA-0486-060. Laboratoire d'Aérologie improved the instrument accuracy with addition of periodical (every 20 minutes), in-flight accurate zero measurements, new IR detector with better cooling and temperature regulation, pressure increase and regulation in the absorption cell, increased flow rate to 4 l/min, water vapour trap and ozone filter. The precision achieved for 30 seconds integration time (corresponding to the response time of the instrument) is 5 ppb or 5% CO, with a lower detection limit of 10 ppb.

3.6.4. Meteorological parameters

Temperature, humidity and wind vector are measured routinely onboard using HYCAL sensor model IH-3602-C of Honeywell Inc. Temperature range is from -70 to +70°C and accuracy is 0.5°C. Relative humidity range is from 0 to 100% and accuracy is 7%.

3.7. Synoptic situation and transport

3.7.1. Lagrangian particle transport model

Atmospheric transport was investigated using FLEXPART (Stohl et al., 2005, Seibert and Frank, 2004). The model was run backward in time from small boxes (0.5°x0.5°x100m) arranged along the flight tracks. The backward simulation method can be used to analyse air mass transport, relating potential source regions to the aircraft position. Each simulation consists of 20000 particles released in the volume of air sampled, which were followed 20 days backward in time. The Potential Emission Sensitivity (PES) function is defined as the residence time of the backward particles in each particular grid box below a given threshold altitude. The PES is a measure for the simulated mixing ratio at the receptor that a source of unit strength in the respective air column below the threshold altitude would produce, disregarding loss processes (passive tracer case). Two different FLEXPART setups are used to calculate PES in this paper: 1) the runs presented for analyzing transport patterns (sections 3.2 and 3.3 below) are done 10 days backward with PES up to 3000 m, and 2) the run for the case study of north-eastern Asian emission uplift contributions (section 5.1.) is done 20 days backward with PES up to 300m.

3.7.2. Synoptic situation during April 2006 campaign

There were fair weather conditions during most of the campaign with occasional fair weather cumulus. The weather was, however, cloudy during Flight 1 (1000-1200 UTC) and precipitations occurred during Flight 4. The BL was shallow and stable during most of the campaign, due to cold near-ground temperature (between -5 and -15°C). During Flight 2 a strong temperature inversion was observed at ≈ 2 km altitude.

Figure 3.3a shows the ECMWF geopotential height at 500 hPa for 12 April 2006. Fig. 3.3b-d shows the FLEXPART PES functions (< 3000 m) up to 10 days backwards. The PES are summed for all the receptor locations corresponding to the aircraft route each day (panel 3c sums Flights 2 and 3). Red squares correspond to space borne fire detection from ATSR World Fire Atlas fire maps for periods 5-12 April (Fig. 3.3b-d) and 1-7 September (Fig. 3.3f-h), retrieved from http://dup.esrin.esa.int/ionia/wfa/. Stationary fires occur in North-western Siberia near 65°N, 80°E, associated to industrial gas flaring in the Norilsk region. Just before the April campaign, two local geopotential minima, over northern and eastern Siberia, cause advection of polar air in the Siberian troposphere. This is confirmed by the PES of Flights 1-3 (Fig. 3.3b-c), showing that the aircraft sampled mainly polar air below 3 km. Across Southern Siberia, a westerly flow is associated to a low pressure system centred at 65°N, 120°E (Fig. 3.3a). Between 11 and 13 April, stagnant conditions at 500 hPa lead to very slow stirring, or filamentation, of FT air. Under these stagnant conditions, there is no advection of European emissions and the footprint (Fig. 3.3b-c) remains concentrated over Siberia. During 11-12 April (Flights 1-3, Fig. 3.3b-c), advection in the lowermost troposphere toward the aircraft route occurs mostly from central Siberia.

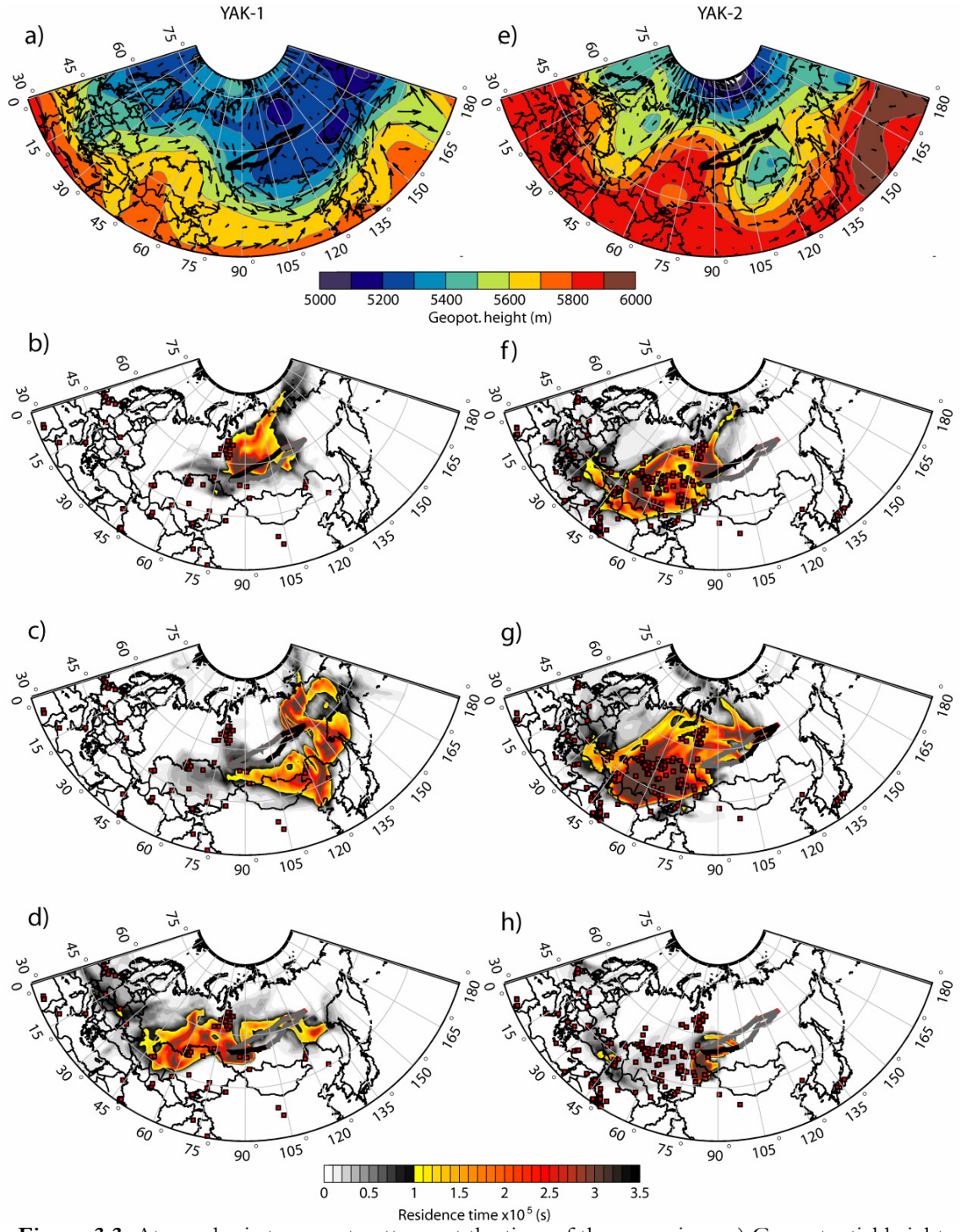

Figure 3.3. Atmospheric transport patterns at the time of the campaigns. a) Geopotential height and wind at 500 hPa from ECMWF analyses for 12 April at 0600 UTC. b) 10-days potential emission sensitivity (PES) for simulated retro-transport of particles released along Flight 1, c) same for Flights 2 and 3, and d) for Flight 4. e) same as a) for 7 September at 0600 UTC, f) PES for Flight 5, g) for Flights 6 and 7 h) for Flight 8. Red squares represent ATSR World Fire Atlas for 5-12 April (b-d) and 1-7 September (f-h).

Figure 3.4a shows the synoptic weather chart for 11 April 2006, at 0600 UTC. Prior to and during Flights 2-3, a series of fronts passed over north eastern Asia during four consecutive days. These fronts caused uplift of BL air from north eastern Asia. The combination of 1) stagnation in the middle FT, and 2) uplift by the frontal passages of moist and warm air from Northern China and eastern Mongolia (see PES in Fig. 3.3c) resulted into the presence of a polluted air mass in the FT which was sampled by the aircraft (section 5.1). For Flight 4 the situation is different, and the main PES, in addition to local Siberian sources, is found to occur just east of the Ural Mountains and in Central and Eastern Europe. According to ATSR fire maps, our measurements are sensitive to agricultural fires in Kazakhstan and to gas flaring emissions in the Norilsk area.

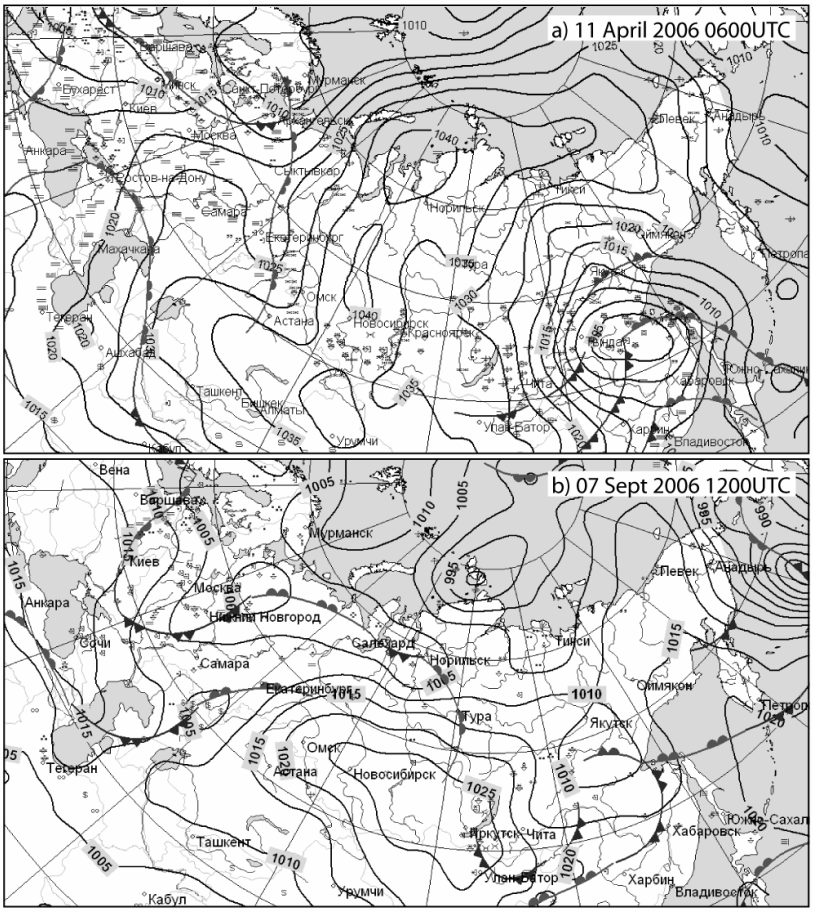

Figure 3.4. Russian weather service Hydrometcenter charts. a) 11 April 2006 at 0600 UTC. A series of fronts associated with a depression are moving south-eastward on the Eastern Asia coast. b) 7 September 2006 at 1200 UTC. A warm front stretching between Norilsk and Krasnoyarsk was crossed by the YAK-AEROSIB aircraft during Flight 5.

3.7.3. Synoptic situation during September 2006 campaign

The September campaign experienced mixed, variable weather. Fair weather occurred only during Flight 5, except at 0545 UTC, were a cloud formation was crossed (warm front). There were precipitations at the end of Flight 6 and beginning of Flight 7 with cold near-ground temperature, and intense convection afterward (Flight 7 at 0800 UTC). The end of Flight 8 also crossed convective conditions.

Figure 3.3e shows the ECMWF geopotential height at 500 hPa on 7 September 2006. Figures 3f-h show the FLEXPART PES (< 3000 m) up to 10 days backwards reaching the aircraft locations. Figure 3.3g show the cumulated PES summed for the route of Flights 6 and 7. The period is characterized by a typical 'omega circulation' whirling around troughs over Eastern Europe and Eastern Asia. A ridge is located over central Siberia, associated with weak fronts (Fig. 3.4b). The European outflow is partially channelled towards 1) Turkey and the Black Sea by a low pressure system in European Russia (Fig. 3.3e, at 60°N-45°E), and 2) central Siberia by a ridge moving eastward (over Kazakhstan at 50°N-70°E on 7 September). The polar low causes a fast north-westerly flow over central Siberia. The combination of zonal 'Omega' circulation and baroclinic perturbations in European Russia mixed up European emissions into the FT over Siberia at the time of the campaign. In addition to this influence from Europe, a significant part of the PES for this campaign (Fig. 3.3f-h) is located over Siberia and Kazakhstan, in presence of regional perturbations leading to local uplift of BL air.

Figure 3.4b shows the synoptic weather chart for 7 September 2006, at 1200 UTC (Flight 5). The dominant synoptic feature of the campaign is a warm front moving towards the South East on 7-8 September. The corresponding FLEXPART simulations of PES across both sides of the warm front indicate sharply distinct origins for the sampled air masses (not shown). For aircraft altitudes below the warm frontal surface (< 1.5 km), the air has a polar origin, and spent at least 15 days into the Arctic. In contrast, for aircraft altitudes above the warm frontal surface (1.5 to 5 km), the air has a western origin and is sensitive to fire emissions in the Caspian Sea area (Fig. 3.3f-g). For altitudes greater than 5 km, the air has a remote origin, and has been entrained by a jet. The consequences on the measured CO_2 and CO profiles are discussed in sections 4.1.1 and 4.1.2.

Figure 3.5 shows example vertical profiles of meteorological variables for 7 September 2006 (Flight 5), and the BL height diurnal variation deduced from these data. Figures 5a-b show the vertical profiles of temperature, wind vector, potential virtual temperature, relative humidity and water vapour mixing ratio (WMR), during the two first ascents of Flight 5. The BL height in Fig. 3.5c is determined from consecutive profiles of virtual potential temperature, humidity and CO_2. On average across the flights, the mid-day average BL height during the September 2006 campaign was ≈1.2 km, and occasionally convective.

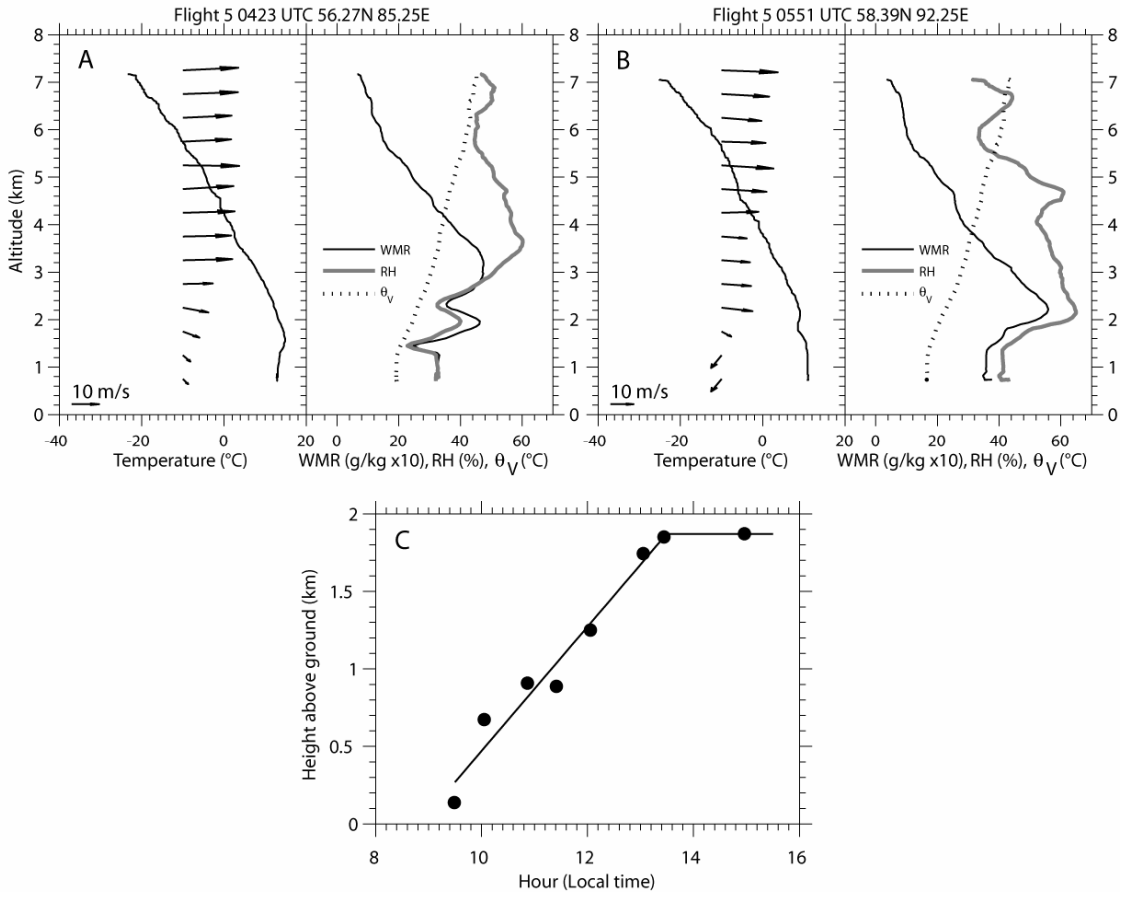

Figure 3.5. Meteorological soundings of Flight 5. A) vertical profile of (left) temperature and wind vector and (right) water vapour mixing ratio, relative humidity and virtual potential temperature during the ascent starting at 0423UTC. B) Same as A for the ascent starting at 0551 UTC. C) Boundary layer height above ground level deduced from virtual potential temperature, humidity and CO_2 profiles during Flight 5. Only BL heights with unambiguous profiles are included.

3.8. Tracers variability

Figure 3.6 and 3.7 show selected individual profiles for flights of the April and September campaigns. Time series from each campaign are further shown in Annex 1, figures A1 and A2. Figure 3.8 shows the average vertical profile of each flight, calculated for altitude bins of 1 km. Horizontal error bars represents the 10th and 90th percentiles of each bin. Monthly smoothed CO_2 and CO concentrations recorded at coincident times are shown for stations KZM (letter K), KZD (letter D), BRW (letter B) and PAL (letter P). The smoothed data were obtained from the NOAA ESRL website (http://www.esrl.noaa.gov/gmd/ccgg/iadv/, see stations location in Fig 1). The spring and fall O_3 seasonal concentrations for the period 1997-1999 from Pochanart et al. (2003) are shown in Fig. 3.8c and Fig. 3.8f at the MND (letter M) mountain station, near the Baikal lake.

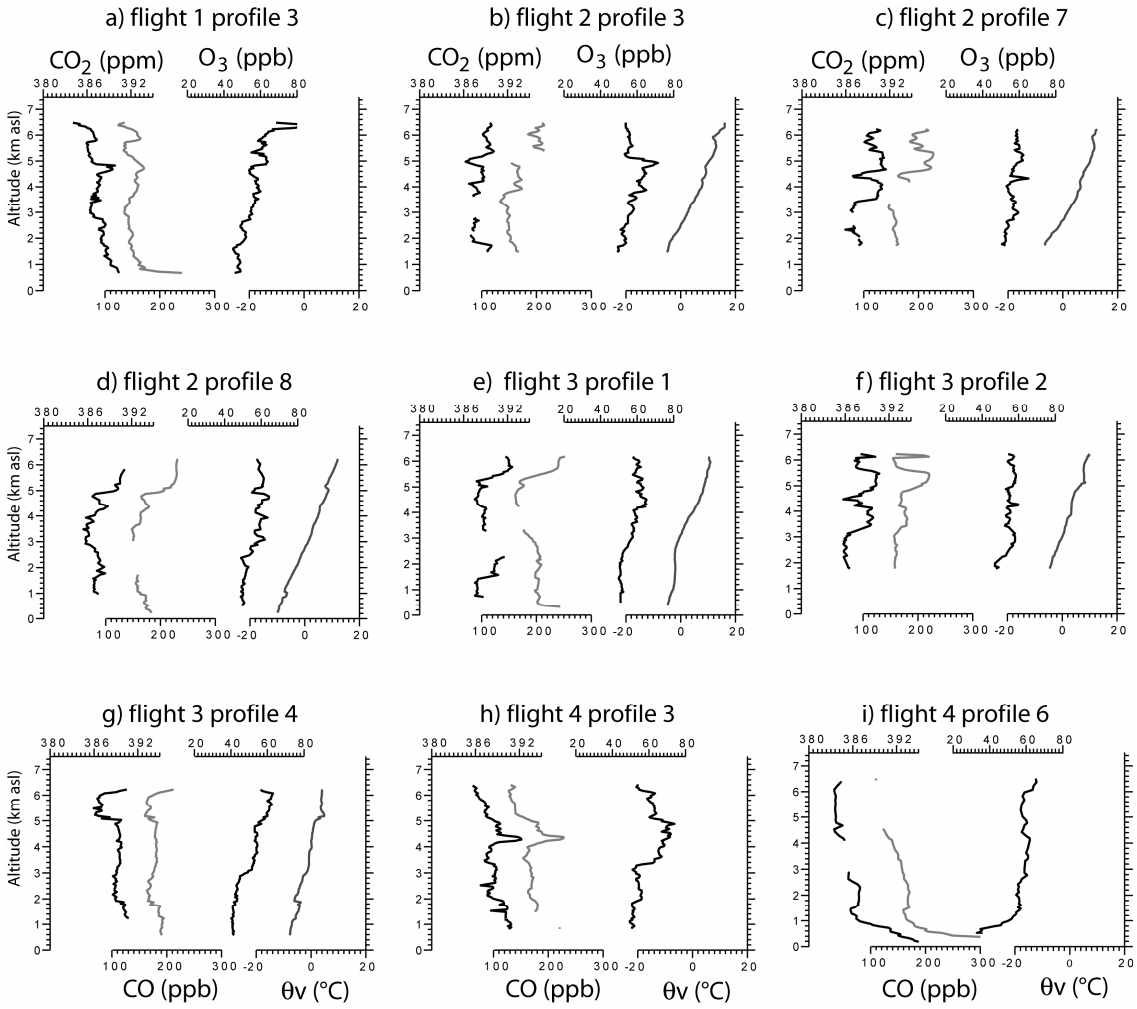

Figure 3.6. Nine selected vertical profiles of the April 2006 campaign which are discussed in the text. The CO_2 profiles are in thick black to the left of each plot, CO in light grey, O_3 in black and potential temperature in dark grey to the right of each plot.

3.8.1. April 2006 campaign

3.8.1.1 CO2 concentrations

An estimate of the background CO_2 concentration was calculated from the data, based on CO variability criteria. We binned the CO_2 data into 2 minutes intervals, rejected the bins where the std. dev. of CO exceeded 10 ppb, took the 33rd percentile of CO_2 in each selected bin, and finally averaged all these values to define the background CO_2 of the campaign. This selection of low variability CO episodes is capable of efficiently discarding CO_2 in polluted layers. The April CO_2 background is 386.2±1.7 ppm (grey line and shaded area in Fig. 3.8a), very close to the monthly smoothed KZM data (385 ppm in Fig 8a). Note that the corresponding background CO for the

campaign also agrees well with the KZM data (see below). The CO_2 and CO excesses above the background therefore reflect regional variability of transport. Elevated CO_2 concentrations near the surface, up to 393 ppm, were observed above Novosibirsk and Tomsk (Fig. 3.6i, Flight 4), or in layers separated from, but close to the surface (see e.g. Fig. 3.6e, near the city of Lensk at 1.5 km altitude). The coincident high concentrations of CO confirm that these elevated CO_2 values reflect the city plumes where regional anthropogenic emissions accumulate in April below stable inversion layers.

3.8.1.2 High CO concentrations

The mean CO concentration measured during the April 2006 campaign is 174±28 ppb, whereas the background concentration (defined on the same basis as above) is 135±21 ppb (grey line and shaded area in Fig. 3.8b). The background CO is reasonably close to the 139 ppb value recorded in altitude at KZM, like for CO2 (Fig 8a-b). The YAK background CO is however lower than the values recorded at the surface at BRW and KZD stations by 27 ppb and 20 ppb respectively. The mean CO concentration is 9 ppb higher than the MND 1997-1999 spring average value (Pochanart et al., 2003). The median CO concentration below 1 km of altitude during Flight 1 and 2 are very close to the PAL concentration of about 172 ppb (Fig. 3.8). However, the footprint pattern in Fig. 3.8b-c suggests that, if advection of air from Northern Europe is the source of this similarity, the contact with pollutant emissions must have occurred earlier than 10 days before. Using the MOZAIC passenger aircraft data, Nédélec et al. (2005) found an April median value of 125 ppb in the upper troposphere (8-10 km altitude). Below 1.5 km, the CO profiles show a high variability, ranging from near-background values over the forests (Fig. 3.6f, below 4 km) up to CO > 300 ppb in city plumes (Fig. 3.6i Flight 4 near Novosibirsk). Between 1.5 and 4 km, the CO vertical distribution is more homogeneous. On the whole, CO_2 and CO are highly correlated during the April 2006 campaign (see Fig. 3.9a). This is further analyzed in section 5.2.

3.8.1.3 O_3 concentrations

The O_3 concentration distribution measured in April 2006 is vertically fairly homogeneous in the FT, in the range of 50 to 60 ppb, although a well-defined increase of O_3 with height of 3 ppb km^{-1} can be observed between 1 and 6 km (Fig. 3.8c). The mean O_3 concentration measured during the entire campaign is 50±5 ppb (Fig. 3.8c). The homogeneous O_3 distribution suggests no strong spatial gradients in chemical sources or sinks of O_3 affecting our profiles. 10-40 ppb depletion in O_3 is observed near the surface below 1km, as compared to the FT above. The lowest O_3 near-ground minima are found over landing air-strips in polluted city plumes, which are easy to identify because of their elevated CO concentrations. This suggests a strong titration of O_3 by NO (Fig. 3.6i) near the surface. Note however that the anti-correlation between CO and O_3 is not systematic in high CO air masses.

During Flight 1, higher (> 80 ppb) O_3 values above 6.5 km are observed. Highest O_3 concentrations range between 101 and 107 ppb and coincides with relatively low CO (126±6 ppb) and low CO_2 values (385.0±0.3 ppm) at 6.4 km altitude (Fig. 3.6a). This suggests a stratospheric contribution to the O_3 enhancement.

The mean O_3 concentration matches well the MND monitoring station spring value (Fig. 3.8c; Pochanart et al., 2003). This good match also suggests that there is little year-to-year variability in springtime tropospheric O_3 concentration over Siberia.

3.8.1.4 Free tropospheric CO_2 and CO layer structure

Filaments with elevated CO_2 concentrations (4-6 ppm enhancement above background) and CO (60 ppb enhancement) were encountered at all altitudes, especially during Flight 2 and 3 (Fig. 3.6c-f). Associated CO values reach up to 250 ppb. The typical thickness of the layers is between 200 m and 2000 m. The vertical profiles (e.g. Fig. 3.6d-e) suggest that the layered structure extends above the flight ceiling. This distribution of CO_2, also clearly visible in CO data, is due to slow stirring in the troposphere under reduced vertical mixing (Stohl, 2001; Newell et al., 1999; see CO-CO_2 scatter plots in Fig. 3.9a-d). Both the number of layer occurrence and their CO_2 excess above the background are higher in Flights 2 and 3 (which correspond to the easternmost part of the campaign flight track), than in Flight 1 and 4 over south-western Siberia (see also Fig. 3.8a-b). O_3 shows no clear enhancement or depression in these layers. The reasons of this distribution will be examined in section 5.1.

3.8.2. September 2006 campaign

3.8.2.1 CO_2 concentrations

In the September 2006 campaign, the background CO_2 concentration is 377.1±0.9 ppm (same method as April, see section 4.1.1) which is 9ppm less than in April 2006. The September 2006 CO_2 concentrations show no thin, stratified structure as in April, but plumes are observed in CO data. However, the meteorological conditions and the complex PES footprints shown by Fig. 3.3f-h suggest the contribution of air masses with distinct origins to the vertical profiles. From an analysis of the FLEXPART results, we inferred mostly an Arctic/boreal origin for CO_2 anomalies in the BL, and influence from more remote western sources (Kazakhstan) for CO_2 in the FT.

All the September individual CO_2 profiles (Fig. 3.7 and 3.8d) are characterized by decreasing values towards the surface. On Flights 5 and 7, CO_2 in the BL is depleted by an average of 4 ppm compared to the FT above (Fig. 3.8d). The BL CO_2 values during the entire campaign are on average 8 ppm lower than the ground based KZD station data (~378 ppm) and 5 ppm lower than the BRW station data. The mean vertical September CO_2 gradient between KZM (2519 m a.s.l.) and KZD (412 m a.s.l.) is only ≈0.5 ppm, whereas in our data the Flight 5 CO_2 gradient at

equivalent altitudes is 2 to 5 ppm (Fig. 3.8d). The FLEXPART analysis (section 3.3 and Fig. 3.3b) shows that the air mass origin of the lowermost 1.5 km section of Flight 5 (BL) is from the Arctic, with a slow southward motion of air and lack of entrainment across the top of the BL. BRW is representative of mean Arctic air concentration. The September campaign background CO_2 value is also very close to the BRW data (374.9 ppm). Therefore the 5 ppm CO_2 gradient between YAK concentrations in the BL (Flight 5) and BRW must be caused by regional biospheric uptake. FLEXPART backward transport analysis suggests that, in addition to regional differences in ecosystems uptake, associated with cropland and grasslands in Southern Siberia and Kazakhstan, regional variations in transport patterns between YAK (Flight 5) and KZD could contribute significantly to the gradient between these two locations.

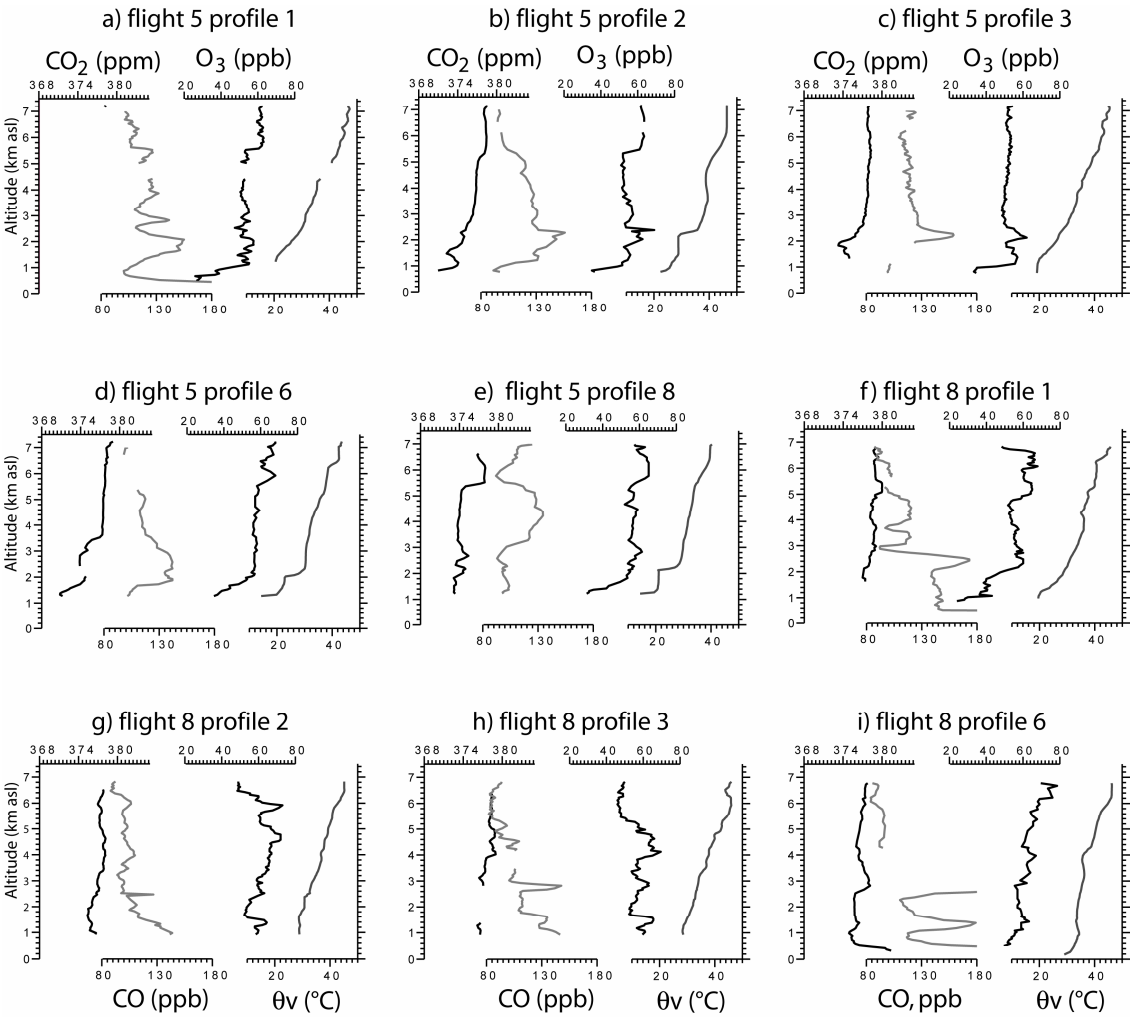

Figure 3.7. Same as Figure 3.6 but for the September 2006 campaign.

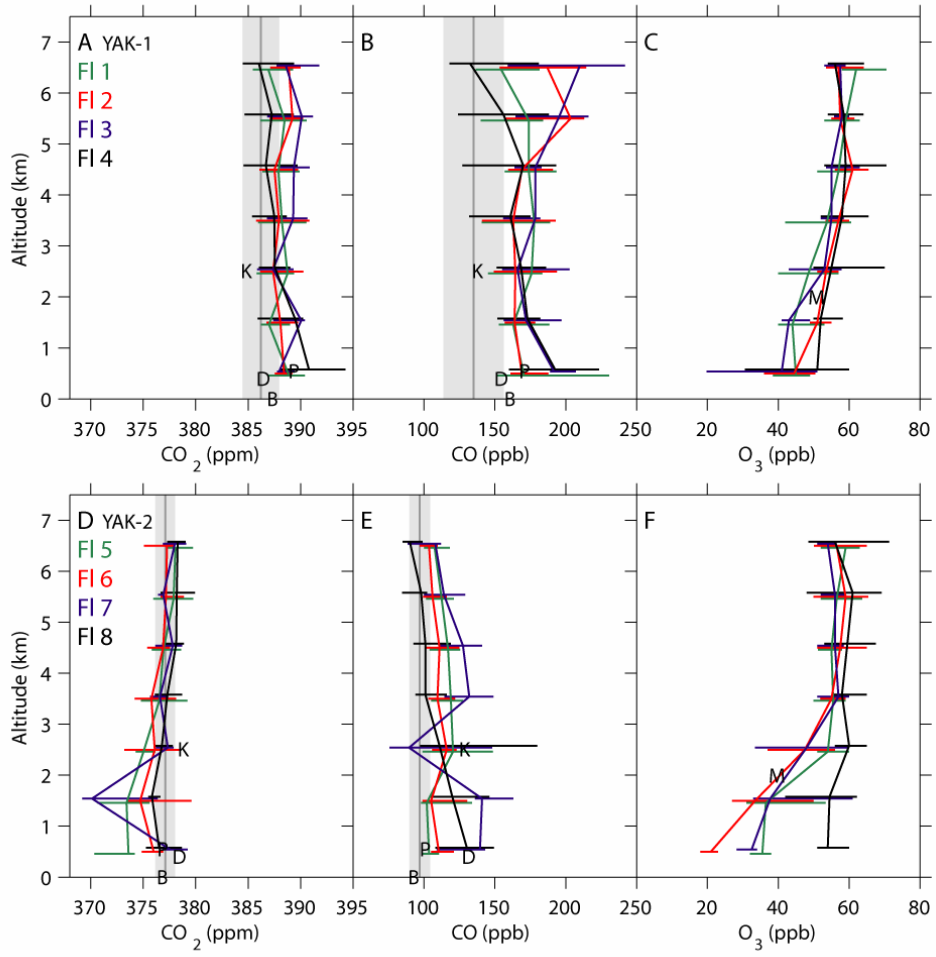

Figure 3.8. CO_2, CO and O_3 average concentration profiles, for each flight. a) April 2006 CO_2 profiles for Flights 1-4. The campaign background mean value and the associated 1σ uncertainty are indicated by the dark grey line and the light grey surface respectively. b) Same as a), for April 2006 CO profiles. c) April 2006 O_3 profiles. d) September 2006 CO_2 profiles and background for Flights 5-8. e) September 2006 CO profiles. f) September 2006 O_3 profiles. The horizontal error bars indicate the 10th and 90th percentiles. Also shown are the NOAA ESRL network interpolation of measured CO_2 and CO at 10 April 2006 (a-b) and 15 September 2006 (d-e), represented by a letter for KZM (K), KZD (D), PAL (P) and BRW (B). O_3 is compared with 3 year seasonal average at MND (M) for spring and fall.

Vertical profiles regularly collected at Zotino (65°45N, 89°23E; Lloyd et al., 2002) show that the mean BL-FT gradient at Zotino is slightly positive in September (1.39 ppm). The local afternoon BL height in September (Lloyd et al. 2002) is on average lower (0.7 – 1 km) than that observed during our campaign. The variability of CO_2 in the FT reflects advection of fossil fuel and biomass burning CO_2 (see Fig. 3.3f-h, red squares), regional differences in uptake by ecosystems, and stratospheric air influence. During Flight 5, both profile 2 (Fig. 3.7b) and profile 8 (Fig. 3.7e) at ~6 km altitude show a coincident excess in O_3 and deficit in CO. In profile 2, the O_3 excess is 12

ppb and the CO deficit is 20 ppb (respectively 8 ppb and 30 ppb in profile 8). Excess is defined here as the difference with the lower part of each profiles. This signature is consistent with a stratospheric influence. Profile 2 and profile 8 (Fig. 3.7b and Fig. 3.7e) also show a positive excess of CO_2, (respectively 1 ppm and 4ppm) indicating that at this time of the year (end of the growing season), the mean lower stratospheric CO_2 is higher than the tropospheric CO_2 value depleted by net plant uptake.

3.8.2.2 CO concentrations

The CO background value for the September 2006 campaign is 97±7ppb (to be compared to 135±21 ppb in April). This background CO is 30 ppb lower than measured further south at KZD and KZM, which may be more influenced by biomass burning (see fire counts in Fig. 3.3). The YAK CO background is comparable however to the value recorded further north at PAL and BRW stations (Fig. 3.8e).

The CO mean and standard deviation are 113±30 ppb. In contrast to April, the air masses that were sampled in September were mostly influenced by surface fluxes from Siberia and Europe entrained by zonal 'Omega' advection (see PES in Fig. 3.3). More active photochemical sink of CO oxidation contributes to decrease the CO September background concentration.

In the September profiles, plumes with CO enhancements up to 140-150 ppb were observed in the FT (mainly during Flight 5, at approx. 2 km altitude in Fig. 3.7a-c). As discussed in section 3.3, this is due to remote fires in Kazakhstan area and anthropogenic emissions advected in a warm air mass. These plumes also exhibit marked O_3 enhancements (Fig. 3.7b-c, at 2.5 km altitude). These CO September enhancements are much lower than in April.

3.8.2.3 Comparison of CO data with MOZAIC flights

Both in April and September, our CO average profiles in Siberia are higher than the European average concentration profiles, and lower than East Asian profiles, showing pollutant enrichment along the zonal flow. In the MOZAIC passenger aircraft CO climatology (http://mozaic.aero.obs-mip.fr), the CO profiles over Frankfurt (Germany) are in the range 130-140 ppb in April and 100-110 ppb in September. The MOZAIC CO concentrations are found to be higher over Nagoya, Osaka and Tokyo (Japan), with values of 140-180 ppb in April, and 120-130 ppb in September. The MOZAIC CO range between Germany and Japan brackets the values observed for each YAK-AEROSIB campaign. However, the CO profiles over Japan are influenced by Southern Asian sources, and not by the result of simple zonal advection of integrated northern Eurasian fluxes.

3.8.2.4 CO-CO_2 correlations

The scatter plots of ΔCO vs. ΔCO_2 for each flight of the September 2006 campaign are shown in Figure 3.9e-h. Near the surface, we observe a CO concentration increase (Fig. 3.7a, 3.7f,

3.7h-i) over cities, especially during Flight 8 over Bratsk and Novosibirsk (Fig. 3.7f and 3.7h-i). However in the presence of biospheric CO_2 uptake and photochemical activity, CO has no correlation with CO_2 in these city plumes in September. For comparison, in April we observed R^2 = 0.95 and 0.82, in the Novosibirsk and Tomsk plumes (see Flights 4 and 1). In September, the overall correlation between ΔCO and ΔCO_2 is small. This is seen in Table 3.2 and Fig. 3.9e-h. Comparing altitudes below 3.5 km, which are more influenced by regional fluxes, the correlation is much lower in September (R^2 range = 0.10 – 0.30) than in April (range = 0.24 – 0.60; Table 3.2). This shows the influence of biogenic sinks (no CO-CO_2 correlation in fluxes) superimposed with the one of anthropogenic emissions. In addition, during spring and summer, CO has additional sources and sinks (production from BVOC, and OH reaction) which de-correlate ΔCO and ΔCO_2 in the atmosphere (Turnbull et al. 2006). Rivier et al. (2006) also showed, using a model, that the CO to fossil fuel CO_2 regression slopes also have a maximum noise in summer.

Table 3.2. Summary of CO-CO_2 correlation by flight and by altitude

	All altitudes		z>3.5 km		z<3.5 km	
Flight	N	R^2	N	R^2	N	R^2
1	1315	0.44	939	0.59	376	0.24
2	858	0.53	646	0.59	212	0.50
3	553	0.54	371	0.65	182	0.35
4	711	0.74	484	0.87	227	0.60
5	1251	0.00	557	0.25	694	0.09
6	994	0.00	486	0.05	508	0.09
7	310	0.24	179	0.19	131	0.30
8	842	0.02	407	0.00	435	0.10

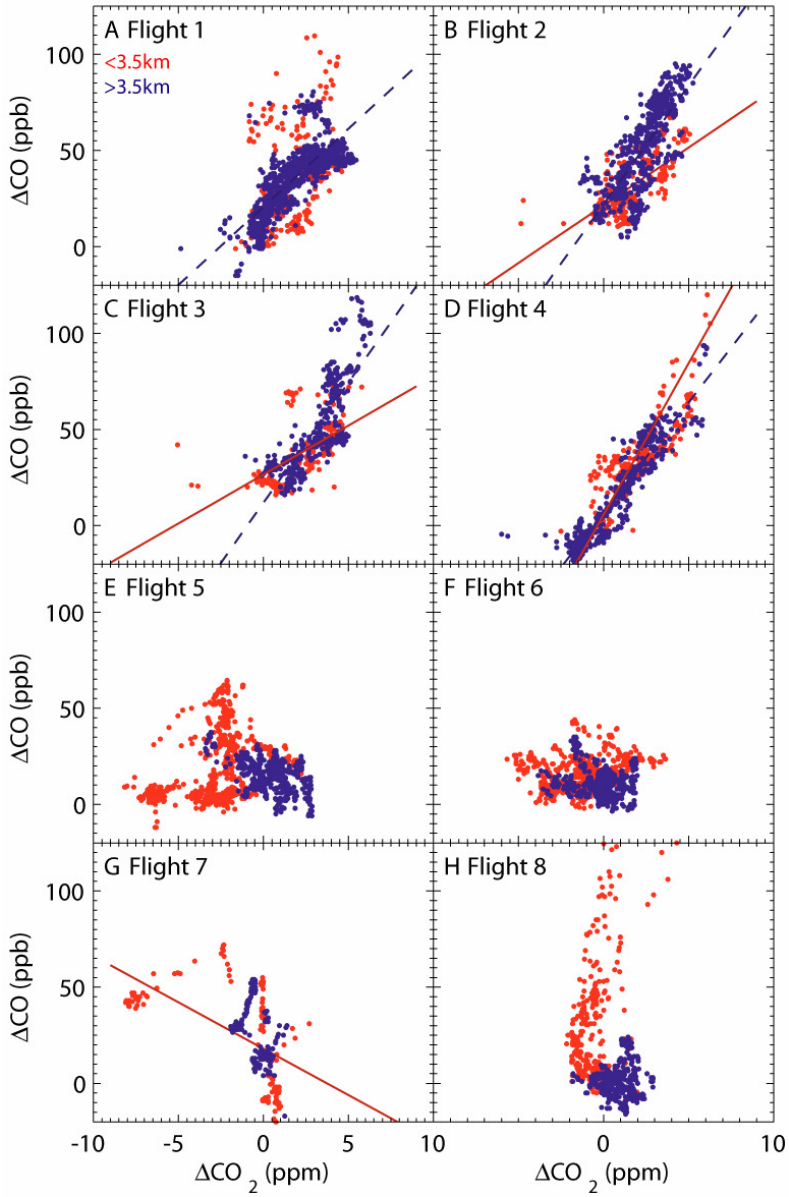

Figure 3.9. Scatter plots of CO vs. CO_2 for all April and September flights. Red dots are for data below 3.5 km, blue dots are above 3.5 km. Regression slopes above (dashed blue line) and below 3.5 km (red line) are shown when correlation coefficient R^2>0.25. a-d) Flights 1-4 in April 2006. e-h) Flights 5-8 in September 2006. Note the absence of correlation for the September flights.

3.8.2.5 O_3 concentrations and possible contributions

Beekman et al. (1994) have shown that free tropospheric O_3 concentrations in the northern hemisphere peaks in spring with a secondary maximum in summer. In our data the September O_3 tropospheric concentrations were slightly higher (55-65 ppb) than in April (50-60 ppb), consistent with either a higher global northern hemisphere summer ozone production or stratospheric intrusions occurrence. High O_3 layers (>70ppb) coinciding with low CO concentrations (~110 ppb)

are encountered on Flights 5, 6 and 8 (Fig. 3.7), at altitudes above 5 km, and usually at the highest points of the flight (7 km). According to the weather and transport analysis of this campaign (see section 3) this is due to a fast zonal transport with a footprint spanning North America, North Atlantic and Europe. For instance on Flight 5 an air mass (profiles 5-6 at 6-7 km, Fig. 3.7d) with high O_3 and low CO (respectively 65.0±4.0 ppb and 101.7±5.8 ppb) also exhibits a low (5±3 %) relative humidity. This is consistent with a stratospheric contribution to higher O_3 concentrations, although our transport model also suggests a significant contribution to O_3 precursors from long range transport of biomass burning plumes. Enhanced O_3 and CO concentrations occur in lower troposphere biomass burning plumes on Flight 5 (Fig. 3.7b-c; see section 4.2.2).

On Flights 5-7, below 1.5 km (in the BL), O_3 concentrations are systematically lower than 40 ppb. These BL O_3 anomalies are not correlated with any CO enhancement (Fig. 3.9d). Below 3 km, at best, a correlation of $R^2 = 0.08$ is found during Flight 7. This absence of relation discards the role of local pollution in the O_3 depletion, via reaction with recently emitted NO. The BL lower O_3 concentrations are attributed to deposition on the vegetation and soil on large scales. O_3 dry deposition seems to be stronger in September than in April. In the BL, this large, continental-scale deposition is consistent with lower summer values relative to spring despite higher summer photochemical production.

3.9. A case study for the source attribution of CO and CO_2 enhancements in April 2006

3.9.1. Uplift of elevated CO concentrations from China in April

We investigated the origin of abnormally high CO and CO_2 concentrations (mean CO 220 ppb and CO_2 391 ppm) encountered on 12 April 2006 in the upper parts of Flight 2 and 3, in eastern Siberia (Fig. 3.6c-f). Note that Flight 1 is not reached by the abnormally high CO and CO_2 concentrations. Maximum CO and CO_2 values in the FT reached 255 ppb and 392.2 ppm, respectively, on Flight 3 (Fig. 3.6e at 6 km altitude). This air mass has a distinctly high positive correlation between CO_2 and CO ($R^2 = 0.53$ when taking all the 12 profiles of Flights 2-3 above 3.5 km) and there is a finely (500-1000 m) stratified structure. Under 3 km, in contrast, CO and CO_2 exhibit near-background concentrations.

3.9.1.1 Fast transport modelling related to a baroclinic perturbation

Figure 3.10 shows the uplift event as described by backward transport analysis. At the altitude where they are observed, these elevated CO and CO2 concentrations are unlikely to reflect emissions from Siberian cities. This is confirmed by the 6-days HYSPLIT back-trajectories analysis and by the surface PES footprints calculated with the FLEXPART model (Fig. 3.10a). HYSPLIT

version 4 (Draxler et al., 1997) back-trajectories were run from the position and time where the highest CO concentration was recorded during Flight 2 over Yakutsk. The green circles on each trajectory mark 24 hours intervals. Back-trajectories were computed 6 days backwards from 3 different starting times bracketing the actual sampling time by ±1 hours. In Figure 3.10a the FLEXPART model was limited to 10 days of backward transport, with clouds of particles being released at locations where measured CO exceeded 220 ppb. Fig. 3.10a also shows ATSR hot spots.

Figure 3.10b shows the back-trajectory vertical displacement. Together with Fig. 3.10a it reveals the following sequence: a flow toward the Pacific was dominant at low altitudes over north-eastern China. This air stream was eventually redirected northward by frontal activity near the coast between China and Japan and uplifted from the BL. The uplift happened between 30 and 50 hours prior to the sampling and lofted polluted air at 6 km altitude. The airstream finally remained homogeneous and reached Flight 2 in thin polluted layers as shown by our data.

Figure 3.10c-d shows the measured and simulated CO enhancements during Flights 2 and 3. Retro-transport was extended here to 20 days backward to probe sensitivity to remote influences. The EDGAR 3.2 FT 2000 emissions (Olivier et al., 2005) emission inventory is used. The CO enhancement above background, caused by recent sources, is obtained by convolving the PES with the CO emission map. Therefore, as the backward transport is run only for 20 days, the pertaining CO concentrations are only the enhancements due to contact with emissions in the last 20 days, with a prescribed chemical lifetime. There is no model spin-up with respect to chemical composition and therefore in this case, FLEXPART cannot simulate a background concentration.

The CO enhancement in Flight 2 at 0330 UTC is correctly modelled but underestimated by a factor of 3. The CO peak at 0445 UTC is also underestimated and located 1.5km too high by the model. Some peaks are underestimated by a factor of 10. The sources of error in this comparison are 1) time or altitude mismatch (phase error) in the model, 2) under-estimation of CO emissions from Chinese industrial activities and biofuel burning in EDGAR, leading to too low concentrations in Asian outflow (Petron et al., 2002; Akimoto et al., 2006; Streets et al., 2003; Forster et al., 2004) or 3) additional CO from biomass burning (fires are not included in our simulation). In a multi-year study, Petron et al. (2002) highlighted the need for nearly a doubling of Asian emissions compared to a priori inventory (EDGAR) to keep consistency between atmospheric measurements and emissions. Additionally, FLEXPART simulates poorly local pollution at low altitudes, probably due to non-representation of 1) emissions in Siberia and 2) night-time accumulation of pollutants.

The FLEXPART model predicts high CO enhancements between 5 and 7 km altitude from North East Asian emissions, and a clean lower troposphere, reflecting the observed CO concentrations. Despite phase errors and underestimations the model is able to show that the middle troposphere (5-7 km altitude) has marked CO enhancements compared to the lower troposphere, and that these enhancements originate from transport of Asian pollution. Figure 3.10a shows that the sensitivity to Asian emissions is particularly marked over North Eastern China.

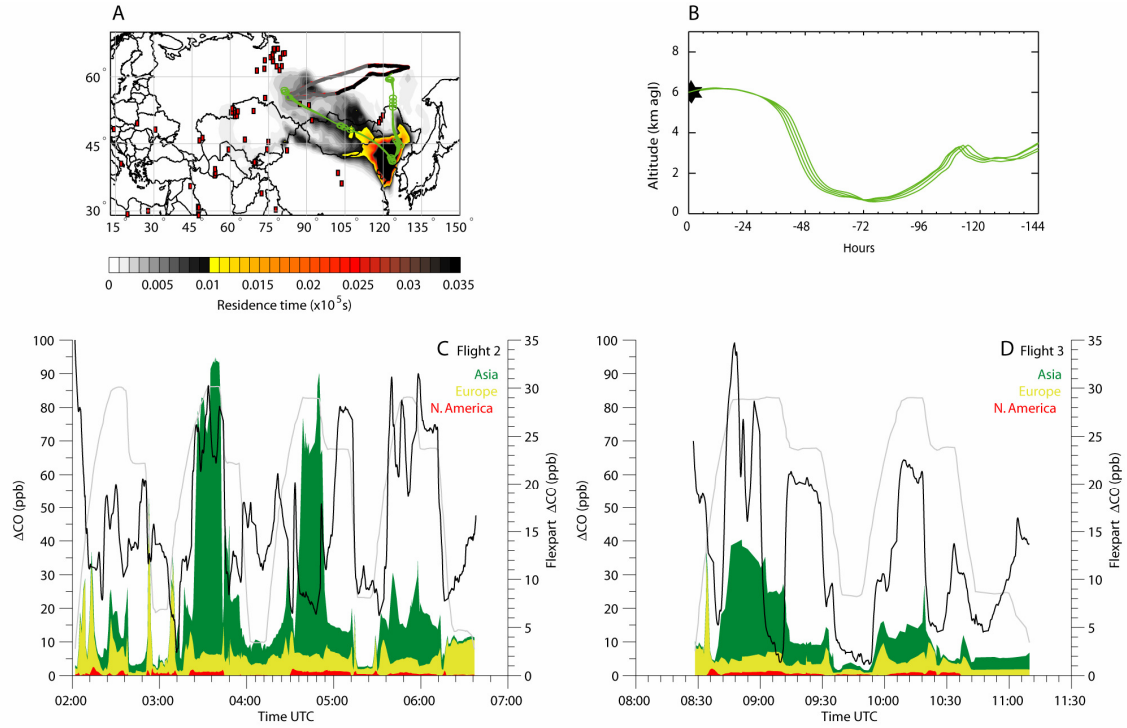

Figure 3.10. Flights 2 and 3: Export of polluted boundary layer air with high CO concentrations to Eastern Siberia, 12 April 2006. a) FLEXPART residence time below 1.5km for 10 days backward. Model particles are released at aircraft times and positions only when actual measured CO > 220 ppb. As a complement, the light green track represent 4 HYSPLIT backtrajectories run at 1 hour interval around aircraft passage at 0600 UTC, at 129°E 62°N and altitude 6km (matching detection of a CO peak). b) Vertical movement of the same backtrajectories with 4 releases at 1h interval. Note the rapid uplift 2 – 3 days prior to detection. c) Measured ΔCO (black line) and simulated ΔCO by origin during Flight 2 (Asia in green, Europe in yellow and North America in red, cumulative filled areas, right Y axis scale). Altitude is shown normalized as grey line. d) same as c) for Flight 3 (same day).

Spring is the peak season of desert dust storms in north-eastern Asia. An extremely high atmospheric dust load was observed in April 2006 over Beijing (Papayannis et al., 2007), corresponding to a large fraction of coarse particles (AOD>3 at 440 nm). After its passage over industrialized regions of northern China, this dust-loaded air mass was later sampled during our Flight 2. The high dust load could explain low O3 concentration of this plume.

3.9.1.2 Warm conveyor belts role on Asian pollutants redistribution

To our knowledge, no direct observation of fast upward transport of a polluted airstream from northern Asia into the Siberian mid troposphere has been made before. Rapid uplift and subsequent transport of BL air occurs generally in mid-latitude cyclones (Cooper et al., 2001). Warm conveyor belts (WCB) vigorously uplift moist boundary-layer air ahead of cold fronts

(Berkowitz et al., 1996; Vaughan et al, 2003). They are most frequent on the eastern coast of continents (Eckhardt et al., 2004), so Siberia is expected to be only a marginal receptor of recently uplifted WCB air masses (Stohl, 2001; his Plate 1). To separate the contributions of uplifted Asian pollution and other sources to the CO enhancements (ΔCO) observed in Flights 2 and 3, the CO enhancements simulated by FLEXPART (Fig. 3.10c) have been split by continent of origin (results for all flights available at http://zardoz.nilu.no/~andreas/YAK/).

When averaging the modelled enhancement ΔCO time series over the whole flight, European emissions contribute 32.4% to ΔCO, Asia 64.4%, and North America 3.2% only. The modelled contribution of European CO emissions is homogeneously distributed throughout the time series whereas the contribution of Asian emissions is more localized into layers above 3.5 km (Fig. 3.10c). As a result, below 3.5 km, the European contribution to the anomaly represents 71%, but conversely the Asian contribution constitutes 71% of the ΔCO above this altitude. As an example, in the layer observed at 0330 UTC in Fig. 3.10c, CO from Asian sources has a 10-fold higher contribution than CO from European sources.

In their characterization of the mean transport of pollutants across Siberia, Newell and Evans (2000) show that maximum zonal flow is usually prevailing in winter and early spring, which is associated to a European footprint. Ramonet et al. (2002) identified European anthropogenic emissions to be the main contributor to the synoptic variability of CO_2 at an aircraft site located 300 km from Moscow. The April 2006 YAK-AEROSIB campaign data suggests that episodic and rapid transport of north-east Asian emissions can contribute to the mid and high Siberian troposphere composition, in addition to the zonal advection of European emissions. The delivery of pollutants to the Siberian troposphere by WCB airstreams could be underestimated in coarse resolution global Chemistry Transport Models, which do not capture correctly these synoptic events.

3.9.1.3 Limited chemistry in the plume

The O_3 concentrations in the polluted (CO>200ppb) air mass is in the range 55-60 ppb (Fig. 3.6c-f). It shows no correlation with CO (R^2 = 0.08). In addition we found evidence for enhanced (up to 2.10^{-2} cm^{-3} i.e. one order of magnitude above background) concentrations of fine particles (CCN aerosols) in these pollution layers from onboard instruments measuring particles with diameter d<200 nm (Arshinov et al., 2007). Coarse dust particles were not measured during the campaign. High concentration levels of fine aerosol particles, and potentially coarse particles, in the air stream might have led to additional O_3 destruction via heterogeneous reactions (e.g. Bonansoni et al., 2004).

3.9.1.4 Contributions of biomass burning and fossil fuel combustion

The elevated CO and CO_2 levels are consistent with a mix of urban pollution and biomass burning emissions (wildfires or agricultural fires). Several fires were detected in April 2006 in the

footprint of Flight 2 (see ATSR fire counts, red squares, on Fig. 3.3b-d and Fig. 3.10a,). According to FLEXPART simulations Flight 2 sampled CO and CO_2 from fire emissions from northern Mongolia (in the region 50°N and 105-120°E) and northern high latitudes in addition to heavy anthropogenic emissions from northern China. The CO/CO_2 regression slope ($S = 1.17\times10^{-2}$) in Flight 2 is consistent with a predominant contribution of anthropogenic emissions; this will be discussed in section 5.2.

3.9.2. Interpretation of CO/CO_2 ratio for selected cases

3.9.2.1 CO as a surrogate tracer for fossil fuel CO_2

We investigated whether CO can be used quantitatively to identify the fossil fuel component of CO_2, given that fossil fuel combustion emits both CO and CO_2 (see also e.g. Levin and Karstens, 2007; Gamnitzer et al., 2006, Rivier et al., 2006, Turnbull et al, 2006). The difficulty in using CO as a proxy of fossil fuel CO_2 is that the CO/CO_2 emission ratio varies spatially and temporally, according to the mix of combustion processes (from 1.38×10^{2} mol mol^{-1} for western northern hemisphere industrial processes to 6.83×10^{2} mol mol^{-1} for world average road transportation, according to the EDGAR inventory). For this study we use the ratio of CO to CO_2 in anthropogenic emissions as given by the EDGAR 3.2 Fast-Track 2000 dataset (Olivier et al., 2005). The average fossil fuel CO/CO_2 emission ratio is 1.08×10^{-2} mol mol^{-1} in Western Europe, compared to 2.13×10^{-2} in China (Table 3.3, see following section for a discussion on uncertainties). The CO/CO_2 emission ratio of biomass burning is higher than the one of fossil fuel combustion: $10.7\pm3.8\times10^{-2}$ for extratropical forest fires, $7.9\pm3.2\times10^{-2}$ for bio-fuel burning, $12.0\pm2.5\times10^{-2}$ for charcoal burning, and $9.5\pm8.8\times10^{-2}$ for agricultural residues burning (Andreae and Merlet, 2001).

The distribution of CO/CO_2 ratios in the global atmosphere results from 1) atmospheric transport which mixes the ratios of different emission sources, 2) secondary CO production from biogenic volatile organic compounds (BVOC) and atmospheric sinks of CO from OH oxidation which change CO but not CO_2, 3) terrestrial and oceanic surface CO_2 fluxes which change CO_2 but not CO.

In winter-times, the effect of processes 2) and 3) is limited. Note the significantly higher CO-CO_2 correlation for flight 4 which was sampled only in the morning, unlike the other April flights (see Table 3.2). Positive correlations between CO and CO_2 are frequently found at northern hemisphere stations (Potosnak et al., 1999; Rivier et al., 2006; Gamnitzer et al., 2006; Suntharalingam et al., 2004; Palmer et al., 2006). Potosnak et al. (1999) observed that using CO as a predictor for CO_2 was more effective in winter. In a northern hemisphere modelling study, Rivier et al. (2006) predicted ubiquitous wintertime correlations between CO and fossil CO_2. They also showed that the modelled scatter between CO and fossil CO_2 was caused by advection of air masses with different CO/CO_2 emission ratios (see their Fig. 6).

Table 3.3. CO/CO_2 ratio for regional emissions and $\Delta CO/\Delta CO_2$ as measured during theYAK-1 campaign. Units are $\times 10^{-2}$ mol mol^{-1} for EDGAR emissions and $\times 10^{-2}$ ppm ppm^{-1} for the measurements. The EDGAR ratio uncertainties are given in the 95% confidence interval.

CO/CO_2, *EDGAR* ($\times 10^{-2}$)		
China[1]	2.13 ± 2.20	
Europe[2]	1.08 ± 0.50	
$\Delta CO/\Delta CO_2$, *Our data* ($\times 10^{-2}$)		
Flight 2, <3km	0.66	
	CO>200 ppb	**CO<200 ppb**
Flight 2, Profiles 7-8	1.25	0.69
Flight 3, Profiles 1-4	1.39	0.52
Flight 2, Profile 6, in high CO plume	1.94	-

[1] Average over the region bracketed in latitude by [25N 52N] and in longitude by [80E 135E].

[2] Average over the region [35N 65N], [10W 55E].

3.9.2.2 CO/CO_2 ratios during Flights 2 and 3 and source attribution

One can decompose the CO_2 and CO concentration as the sum of the background value (determined as in section 4) and an anomaly called ΔCO_2 and ΔCO respectively. We regressed the observed value of ΔCO as a function of ΔCO_2 for all flights (see Fig. 3.9 and Table 3.2 for correlation coefficients). In the April campaign, there is a significant positive correlation between ΔCO and ΔCO_2, with a clear distinction between data above and below 3.5 km (for Flight 2 $R^2 = 0.58$ below 3.5 km and $R^2 = 0.55$ above). Above 3.5 km in April Flights 2 and 3 (Fig. 3.9b-c), the regression slope is clearly higher than for Flight 1 and 4 (Fig. 3.9a and 9d), and also higher than below 3.5 km for the same flights. The $\Delta CO/\Delta CO_2$ linear regression slopes are 6.8 and 11.3 ppb/ppm respectively below and above 3.5 km. This high, positive CO-CO_2 correlation coefficient suggests that the contribution of natural CO_2 fluxes and photo-chemical CO sinks to this flight is small. This is further confirmed by combining the CO_2 Net Ecosystem Exchange (NEE) fluxes calculated by the ORCHIDEE process-based ecosystem model (Krinner et al., 2005) at 0.4 by 0.4° in April 2006 with the FLEXPART footprints. For the entire April 2006 YAK-AEROSIB campaign, we found that the contribution of NEE is negligible relative to anthropogenic fluxes: -0.5% for Europe (i.e. small biospheric uptake) and +1.1% for Asia relative to fossil fuel emissions. Thus, neglecting the impact of natural CO_2 sources to the vertical variability in the April profiles, ΔCO_2 can be expressed from ΔCO by:

$$\Delta CO_2(\text{obs}) = \Delta CO(\text{obs}) * S^{-1} + \text{constant} \qquad (1)$$

where the constant term represents the background CO_2 component, assumed to be vertically uniform in each profile. For the situation of Flights 2 and 3 we assumed that, in presence of fast horizontal transport of remote emissions and comparatively lower vertical mixing, the value of S reflects the ratio of fossil fuel emissions, weighted by the emitted flux over each grid point (see Gamnitzer et al., 2006). Using the EDGAR 3.2 Fast-Track 2000 fossil fuel CO and CO_2 emission maps, the emission ratio are $S = 2.13\times10^{-2}$ mol mol^{-1} for China, $S = 1.08\times10^{-2}$ mol mol^{-1} for Europe. Thus, the *ratio* of Chinese emissions CO/CO_2 ratio to the European CO/CO_2 is 1.97. In the YAK-AEROSIB data, the ratio of Asian (above 3.5 km) to European (below 3.5 km) CO/CO_2 ratios in the Eastern part of the campaign is 1.8.

3.9.2.3 Analysis of errors

The ratio of European to Asian $\Delta CO/\Delta CO_2$ in the YAK measurements is consistent with that of emission inventories. However, the values of the $\Delta CO/\Delta CO_2$ slope S determined from the YAK measurements are half the values given by inventories (Table 3.3). Significant error sources in the inventories propagate to the slopes. We computed a 95% confidence uncertainty for Asian and European emission CO/CO_2 slopes using a Monte Carlo analysis. We assume a weak correlation (R^2=0.1 as suggested by Palmer et al., 2006) between CO and CO_2 emission uncertainties, due to the presence of correlated error sources in the underlying emission factors and activities. A rough estimate of the error for CO and CO_2 Asian emissions is 50% and 20% respectively (Streets et al., 2003), and for European emissions of 30% and 10% respectively. The Monte-Carlo simulation gives emission CO/CO_2 slopes $S = 2.1 \pm 2.2 \times 10^{-2}$ mol mol^{-1} for Asian and $1.1 \pm 0.50 \times10^{-2}$ mol mol^{-1} for Europe.

Into the polluted air masses of Flights 2-3 where CO > 200 ppb, we determined $S = 12.5$ ppb/ppm for Flight 2 (profiles 7-8, and $S = 13.9$ ppb/ppm for Flight 3 (profiles 1-4). Taking only data inside the plume of profiles 6-7 of Flight 2 at 5 km altitude (Fig. 3.6c) we obtain $S = 19.4$ ppb ppm^{-1}. All these values are given in Table 3.3. Therefore, the more we restrict the CO data selection towards elevated values representative of polluted air masses, the better agreement is found for S between atmospheric data and inventories, and the more accurate our discrimination of Asian vs. European emissions. This suggests that the $\Delta CO/\Delta CO_2$ signal is significantly diluted 1) as a methodological flaw when averaging over distinct air masses, and 2) physically when mixing with the surrounding air takes place. This dilution can result in lower $\Delta CO/\Delta CO_2$ ratio because the enhancement relative to background is higher for CO than for CO_2.

The precision of our method, based on deviation from background concentration, is affected by other factors, such as the absence of simple (e.g. marine) background. However the *ratio* between S in the lower and S in the upper part of the profiles is consistent with the retro-transport analysis of a dominant Chinese pollution influence above 3.5km, and of a dominant European origin below that altitude. Due to limited mixing, the conservation of CO/CO_2 ratios in the YAK easternmost flights was similar to that of the TRACE-P flights with high (R^2>0.7) CO-CO_2 correlations at all altitudes analyzed by Suntharalingam et al. (2004), which allowed Palmer et al.

(2006) to use CO-CO_2 error covariance for better separating Asian fossil from biogenic CO_2 fluxes. Under most common conditions, CO/CO_2 ratio is not a conservative tracer. The uplift situation of April 2006 was specifically favourable to preserve high CO/CO_2 correlations over long distances because: 1) there was no biotic CO_2 sinks in Siberia at this time of the year, 2) the air mass was sampled after uplift, before being homogenized and mixed by transport, and thus contained a well defined CO/CO_2 signature.

3.10. Conclusion

The set-up and preliminary results of two YAK-AEROSIB aircraft campaigns across Siberia in April and September 2006 have been presented. Each campaign comprises four flights and a total of 26 vertical profiles spaced by 200 km between 0 and 7 km. We report here on the in-situ measurement of CO_2, CO and O_3. The April 2006 campaign was characterized by a slow zonal flow, and the influence of Siberian cities and remote Asian emissions in the vertical profiles. The September 2006 campaign was dominated by meandering zonal flow, variable synoptic conditions and a descent of arctic air in the boundary layer (BL). Both CO_2 and CO values were very high in April 2006 (respectively 385-390 ppm and 160-200 ppb) due to both near-ground accumulation of Siberian cities emissions, and long-range transport in the middle troposphere. The lowest CO_2 concentration values were observed in the BL during September, which support the view of a strong biospheric CO_2 sink in Siberia at that time of the year. The next step will be to analyze the CO_2 data within a regional inverse model (Lauvaux et al., 2008) in order to exploit quantitatively the information contained in the CO_2 gradients.

In the free troposphere (FT), the O_3 concentrations were much more homogeneous than those of CO_2 and CO across the whole aircraft transect. In April O_3 values smoothly increased with altitude up to the flight ceiling. In September a 20 ppb gradient of O_3 was observed between the FT and the ozone-depleted BL. This gradient is likely due to O_3 deposition over the forests and to a stronger late summer turbulent mixing. The relationships between O_3 and CO (indicator of O_3 precursors) analyzed from the April 2006 campaign have not shown important active photochemistry from regional fresh emissions. Relatively high O_3 levels (50-65 ppb) in the FT (both in April and September) reflect the global northern hemisphere O_3 enhancement.

The mid troposphere in the eastern part of the April campaign exhibited very high CO and CO_2 values. Analysis of this air mass using back-trajectories and a Lagrangian transport model revealed the effect of a sequence of baroclinic perturbations followed by stagnant conditions in the middle troposphere. This led to the fast injection and persistence for several days over Siberia of thin layers of polluted air originating from north-eastern Asian sources. The export of Asian pollution to the East through the Pacific Ocean at mid-latitudes is partially driven by cold front uplift (see e.g. Mari et al., 2004). This export pathway has been extensively documented (see e.g. Jacob et al., 2003; Suntharalingam et al., 2004), contrarily to the northward transport of Asian

emissions towards Siberia. Our observations has shown that the advection of BL air exposed to Asian emissions and uplifted Warm Conveyor Belt contributed significantly to the CO_2 and CO enhancement of the upper Siberian troposphere during April 2006. This case of export pattern deserves further investigation, especially using chemistry – transport modelling.

CO has been suggested as a tool for separating the fossil CO_2 component in the observed total CO_2 signals. In our study we have been able to use CO/CO_2 ratio in the free troposphere, even far from the emission regions, as a quantity representative of surface emissions characteristics. Therefore, under specific conditions, atmospheric CO/CO_2 ratios could be used for separating source regions with contrasted emission ratios, like Asia and Europe. In September, with more active chemistry and production of CO from VOCs, this property was no longer valid.

Chapitre 4.
Relations source-récepteur pour les mesures de gaz trace

Ce chapitre est dans la continuité du précédent en ce qu'il interprète la variabilité des gaz traces mesurés durant les campagnes. Les trois premières campagnes YAK-AEROSIB représentent au total environ 70h de mesures continues de CO_2, CO et O_3. L'analyse des données repose ici sur une technique de clustering des fonctions d'influence (ou « rétropanaches ») obtenus avec le modèle lagrangien de dispersion de particules FLEXPART. Il est montré que cette technique est capable de séparer efficacement les concentrations de traceurs de manière indépendante. Fondamentalement, la technique exploratoire de clustering permet de tester l'hypothèse selon laquelle deux mesures de concentrations différentes sont expliquées par des différences entre la répartition géographique de leur sensibilité à des émissions de surface. Pour valider la technique, je vérifie que deux mesures attribuées à des clusters différents auront des concentrations différentes. Ensuite une analyse cluster par cluster est possible et permet de dégager les grandes zones qui influencent les concentrations de CO_2, CO et O_3 en Sibérie. Le résultats principal est que d'une part les émissions européennes peuvent se combiner avec des émissions de feux de forêt en Asie Centrale pour contribuer fortement à la charge de CO présente en Sibérie, et que d'autre part cet export d'air européen a été identifié non pas dans la couche limite mais dans la moyenne troposphère.

4.1. Contexte

4.1.1. Relier les mesures de concentrations aux émissions à l'aide d'un modèle lagrangien

Dans ce chapitre je m'attache à différentes questions liées à l'attribution de sources pour les concentrations mesurées au dessus de la Sibérie. La contribution de chaque source ou région source dépend de trois facteurs : (i) le transport associant la région émettrice et la concentration au récepteur, (ii) le flux d'émission des espèces concernées (ou des précurseurs des espèces concernées) dans la région, et (iii) les pertes ou la création de cette espèce durant le transport. Le transport lui-même influence la relation source-récepteur de deux manières : (i) le transport direct sous forme de panache (clairement identifiable par exemple par un excès marqué de l'espèce dans des mesures effectuées sur un profil atmosphérique) et (ii) par la contribution de la source à la concentration de fond de l'espèce, qui ne peut être attribuée à un panache particulier. Dans le cas de la pollution européenne, il s'agira plutôt d'un transport du deuxième type en l'absence de panaches particuliers, dû au mélange vertical affectant les masses d'air durant la circulation zonale.

Un premier objectif de l'étude présentée dans ce chapitre est de tester l'hypothèse (prédite par les modèles ; Wild et al., 2003 ; Stohl et al., 2002 ; Duncan & Bey, 2004 ; Liu et al., 2002) selon laquelle l'advection des polluants européens au dessus de la Sibérie se produit dans la basse troposphère. Cette hypothèse est testée par une analyse de l'ensemble des données à l'aide de rétropanaches, c'est-à-dire l'équivalent de panaches se dispersant en temps inverse à partir du récepteur, vers d'éventuelles sources. Ces rétropanaches sont simulés par le modèle de dispersion lagrangien (LPDM, *lagrangian particle dispersion model*) FLEXPART. La technique de clustering des rétropanaches introduite dans ce chapitre permet de faire émerger les grandes régions affectant les concentrations observées en Sibérie. Un certain nombre de régions est examiné ainsi, définies entre autre selon l'importance des émissions qui y ont lieu (comme par exemple en Europe ou en Chine du nord-est).

A travers l'établissement de relation source-récepteur focalisées sur le transport, je m'attache à identifier la contribution des sources anthropiques européennes (incluant la Russie occidentale) aux concentrations de CO_2 et de CO. D'autres sources anthropiques peuvent également contribuer significativement aux excès de polluants au dessus de la Sibérie, comme nous l'avons démontré dans le chapitre précédent avec le cas des émissions chinoises en avril 2006. Ceci peut également être évalué à l'aide du même type d'analyse.

Les émissions anthropiques peuvent être renforcées par des émissions liées aux feux de forêt ou plus généralement de biomasse. La contribution de ces émissions aux concentrations en CO_2, CO et O_3 est mal connue en ce qui concerne la Sibérie. La végétation pouvant émettre du CO_2 lors d'incendie est également alternativement un puits et une source de CO_2 naturellement de par le processus de photosynthèse. En cumulant le temps de résidence des rétropanaches sur 10 jours il est possible d'avoir accès à un proxy de la production nette de l'écosystème.

Cette étude bénéficie de trois campagnes effectuées à différentes moments de l'année (avril, aout, septembre). Une variabilité saisonnière des relations entre sources potentielles et

concentrations observées peut donc être esquissée à partir des campagnes. Une variabilité saisonnière des concentrations en CO_2, CO et O_3 pourra alors être attribuée à des variations du transport atmosphérique.

4.1.2. Technique de clustering pour le transport

La technique de clustering est utilisée ici comme un outil permettant d'explorer l'information contenue dans les rétropanaches et d'associer ainsi les observations à des sources de surface. Le clustering est basé sur la sensibilité aux émissions potentielles (PES, *potential emission sensitivity*), information dérivée des rétropanaches calculés par FLEXPART. La PES est proportionnelle au temps de résidence à proximité de la surface des particules émises par le modèle. Ainsi si la zone où se trouve un grand nombre de particules émet par exemple une quantité importante de CO, la concentration amont (simulée au récepteur), sera augmentée en proportion.

L'application du clustering non pas à des rétropanaches mais à des rétrotrajectoires a été beaucoup utilisé pour analyser les mesures de composition atmosphérique. Cette technique s'est avérée capable de séparer efficacement des masses d'air différentes ayant des propriétés différentes (Moody & Galloway, 1988 ; Dorling et al., 1992 ; Sirois & Bottenheim, 1995 ; Eneroth et al., 2003). Moody & Galloway (1988) ont appliqué cette technique pour évaluer la déposition humide de composés acides au dessus des Bermudes. Le clustering de rétrotrajectoires a été utilise à l'échelle continentale pour obtenir des relations sources récepteurs pour les concentrations d'O_3 en Sibérie centrale. Ceci a permis d'étayer l'hypothèse que le CO était plus élevé dans les masses d'air influencées par les émissions européennes (Pochanart et al., 2003). Dans le cadre de mesures aéroportées, Traub et al. (2003) ont utilisé les rétrotrajectoires pour analyser un volume important de mesures à travers plusieurs campagnes.

Contrairement aux rétrotrajectoires, les modèles lagrangiens de dispersion de particules prennent en compte la dispersion atmosphérique et la turbulence (Stohl et al., 1998). Han et al. (2005) ont comparé le résultat d'attribution de sources à l'échelle régionale en utilisant des rétro-trajectoires simple et des rétropanaches (dispersion inversée). Le LPDM s'est avéré plus efficace à identifier les sources régionales. L'utilisation de LPDM a été appliquée avec succès dans plusieurs domaines. Elle a été proposée (Gerbig et al., 2003b; Lin et al. 2003) et démontrée (Lauvaux et al., 2008) pour les inversion de flux de surface de CO_2 à l'échelle « méso » (inférieure à la centaine de kilomètres) et régionale (inférieure au millier de kilomètres).

4.2. Résumé

Cette analyse est basée sur les trois premières campagnes YAK-AEROSIB. Une technique de clustering est appliquée aux rétropanaches simulés avec le modèles FLEXPART. La technique de clustering a permis d'identifier de fortes concentrations de CO et d'O_3 en relation avec des émissions situées au Kazakhstan en Septembre 2006, époque durant laquelle on observe

d'importants feux de biomasse. Une forte corrélation (jusqu'à R^2 = 0.68) et une relation linéaire robuste avec des pentes de régression comprises entre -0.10 et 0.24 ppb ppb^{-1} ont été observées dans des panaches individuels. La réduction de la concentration de CO_2 en été (aout 2007, Septembre 2006) est largement expliquée (~50%) par l'exposition aux écosystèmes boréaux et subarctique. Ceci génère un gradient de CO_2 de 5 à 10 ppm entre la couche limite et la troposphère libre durant la campagne d'aout 2007. Les émissions européennes semblent contribuer à des concentrations élevées d'O_3 au dessus de la Sibérie en altitude en combinaison avec une influence stratosphérique. Les processus de déposition à grande échelle réduisent la concentration en O_3 dans la couche limite boréale et subarctique, résultant en un gradient de -20 ppb en moyenne entre la couche limite et la troposphère libre.

Cette première tentative de clustering de rétropanaches est très prometteuse et pourrait également être appliquée à l'interprétation de mesures de surface.

4.3. Article

Source-receptor relationship for CO_2, CO and O_3 measurements in the troposphere above Siberia. Manuscrit préparé pour soumission prochaine à *Atmospheric Chemistry and Physics* par Jean-Daniel Paris, Andreas Stohl, Philippe Ciais, Philippe Nédélec, Boris Belan, Mikhail Arshinov et Michel Ramonet.

We analysed three intensive campaigns above Siberia resulting in a total of ~70h of continuous CO_2, CO and O_3 measurements. The flight route consists of consecutive ascents and descents between Novosibirsk (55°N, 82°E) and Yakutsk (62°N, 129°E). Our data analysis uses clustering of footprints obtained with the Lagrangian particle dispersion model FLEXPART. The model-based technique was found to be able to separate efficiently tracers' concentrations. High CO and O_3 concentrations (median values 121 ppb and 54.5pb respectively) were found in clusters associated with fires in Kazakhstan in September 2006. High correlation (as high as $R^2 = 0.68$) and robust linear relationships with regression slope between -0.10—0.24 ppb ppb^{-1} were found in individual plumes. Summer (August 2007, September 2006) uptake of CO_2 was found to be largely (~50%) explained by exposure to boreal and sub-arctic ecosystems, most likely by photosynthesis. This results in an average 5-10 ppm gradient between the boundary layer and the free troposphere throughout the August 2007 campaign. European emissions seem to contribute to high O_3 concentrations above Siberia in altitude were it is also near stratospheric inputs. Large-scale deposition processes reduce O_3 in the boreal and sub-arctic BL, resulting in a ~20 ppb gradient between the boundary layer and the free troposphere. This first attempt of Lagrangian footprint clustering is very promising and could also be advantageously applied to the interpretation of ground based measurements including calculation of tracers' sources and sinks.

4.4. Introduction

Three airborne campaigns were made across Siberia in April 2006, September 2006 and August 2007 respectively. Numerous vertical profiles of CO, CO_2, O_3 and aerosols were collected, allowing a 'tomography' of the Siberian troposphere at different times of the year. After introducing the new data set, we present a clustering analysis of the tracers' concentrations based on partitioning of footprints obtained with a Lagrangian particle dispersion model (LPDM).

Atmospheric transport can occur both at low altitude in the boundary layer and in the free troposphere, where it can be much faster. Mid-latitude cyclones are responsible for a large part of the pollutant transport into the mid-latitude free troposphere (Cotton et al., 1995, Stohl, 2001). To a large extent, export of North-East Asian and North American emissions is associated with strong uplift in the warm conveyor belts of these mid-latitude cyclones (e.g Cooper et al., 2001; Hess and

Vukicevic, 2003; Liang et al., 2004; Owen et al., 2006). On the opposite, European emissions have a tendency to remain in the lower troposphere and are most frequently channelled to the Arctic or to Siberia (Wild et al., 2003; Stohl et al., 2002; Duncan and Bey, 2004, Stohl et al., 2007; Law and Stohl, 2007; Liu et al., 2002). Precursors transported from Europe produce 2-4 ppb O_3 over Siberia in spring and 2-6 ppb in summer (Wild et al., 2003; Duncan and Bey, 2004). However, faster zonal advection occurs in winter and early spring in association with the Siberian High (Newell and Evans, 2000; Wild et al., 2003; Liu et al., 2002). In April, European pollutants can be mixed in significant amount with the Asian outflow to the Pacific (Liu et al., 2003). This European pollutant export increases with latitude: in the northern Asian outflow toward north Japan (at 40°N), anthropogenic European CO enhancement can be very high in winter (~40-50 ppb), although marginal in summer (Liang et al., 2004). Interannual variations of transport patterns across Eurasia are modulated by the North Atlantic Oscillation (Eckhardt et al., 2003).

Pollutant export to or across Siberia, however, has been studied almost exclusively through modelling studies and lacks measurement-based assessment. Pochanart et al. (2003) has conducted ground based measurements supported by transport model analysis, showing that European emissions lead to a 1-4 ppb increase in O_3 near Baikal Lake. Eneroth et al. (2003) have shown that European emissions were not the cause of the highest CO_2 concentrations in the lowest 3 km, but that stagnant flow conditions were responsible of respiration build-up leading to high concentrations. But both measurements of CO_2 and pollutant distribution are still required over Siberia, along with the possibility to relate them to potentially remote emission sources i.e. source-receptor relationships (SRR).

Aircraft measurements only provide a snapshot of the atmosphere at a particular time, but they have the potential to explore transport processes and impact across transported plumes (Takegawa et al., 2004; Fehsenfeld et al., 2006; Stohl et al., 2007b; Methven et al., 2006; Real et al., 2007) or in the outflow of massively emitting regions (Jacob, 2003). Anderson et al. (1996) successfully reconstructed the seasonal cycle of CO_2 in the upper troposphere based on airborne campaigns. Here we investigate data from three recent YAK-AEROSIB intensive airborne campaigns that sampled the Siberian troposphere at different times of the year (Paris et al., 2008). The present study includes a new data from the August 2007 campaign and makes use of a clustering of SRR from a backward Lagrangian particle dispersion model.

Contrarily to single back-trajectories, the SRR obtained from a LPDM accounts for the atmospheric turbulence and convection (Stohl et al., 1998). Han et al. (2005) compared the result of regional source apportionment using single backtrajectories and backward dispersion. Their backward dispersion model added individual turbulence-related stochastic component to a large number of HYSPLIT backtrajectories. They demonstrated the better ability of LPDM to identify regional point sources of reactive mercury. Use of LPDM has been proposed (Gerbig et al., 2003b; Lin et al. 2003) and eventually demonstrated (Lauvaux et al., 2008) for meso- to regional-scale inversion of CO_2 surface fluxes. Clustering of backtrajectories has been widely used for the analysis of atmospheric composition measurements at fixed observatories and have been found to be an efficient method for separating air masses with different properties (Moody and Galloway, 1988,

Dorling et al., 1992, Sirois and Bottenheim, 1995, Eneroth et al., 2003). Moody and Galloway (1988) were the first to attempt clustering of back-trajectories in order to assess the wet deposition of acid compounds over the Bermuda. Clustering of back-trajectories has been used at the continental scale to derive SRRs for O_3 concentrations in central Siberia and supported the conclusion of elevated CO in air masses influenced by European emissions (Pochanart et al., 2003). Traub et al. (2003) applied a simple back-trajectories' partitioning technique to the extensive analysis of measurements obtained from an aircraft. No attempt has been made yet, to our knowledge, to use a clustering technique based on LPDM footprints.

In the present study we focus on the extent to which the map of potential emission sensitivity (PES) for a given receptor position relate to the air mass chemical composition at this receptor. The PES is expressed here as a residence time. We try to answer the following questions: (i) is it possible to identify the contribution to CO_2 and CO concentrations of European or other remote anthropogenic sources predicted by models? (ii) Is it possible to identify contributions from forest fire or from other types of biomass burning? (iii) To what extent can we explain the seasonal variability in CO_2, CO and O_3 concentrations by variations in atmospheric transport patterns through intensive campaigns? (iv) Is there a consistent signal about the regional carbon source/sink distribution emerging through model analysis of CO_2 concentrations?

Section 2 describes the experimental details and provides model and statistical tools description. Section 3 describes the variability of CO_2, CO and O_3 observed above Siberia during the three campaigns. In Section 4 we discuss, using cluster analysis, the tracer concentrations observed in selected flights. Section 5 investigates the 'seasonal' (inter-campaign) variation of the connection between source regions and trace gas concentrations over Siberia.

4.5. Data and Methods

4.5.1. Campaigns overview and Instruments

Intensive campaigns took place over Siberia between 11 and 14 April 2006 (YAK-1), between 7 and 10 September 2006 (YAK-2) and between 17 and 20 August 2007 (YAK-3). The airborne platform is an Antonov-30 dubbed "Optik-E" chartered by Tomsk Institute of Atmospheric Optics that has been used for various campaigns since the 1990's. It was equipped in collaboration between French and Russian laboratories for the measurement of CO_2, CO, O_3, aerosols and meteorological parameters. The flight route consists in a large, continental-scale loop from Novosibirsk in central Siberia to Yakutsk in eastern Siberia (see Figure 4.1) that is done in four days. The flight route is repeated with minor modifications during each campaign. Flights were conducted in all weather conditions. Thick cloud decks were flown over instead of conducting normal ascent and descent through them. Profiles are collected as often as possible as the flight

tracks consist mainly of ascents up to 7 km altitude and descents. Each intensive campaign comprises 4 flights of up to 8 hours limited by refuelling needs, over 3 days of actual flight.

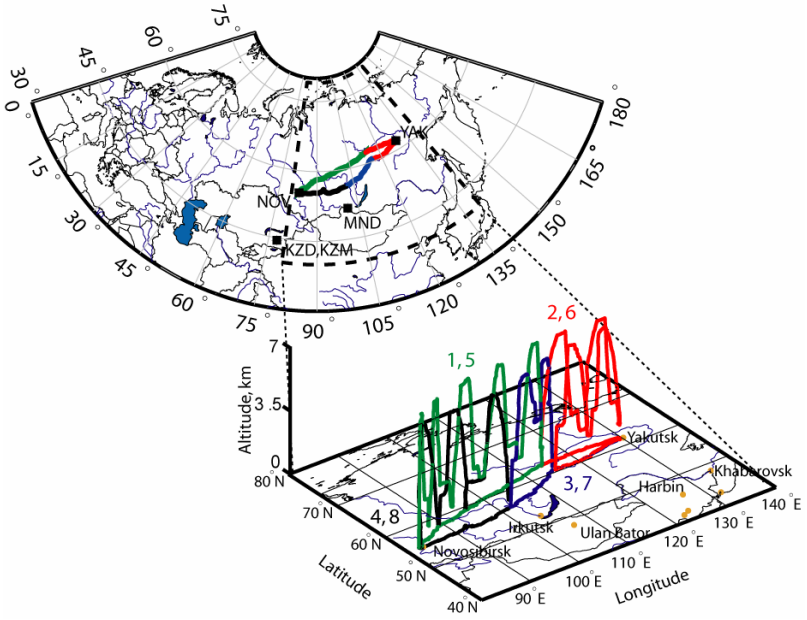

Figure 4.1. Aircraft itinerary (top panel) and vertical flight pattern (bottom panel). Each campaign followed a similar itinerary. The different flights of each campaign (four each, typically one per day) are shown by different colors.

The April campaign was dominated by stagnant flow conditions and low surface temperatures (Paris et al., 2008), with most of the ground covered by snow. In contrast, the September 2006 and August 2007 campaigns were characterized by westerly flow, warmer and highly variable temperatures, and significant frontal activity in the flight area.

Detailed instrument descriptions can be found in Paris et al. (2008); we give here only a short description. CO_2 is measured by a modified Non Dispersive Infrared Analyser based on a commercial Li-Cor 6262, with accuracy and precision of 0.15 ppm, obtained by periodical in-flight calibration against WMO-referenced reference gases bracketing atmospheric concentrations, and regulation of pressure, temperature and flow in the cells. CO is measured by IR absorption gas correlation with an accuracy of 5 ppb or 5%. The instrument is based on a commercial infrared absorption correlation gas analyser (Model 48C, TEI Thermo Environment Instruments, USA; Nedelec et al., 2003). O_3 is measured by a modified UV commercial fast response ozone analyser (Thermo Instruments Model 49) with a precision of 2 ppb, 2% for an integration time of 4 sec.

4.5.2. Atmospheric backward transport model

Atmospheric transport was investigated using the FLEXPART v6.2 Lagrangian particle dispersion model. FLEXPART calculates the trajectories of tracer particles using the mean winds interpolated from the analysis fields plus random motions representing turbulence (Stohl and

Thomson, 1999). Results presented here use ECMWF analysis fields, although both ECMWF and GFS (NOAA/NCEP) fields were used for a prior assessment of transport error. For moist convective transport, FLEXPART uses the scheme of (Emanuel, 1999), as described and tested by (Forster et al., 2007). A backward simulation mode is available, described in more detail by Stohl et al. (2005) and Seibert and Frank (2004). Here the backward method is used to analyse transport pathways from potential flux regions to the receptor position. Each simulation consists of 40000 particles released whenever the aircraft has moved 0.15° in latitude or longitude, or 10 hPa in altitude. This corresponds to about one minute of sampling or to a layer ~ 100 m thick during ascent or descent). Released particles were followed 10 days backward in time. Gridded PESs in three vertical levels (0-300m, 300-3000 m, and 3000-50000m) are stored at 1°x1° resolution every 24 h. The fraction of stratospheric air is recorded as the percentage of all particles originating from the stratosphere. Results are available at http://zardoz.nilu.no/ ~andreas/YAK/.

4.5.3. Cluster analysis

Airborne campaigns can deliver detailed information on the atmospheric state at a particular time. To generalize this information and to organize the YAK-AEROSIB data set, a method is sought that groups the data according to common transport properties. Cluster analysis is such an exploratory tool, which sorts multivariate data into groups as dissimilar as possible but whose properties are not known a priori. We seek to investigate to which extent footprints can explain the air mass chemical composition in CO_2, CO and O_3. Footprints are implemented as 10-days summed spatial distribution of PES (proportional to potential emission sensitivity) obtained from FLEXPART, complemented by 10-days averaged relative contributions from the stratosphere, defined as the region with potential vorticity > 2 PVU. To facilitate analysis we have reduced the number of variables from the gridded PES by further summing these PES over large regions of interest for our study (Fig. 2). A vector $\mathbf{x}_j = \left[\sum_{d=1}^{10} r_{1,j}, \sum_{d=1}^{10} r_{2,j}, \ldots, \sum_{d=1}^{10} r_{M,j} \right]^{\mathbf{T}}$ of daily PES r_k in box m (m=1, 2, …, M) is associated with each consecutive receptor position j. This time series $\mathbf{x}j$ will constitute our set of j realizations of M variables to cluster. Defining j over a single campaign improves the separation capability of the algorithm, whereas defining j over the three campaigns allows inter-campaign comparison.

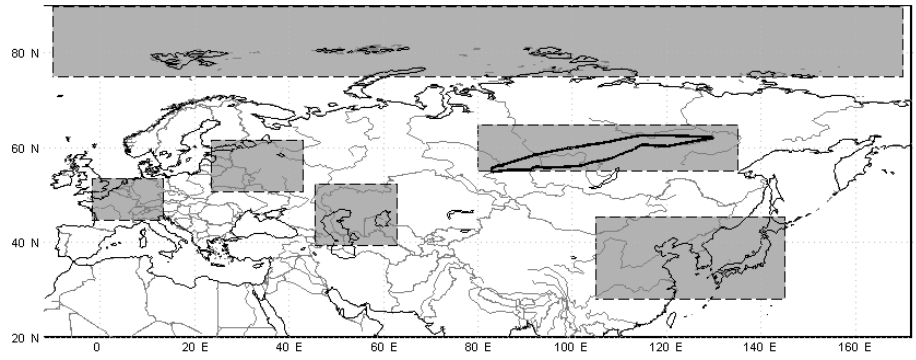

Figure 4.2. Regions chosen for data reduction prior to the clustering analysis. The thick black line shows the itinerary of the aircraft.

The M boxes are identified a priori as regions with specific sources or sink for the species relevant to this study. Such identification is based either on case studies from the April and September 2006 campaigns in Paris et al. (2008), or on the questions to be addressed with this dataset, such as the transport of European emissions to Siberia. The regions identified are:

- Europe: European pollutant emissions and outflow;
- Western Russia: European Russian pollutant emissions and outflow;
- NE China, Japan and Koreas: extratropical cyclones can lift NE Asian pollutant over central or eastern Siberia (Paris et al., 2008);
- Central Asia: Central Asia has a different ecosystem and low anthropogenic sources but it is a potential source of biomass burning (e.g. van der Werf et al., 2006);
- Arctic: Arctic air from beyond the Arctic front can be observed over Siberia during cold air outbreaks;
- Local region: covers the area directly flown over by our aircraft;
- Stratosphere: An extra variable is added which averages the 10-day proportion of stratospheric particles.

The boxes' geographical extent is the result of a trade-off between maximizing differences between transport from the various boxes, and an insufficient number of particles if boxes are chosen to be too small. There are large regions not covered by any box. Theoretically, this could mean that a footprint is located entirely outside all of the boxes. However, the footprints normally cove quite large regions, so they always overlap with one or more of the boxes. By separating the boxes from each other, differences between the various footprints can be maximized by the clustering algorithm. Choosing boxes that are contiguous make the separation more sensitive to horizontal transport error and associated PES less contrasted.

Regions more remote are less connected (few or no particles reaching the region) by transport to the measurements. As a result, remote regions' average footprint distributions are skewed toward 0. To account for this skewness and different region sizes, normalization is applied to the regions' average footprint time series $\mathbf{x}$ according to $\mathbf{x}_N = \left(\mathbf{x} - p_{0.05}\right)/\overline{\mathbf{x}}$ where $p_{0.05}$ is the

5th percentile of **x** and was found to optimally separate clusters. The robustness of data reduction into regions and data normalization was tested by running the clustering algorithm for varying region sizes, locations and number of regions (bootstrapping), and various normalization functions.

The K-means algorithm implemented in the MATLAB software's Statistics toolbox is used for clustering. K-means is a classic partitioning (non-hierarchical) algorithm (see e.g. Wilks, 2006) which attempts to separate observations into a fixed number of groups. (1) It defines *K* centroids with initial random position vector of size $M = 7$ (number of regions); then (2) associates each point $\mathbf{x}j$ to the nearest (in Euclidian metrics) cluster centroid, (3) moves the centroid to the centre of the cluster and (4) repeats steps 2 and 3 until convergence is achieved. In the process, any empty cluster is discarded. In order to maintain the number of clusters, a point having maximum distance to its centroid is singled out and declared centroid of a new cluster.

Figure 4.3 shows the 'silhouette' index ($S \in [-1, 1]$), a measure of the separation capability of the clustering, as a function of the chosen number of clusters. The S index is defined as:

$$S = \frac{1}{N}\sum_{i=1}^{N}\frac{d_{nearest} - d_{centroid}}{\max(d_{nearest}, d_{centroid})} \quad (1)$$

with N number of points, and where point *i* has a distance of to the nearest cluster d_{nearest} and distance to its associated centroid d_{centroid}. The S index informs about how close a point is to its cluster's centroid, relative to the other nearest cluster centroid (Matlab R2006b documentation, Statistics toolbox, http://www.mathworks.com/ access/helpdesk/help/ toolbox/stats/ silhouette.html). The minimum number *k* of clusters was found to be optimally set to 6 in the global clustering option, and 4 in the campaign by campaign option (Fig. 4.3).

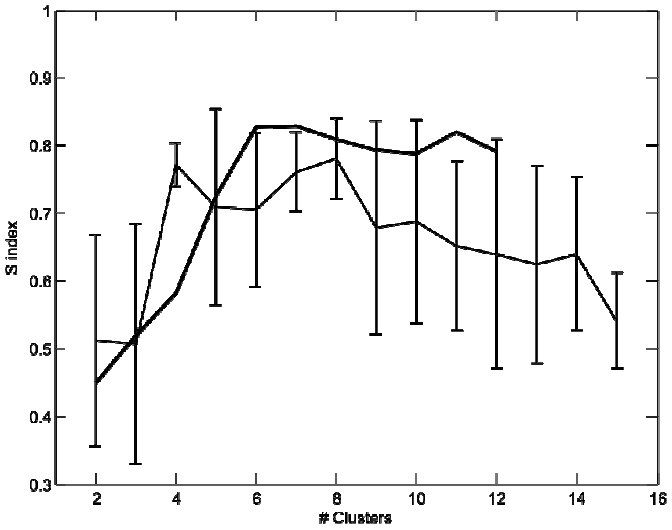

Figure 4.3. S index of the clustering algorithm separation capability as a function of the number of clusters for all data (thick line) and separated campaign by campaign (thin line with error bars showing ±1 std dev)

As the clustering algorithm is sensitive to a priori (random) position of the centroids, the process is repeated 20 times and the result optimizing the separation between centroids is retained. This also ensures a very high confidence in reproducibility of cluster centroids determination. The normalization and the metrics were also found to have a strong impact on the result. In this respect, cluster analysis is not an objective classification technique as the criteria set for the clustering have to be determined subjectively.

4.6. Campaign observations

4.6.1. CO_2 measurements over Siberia

Fig. 4.4a, 4.4d and 4.4g show the observed CO_2 concentrations averaged for each of the 4 flights of each campaign. Among the seasons chosen for our surveys, the minimum BL CO_2 concentrations have been observed in August, namely 366 ppm on average in the lowest 1 km during flight 12 (Fig. 4.4g). Flight 12 occurred mostly over a forested region, with sparse agricultural landscapes and industrial centres (Kemerovo, Novosibirsk) nearby. This CO_2 concentration minimum would be even lower compared to the other campaigns if we would correct the data for the trend in atmospheric CO_2 due to global anthropogenic emissions of ~1.4 ppm yr-1, since this campaign was carried out in August 2007, and the others in April and September 2006. This minimum CO_2 concentration is coincident with a very high BL top (up to 4 km asl, about 3.5 km agl), as deduced from humidity and CO_2 gradients. In the free troposphere, CO_2 was 377—379 ppm in August 2007, comparable (up to the interannual trend) to the 377—378 ppm in September 2006 but much lower than April 2006 (387—388 ppm), reflecting the hemispheric CO_2 seasonal cycle. CO_2 in April 2006 was as high as 392 ppm in filaments of fast lifted pollution encountered at 5—6 km altitude (Paris et al., 2008).

4.6.2. CO and O_3 measurements over Siberia

Figure 4.4b show the average profiles of CO concentrations for each flight during campaigns 1. Throughout the YAK-1 campaign the vertical average CO concentration was 173 ppb. Elevated CO concentrations were repeatedly observed and a warm conveyor belt uplifted a polluted air mass with CO up to 220 ppb from NE China above Siberia (Paris et al., 2008). Figures 4c show the average O_3 profiles during campaign 1. The O_3 profile shows a gradient from 60 ppb on average at 6 km to 44 ppb at 1 km. Measurements in the upper part of the profile have shown significantly lower CO and higher O_3 values, with O_3 up to 85ppb.

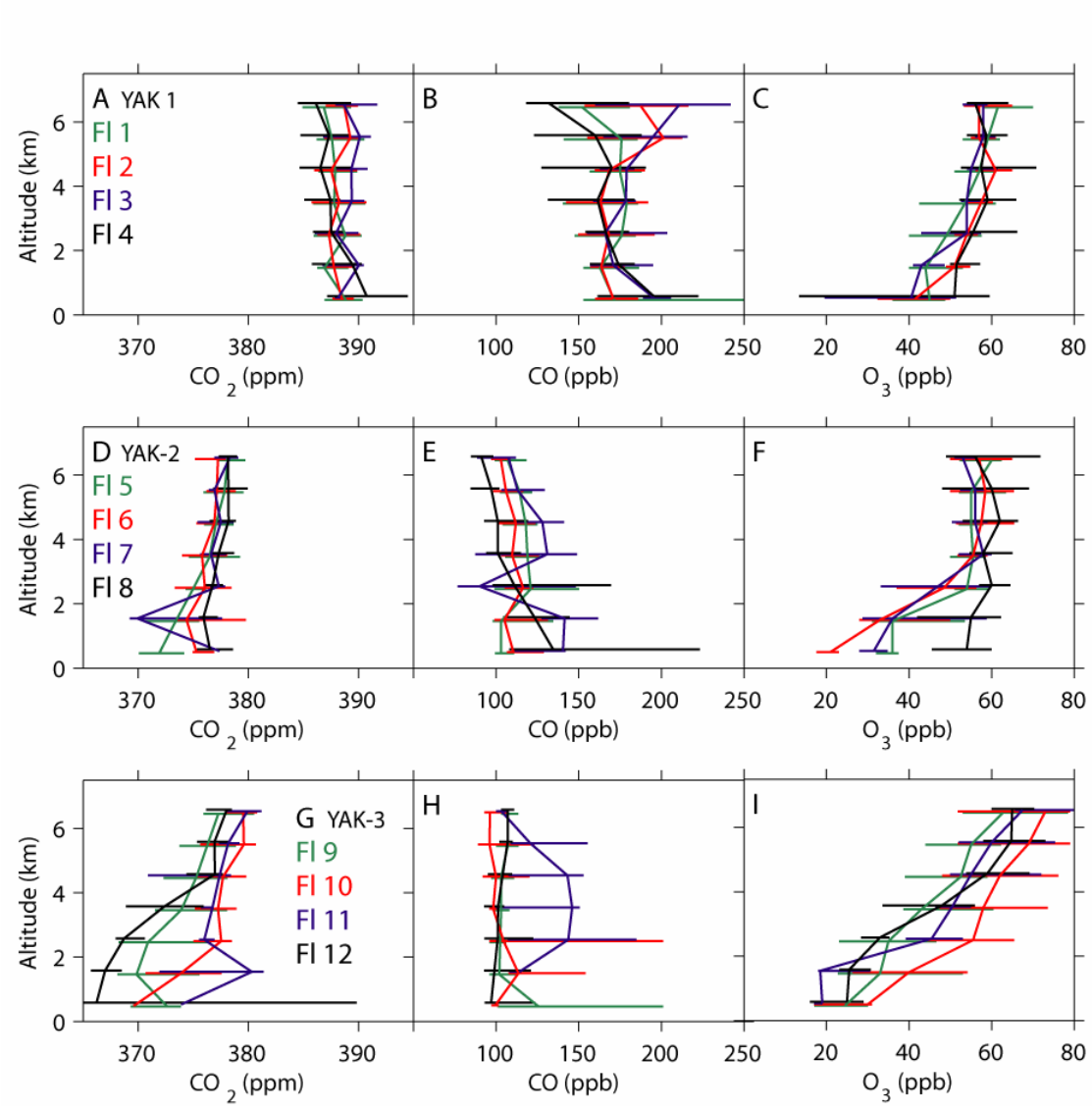

Figure 4.4. Profiles of CO_2, CO and O_3 over the 3 campaigns. Each flight is averaged in 1000m bins. The vertical line joins the median of each bin, while the horizontal lines represent the 10th and 90th percentiles of each bin.

During YAK-2 the average CO concentration was about 100 ppb, with a large variability (Fig. 4.4e). During Flight 5 the aircraft crossed a warm front exhibiting strong tracer gradients across its surface with CO concentration up to 150 ppb immediately above the front, between 2 and 3 km altitude.

High ozone values were found at the highest aircraft altitude during YAK-3 campaign, up to 90ppb (Fig. 4.4i). The O_3 vertical gradient between upper and lower altitudes was therefore the highest of the three campaigns. Except for local emissions in the lower troposphere, the YAK-3 campaign has shown low CO values (background 100 ± 5 ppb) with little variation, although satellite fire detection has shown numerous fires in temperate and boreal Eurasia. O_3 exhibits a nearly linear gradient up to 7 km altitude were the concentrations reach 90 ppb.

4.7. Cluster-based SRR relationships: case studies

In this section we apply and discuss the clustering results to examine the measurements from one flight from each of the three campaigns (Flight 1 on 11 April 2006, Flight 5 on 7 September 2006 and Flight 9 on 17 August 2007). All three flights are going from Novosibirsk to Myrni and correspond to the green route in Fig. 4.1). The clustering is done on a single campaign-basis. The clustering being independent from the observed concentrations, statistical separation of the concentrations across different clusters is interpreted as a validation of the SRR.

4.7.1. Flight 1: pollution from NE China

Figure 4.5 shows the average footprint for each cluster in logarithmic color scale. Footprints classified as Cluster C (n = 255; Fig 5c) are on average dominantly located over South East and East Siberia but have less average sensitivity to potential surface emissions than the other clusters. A marginal number of footprints are associated to Cluster A (n = 5; Fig 5a) with sensitivity to European emissions. Cluster B (n = 68; Fig 5b) gathers a significant amount of data having resided over northern Siberia and the Arctic. Footprints in Cluster D (n = 19; Fig. 4.5d) are exposed to surface exchange in southern Siberia and the Kazakhstan. The four well-differentiated footprint maps illustrate the validity of cluster-based partitioning.

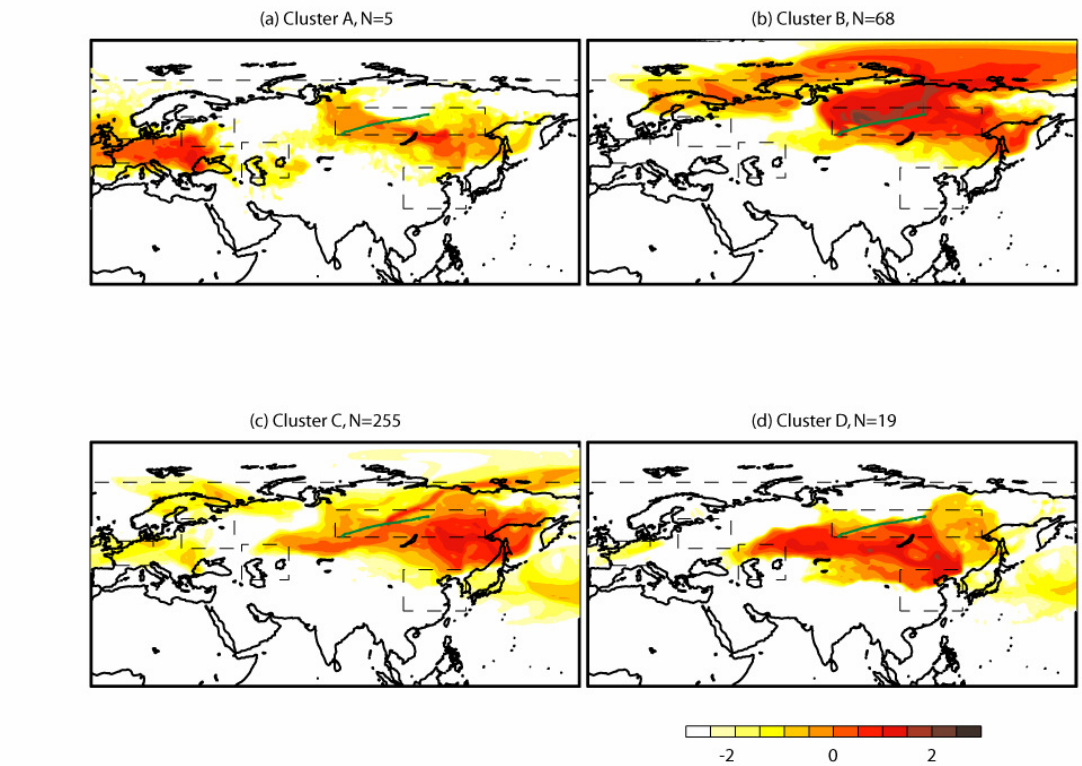

Figure 4.5. Average footprint maps for data belonging to clusters A-D throughout Flight 1 (11 April 2006). Logarithmic color scale gives the mean particles PES <300m. The number of elements N in a particular cluster is given above each map.

Figure 4.6 shows the distribution (quartiles and median) of CO_2, CO, O_3 and water vapour measurements associated to each cluster. Associated altitude is given in Fig. 4.6e, and the four (A-D) clusters' centroid (in std dev-normalized coordinates) position vector is given in Fig. 4.6f. Each cluster's centroid position vector can be related to the cluster average footprint map in Fig. 4.5.

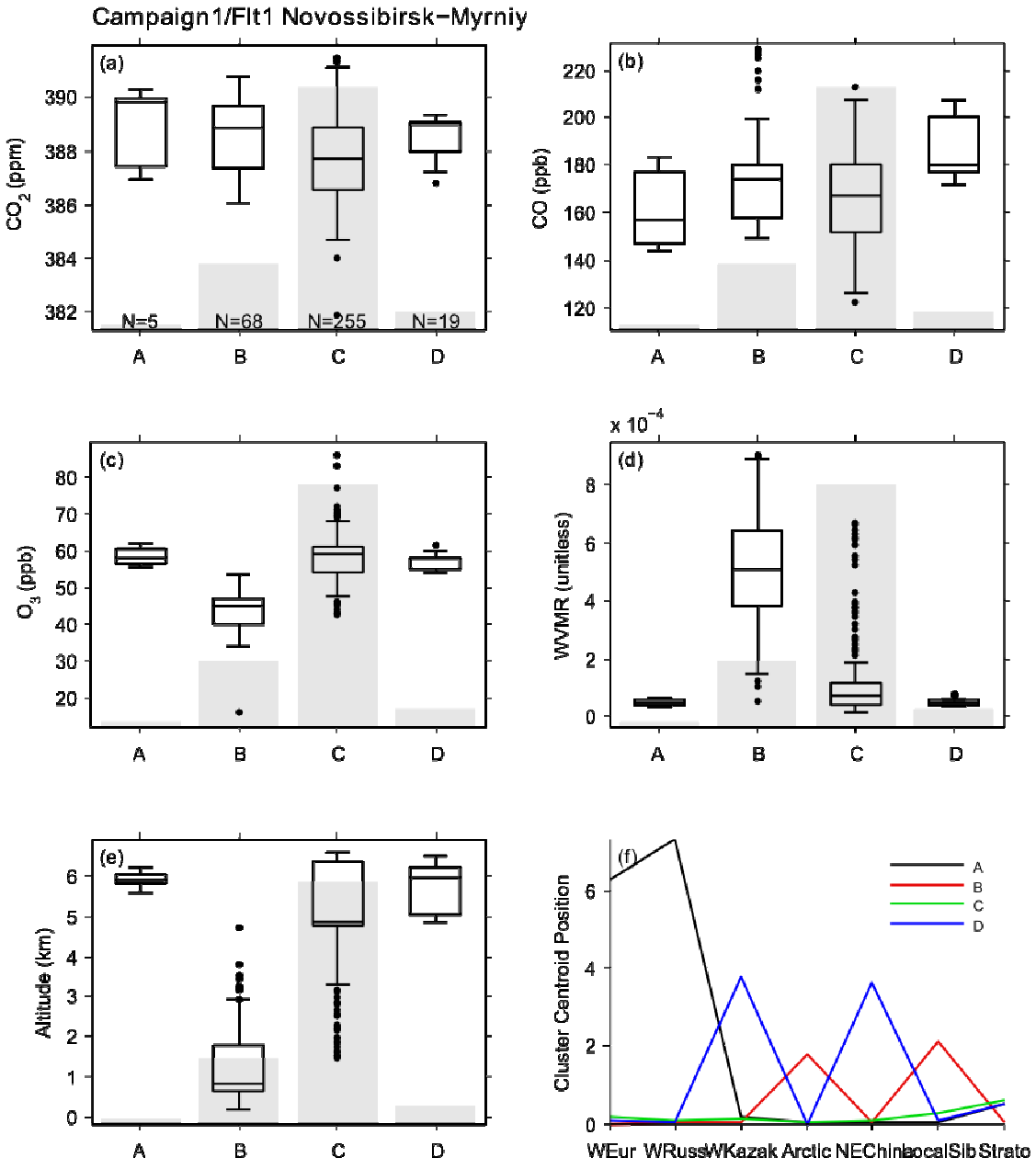

Figure 4.6. Box plots of median and interquartile range (IQR) for CO_2 concentrations measured during Flight 1 in each April 2006 cluster (clusters A-D in abscissa, same denomination as in Fig. 4.5) (a). Outliers within 1 IQD are within the whiskers, outliers beyond 1 IQR are shown as points. (b) Same for CO. (c) Same for O_3. (d) Same for water vapour mixing ratio. (e) Same for altitude. (f) Cluster centroid position vector for each cluster.

The data associated to Cluster D (sensitive to NE China emissions) are encountered between 5 and 6.5 km altitude (Fig. 4.6e) and have a median CO concentration of 180 ppb (Fig. 4.6b), well differentiated from other clusters. On the opposite, CO_2 values (median 388.6 ppm; Fig. 4.6a) are not distinguishably higher. This cluster identifies the transport of North Eastern China emissions to eastern Siberia on 12 April 2006 (Paris et al., 2008). The ability of the LPDM to resolve thin layers associated to synoptic features is a useful advantage over Eulerian models.

Cluster C is ubiquitous throughout Flight 1 and has a higher stratospheric influence reflected in its highest O_3 concentrations (up to 85 ppb). Cluster B has high CO concentrations (median 174 ppb) corresponding to local emission sensitivity of the lower troposphere.

4.7.2. Flight 5: Fires and CO_2 uptake

Figure 4.7 shows the average footprint for each cluster for the 7 September 2006 flight. As in the previous section, clustering was performed on the whole campaign (here, the September 2006 campaign). Data within Cluster B are the most ubiquitous (n = 148, Fig. 4.7b) and were mostly associated to FT zonal flow, resulting in a generally weak footprint mainly over European Russia and the Black Sea. This cluster has the highest stratospheric signature of the dataset (Fig. 4.8f). Cluster D is also ubiquitous in this flight (n=132; Fig. 4.7d) but has a high footprint density region located over Kazakhstan, between Caspian and Aral Seas. A large number of fires detected by ATSR fire count in this region, probably of agricultural origin, were injected in the FT as the region was swept by a front (Paris et al., 2008). Cluster A (n = 47, Fig. 4.7a) is clearly associated to an Arctic air mass channelled southward in the BL. Cluster C (n = 14, Fig 7c) reflects advection of air masses in contact with potential European emissions.

The European (Cluster C) air mass has a median CO concentration of 109.5 ppb (Fig. 4.8b) at a median altitude of 5 km, to be compared to 105.0 ppb for the more ubiquitous Cluster B. Although this is only a single case, it shows that European pollution does not always follow the low level advection pathway (Wild et al., 2003; Stohl et al., 2002; Duncan and Bey, 2004). Other characteristic of this air mass include relatively high CO_2 (median 376.3 ppm) and an O_3 median concentration of 53 ppb.

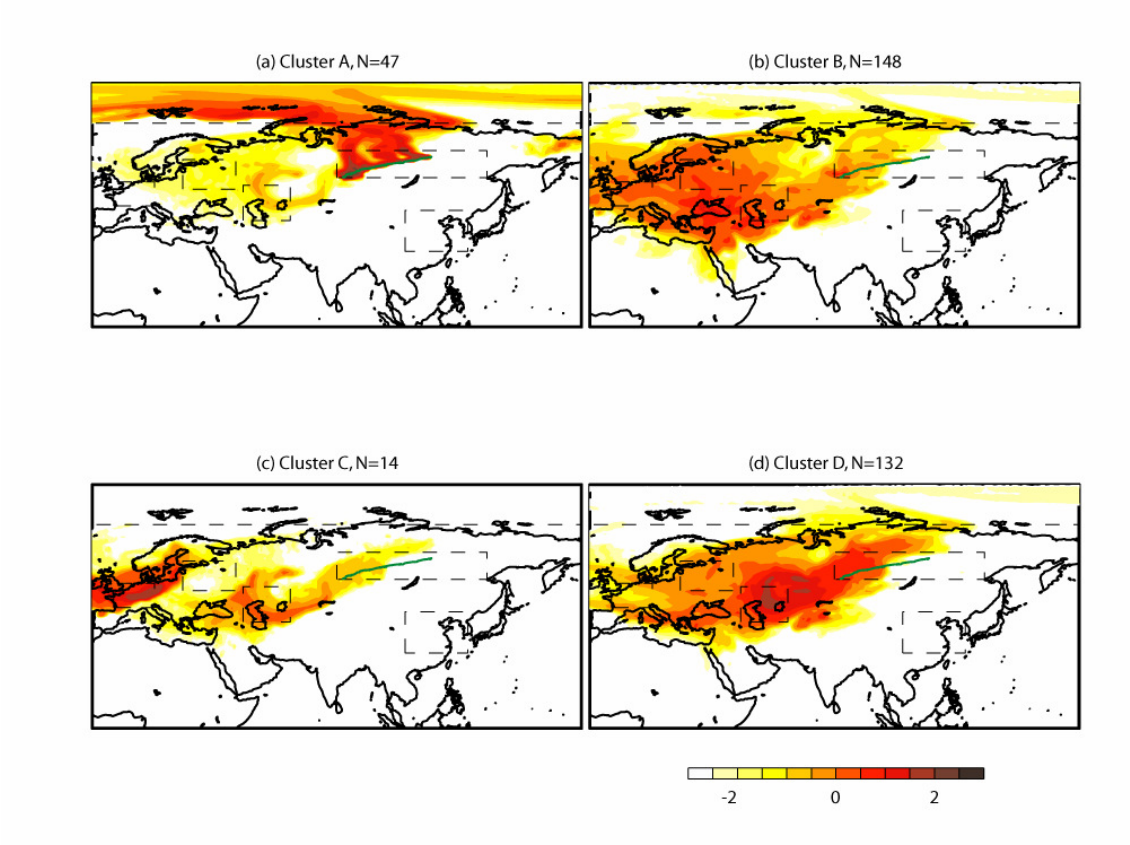

Figure 4.7. Same as Fig. 4.5 for Flight 5 in September 2006

Figure 4.8 shows that Cluster D has the most elevated CO concentration, up to 158 ppb (median 121.0 ppb, third quartile 132.2 ppb). It is also associated to high O_3 (median 54.5 ppb, IQR 51.2-57.0 ppb) but not to high CO_2 (median 375.0 ppm). High CO and O_3 are likely to reflect the sensitivity of Cluster D (Fig. 4.7d) to the biomass burning detected in the Caspian region (especially in Northern Kazakhstan at ~ 50°N, between 50 and 70°E). The ratio of O_3 to CO enhancements reflects a balance between ozone production and loss in the plume (Pfister et al., 2006; Val Martin et al., 2006). A plume with the highest CO concentration (144.3 ± 14.0, O_3 concentration 58.9 ± 3.8 ppb) exhibits a high CO-O_3 correlation (R^2 = 0.68, n = 90 10-s samples). The robust linear regression slope is 0.24 mol mol^{-1}, which is usually associated to ozone production within the plume from combustion-generated precursors like CO. The regression slope in another plume with high CO (134.8 ± 9.1 ppb) was found to be negative (-0.10 mol mol^{-1}). Both of these plumes are encountered at 2-2.5km altitude. The O_3-CO correlation coefficients are comparable to those found in the literature for boreal forest fire plumes (range 0.05 – 0.30 mol mol^{-1}; see Val Martin et al., 2006; Real et al. 2007 and references therein).

Both of these plumes have a high CO-CO_2 correlation (respectively R2 = 0.80 and 0.78) with negative CO-CO_2 regression slopes of -0.06 and -0.09 mol mol^{-1} respectively. These negative slopes reflect competing loss processes such as CO oxidation within the plume and CO_2 assimilation by intact vegetation.

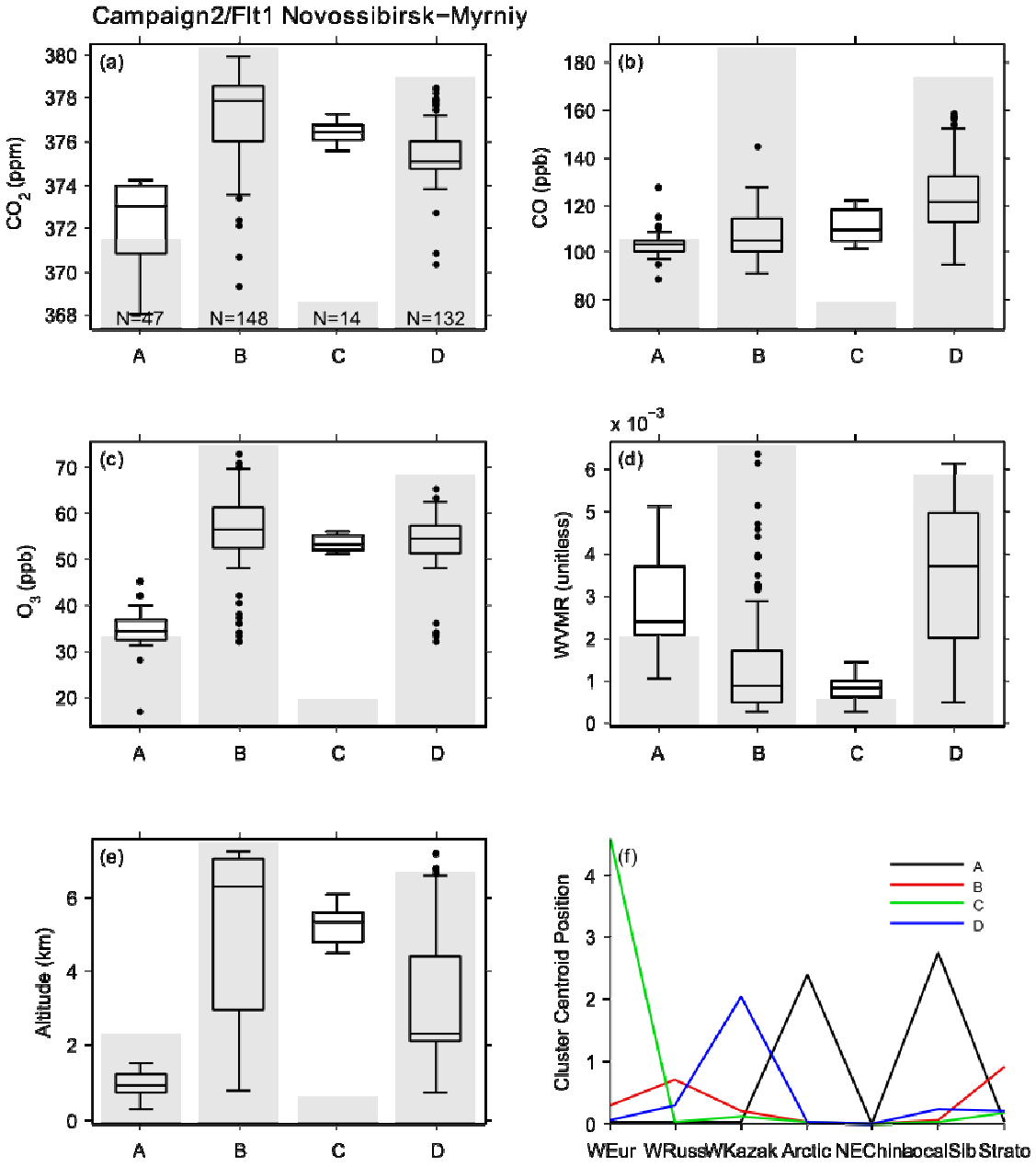

Figure 4.8. Same as Fig. 4.6 for Flight 5 in September 2006

Cluster A gathers observations affected by Arctic air (Fig. 4.8f) with low CO_2, CO and O_3 concentrations values (CO_2 median 373.06 ppm with IQR 370.81—373.94 ppm, CO median 103.0 and O_3 median 34.5 ppb). It is associated to a low altitude (1 km) within the BL and with a high water vapour mixing ratio (Fig. 4.8d). Advection of Arctic air in the campaign domain sampled during September 2006 occurred in the boundary layer. FLEXPART results indicate that total PES over the Arctic was 5 days or more in the last 10 days for the majority of data in Cluster A. The low CO and low CO_2 concentrations are suggestive of a strong isolation from sources in the recent air mass history. During the five days of meridian transport from the Arctic, exposure to uptake by

high latitude vegetation with permanent daylight period and to surface deposition must also have contributed to low CO_2 and low O_3 values respectively.

4.7.3. Flight 9: CO_2 uptake, forest fire and stratospheric input

Figure 4.9 shows the average footprint for each cluster for the 14 August 2007 flight. Cluster B indicates the dominant footprint pattern for this flight (n = 194; Fig. 4.9b). It has a strong stratospheric component (Fig. 4.10f) and the weak footprint density is spread over Western Siberia. Cluster C (n = 50; Fig. 4.9c) has a high sensitivity north of Lake Baikal. Cluster A (n = 26; Fig. 4.9a) is centred over north European Russia and Scandinavia while Cluster D (n = 26; Fig. 4.9d) reflects air of Arctic origin, comparable to Cluster A in the September 2006 case.

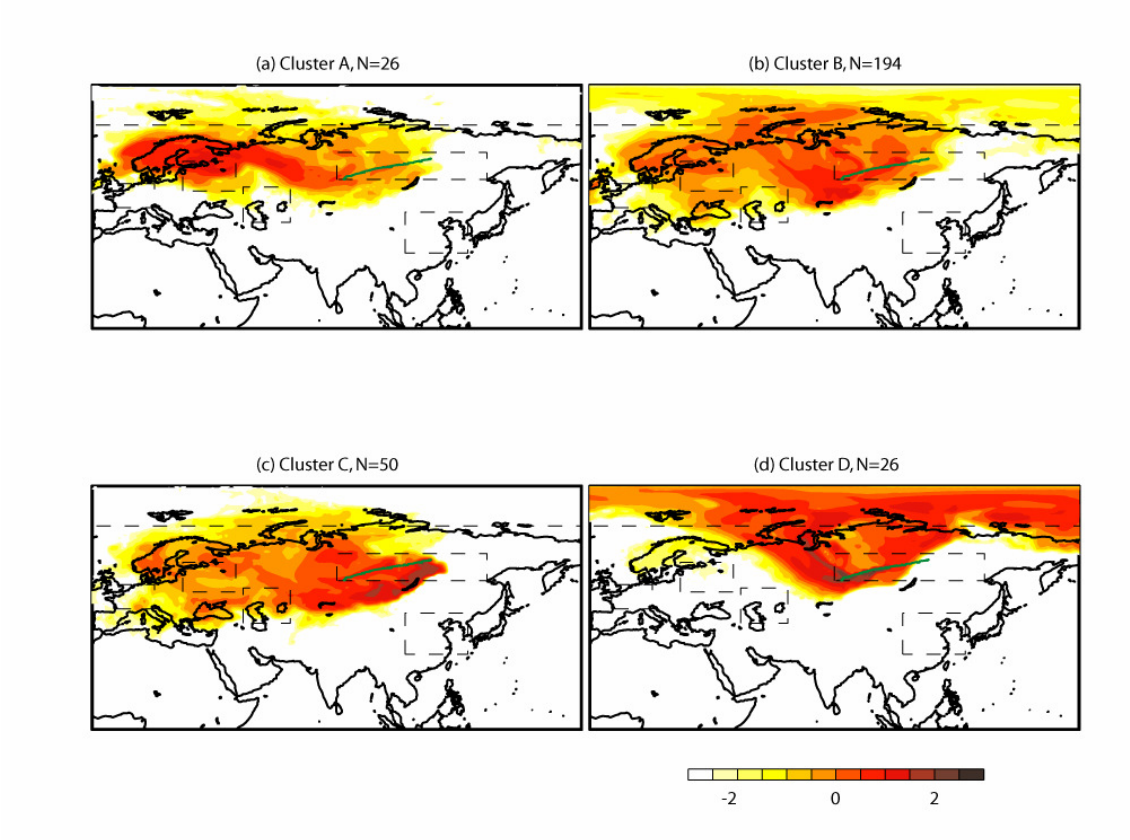

Figure 4.9. Same as Fig. 4.5 for Flight 5 in August 2007

Figure 4.10b-c shows that Cluster C has the highest CO median (122.0 ppb) with a wide IQR within 110.0—190.9 ppb. Such high CO values point to regional fire influence, as seen on ATSR fire atlas for the period of the campaign. The altitude range is very large (1—6 km). The highest CO concentrations (300 ppb) were observed in two layers in the lower FT (Fig. 4.11).

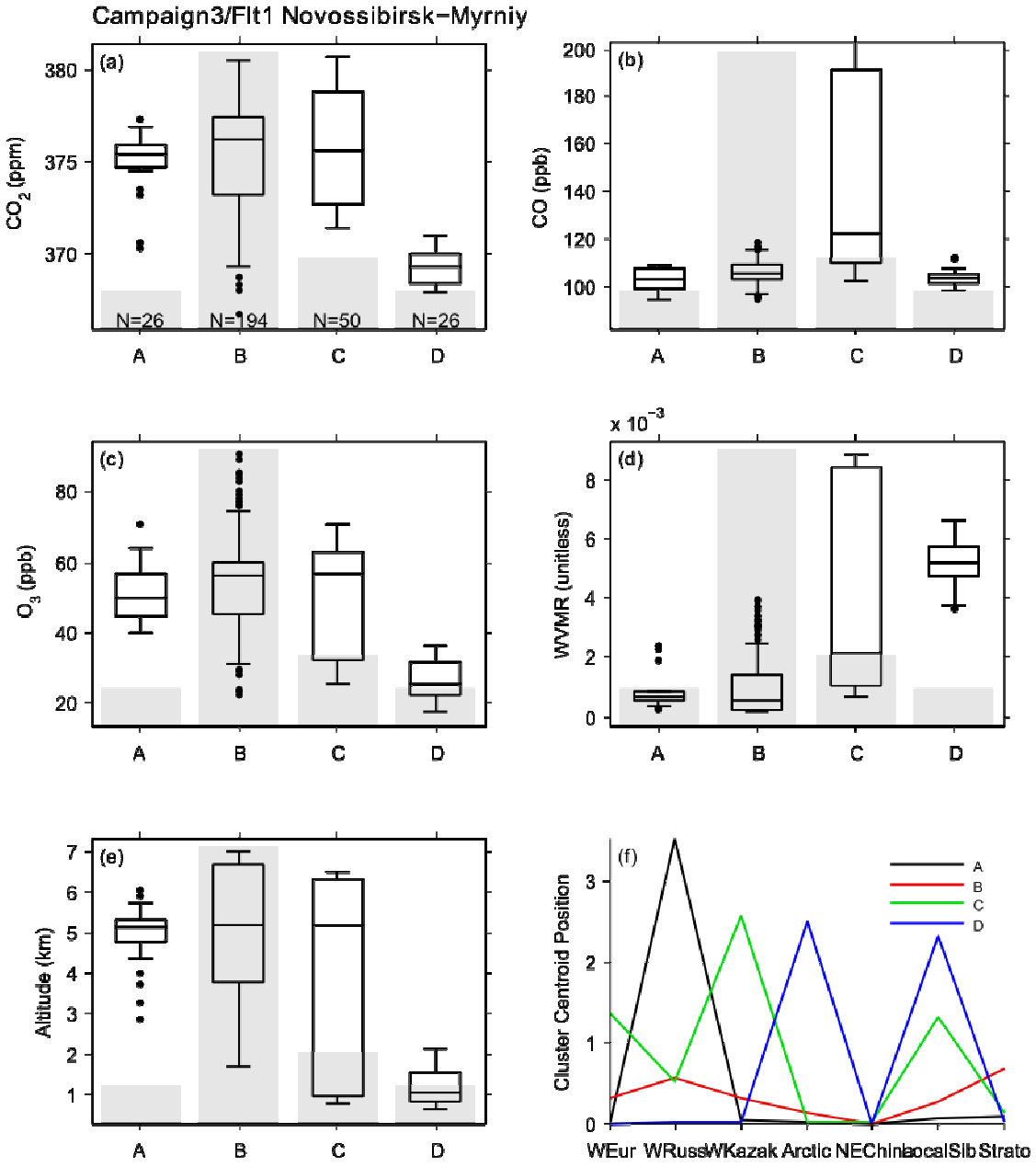

Figure 4.10. Same as Fig. 4.6 for Flight 5 in August 2007

Comparing CO_2 concentrations in the low-altitude Arctic clusters of September 2006 (Cluster A) and August 2007 (Cluster D), the latter (median 369.31 ppm) is lower by ~4 ppm despite anthropogenic inter-annual increase of ~1.5 ppm yr-1. The same is found for O_3 with 25.0 ppb in August 2007 vs. 34.5 ppb in September 2006. In Siberia FT CO_2 concentrations are minimum in August (Ramonet et al., 2002), and September concentrations increase by about 2 ppm in the FT and 5 ppm in the BL relative to August.

Cluster B shows the highest stratospheric component. The highest O_3 values (up to 91 ppb) associated to it are consistent with the 'stratospheric' classification. High O_3 concentrations (up to 90 ppb; Fig. 4.11) are associated to >50% of freshly (2 days) exported stratospheric particles.

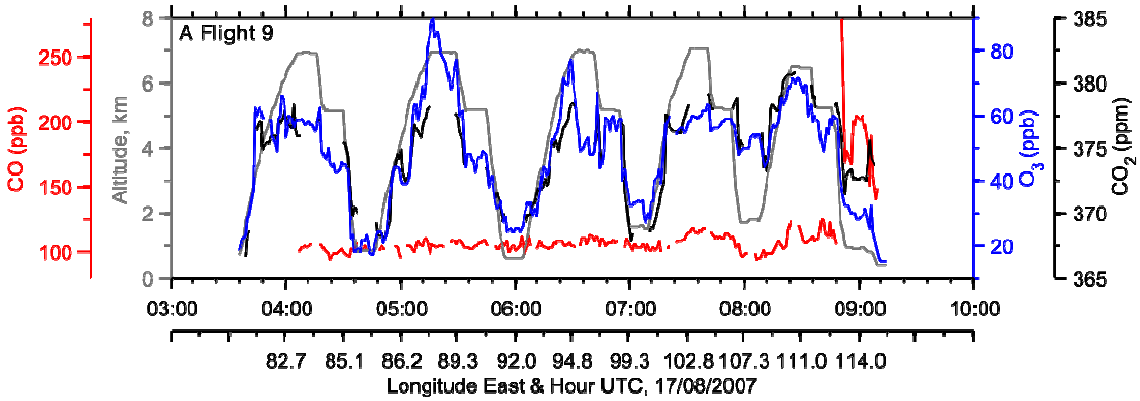

Figure 4.11. Time series of measured CO_2 (black), CO (red) and O_3 (blue) concentrations as well as altitude (grey). Longitude is also given every half hour.

4.8. Statistical relation between regions and species across campaigns

In order to compare between campaigns and generalize the above case studies we resort to pair-wise correlations statistics associating individual trace gases and each region as defined in Fig. 4.2.

4.8.1. Variations of CO_2 associated to source regions

Figure 4.12 shows the scatter plot of all CO_2 measurements against the PES in the Arctic and Siberia regions. Linear regression lines are fitted to the data and results are reported in Table 4.1, as well as correlation coefficients. Pearson correlation coefficients reported in Table 4.1 were calculated after excluding data associated to residence time < 100 s grid^{-1}. Since CO_2 fluxes are highly variable at the sub-day timescale, whereas simulated exposure to fluxes is averaged over 10 days, the relations between CO_2 concentrations and PES over source or sink regions are not expected to be strongly linear. The Kendall τ parameter equally reported in Table 4.1 is a more robust assessment of the strength of such a non-linear relationship (Wilks, 2006).

Table 4.1. Region-concentration pairwise statistics for CO_2.

	April 2006			September 2006			August 2007		
	τ^a	R^b	s^c	τ^a	R^b	s^c	τ^a	R^b	s^c
W Europe	-0.07	0.03	-	0.31	0.03	-	0.42	0.19	-
W Russia	0.05	-0.29	-3.7e-4	0.15	0.11	4.9e-4	0.11	-0.12	-1.9e-3
W Kazak	0.13	-0.04	-	0.01	-0.15	-2.1e-4	0.25	-0.13	-3.0e-3
Arctic	0.06	-0.25	-1.3e-4	-0.29	-0.35	-5.0e-4	-0.40	-0.37	-4.7e-4
NE China	0.31	-0.01	-	0.00	0.68	-	0.14	0.54	5.0e-2
Local	0.40	0.14	5.0e-5	-0.37	-0.20	-1.0e-4	-0.43	-0.41	-3.9e-4
Strato	-0.01	-0.35	-4.0e-2	0.37	0.00	-	0.37	-0.21	-1.4e-2

a Kendall's tau. Values are given in italics if not statistically robust ($p>0.01$)

b Pearson correlation coefficient. Values are given in italics if not statistically robust ($p>0.01$)

c robust linear regression slope (ppm s-1). No values is given if both Pearson and Kendall correlations are not robust, or if only Pearson correlation is not robust with $|R| <0.2$.

Figure 4.12 shows that CO_2 are significantly ($p < 0.01$) correlated to and decrease with PES over local ecosystems both in September 2006 ($R = -0.20$, $\tau = -0.37$, see Table 4.1) and August 2007 ($R = -0.41$, $\tau = -0.43$). Robust linear regression slopes are -1.0 10^{-4} ppm s^{-1} and -3.9 10-4 ppm s^{-1} respectively. Similarly, for the Arctic box in summer, significant correlation is observed between CO_2 concentrations and the PES (in September 2006, $R = -0.35$ and $\tau = -0.29$; in August 2007, $R = -0.37$ and $\tau = -0.40$). As discussed in Section 4, high Arctic signal is typically associated to advection in the BL, and so integrates between 1 and 10 days of exposure to uptake by Siberian sub-arctic ecosystems. Together, 10-day cumulated exposure to local and Arctic fluxes in August 2007 therefore explain ~50% of the total CO_2 variance (approximated as the diagonal sum of correlation coefficients), where boreal and sub-arctic ecosystem uptake is at its annual maximum.

In August 2007 the North Eastern China region seem to has a positive contribution to CO_2 concentrations with a significant correlation ($R = 0.54$, slope = 5.0 10^{-2} ppm s^{-1}, $\tau = 0.14$). In the clustering analysis has produced no cluster with dominant NE China signal (Fig. 4.10). These two diverging results suggest that NE Chinese CO_2 emissions enhanced August CO_2 concentration over Siberia but without a well-defined filamentary structure. In April 2006 both a highly polluted cluster of dominant NE China footprint, and a consistent positive relationship ($\tau = 0.31$) between CO_2 and NE China PES were found.

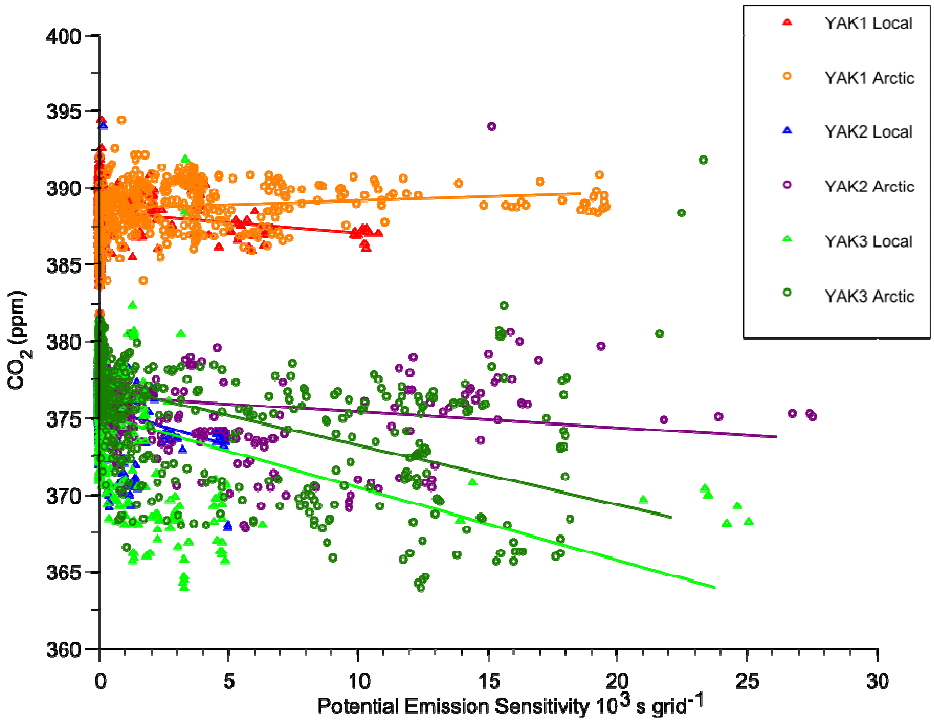

Figure 4.12. CO_2 measurements from the three campaigns plotted against PES in the Arctic and Siberia regions, with robust linear regression fit.

4.8.2. Variations of CO and O_3 associated to source regions

Tables 2-3 show the pairwise statistics associating possible source regions and CO and O_3 concentrations respectively. CO budget over Siberia seems to include anthropogenic sources (NE China in April 2006: τ = 0.32, local sources in all campaigns, see Table 4.2) and Western Kazakhstan sources in September 2006 (τ = 0.29) and August 2007 (τ = 0.26), where it is most likely attributed to biomass burning in both cases. A regression slope of 3.6 10^{-3} ppb s^{-1} is found for both periods. Our calculations fail to identify O_3 production in these fire plumes (Table 4.3) in relation to the Western Kazakhstan source region.

O_3 statistics exhibit good correlations with most regions excepted in September 2006. As can be expected the stratosphere is a significant contributor to the O_3 concentration (τ ranges between 0.41 and 0.53) in all campaigns with linear regression slopes of 0.1 in April and 0.58 in September. Paralleling CO_2 patterns, exposure to ground influence in the Siberian BL consistently reduce O_3 concentrations in all campaigns. Linear correlation is stronger (R between -0.76 and -0.45, see Table 4.3) and the slopes are steeper by almost one order of magnitude in summer months. Influence of Europe (Western Europe and European Russia) seems to result in overall higher O_3 concentrations, confirming the case studies of Section 4. This influence is clear ($p<0.01$) for Western Europe in April (R = 0.35) and August (R = 0.34), and for Western Russia in April only (R = 0.24).

Table 4.2. Region-concentration pair-wise statistics for CO

	April 2006			September 2006			August 2007		
	τ^a	R^b	s^c	τ^a	R^b	s^c	τ^a	R^b	s^c
W Europe	-0.08	-0.04	-	0.02	-0.01	-	0.18	-0.28	-7.9e-02
W Russia	0.03	-0.25	-5.3e-03	0.09	0.02	-	0.03	-0.07	-
W Kazak	0.17	-0.11	-	0.29	0.21	3.6e-03	0.26	0.17	3.6e-03
Arctic	0.03	0.04	-	0.15	-0.18	-4.1e-03	-0.06	-0.13	-
NE China	0.32	0.00	-	-0.03	-0.86	-	0.17	-0.22	-1.7e-01
Local	0.29	0.01	-	0.27	0.06	-	0.14	0.36	-3.8e-05
Strato	-0.04	-0.36	-6.3e-01	-0.15	-0.42	-1.1e+00	0.03	0.26	-

a Kendall's tau. Values are given in italics if not statistically robust (p>0.01)

b Pearson correlation coefficient. Values are given in italics if not statistically robust (p>0.01)

c robust linear regression slope (ppm s-1). No values is given if both Pearson and Kendall correlations are not robust, or if only Pearson correlation is not robust with |R| <0.2.

Table 4.3. Region-concentration pair-wise statistics for O_3

	April 2006			September 2006			August 2007		
	τ^a	R^b	s^c	τ^a	R^b	s^c	τ^a	R^b	s^c
W Europe	0.28	0.35	8.5e-03	0.31	0.01	-	0.39	0.34	1.2e-01
W Russia	0.18	0.24	1.1e-03	0.07	-0.06	-	0.13	-0.10	-8.2e-03
W Kazak	0.12	-0.20	-3.7e-04	0.07	0.06	-	0.17	-0.05	-
Arctic	-0.44	-0.36	-6.3e-04	-0.33	-0.47	-3.8e-03	-0.45	-0.45	-1.8e-03
NE China	0.08	-0.36	-1.7e-03	-0.10	0.15	-	0.16	0.44	2.1e-01
Local	-0.47	-0.53	-9.8e-04	-0.44	-0.76	-2.5e-03	-0.50	-0.69	-2.3e-03
Strato	0.45	0.43	1.0e-01	0.41	0.30	5.8e-01	0.52	-0.02	-

a Kendall's tau. Values are given in italics if not statistically robust (p>0.01)

b Pearson correlation coefficient. Values are given in italics if not statistically robust (p>0.01)

c robust linear regression slope (ppm s-1). No values is given if both Pearson and Kendall correlations are not robust, or if only Pearson correlation is not robust with |R| <0.2.

4.9. Conclusion

We analysed three intensive campaigns above Siberia resulting in a total of ~70h of CO_2, CO and O_3 measurements. The sampling strategy was to perform consecutive ascents and descents to obtain a tomography of the atmosphere above Siberia. Our data analysis was based on a novel application of clustering to Lagrangian particle dispersion model footprint. The technique was found to be able to separate tracers concentrations although it was based solely on atmospheric transport modelling. CO concentrations of ~109 ppb were observed in clusters associated to a

dominant European emissions sensitivity in September 2006 and ~105 ppb in August 2007. Dominant NE China PES was associated to concentrations of 180 ppb in April 2006. High CO and O_3 concentrations (median values 121 ppb and 54.5pb respectively) were found in clusters associated with fires in Kazakhstan in September 2006. High correlation (R^2 = 0.68) and robust linear relationships with regression slopes ranging between -0.10 – 0.24 ppb ppb^{-1} where found in individual plumes.

Summer (August 2007, September 2006) uptake of CO_2 was found to be largely (~50%) explained by exposure to boreal and sub-arctic ecosystems, most likely by photosynthesis. It is likely that permanent sunlight exposure of vegetation above 66°N contributes to a more constant uptake in this region, therefore strongly depleting CO_2 in transiting air masses.

Discernable influence of air exposed to European emissions was observed toward higher O_3 concentrations, besides large removal in the Siberian BL and constant stratospheric contribution.

LPDM-based clustering has a large potential and the technique used here, although it has demonstrated its resolving power, require more refinements.

Chapitre 5.
Distribution des aérosols fins dans la troposphère

La variabilité des gaz traces mesurés a été présentée dans les deux chapitres précédents et la contribution du transport atmosphérique à partir de sources distantes a été analysée en général dans le chapitre 4. La contribution du transport pour l'étude du CO_2, du CO et de l'O_3 est pertinente car le temps de vie de ces espèces est suffisamment long pour que les concentrations soient importantes loin des sources. A l'inverse, les aérosols sub-micrométriques, également mesurés durant les campagnes, ont un temps de vie très court, allant de quelques heures à quelques jours. Leur observation loin des sources (primaires ou secondaires) ne peut donc être expliquée uniquement par des processus de transport. Ce chapitre présente ces mesures d'aérosols et se focalise sur la distribution du processus de nucléation en atmosphère propre, la nucléation étant le processus de formation des particules ultrafines. Je montre ainsi que ces données, bien que limitée en résolution granulométrique, permettent de mettre en évidence un possible maximum saisonnier en été de nucléation in situ dans la troposphère continentale propre.

5.1. Contexte

La mesure systématique des aérosols dans la troposphère fait partie des missions que s'est donné l'Institut d'Optique Atmosphérique de Tomsk. A ce titre l'Antonov-30 est équipé pour mesurer les aérosols de 3 à 200 nm de diamètre, ainsi que pour collecter des échantillons pour analyse de composition en laboratoire. Une analyse des implications possibles de la distribution observée est présentée ici, basée sur les mesures effectuées lors des campagnes d'avril et septembre

2006, ainsi que lors de profils réguliers obtenus au dessus de Novossibirsk dans le cadre d'un autre programme de recherche.

L'aérosol nanométrique est une étape du cycle de vie de l'aérosol qui reste mal connue, notamment dans la troposphère libre continentale propre. Les sources des aérosols nanométriques en troposphère libre restent mal connues. En effet, la formation d'aérosols secondaires a été observée dans la couche limite, généralement au printemps ou en automne, sous forme de *nucleation burst*. De grande quantité d'aérosols sont ainsi formées en quelques heures et où la taille moyenne augmente très rapidement. On a donc imaginé que les aérosols secondaires peuvent parvenir à la troposphère libre « en l'état ». A l'inverse, certaines études dans la troposphère libre suggèrent une formation in-situ des aérosols, à partir de précurseurs émis à la surface mais capable de franchir la couche limite.

De manière générale, les mesures de particules ultrafines sont peu nombreuses. Très peu d'observation peuvent prétendre être représentatives de zones continentales propres (Seinfeld & Pandis, 2003). Cet article propose d'étudier les données obtenues au dessus de la Sibérie par les campagnes YAK-AEROSIB ainsi que par le programme de mesure régulier au dessus de Novossibirsk. Ce chapitre n'a pas vocation à caractériser le processus de nucléation, domaine d'étude très spécifique et exigeant, mais prétend illustrer le potentiel des mesures aéroportées en Sibérie pour étudier cette nucléation car la troposphère y est représentative d'un environnement propre et continental.

5.2. Résumé

La concentration des particules ultra fines a été mesurée au dessus de la Sibérie durant deux campagnes intensives YAK-AEROSIB à l'échelle continentale en avril et en septembre 2006. Ce jeu de données est complété par des profils mensuels au dessus de Novossibirsk. La concentration en nombre d'aérosols est mesurée pour les particules avec des granulométries comprises entre 3 et 70 et entre 70 et 200 nm, en combinaison avec des mesures de CO et autre gaz traces. La concentration de particules dans la troposphère libre varie entre 80 et 200 cm^{-3}. Des concentrations de ~500 cm^{-3} ont été échantillonnées à 5—6 km altitude en Sibérie orientale en avril, dans une masse d'air polluée soulevée depuis la Chine du nord est quatre jours au préalable. La répartition en granulométrie est approximativement égale dans les deux canaux entre 3—70 nm et 70—200 nm, ne suggérant pas la formation de nouvelles particules par nucléation. En septembre, le rapport entre la concentration des particules ultrafines (avec des tailles comprises entre 3 et 70 nm) et les particules fines (entre 70—200 nm) augmente avec l'altitude. Les particules ultrafines représentent ainsi 90% de la concentration totale mesurée dans la troposphère à 6—7 km d'altitude. La troposphère libre est particulièrement propre en septembre 2006, comme indiqué par les faibles concentrations de CO. La formation in situ dans la troposphère sibérienne est plausible au vue de la courte durée de vie des particules ultrafines. La nucléation in situ au dessus de la Sibérie semblerait

plus importante au printemps et en automne dans la couche limite, et en été dans la moyenne troposphère, comme indiqué par les profils mensuels à Novossibirsk. En effet, les concentrations $N_{3—70}$ représentent ~90% du total ($N_{3—200}$) en juillet-aout entre 6—7 km altitude. Notre jeu de données souffre toutefois d'une résolution de granulométrie très limitée.

5.3. Article

Large-scale aircraft observations of ultra-fine and fine particle concentrations in the remote Siberian troposphere: New particle formation studies. Accepté avec révisions dans *Atmospheric Environment,* par Jean-Daniel Paris, Mikhail Yu. Arshinov, Philippe Ciais, Boris D. Belan et Philippe Nédélec.

Ultra fine particles number concentrations were measured over Siberia during two large-scale airborne measurement campaigns in April and September 2006. During both campaigns, an aircraft flew between Novosibirsk and Yakutsk, collecting every 200 km vertical profiles up to 7 km. This dataset was completed by 5 years of monthly profiles above Novosibirsk. Particle number concentration was measured in the size ranges 3–70 and 70–200 nm, along with other tracers. Free troposphere (FT) particle concentrations ($N_{3–200}$) varied between 60 and 460 cm^{-3}, inferior to boundary layer concentrations (100–7000 cm^{-3}). In April, high concentrations of ~500 cm^{-3} were observed in a polluted air mass recently uplifted at 5–6 km altitude over eastern Siberia, with no sign of significant new particle formation. In September, particle concentrations decreased with altitude, but with a steeper gradient in $N_{70–200}$ compared to $N_{3–70}$, the later accounting for 90% of the total particle concentration in the free troposphere at 6–7 km altitude. Because ultra-fine particles presumably have short lifetimes, these observed particles could have been formed in-situ in the clean Siberian atmosphere. Two cases of possible nucleation with high concentration and $N_{3–70}/N_{70–200}$ ratios are reported for the September campaign, in the upper troposphere and in cloud outflow in the mid-troposphere. In the seasonal analysis, a FT $N_{3–70}$ maximum is found in July-August between 6–7 km altitude, with $N_{3–70}$ accounting for ~90% of $N_{3–200}$ supporting the hypothesis of in-situ formation in the FT. A secondary FT maximum of $N_{3–70}$ was identified later in autumn. In the boundary layer, seasonally maximum $N_{3–70}$ concentrations were found over Novosibirsk in May and September, but not in summer, possibly due to scavenging by precipitations and a large condensational sink from biomass burning aerosols. Our dataset has a limited size resolution and no speciation capability; more investigation is thus required to understand the conditions leading to in-situ nucleation processes in the Siberian air shed.

5.4. Introduction

Aerosols play an essential role in the Earth system and impact the Earth energy balance due to their ability to interact with light and to nucleate clouds (Charlson et al., 1990). Free tropospheric particles are either uplifted from the boundary layer or formed in-situ from gaseous precursors. Gas-to-particle conversion occurs as two competing processes: condensation on pre-existing particles or as nucleation. Binary homogeneous nucleation of sulphuric acid and water vapour is a

dominant nucleation mechanism. High nucleation rates have also been observed at ultra-low sulphuric acid concentration (Hoppel et al., 1994; Covert et al., 1992, Weber et al., 1996), suggesting ternary formation of new particle e.g. with ammonia is also a significant nucleation mechanism (Korhonen et al., 1999). Also, ion-induced nucleation (e.g. Lee et al., 2003) or activation of existing clusters (Kulmala et al., 2006a) can be important. Ultra-fine particles either grow or evaporate. Particles with size ~10 nm have a lifetime of about two hours in the FT (Williams et al., 2002), increasing with decreasing condensational sink.

Freshly nucleated aerosols have been observed at many locations in the free troposphere (FT) (Covert et al., 1992, Weber et al., 1996; Nyeki et al., 1999; de Reus et al. 2000; Clarke et al, 1998, 1999; Twohy et al., 2002; Lee et al., 2003; Minikin et al., 2003; Young et al. 2007; Benson et al., 2008). Twohy et al. (2002) in particular observed high condensation nuclei concentration up to 45000 cm^{-3} from nucleation in the outflow of a mesoscale convective system. These observations are summarized in Table 5.1. Observations of nucleation in the clean continental free troposphere remain sparse. Leaitch and Isaac (1991) argued that continental free troposphere surveys are likely to be affected by lateral advection of DMS-rich marine air.

Table 5.1. Observed concentration distribution in the FT from the literature, mostly during nucleation events. Range is given between square brackets.

Reference	Concentrations (cm^{-3})	Size range (nm)	Location	Latitude	Altitude
Schröder and Ström, 1997	50	7–18	West Europe	mid lat	LT
–	300	7–18	–	–	UT
–	1500	>18	–	–	FT
Nyeki et al., 1999	[35–550]	5–15	Germany	46°N	FT
–	[1000–2000]	>15	–	–	–
De Reus et al., 2000	[50–100]	6–18	Tenerife	29°N	FT
–	[500–1000]	>18	–	–	–
Hermann et al., 2003	[50–500]	4–12	Europe	Mid lat	UT/LS
–	[1000–6000]	>12	–	Mid lat	UT/LS
Minikin et al., 2003	1400 [450–15000]	>5	NH	NH	UT
–	770 [290–9600]	>14	–	–	–
–	40 [16–90]	100–1000	–	–	–
Twohy et al., 2002	Up to 45000	>25	Central US	Mid lat	UT
Lee et al., 2003 [a]	330	4–9	NH	Mid & high lat	UT/LS
– [b]	60	4–9	–	–	–
–	200–500	4–2000	–	–	–
Young et al., 2007[c]	700–3960	4–9	US	Mid lat	UT/LS
Benson et al., 2008 [a]	200–400	4–9	US	Mid lat	FT
– [a]	250–750	4–2000	–	–	–
This study[d]	50–350	3–70	Siberia	Boreal	FT
–[d]	90–580	3–200	–	–	–
–[e]	50–1100	3–70	–	–	–
–[e]	75–1500	3–200	–	–	–

[a] Average concentration reported in the presence of identified nucleation

[b] Average concentration reported in the absence of identified nucleation

[c] within tropopause fold

[d] April 2006 campaign, all data

[e] September 2006 campaign, all data

No extensive study has been reported for the clean continental free tropospheric air shed of Siberia. Previous boundary layer studies in this region highlighted the contribution of anthropogenic and biogenic emission to aerosols concentrations (Bashurova et al., 1992; Koutsenogii et al. 1993, Koutsenogii, 1997; Vartiainen et al. 2007; Heintzenberg et al., 2008; Dal Maso et al., 2008). Most of Siberia exhibits deep atmospheric boundary layers in summer, as the

relatively dry boreal conifer forests tend to produce high sensible heat fluxes (Baldocchi et al., 2000). The diurnal growth of a deep convective boundary layer will ensure vigorous ventilation of surface emissions such as biogenic volatile organic compounds (Lathiere et al., 2006) in summer, which may in turn favour nucleation (O'Dowd et al., 2002).

We present new aerosol size distribution data from two continent-wide campaigns carried out over Siberia (between 55°N and 63°N) in September and April 2006 and from 5 years of monthly vertical profiles over Novosibirsk. The question of a nucleation signal in ultra fine aerosols concentration in the Siberian FT, and its seasonal variation, is addressed.

Particles number concentrations are measured in the ranges 3–70 nm and 70–200 nm. Ultra-fine particles number concentration in the 3–70 nm range (N_{3-70}) accounts for most of the total number of particles in remote clean continental air (Seinfeld and Pandis, 1998), but only for a negligible fraction of the aerosol mass. Particles concentration in the 100–1000 nm size range is proportional to aerosol total surface and hence to the gaseous precursors aerosol surface sink. This coarse size resolution information is used to assess the large-scale distribution of ultra fine particles in the free troposphere.

CO enhancement is used here as a tracer of pollution from anthropogenic sources and biomass burning. SO_2 was not directly measured during our campaigns so we instead use CO as a proxy of potential gaseous precursors such as SO_2. CO and SO_2 have common anthropogenic sources, such as combustion of coal and other fuels, also emitting submicron particles of black carbon and organic carbon (e.g. Ohara et al., 2007). CO enhancements may not necessarily be correlated with enhancements in SO_2 because of their different lifetimes against reaction with OH (one month or more and a few days respectively; Seinfeld and Pandis, 1998).

5.5. Methods

The YAK-AEROSIB campaigns have been conducted in April and September 2006 (Paris et al., 2008) using a chartered Antonov-30 operated by Institute of Atmospheric Optics in Tomsk. The two campaigns were carried so as to allow maximum sampling of the troposphere below 7 km, with a see-saw flight pattern combining 26 vertical profiles between 0.5 and 7 km of altitude spaced horizontally by ~300 km (Fig. 5.1). Each campaign consists of four flights, numbered 1 – 4 during the April campaign and 5 – 8 during the September campaign. Campaigns measurements are completed by monthly vertical profiles near Novosibirsk (NOV in Fig. 5.1 top panel; Arshinov and Belan, 2004) collected between December 2002 and November 2007. The monthly flights use the same aerosol instrument and aircraft as the intensive campaigns. The NOV profiles were always collected between 1200 and 1600 local time, from the ground to 7 km altitude.

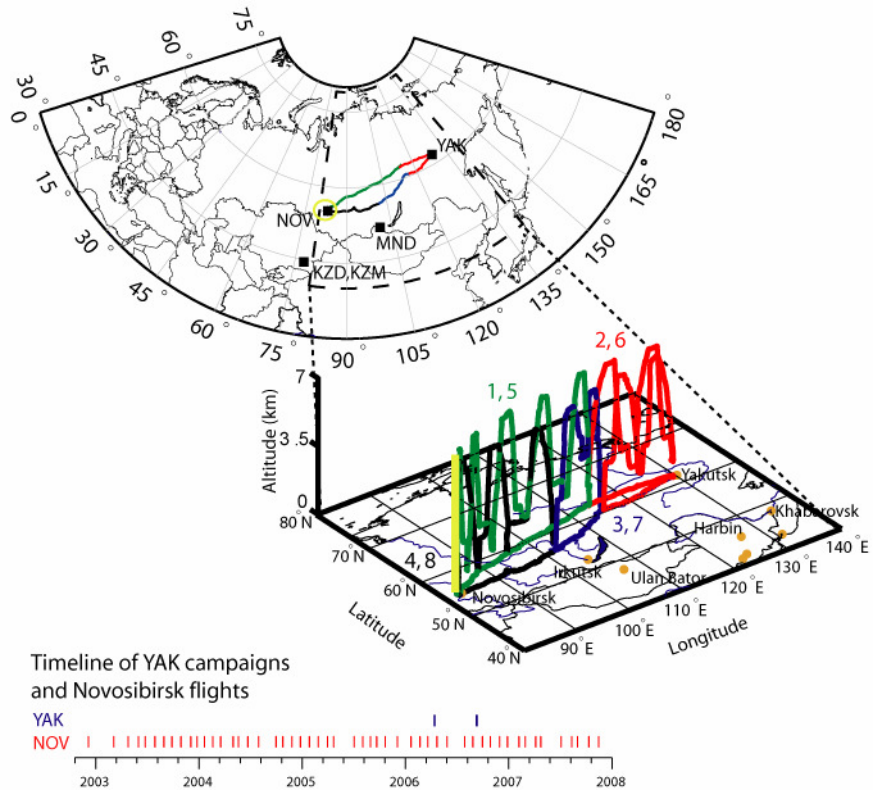

Figure 5.1. Flight route during the campaigns. The April 2006 and September 2006 campaigns followed the same route. Each of these two campaigns was split into the same four flights (in the top panel, numbered 1 to 4 in April and 5 to 8 in September 2006 and differentiated by colours: green, red, blue and black). Novosibirsk profiles site is also shown in yellow. Bottom panel shows the timeline of measurements (red: regular profiles in Novosibirsk, blue: YAK intensive campaigns).

Ultra fine particles concentration in the diameter range from 3 to 200 nm are measured using an 8-channel automated diffusion battery (ADB; designed by ICKC SB RAS, Novosibirsk; Reischl et al., 1991; Ankilov et al., 2002a, 2002b) coupled to a condensation particle counter (Arshinov and Belan, 2004). Air is sampled using a quasi-isokinetic inlet (Zuev et al., 1992) at the front side of the aircraft. The ADB system has been specially designed for airborne applications with regulated flow rate, compensating for outside pressure variations and minimising particle losses. In order to reduce integration (scanning) time and hence improve precision, only two channels of the battery are used in the instrument. This also improves the total particle concentrations retrieval. Size response of the instrument is homogeneous over the 3–200 nm size range (Ankilov et al., 2002b) and for different aerosol compositions. Transmission efficiency for the airborne instrument is corrected for and is ~0.997 in the 70–200 nm range and between 0.82 at 400 hPa and 0.89 at 1000 hPa for the 3–70 nm size range. All concentrations are reported at standard pressure and temperature (STP) conditions.

The CO airborne analyser used for the YAK-AEROSIB campaigns is described in Nédélec et al. (2003). It is an automated instrument modified from the commercial infrared absorption correlation gas analyser (Model 48C, Thermo Environment Instruments, USA) to reach an accuracy

of 5 ppb or 5% for 30 seconds integration time. Periodical (every 20 minutes), in-flight accurate zero measurements were performed during the campaigns. The O3 instrument is derived from the commercial Thermo 49 instrument based on UV absorption with a precision of 2 ppb or 2 % (e.g. Paris et al., 2008).

5.6. Results and discussion

5.6.1. Particle concentrations during the intensive campaigns

The total (sizes 3–200 nm) particle number concentration measured during the YAK-AEROSIB campaigns had a modal distribution of 150 cm^{-3}. In the April 2006 campaign, the median concentration was 190 cm^{-3}, and ranged from 90 to 580 cm^{-3} (10^{th} and 90^{th} percentile respectively; Fig. 5.2). 1% of the data exhibited concentrations higher than 10^4 cm^{-3}, mostly in the vicinity of airports (at take off and landing). Above 3km, April concentrations are in the range 80–460 cm^{-3}. The distribution of ultra-fine aerosols has a maximum in the boundary layer (BL) where anthropogenic and biogenic emissions of aerosols and precursors are injected. In the lowest 1 km, in a very stable and shallow boundary layer, the April concentration ranged between 10^2–7×10^3 cm^{-3}.

During the September 2006 campaign, the particle number concentrations observed were in the range 75–1.5×10^3 cm^{-3}, (again, respectively 10^{th} and 90^{th} percentile; Fig. 5.3), with a median of 215 cm^{-3} and skewed toward lower concentrations. Above 3 km, typical September concentrations are between 60–340 cm^{-3}, and 1% of the data is above 3×10^3 cm^{-3}. In the September BL (approximated by the lowest 2 km), variability was less important than the lowest 1 km in April, with a range 350–2×10^3 cm^{-3}.

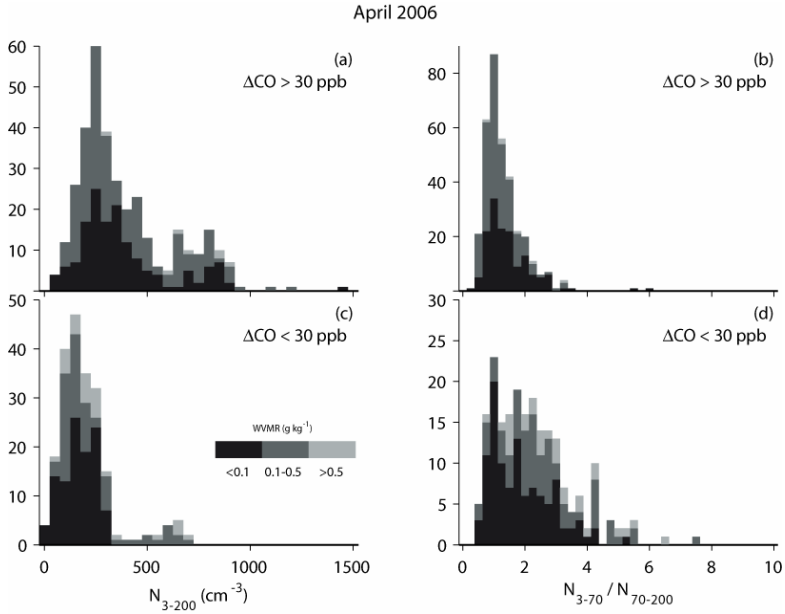

Figure 5.2. (a) Free troposphere (z>3km) particle number concentration frequency distribution in the April 2006 campaign for samples with **ΔCO**>15ppb (polluted air). **ΔCO** is defined in section 3.3. (b) R ratio in polluted air. (c) Particle number concentration in clean air (**ΔCO**<15ppb). (d) R ratio in clean air. Grey shading represent the water vapour mixing ratio.

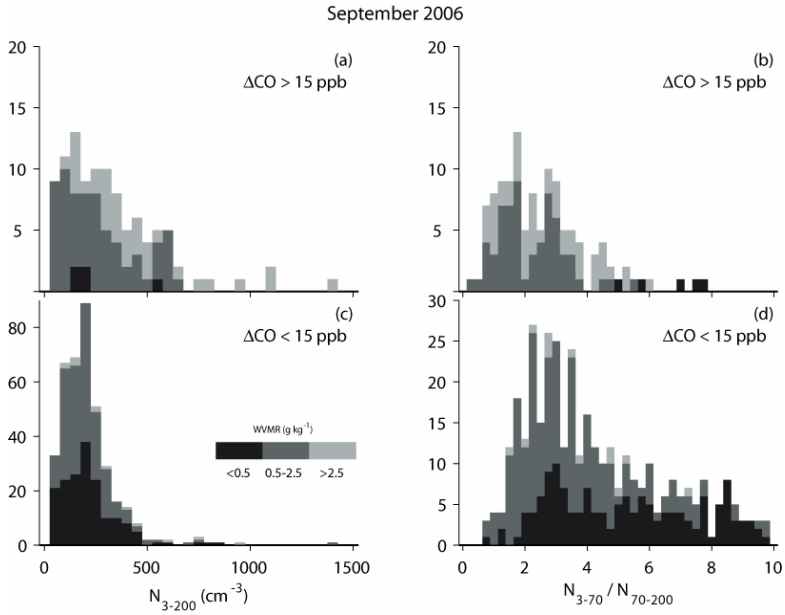

Figure 5.3. (a) Free troposphere (z>3km) particle number concentration frequency distribution in the September 2006 campaign for samples with **ΔCO**>15 ppb (polluted air). (b) R ratio in polluted air. (c) Particle number concentration in clean air (**ΔCO**<15 ppb). (d) R ratio in clean air. Grey shading represent the water vapour mixing ratio.

Figure 5.4 shows three examples of the distribution of particle number concentration in vertical profiles, each profile being averaged over a given flight (6±2 hours). Also shown are the CO and water vapour mixing ratios. The September flights (shown in Fig. 5.4c; flight 8, 10 Sept 2006) exhibit larger $N_{3–200}$ value in the BL or immediately above the BL. The strong sensible heat flux from the forest mixes efficiently biogenic volatile organic compounds (VOC) emitted by the vegetation (Lathière et al., 2006; Tarvainen et al., 2007; O'Dowd, 2002) into deep convective BL (Baldocchi et al., 2000), lofting these compounds up to the entrainment zone, where they can reach into the FT by night (Stull, 1988). Conditions favourable to nucleation were met during the September campaign. No local, fresh biomass burning plume was observed at that time. Only one aged fire plume from (agricultural) biomass burning transported from Kazakhstan and the Caspian Sea area was measured, which exhibited the highest CO concentrations of the campaign. In the September data above 4 km altitude, $N_{3–70}$ is higher by up to one order of magnitude than $N_{70–200}$. On the opposite, the April flights (April 11 and 14, 2006, Fig. 5.4a-b) has concentrations of $N_{3–70}$ and $N_{70–200}$ particles approximately equal, from the ground to flight ceiling.

5.6.2. Size distribution and the limitation of size resolution

Here we rely on the relative concentration of particle in the two size ranges to discriminate fresh particles (roughly, nucleation and Aitken modes) from condensation nuclei (CN). In the troposphere, under specific conditions of humidity, temperature and incoming radiation, nucleation yields a larger number concentration of ultrafine particles relative to concentration nuclei. Studies on airborne aerosol measurements (using finer size resolution instruments) proposed nucleation event to be characterized by a modal distribution increased toward the finer sizes with specific criteria (see e.g. Covert et al., 1992; Lee et al., 2003; Young et al., 2007). We speculate here that a large increase in the ratio $R = N_{3\text{-}70}/N_{70\text{-}200}$ is sufficiently discriminative of freshly nucleated particles. The median of the R value is 1.5 for the April campaign (see Fig. 5.2), and 2.5 for the September campaign (see Fig. 5.3). In the September 2006 campaign 20% of the data had $R>5$, and 5% had $R>10$. In the free troposphere above 4 km altitude, 65% of the data had $R>5$ and 10% had $R>10$. No more than 4% of the data reached R>5 in the April campaign. 11% of the September FT data had both $R>5$ and $N_{3–70}>100$ cm^{-3}, which can be considered a possible criteria for the assessment of recently nucleated particles in the FT. Only 2% of the April data responded to this criterion.

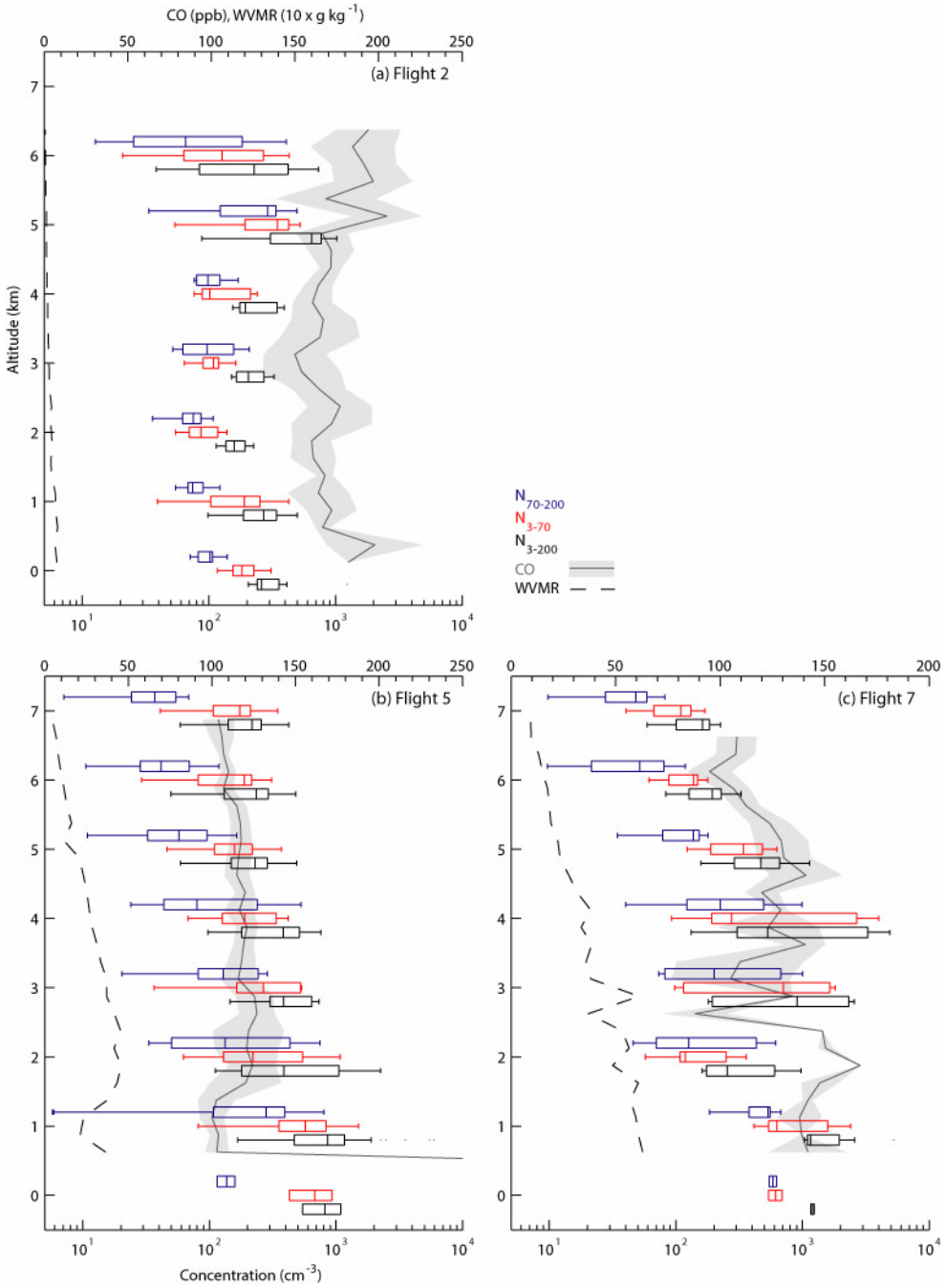

Figure 5.4. Vertical profile of particle number concentrations and trace gases for (a) Flight 1 (11 April 2006), (b) Flight 3 (12 April 2006), and (c) Flight 8 (10 September 2006). Blue box plots represent the N3-70 concentrations, red box plots the N70-200, black box plots the total N3-200. The box-and-whiskers indicate the median, first and third quartile of the data in each 1km altitude bin. Bars extending from the box encompass outliers residing at less than 1.5 inter-quartile range, more extreme outliers being marked as points. The magenta line represents CO mixing ratio, with 1 standard deviation shaded in grey. The green line shows the water vapour mixing ratio. Each profile shown here is averaged over between 4 and 8 ascents and descents.

5.6.3. Long range transport of surface tracers and particle concentrations: April 2006 case

High particle concentrations coincided with CO enhancements (Fig. 5.2 and Fig. 5.4a) in the mostly dry April troposphere, irrespective of altitude. During flights 2 and 3 in April 2006 Uplifted boundary layer air from polluted regions of China was identified in the mid-troposphere in Siberia above 5 km by Paris et al. (2008). Elevated CO concentrations were observed in this uplifted pollution (Fig. 5.4a), alongside with an absence of O_3 enhancement. The presence of Chinese pollution suggests the possible presence of coarse particles (anthropogenic and dust from dust storm in China), which could explain the absence of O_3 enhancement. Additional gas to particle conversion may occur in this plume.

In our sampled air mass from China, the observed $N_{3–200}$ had median 300 cm^{-3} and third quartile ~500 cm^{-3}, and was higher than in surrounding cleaner air (between 10 and 80 cm^{-3}), but remained low pointing out to a condensational growth of existing aerosols. At 5km altitude in the uplifted pollution plume, $N_{3–70}$ was higher than $N_{70–200}$, possibly reflecting a distinct layer where fresh nucleation occurred in the recent air mass history.

In the flights of April 2006, outside the well-defined uplifted pollution plume described above (which was encountered during Flight 2 and Flight 3), the FT is characterized by very low $N_{3–200}$ (~10^2 cm^{-3}) even in polluted air masses with CO excess (ΔCO) of ~100 ppb (Fig. 5.5). ΔCO is defined relative to the clean-air background according to Paris et al. (2008). There was no clear relation between ΔCO and the *R* ratio in the April 2006 campaign dataset. Within the clean FT air masses, the *R* ratio remained close to unity, suggesting a flat, or symmetric, size distribution. Over eastern Siberia (Flights 2 and 3), the *R* ratio is 0.99±0.05 in air masses having ΔCO>50 ppb (associated to Chinese pollution), whereas it is 1.28±0.11 for surrounding air. This observation suggests that new particle formation must have been very limited in a recent history of the sampled air mass, possibly with preferential sink on pre-existing particles.

Using CO as a surface tracer suggests that this air mass was exposed to large concomitant sources of both CO and SO_2 (Ohara et al., 2007). A literature survey suggest likely CO/SO_2 ratios in the outflow of NE Chinese boundary layer. During Chinese pollution export event over Taiwan, Lin et al. (2007) show well correlated SO_2 and CO measurement, with ratios of about 0.01–0.02 ppb(SO_2)/ppb(CO) after ~1 days of transport. By comparison, emissions ratio from Ohara et al. (2007) are in the range 0.08–0.10 mol(SO_2)/mol(CO). In the polluted air that we sampled in April 2006, the 50–60 ppb CO enhancements could therefore be translated into SO_2 enhancements of about 0.5–1.2 ppb. In the immediate outflow of China in April Buzorius et al. (2004) found elevated CN concentration, coincident with high SO_2 concentrations (10ppb), and alternating with layers of high CO and coarser particles acting as condensational sink, similar to the Chinese outflow described above.

5.6.4. Upper troposphere particle formation: September 2006 case

In September 2006, increasing *R* ratio was observed with decreasing CO enhancements (Fig. 5.3 and Fig. 5.4c). Dry FT air (4-8 km) has a lower concentration of particles but is characterized by R ratio values up to 10. Due to a lower amount of anthropogenic pollution (for which we use ΔCO as a proxy) in the Siberian air shed at that time, the formation of new particles is able to dominate over the condensational sink.

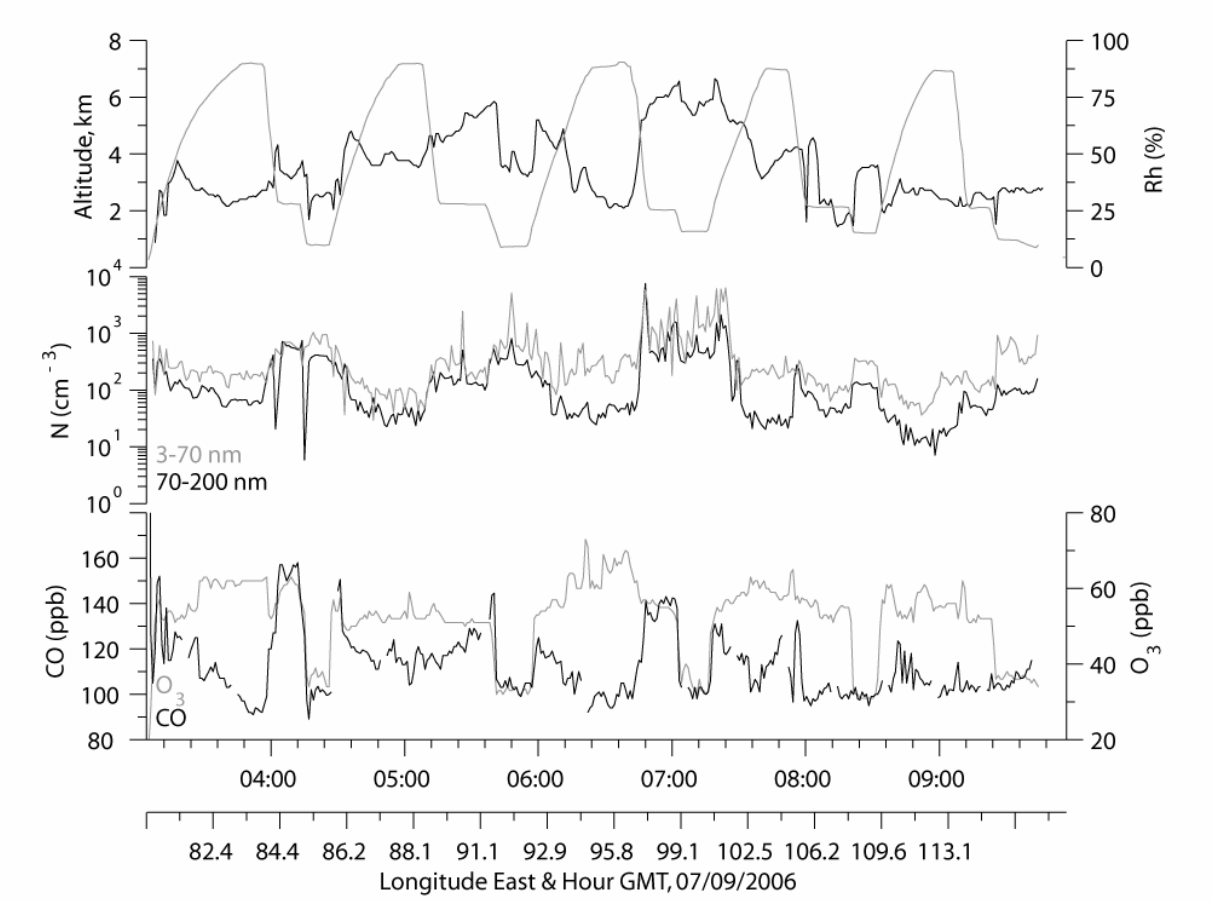

Figure 5.5. Time series of relative humidity, altitude, and particle, CO and O_3 concentrations for Flight 5 on 7 September 2006.

Figure 5.5 shows measured particles concentrations as well as relative humidity, CO and O_3 for Flight 5 on 7 September. Note the elevated CO concentrations (ΔCO ~ 60 ppb, with large O_3 concentrations of 55–60 ppb) at about 2 km altitude at 0400-0415 UTC resulting from the encounter with a biomass burning plume originating from Kazakhstan (Paris et al., 2008). The plume was encountered while crossing a warm front with heavy cloud cover (the cloud cover corresponding to the two sharp drops in particle concentration). The observed CO background in late summer is between 90–110 ppb, denoting a rather clean atmosphere. Particle concentrations are highly variable throughout the flight but two regimes emerge: high particle concentrations (a few thousands cm^{-3}) in the BL (identified by high humidity and very low O_3 concentrations); and

two occurrences (time between 0600 and 0800) of a stratospheric influence (marked by O_3 concentrations up to 70 ppb, and) in the upper troposphere, where $N_{3–70}$ is of the order of 100–200 cm^{-3} against $N_{70–200}$ concentrations of 10–20 cm^{-3}. This results in R ratio value of about 10, denoting the influence of new particle formation. Surface tracer CO is very low during these cases, further confirming the isolation from surface sources and suggesting ion-induced or ion-mediated nucleation as a contribution to new particle formation (Lee et al., 2003). In order to test the possibility that we observe export of particles that have nucleated in the BL we have investigated the sensitivity of the R ratio to surface emissions influence within a characteristic lifetime of 48 hours. Using the FLEXPART Lagrangian particle dispersion model (Stohl et al., 2005; Paris et al., 2008, results available online at http://zardoz.nilu.no/~andreas/YAK/) throughout the September 2006 campaign it was found that on average, in the air sampled above 4km, less than 1% of the sampled 'air parcels' have resided in the lowest 300m of the troposphere, and hence would have been possibly influenced by surface emissions, within the last 48 hours. Due to their rather short lifetime, this rules out the vertical transport of particles originally nucleated in the BL to the FT. As a result our case study suggests that fresh particle nucleation occurred in the remote continental upper troposphere, with air well isolated from the BL. This could be attributed to the specific conditions (steep temperature and humidity gradients) in tropopause folds (Young et al., 2007).

5.6.5. New particle formation in mid-tropospheric cloud outflow: September 2006 case

The aircraft flew over convective clouds between 0750 and 0815 (Fig. 5.6) at 4 km altitude during Flight 7 (8 September 2006). The convection is reflected by a local increase in relative humidity to ~80%, and in CO concentrations to ~150 ppb, about 50 ppb above tropospheric background concentrations. Immediately past the outflow of the convection, concentrations of $N_{3–70}$ increase by one order of magnitude up to 4000 cm^{-3} while $N_{70–200}$ increases only up to 700 cm^{-3}. As a result the R ratio increased from unity at 0800 to about 6. Ruling out size-dependent effects in aerosol load scavenging during convection, this strongly suggests the occurrence of new particle formation in the cloud outflow. According to FLEXPART up to 90% of the air parcels sampled with highest R ratio values had resided in the BL in the last two days prior to sampling, confirming the influence of uplifted BL air in the measurement. The contribution of surface tracer such as CO is suggestive of a concomitant uplift of elevated SO_2 or insoluble organic compounds concentrations, potentially participating to the new particle formation event. Twohy et al. (2002) described a similar event although in their case it was observed in the upper troposphere, and fine particle concentrations were much higher.

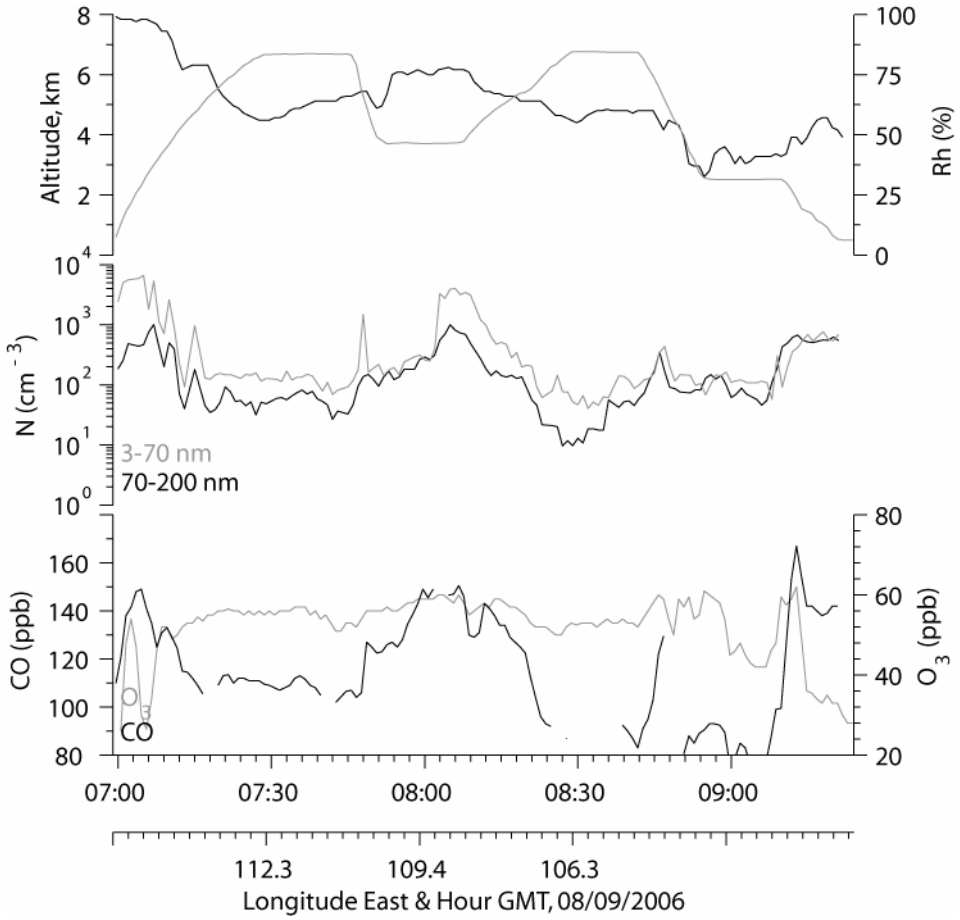

Figure 5.6. Time series of relative humidity, altitude, and particle, CO and O_3 concentrations for Flight 7 on 8 September 2006.

5.6.6. Seasonal variation

Figures 4a-b show respectively the seasonal evolution of $N_{3–70}$ and N_{70-200} derived from the 5 years of monthly vertical profiles in Novosibirsk (Arshinov and Belan, 2004). Median ultra-fine particles (3–70 nm) concentrations range between ~300 cm^{-3} in summer and 30 cm^{-3} in winter. Fine particles (70–200 nm) range between 10 and 30 cm^{-3} in winter and summer, respectively. Variability of ultra-fine particles is higher in June and July, suggesting a shorter lifetime (Williams et al., 2002). The most important feature of Fig. 5.7 is the difference in concentration between the BL and the FT. The BL height seasonal variation is clearly visible in the data, except for an apparent drop in particle concentration between June and August. The concentrations are maximal in May and September (with both N_{3-70} and N_{70-200} > 500 cm^{-3}). Kulmala et al. (2004) and Lyubovtseva et al. (2005) observed spring and fall maxima in nucleation events frequency at the Hyytiälä station in Finland.

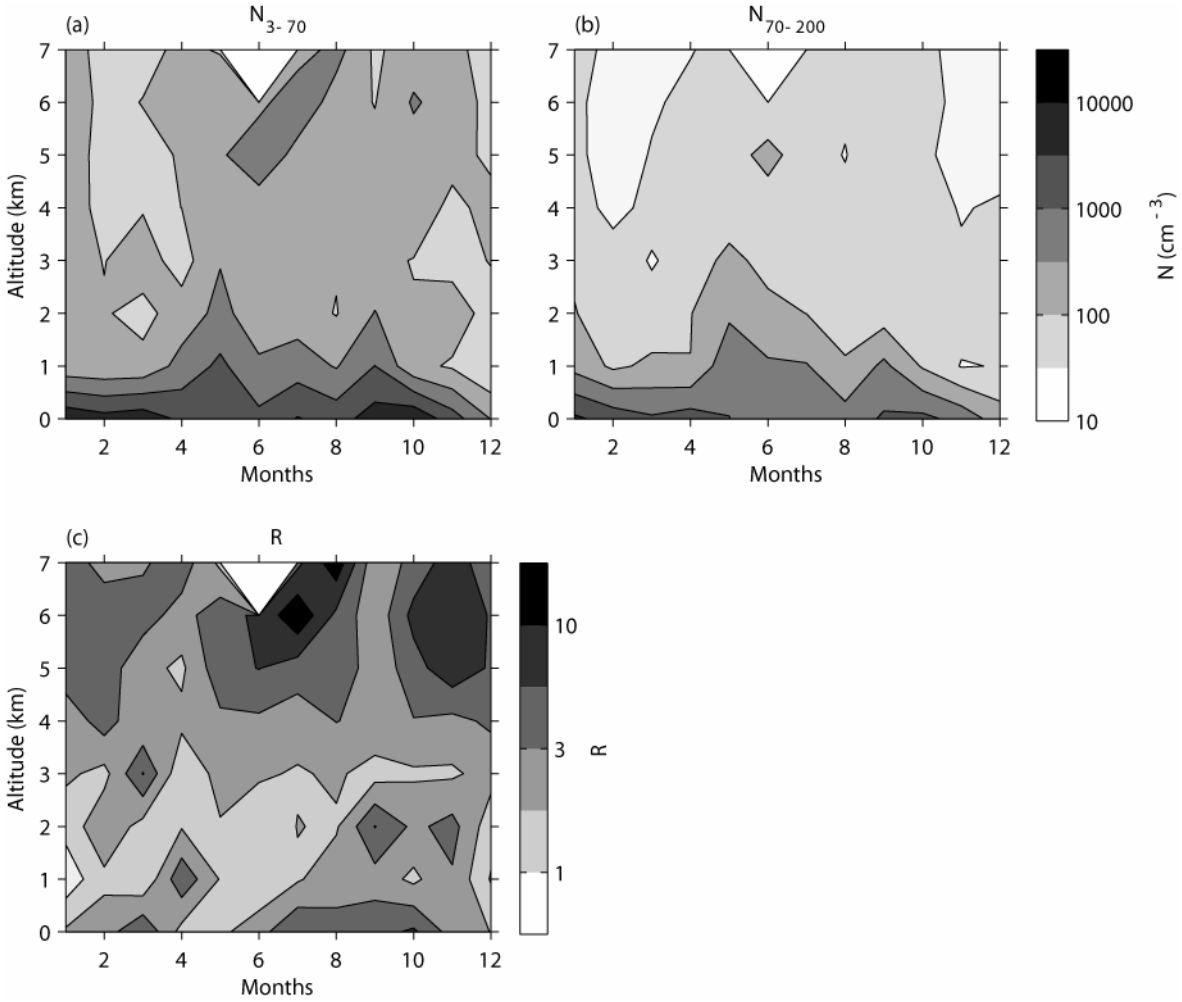

Figure 5.7. Seasonal variation of the particles number concentrations and ratio *R* of ultrafine (3-70nm) and fine (70-200nm) in the troposphere obtained from regular vertical profiles near Novosibirsk. (a) Total concentration in the 3-70 nm range. (b) Total concentration in the 70-200 nm range. (c) R ratio. Greyscales are logarithmic. There were not enough good data in June at 7 km to provide a robust value.

Our data do not allow explaining the summer drop in BL particle concentrations. In summer, conditions typically include a high BL top, higher biogenic precursors emissions (Lathière et al., 2006) and higher growth rates of ion clusters and ultrafine particles (Hirsikko et al., 2005). In Siberia the months of June, July and August account for 50–60% of the annual precipitation (Soja et al., 2004), leading to scavenging in the lower troposphere, and are also the period for highest evapo-transpiration. Lower fine particle concentrations in summer could additionally be influenced by the presence of coarser carbonaceous particle from forest fires (Soja et al., 2004), which could increase the condensational sink.

In the free troposphere there is a significant maximum of ultra-fine particles in July and August, which could be in-situ formation. Figure 5.7c shows the seasonal and vertical distribution of the R ratio. The FT median size ratio *R* shows a large variability from 0.1 to 10, possibly

reflecting sporadic fresh particle nucleation. This ratio is maximum in July between 5–7 km altitude (R inter-quartile range being here 4–12), which suggest summer maximum in-situ particle formation, despite wet scavenging by widespread continental convection. A secondary maximum occur in November, whose origin is unclear. At 5 km there is a minimum in the R ratio in April, which could be compared to our case study of Asian pollutant export to Siberia during dust storms outbreak (Paris et al., 2008). This minimum is therefore possibly explained by an increased condensational sink preventing new particle formation.

Our September case study identified that uplift of BL air by convection in the mid troposphere and UT/LS conditions can enhance ultrafine particle concentrations in the FT. These conclusions could explain the summer maximum in the R ratio at 5 – 7 km altitude. Alternatively, this finding could also be explained by the hypothesis by Kulmala et al. (2006b) that deep convection of water-insoluble trace gases to the FT are a possible in-situ nucleation source in the absence of sulphuric acid.

5.7. Summary and Conclusions

Fine (7–200 nm) particles number concentration measurement during two intensive airborne campaigns in the troposphere above Siberia between Novosibirsk and Yakutsk (the YAK-AEROSIB project) and monthly vertical profiles near Novosibirsk have been presented. During the campaigns, low concentrations of the order of 200 cm^{-3} have been observed in the free troposphere (FT). Our data are consistent with a possibly widespread gas-to-particle conversion in the free troposphere. In April, no strong excess of fine particles were found in a filament of polluted air originating from NE China, suggesting dominant effect of condensational sink.

In September 2006, particle concentrations decreased with altitude to reach ~50–200 cm^{-3} at 7 km. $N_{70–200}$ exhibited a gradient steeper than that of $N_{3–70}$. $N_{3–70}$ account for 90% of the total particle concentration in the free troposphere at 6–7 km altitude. Two cases of possible nucleation with relatively high concentrations (~200 cm^{-3}) and $N_{3–70}/N_{70–200}$ ratios are reported for the September campaign, in the upper troposphere and in cloud outflow in the mid-troposphere. The latter case lead to concentrations of ~4000 cm^{-3} in association with surface emissions as denoted by elevated CO concentrations.

In the seasonal analysis, we found high concentrations (>1000 cm^{-3}) and $N_{3–70}/N_{70–200}$ ratios in summer in the mid- and upper troposphere, consistent with in-situ nucleation. This could be related to either one of the two processes described by our case studies. The summer precipitations maximum, and the high altitude of this maximum could also support Kulmala et al. (2006b) hypothesis of in-situ FT nucleation from water-insoluble precursors. Maximum concentrations in the BL are observed in spring and fall.

Our aircraft was not equipped to provide high-resolution size distribution or precursors' concentration measurements. Therefore our preliminary results strongly suggest, but cannot diagnose unambiguously, fresh nucleation. Instead, this calls for new, targeted investigation in the clean, continental air shed above Siberia.

Chapitre 6.
Apport des mesures pour la contrainte des modèles

Les chapitres précédents ont analysé les observations de gaz trace et de particules obtenues durant les campagnes. Ces analyses, dans les chapitres 3 et 4, sont basées sur l'utilisation de modèles permettant de fournir des informations sur l'origine des masses d'air difficilement accessibles à travers un jeu de données in situ. Avec un angle d'approche opposé, ce chapitre, tout en synthétisant les observations présentées préalablement, approche la question de l'utilisation de ces mesures pour apporter une validation des modèles utilisés pour prédire le transport atmosphérique et notamment ceux utilisés pour transporter les flux de CO_2.

6.1. Contexte et résumé

Le CO_2 est échangé par les forêts sibériennes avec une forte variation saisonière. Il est émis parallèlement au CO dans les processus de combustion. L'article dont est tiré ce chapitre se veut une synthèse des résultats obtenus sur les campagnes YAK-AEROSIB. Le CO_2 et le CO ont la propriété d'être des espèces à longue durée de vie et donc soumises au transport atmosphérique. Les mesures réalisées durant les campagnes contiennent donc un signal un signal utile pour valider la réprésentation du mélange atmophérique dans les modèles utilisés pour les estimations de flux de CO_2. On peut ainsi utiliser ces mesures pour étudier d'une part le mélange vertical à grande échelle dans les modèles, et d'autre part le transport synoptique associés par exemple aux systèmes frontaux. Symétriquement, on peut s'attacher à retrouver dans les observations la prédiction des modèles concernant l'advection à basse altitude des polluants européens vers la Sibérie et l'Arctique.

Ces campagnes permettent également de valider les modèles lagrangien de transport capable de caractériser des panaches de quelques centaines de mètre d'épaisseur seulement.

6.1.1. Mélange vertical et *rectifier*

La mesure aéroportée du CO_2 peut contribuer à la validation des modèles en termes de mélange vertical. Le gradient vertical de CO_2 à grande échelle au dessus des zones continentales de l'Hémisphère Nord, et en particulier en Eurasie, est sensible à la covariation saisonnière entre le transport vertical et les flux de surface. Cette covariation, appelée effet *rectifier* (Denning et al. 1999 ; voir également Yang et al 2007 ; Chan et al 2008, Larson and Kolmer, 2008) génère des gradients horizontaux moyens de CO_2 entre les stations de surface. Malheureusement, les modèles de transport globaux utilisés pour la modélisation du CO_2 donnent des résultats divergents dans le calcul de ces gradients pourtant fondamentaux pour le calcul des flux (Rayner and Law 1995; Law et al. 1996). Cette erreur dans les modèles de transport se propage donc au diagnostic des flux de surface (Gurney et al. 2002; Peylin et al. 2002). Puisque l'écart entre modèles en termes de cycle saisonnier du CO_2 simulé illustre leurs différences en mélange vertical et horizontal, il a été proposé (Gloor et al. 2004) et récemment démontré (Stephens et al. 2007, Yang et al. 2007) que des profils verticaux indépendants fournissent une contrainte supplémentaire qui permette de valider la représentation par les modèles du couplage entre flux de surface et transport.

Stephens et al. (2007) ont évalué, avec une collection de 12 sites de profils verticaux aéroportés dans l'hémisphère nord, les modèles de transport globaux prescrits avec des flux optimisés contraints par les stations de surface (selon le protocole TRANSCOM décrit par Baker et al., 2006). Malgré l'utilisation de flux prescrits optimisés pour les mesures de surface, la quasi-totalité des modèles s'est montré systématiquement biaisée par rapport aux gradients verticaux observés. Ces biais suggérèrent que le mélange vertical est sous-estimé en hiver et surestimé en été, avec un impact important sur l'inférence des puits entre hémisphère nord et tropiques. Les modèles de transport peuvent ainsi être efficacement différenciés, dans le cadre d'une modélisation inverse du CO_2, à travers leur représentation des gradients verticaux observé.

6.2. Résumé

L'ensemble des profils verticaux de CO_2 obtenus durant les trois premières campagnes YAK-AEROSIB constitue un jeu de données unique capable de fournir de nouvelles contraintes sur la représentation du transport synoptique dans les modèles, notamment dans le cas d'un transect à travers une zone de perturbation barocline. Le cycle saisonnnier observé pour la distribution verticale du CO_2 permet de contraindre le *rectifier effect* mal compris. Dans une application préliminaire de ces données pour valider les modeles globaux de transport du CO_2, nous montrons que le model de transport LMDZ est probablement biaisé vers une sous-estimation du mélange vertical en hiver, révélé par un gradient vertical excessif de CO_2 en comparaison des

observations. Dans une étude de cas appliquée à un vol de septembre 2006, je montre que la représentation du transport synoptique est correctement modélisée. En particulier, la hauteur de couche limite (déterminée par le gradient de CO2) et le gradient associé à un front chaud sont correctement positionnés.

Par ailleurs cet article synthétise certaines observation établies dans les précédents chapitre, comme par exemple le transport des emissions d'Europe et de feux de biomass dans la région entourant la Mer Caspiennne (et notamment au Kazakhstan), identifié immédiatement au dessus d'un air beaucoup plus propre en provenance de l'Arctique.

Nous concluons sur les perspectives offertes par les campagnnes de Juillet 2008, plus spécialement dédiées à l'étude des feux de forêts dans le cadre du projet POLARCAT de l'Année Polaire Internationale, projet d'envergre internationale pour lequel les campagnes en Sibérie furent soutenues par des partenaires français (Service d'Aéronomie et laboratoire partenaires) et norvégiens (NILU).

6.3. Article

Transcontinental flights over Siberia: overview of first results of the YAK AEROSIB project. Soumis au *Bulletin of the American Meteorological Societey*, par J.-D. Paris, P. Ciais, P. Nédélec, A. Stohl, B. D. Belan, M. Yu. Arshinov, C. Carouge, G. S. Golitsyn, I. Granberg.

The YAK-AEROSIB aircraft campaigns, part of a joint French-Russian research program, measured the vertical distribution of CO_2, CO and O_3 in the Siberian troposhere, in April 2006, September 2006 and August 2007. Siberia is a vast region lacking measurements so far, and its role as a possible CO_2 sink is not well understood. The unique set of dense CO_2 vertical profiles provided new constraints on the representation of synoptic transport patterns and mixing associated to frontal transport in models. Further, the observed seasonal cycle in vertical CO_2 distribution constrained the poorly known covariance between vegetation fluxes and vertical mixing, known as "rectifier effect". In a first but promising illustration of the usefulness of the YAK-AEROSIB data to cross-validate global CO_2 transport models, we show that the LMDZ transport model is likely to be biased towards too low mixing in winter times, as it produdes a too large CO_2 vertical gradient compared to the observation. Detailed case studies found occurences of CO enhancements of 30-50ppb above background values, coincident with high O_3, that were related to the transport of emissions from Europe and from wildfires in the Caspian Sea area, over much cleaner Arctic air. Another case in April 2006 revealed large CO pollution in the troposphere (5-7 km) over Eastern Siberia, due to the very fast transport of Chinese emissions provoked by a cold front. YAK-AEROSIB was continued with campaigns in spring and summer 2008, which were targeted at examining the extent and composition of Siberian forest fire plumes, in the frame of the POLARCAT project.

6.4. Introduction

The atmospheric composition of the Siberian air shed is not well measured. We present new data from the YAK-AEROSIB campaigns, performed as a joint French-Russian research program ongoing since 2004. Three campaigns have been executed using an ANTONOV-30 research aircraft equiped with new instruments, in April 2006, September 2006 and August 2007 respectively. Numerous vertical profiles of CO, CO_2, O_3 and aerosols have been collected, allowing a 'tomography' of the Siberian troposphere at different times of the year.

6.4.1. Why are measurements needed over Siberia?

Partitioning the sources and sink of CO_2,the main anthropogenic greenhouse gas, remain a difficult task. The top-down approach infer surface fluxes from the measured atmospheric concentrations by accounting for atmospheric transport of integrated fluxes. Uncertainty in modelled transport and sparseness of measurement network limit the ability of inverse methods (Gurney et al. 2002). The spread across transport models results can be matched against independent vertical profiles to cross validate models (Gloor et al. 2004, Stephens et al. 2007). In large continental areas such as Eurasia, the vertical CO_2 gradient is affected by the seasonal co-variation, called rectifier effect (Denning et al. 1999), between vertical mixing and surface fluxes. Such co-variation propagates into large discrepancies between models that can be best assessed using dense profiles above Siberia, the region that is most sensitive to this effect.

Atmospheric pollutants released by human activities in mid-latitude regions of the Northern Hemisphere are quickly moved over long distances by atmospheric transport. For instance, intercontinental pollution transport has become of increasing concern because of its effect on local and regional air quality levels The main pollution transport pathways, schematically depicted in Fig. 6.1, differ qualitatively between North Asia and Siberia, Western Europe and North America. European pollutants are predominantly dispersed westwards over Siberia in summer, or westwards and northwards towards Siberia and into the Artic in winter (Stohl and Eckhardt 2004). Unlike the export of North Asian emissions which has a higher probability to be mixed by convection, injecting pollutants in the high-troposphere, the export of O_3 and its precursors from Europe tends to remain confined to below 3000 m (Wild et al. 2004, Stohl et al. 2002, Duncan and Bey 2004). This pattern is diagnosed upon large scale model simulation results, and thus depends critically on how well these models simulate vertical transport and mixing. The main pathways of intercontinental transport across the Northern Hemisphere have been characterized by campaigns down-wind from and in emission regions (Andreae et al. 1988, Lelieveld et al. 2002, Jacob et al. 2003), and by using satellite observations (Edwards et al. 2004) interpreted with models (Heald et al. 2004). However, no data are available from the vast region of Siberia, which according to the models is heavily impacted by the transport of pollution from Europe but where boreal forest fires can episodically also be an important local pollution source.

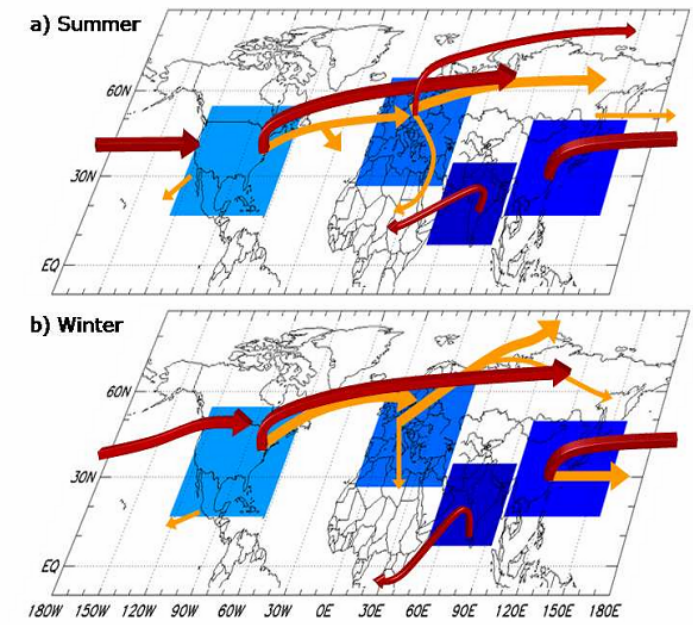

Figure 6.1. Illustration of pollutant long range transport patterns. From Task Force-HTAP, interim rep., 2007 [www.htap.org]; Originally from Stohl and Eckhardt, 2004

Using the YAK-AEROSIB data, we seek to obtain a better understanding of the following science questions: What is the vertical distribution of CO_2, CO and O_3 over Siberia and its seasonal variation? What does CO_2 which is exchanged by Siberian forests with a strong seasonal variation as well as co-emitted with CO in the combustion of fossil fuels, tell us as a transport tracer to constrain vertical mixing in models ? What can we learn from such a dense set of vertical profiles about synoptic transport and tracer mixing associated with frontal systems ? Can we confirm by observations the model predictions that European pollutants are mainly exported to Siberia and the Arctic at low altitudes ? After presenting the YAK-AEROSIB campaigns and measurements, these questions are addressed, using results from the first three campaigns. Illustrative examples of the use of vertical profile information are presented and discussed, rather than an in-depth data analysis or model evaluation.

6.5. Experimental strategy and operations

The three YAK-AEROSIB campaigns sampled exactly the same transect of the Siberian troposphere shown in Fig. 6.2, using *Optik-E,* an Antonov -30 research aircraft,operated by the Tomsk Institute of Atmospheric Optics (Fig. 6.3). The YAK-AEROSIB campaigns transect is extending from Novossibirsk to Yakutsk, in a domain bounded by 55°N to 63 °N and 80°E to 130°E. Vertical profiles between 0 and 7 km are made roughly every 200 km. The dominant vegetation type is deciduous (larch) and evergreen (spruce, pine) conifer forests, with forested bogs in the Yakutsk region, and agricultural regions and steppes further south and west of the domain.

The region has an extensive rivers and ponds network, including the Yenissei and Lena rivers and their tributaries. The flight track passes over several major cities, industrial or mining centres : Novosibirsk, Tomsk, Myrni, Ieniseisk, Irkutsk, Bratsk, Krasnoyarsk and Kemerovo. Agriculture is also present in the surroundings of Krasnoyarsk and Novosibirsk.

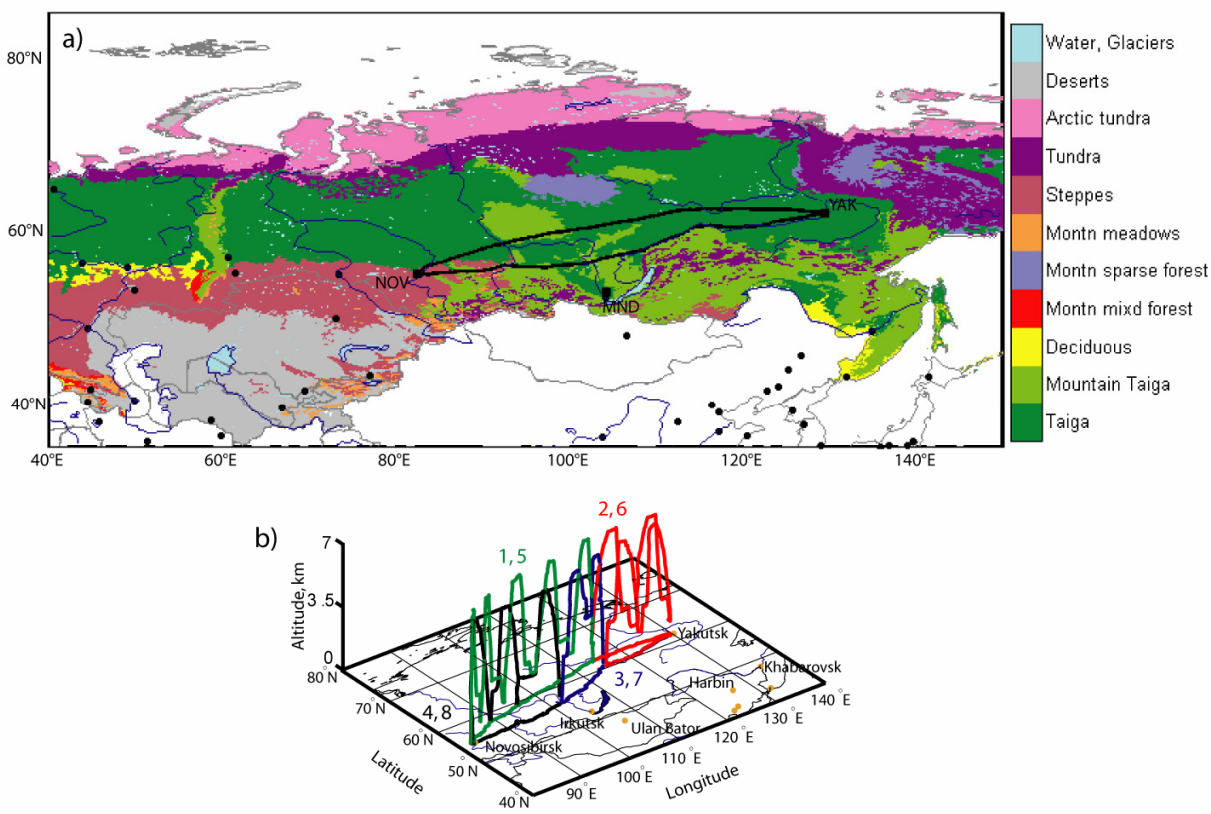

Figure 6.2. Flight route and landscape classification. Each campaign follows a similar route, starting from Novosibirsk (NOV) in central Siberia, to the pivot point Yakutsk (YAK) and back to NOV. A campaign is composed of 4 flights; the first is depicted in green, the second in red, the third in blue, and the fourth in black. The landscape classification is derived from (Shvidenko et al. 2007)

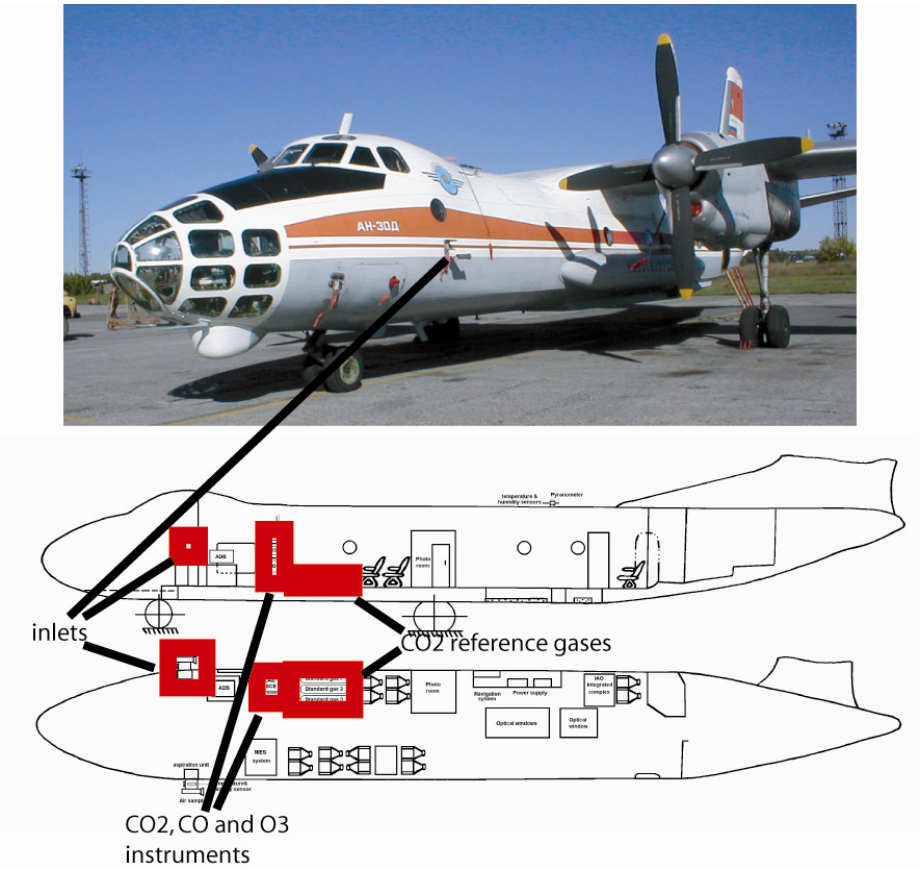

Figure 6.3. Aircraft picture and schematics of interior.

Each campaign consists of four flights, each containing between 4 and 10 vertical profiles. The first campaign YAK-1 was conducted in April 2006 and 26 vertical profiles were collected. Each profile takes about 30 minutes, including horizontal plateaus at lower level, at 5 km during descent, and at upper level. The campaign YAK-2 was conducted in September 2006 and YAK-3 in August 2007 (see Table 6.1). The two-propeller Antonov-30 aircraft operated by the Institute of Atmospheric Optics of Tomsk (Zuev et al., 1992) is equipped for meteorological measurements. Aircraft horizontal speed during measurement is about 85 m s-1 and vertical speed is about 3.5 m s-1 on ascent and 7 m s-1 on descent during profiles.

Table 6.1. Flights information.

Flight nb	Date	Time (local)	Time (UTC)	Nb profiles	Itinerary
1	11 Apr 06	1200-2100	0600-1200	8	Novosibirsk-Myrni
2	12 Apr 06	1100-1530	0200-0630	8	Myrni-Yakutsk-Lensk
3	12 Apr 06	1730-1900	0830-1100	4	Lensk-Bratsk
4	14 Apr 06	0830-1030	0030-0430	6	Bratsk-Novosibirsk
5	07 Sept 06	0900-1900	0300-1000	10	Novosibirsk-Myrni
6	08 Sept 06	0945-1430	0045-0530	8	Myrni-Yakutsk-Lensk
7	08 Sept 06	1600-1730	0700-0930	2	Lensk-Bratsk
8	10 Sept 06	0900-1115	0100-0515	6	Bratsk-Novosibirsk
9	17 Aug 07	0930-1815	0330-0915	10	Novosibirsk-Myrni
10	18 Aug 07	0725-1200	2225-0300	8	Myrni-Yakutsk-Lensk
11	18 Aug 07	1315-1445	0415-0645	4	Lensk-Bratsk
12	20 Aug 07	0830-1000	0030-0400	6	Bratsk-Novosibirsk

[a] started on 17 Aug 07, 2225 UTC, most of the flight occurred on the 18th by UTC dates.

The CO_2 analyser is a modified non-dispersive infrared (NDIR) analyser Li-Cor 6262 (see Table 6.2). The instrument is regulated for temperature, flow and pressure. Incoming air is chemically dried. Three calibration gases, traceable to a suite of primary WMO-CO_2 standards from NOAA/ESRL, bracketing ambient concentrations are used sequentially at ~30min intervals in order to cope with potential drift of the measurement. Approximately 5% of the data were rejected on average based on pressure, flow and temperature anomalies.

Table 6.2. Instruments characteristics.

Species measured	Core Technique	Acquisition frequency	Accuracy	Reference
CO_2	NDIR	2 s	0.15 ppm	Paris et al., 2008
CO	Gas filter correlation	1 s[a]	5 ppb / 5%	Nedelec et al., 2003
O_3	UV absorption	4 s	2ppb / 2%	Paris et al., 2008
Aerosols concentration	Diffusion battery	1 min	10%	Reischl et al., 1991
Relative humidity		1 s	7%	Zuev et al., 1992
Temperature		1 s	0.5°C	Zuev et al., 1992

[a]: after 30 s slide-averaging

The O_3 analyser is a modified Model 49 (Table 6.2) of Thermo Environmental Instruments (TEI, USA), with added internal calibration and compensated pressure and temperature. It is based

on UV absorption in two parallel ("zero" and sample) cells. Laboratory calibration with a O_3 generator is performed before and after the campaigns. Before entering the O_3 and CO instruments, air is pressurised to cabin level.

The CO analyzer (Nedelec et al. 2003, Table 6.2) is a heavily modified IR gas filter correlation analyser TEI Model 48C. Periodical accurate zero measurements, new IR detector with better cooling and temperature regulation, pressure increase and regulation in the absorption cell, increased flow rate to 4 L min^{-1}, water vapour trap and ozone filter have been introduced.

Aerosols are measured using a diffusion battery (Reischl et al., 1991; Arshinov et al., 2007) but are presented in another paper (Paris et al., 2008, manuscript in preparation). Meteorological parameters are measured routinely onboard using HYCAL sensor model IH-3602-C of Honeywell Inc.

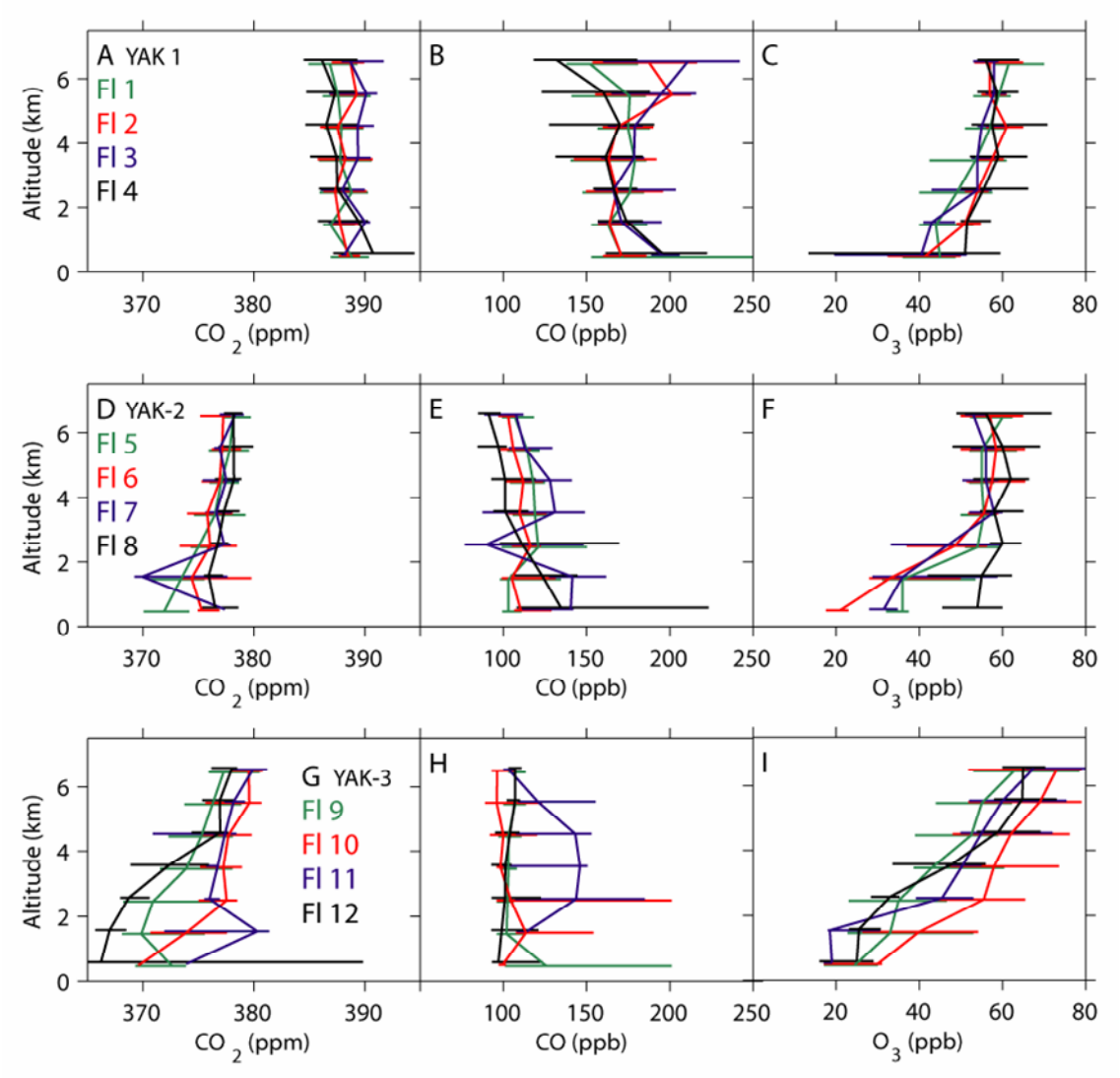

Figure 6.4. Profiles of CO_2, CO and O_3 over the 3 campaigns. Each flight is colour-coded as in Fig. 6.3. Each flight is averaged in 1000m bins. The horizontal bars at each altitude bin represent its 10^{th} and 90^{th} percentile.

6.6. Vertical and horizontal variability of CO_2, CO and O_3 over Siberia

We present here the seasonal variations of CO_2, CO and O_3 obtained during the YAK-AEROSIB campaigns, as well as their vertical and horizontal distribution. Figure 6.4 shows average tracer profiles.

6.6.1. Carbon dioxide

The CO_2 distribution is sensitive to the diurnal cycle of CO_2 exchange (i.e. during growing season, photosynthesis during daytime counteracts the diurnally less variable emissions from respiration) but this bias was minimized because sampling was conducted on average over all daylight hours. Individual profiles averaged for each flight into 1 km altitude bins are shown in Fig 4. One can see that the peak-to-peak amplitude of CO_2 between April and September is 14.3 ppm below 2 km, and 10.8 ppm between 3 and 7 km. April corresponds to the seasonal maximum of CO_2 over Eurasia, and more generally at high northern latitudes. During the April 2006 campaign, most of Siberia was covered with snow (Mc Donald et al. 2007) and surface soils were frozen (Smith et al. 2004), implying no uptake by plants and presumably a very small respiratory source of CO_2 to the atmosphere (Shibistova et al. 2002). In Western Europe and temperate Asia on the other hand, satellite observations of vegetation greenness index (Zhou et al. 2001, Maignan et al. 2008) indicated active photosynthesis, and eddy-covariance flux tower observations in Western Europe (Reichstein et al. 2007) confirmed net carbon uptake. August corresponds to the termination of the carbon uptake period over Siberia, with flux tower data consistently indicating a change in Net Ecosystem Exchange (NEE) of CO_2 from a sink to source at around day 250 $\pm$ 10 (Van der Molen et al. 2008). Consequently, atmospheric CO_2 in the lower Eurasian troposphere usually reaches its seasonal minimum in August (Levin et al. 2002, Lloyd et al. 2002, Ramonet et al. 2002, Machida et al. 2001), reflecting NEE zero-crossing from sink to source. Note that the August 2007 weather conditions (especially flight 9) were highly convective, with cumulus clouds fields and rain bands crossed in two occasions. In August, the regional ecosystems behave as a strong and apparently homogeneous sink, causing a CO_2 depletion of 6 ppm or more (Fig. 6.5) into the low troposphere west of 110°E. In September 2006, although the vegetation was still active (green from space) over Siberia, ecosystems were net sources of CO_2.

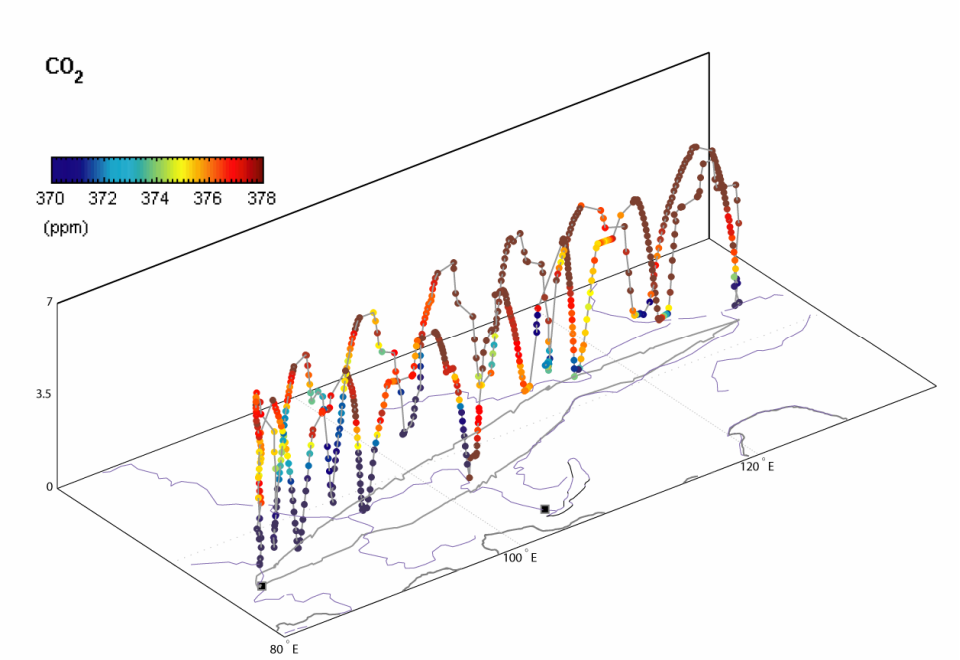

Figure 6.5. 3D representations of CO_2 measurements during August 2007. The cities of Novosibirsk and Irkutsk near Lake Baikal are represented by black squares.

6.6.2. Ozone

Figure 6.4 (panels c, f, and i) provides the O_3 average vertical profiles. The vertical gradient of O_3 is 2.6 times steeper in August 2007 than in April or September 2006, with a more pronounced O_3 depletion near the surface in August. In August, the mid tropospheric O_3 concentrations between 5 and 7 km ranged from 60 to 80 ppb, whereas they reached only 50-65 ppb in April and September. Thin layers with high O_3 concentrations (80—100 ppb and higher) probably originating from the stratosphere were repeatedly observed in the mid troposphere. The August steeper O_3 vertical gradient can be explained by a combination of factors: (1) More intense photochemical production of O_3 in August 2007, coupled to convective injection to the middle troposphere of precursors initially emitted in the BL. (2) Higher surface biogenic volatile organic compounds (BVOC) emissions contribute to higher O_3 production in August (Chameides et al. 1992). Boreal deciduous trees and spruce monoterpene emissions are indeed maximum in July-August (Tarvainen et al. 2007), while pine emissions peak in the early summer. A model study indicates that Siberian ecosystems are a large source of monoterpenes in summer (Lathiere et al. 2006). (3) Maximum foliar and surface deposition in summer cause a depletion of O_3 in the BL, and (4) the temperature-dependent O_3 reaction with BVOC within the canopy could act a as significant additional surface sink of O_3 (Goldstein et al. 2004).

The summer O_3 gradient increased with time of day, with the O_3 concentration in the BL dropping at a rate of 2.6ppb hr-1 (noted between 10 and 16h on August 16, 2007). This decrease of O_3 was spatially very homogeneous despite the large distance between profiles (200 km) and the

rather heterogeneous vegetation coverage. This suggests that strong near-surface deposition and photochemical processes are the dominant cause of the observed pronounced O_3 vertical gradient in the August 2007 flights.

6.6.3. Carbon monoxide

CO concentrations were highest during the April 2006 campaign, as shown by Fig 4b. The mean tropospheric CO level during that campaign is 170 ppb, a surprisingly high value for the supposedly "clean" Siberian air, which is not subject to local CO emissions from industry or wildfires. The background CO value was determined in each campaign from the profile sections with the lowest CO variability (Paris et al., 2008) and is 135 ppb in April 2006. The CO concentration measured by the YAK-AEROSIB flights in April 2006 is in fact even higher than the one routinely measured in ascent and descent over Frankfurt, in Germany by the MOZAIC aircraft programme (Marenco et al. 1998), which suggests a contamination by pollution transported from Eurasian sources. Indeed, pollutants and dust accumulated in the boundary layer over northern China in April 2006 (Papayannis et al. 2007) were found to be swept by a series of cold fronts and uplifted over Eastern Siberia, and recorded by Flight 2 and 3 of the campaign (Fig. 6.5b). This quickly uplifted pollution episode from China was partly uplifted over Western and Eastern Siberia, and partly entrained directly in altitude towards the North Pacific.

6.7. CO_2 as a tracer of vertical and horizontal mixing in models

The YAK-AEROSIB dataset provides a useful test bed for model validation, thanks to the large geographical extent of the flights and the density of vertical profiles. CO_2 is a long-lived transport tracer capable to constrain vertical mixing in models (Stephens et al., 2007). Its atmospheric budget is dominated by emissions from fossil fuel combustion, ameliorated by ocean uptake and by seasonally varying plant uptake. Surface CO_2 gradients of a few ppm are mixed in the vertical at the synoptic scale (e.g. Yi et al. 2004; Chan et al. 2004) and advected over very long distances (e.g. Wada et al. 2007).

6.7.1. Vertical mixing of CO_2 and rectification gradients

The large-scale CO_2 vertical gradient over the Northern Hemisphere continents, in particular Eurasia, is sensitive to the seasonal co-variation between vertical transport and surface fluxes. This co-variation, called rectifier effect (Denning et al. 1999) causes horizontal CO_2 gradients between surface sites. Unfortunately, global transport models used for CO_2 studies give very different results in simulating these gradients (Rayner and Law 1995; Law et al. 1996). This uncertainty of transport models plagues the diagnostic of surface fluxes in inversions (Gurney et al. 2002; Peylin et al. 2004). Because the spread of transport model results for CO_2 reflects their differences in vertical and

horizontal mixing, it has been suggested (Gloor et al. 2004) and recently demonstrated (Stephens et al. 2007, Yang et al. 2007) that independent vertical profile data can help to cross validate models.

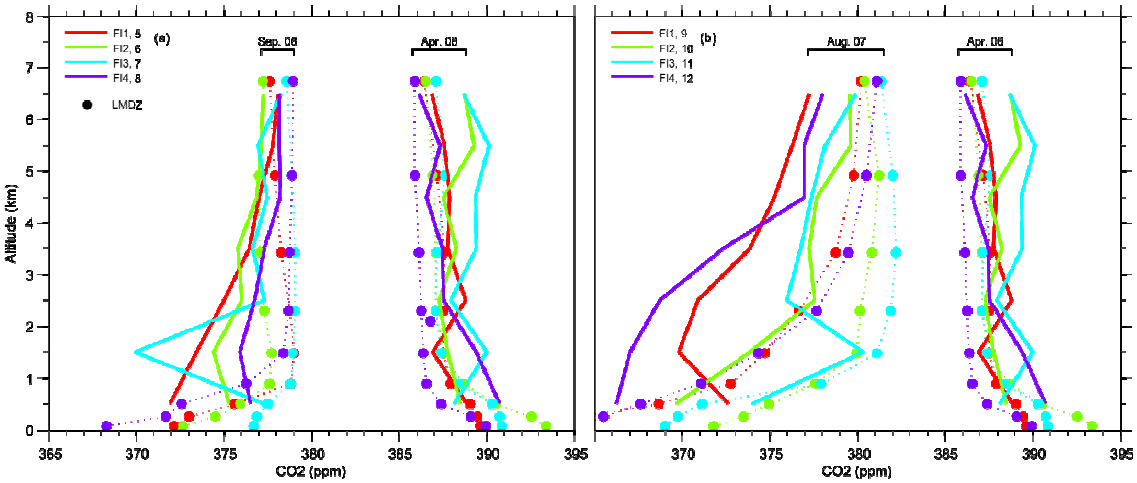

Figure 6.6. Estimation of model vertical mixing with CO_2 as a tracer of transport. Each profile corresponds to a flight averaged in 1000m bins. (a) Comparison of April 2006 and September 2006 campaigns. (b) Comparison of April 2006 and August 2007 campaigns. Model results are shown as colour dots on dotted lines, measurements are thick lines.

Stephens et al. (2007) performed their cross-validation study of transport models prescribed with optimized fluxes constrained by surface stations, using vertical profiles. They compiled a climatology of the northern hemispheric vertical CO_2 distribution from 12 aircraft sites, and applied it to the TRANSCOM group of transport models (Baker et al. 2006). Despite being prescribed with fluxes which fit optimally the surface data, nearly all the TRANSCOM transport models exhibited systematic biases compared to the observed vertical profiles. The sign of these biases suggests that vertical mixing is being underestimated in wintertime and overestimated in summertime. Moreover, a clear relationship was found between vertical model biases and the balance between tropical and temperate carbon sinks. Thus, transport models can be differentiated as having greater consistency with the observed CO_2 vertical gradient information.

We applied the YAK-AEROSIB data to evaluate model vertical transport. Unlike Stephens et al., we do not use a large number of sites nor coverage of all the months, but the large spatial representativeness of the campaigns allows for substituting to a low temporal density a high spatial density of vertical profiles across Siberia, the region where transport models differ most (Denning et al. 1999 ; Law et al. 1996). Fig. 6.6 provides a comparison between a modelled CO_2 vertical distribution and the three YAK-AEROSIB campaigns. The LMDZ-INCA model without optimized fluxes is shown here as an example. LMDz-INCA is a global chemistry climate model (Sadourny and Laval 1984, Hauglustaine et al. 2004, Brunner et al. 2005). Resolution is 3.75° x 2.5° with 19 vertical levels. It can be seen that this particular model underestimates wintertime mixing and overestimate summertime mixing (Fig. 6.6). As Siberia is the region of the Northern Hemisphere where transport models are particularly deficient and where model results deviate

strongly from each other (Gurney et al. 2002) , reducing the inversion spread over this region by systematic cross-validation will also help to reduce uncertainties elsewhere in the Northern Hemisphere.

6.7.2. Horizontal mixing of CO_2 and cross PBL transport

Figure 6.7 shows a LMDZ-INCA simulation of CO_2 during Flight 5 (7 September 2006; Paris et al. 2008). Flight 5 was selected because the aircraft crossed a weak front during second and third profiles, and the imprint of the synoptic circulation near the front is clearly visible in the CO_2 data (colour dots in Fig. 6.7, see also Fig. 6.4b). The biogenic CO_2 fluxes are prescribed from the CASA terrestrial ecosystem model (ref) and anthropogenic emissions are from the EDGAR FT2000 database (Olivier et al. 2005). Biomass burning emissions are not included in this model simulation. The modelled CO_2 field interpolated to the aircraft positions is in good agreement with the observations (R^2=0.46, n=412), but the CO_2 variability is underestimated by a factor 2.5. The LMDZ-INCA model is found to reproduce qualitatively the position of the boundary layer CO_2 gradient (at ~1 – 3 km altitude) and synoptic patterns crossed between 0400 and 0600 UTC. However, it remains difficult to unambiguously define in the model a BL height for CO_2 mixing, below which CO_2 would be more depleted than in the FT above, because the CO_2 vertical gradients in the model are not as steep as in the data. Another limitation of such a model-data comparison for a particular episode is the difficulty to accurately represent biogenic CO_2 fluxes. As an example, the elevated modelled CO_2 (~379ppm) below 400 m from 0300 to 0500 UTC (1000-1200 local time) in Fig. 6.7 can be due to an overestimated CO_2 source by the vegetation.

This observation-model comparative case study provided by Fig. 6.7 suggests that in September 2006, the anthropogenic European CO_2 emissions reached Siberia between 50°N and 70°N and enhanced CO_2 concentrations by ~0.5 ppm between 2-4 km altitude. In the next section it will be shown that this is consistent with the FLEXPART analysis of the air mass origin.

6.8. Pollution over Siberia and source regions

Little is known about how remote pollution sources influence Siberia. Models predict a dominance of low level advection of European pollutants to Siberia (Wild et al. 2004, Duncan and Bey 2004) but this has received little experimental support (Pochanart et al. 2003). In this section, we use a backward Lagrangian transport model to attribute two observed CO_2 and CO plumes to pollution sources.

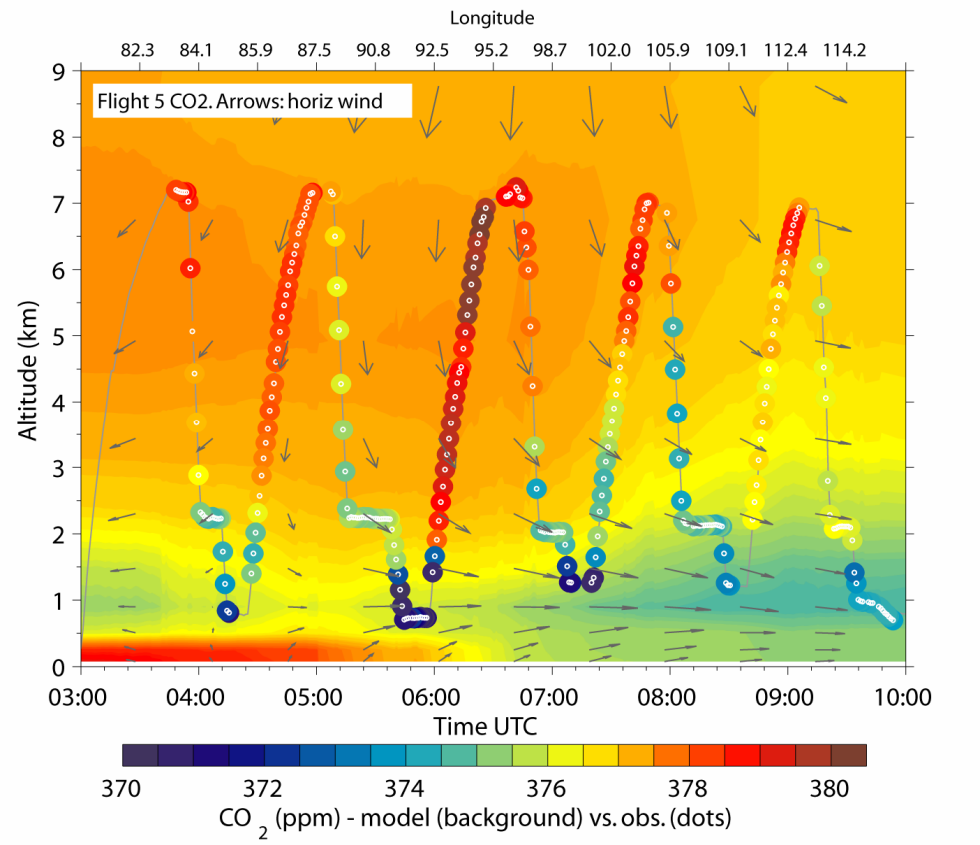

Figure 6.7. CO_2 along flight 5 on 7 September 2006. The in-situ measured CO_2 (dots) is superposed on the CO_2 profile interpolated from the LMDZ-INCA chemistry-GCM (background). Note that the colour scale is the same for data and observations. The grey arrows represent the horizontal wind (north upward).

6.8.1. Long-range transport of fires and European emission vs. clean Arctic air (September 2006)

The first illustrative case of transport is taken from the September 2006 campaign. We developed an orthogonal classification of the FLEXPART footprints in order to identify and further inter-compare air masses sampled in different profiles (Paris et al, manuscript in preparation). The classification scheme is based on similarity between footprints associated to each data. Figure 6.8 shows an example of the footprint classification results for 7 September 2006 (Flight 5). Two footprint classes are dominant, describing respectively airstreams either with a European / Caspian Sea or an Arctic origin. These two classes are well separated in terms of tracer concentrations. The Arctic class predominates at altitudes below 1700 m and is associated with low CO, O_3 and CO_2 concentrations (see values in Table 6.3). In contrast, the European / Caspian Sea class is present at ~2500 m in the profiles, and it is characterized by high CO and intermediate O_3 and CO_2 (Table 6.3).

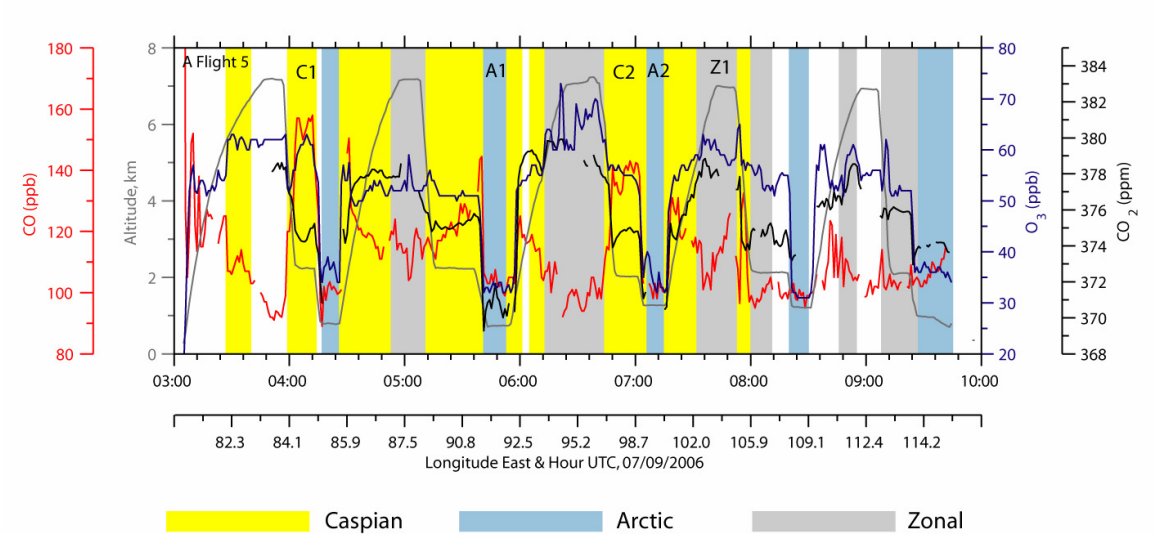

Figure 6.8. CO_2, CO and O_3 concentrations during flight 5. The shading corresponds to the occurrence of "Caspian/Europe" air masses (yellow) and "Artic" air mass. The grey shading corresponds to fast zonal transport pattern, encountered mainly in the mid to upper troposphere.

Air classified as belonging to the Arctic class (light blue in Fig. 6.8) is marked by a long residence time (>10 days) inside the polar vortex. The low CO and CO_2 concentrations suggest a strong isolation from sources in the recent air mass history. The mean residence time of air in the Arctic is maximum in summer (Stohl 2006), but decreases with altitude. The FLEXPART footprints indicate that advection of Arctic air in the campaign domain sampled during September 2006 occurred in the boundary layer. During the five days of meridian transport from the Arctic to Flight 7, contact with high latitude vegetation must also have contributed to low CO_2 and O_3 concentrations through plant uptake and dry deposition, respectively.

The European / Caspian Sea class (yellow in Fig. 6.8) is the most ubiquitous air mass sampled during Flight 5. Its footprint potential emission sensitivity (PES) is largest around the Caspian Sea but it extends towards Europe. CO concentrations are higher (Table 6.3). By spatially multiplying the FLEXPART PES with the EDGAR anthropogenic emissions and GFED fire emissions we obtain a CO enhancement (ΔCO) associated to European anthropogenic emissions of ~10 ppb, and a roughly equal ΔCO associated to regional fire emissions around the Caspian Sea. Fires occurred mostly in Northern Kazakhstan (50°N, 50-70°E), probably from agricultural burnings. In Southern Siberia, Pochanart et al. (2003) found a difference in median CO concentration of 24 ppb in air masses showing European influence compared to cleaner air masses from the Arctic.

Table 6.3. Altitudes and tracers concentrations associated with the European and Arctic classes.

Class	Altitude (m)	CO_2 (ppm) [a]	CO (ppb) [a]	O_3 (ppb) [a]
European / Caspian	~2500	375.63 ± 1.97	122.29 ± 14.53	53.43 ± 6.72
Arctic	900 – 1700	372.53 ± 1.67	102.71 ± 4.30	34.92 ± 3.24

[a]: values are given as mean ± 1 std dev

Individual plumes in the European / Caspian Sea class exhibit correlated CO and O_3 concentrations. In a plume with the highest CO concentration (144.26+13.97 ppb, sampled at 0400UTC; Fig. 6.8), the CO-O_3 correlation is high (R^2=0.68, n=90) and the regression slope is 0.24, which is typical of ozone production from fire-emitted precursors. A polluted airstream sampled at 0700 UTC (Fig. 6.8; CO = 134.78+9.12 ppb, $R_{CO-O3}{}^2$=0.39, n=108) exhibited an unusual negative CO vs. O_3 linear regression slope (s = -0.10 ppb ppb^{-1}). The photochemical processes leading to negative CO-O_3 slopes in biomass burning plumes remain debated (Val Martin et al., 2006; Real et al. 2007). These two plumes are advected at 2.5 km altitude, and both contain low CO_2 concentrations although the CO_2-CO correlation is significantly positive (R^2~0.80). Regression slopes of CO vs. CO_2 are negative (-0.06 – -0.09 ppb ppm^{-1}) in these plumes. In the absence of CO_2 sources or sinks other than combustion, the enhancement of CO should be paralleled by high CO_2 values, which is not the case here; suggesting that regional CO_2 uptake by plants offset part of the CO_2 increase due to combustion emissions.

6.8.2. Uplift and northward transport of pollution from China (April 2006)

Another interesting transport episode was observed during the April 2006 campaign. Abnormally high excesses of CO (90 ppb above background) were detected between 5-7 km altitude, on the easternmost part of the flight track, on April 12, 2006. Because of its high altitude, this signal can readily be attributed to remote sources, which we investigated using the Lagrangian particle dispersion model FLEXPART (Stohl et al. 2005) complemented with back-trajectories from the HYSPLIT version 4 model (Draxler et al. 1997)

Figure 6.9 shows the results of FLEXPART 10-days backward particle dispersion simulations started from each aircraft position with high CO (>200 ppb). The footprint (emission sensitivity (averaged between the ground level and 1500 m above) shows the regions where emissions could have contributed to the measured concentrations. The back-trajectory HYSPLIT simulation was run 6 days backward only. Both model tools reveal that North Eastern Chinese emissions must have been the main contributor to the excess CO and CO_2, and that these emissions were transported quickly to above 5 km altitude (Paris et al. 2008). The transport calculations cannot resolve whether fossil fuel emissions in China or fires in Northern Mongolia caused the observed CO and CO_2 enhancements, but the measured CO/CO_2 ratios suggest a dominant fossil fuel origin. During the episode, the transport of pollution to the mid-troposphere was caused by a series of extra tropical cyclones and their associated warm conveyor belts (WCB). Such WCBs passing over Eastern Asia are important for trans-Pacific pollution transport (Yienger

et al. 2000). As evidence is growing that Asian emissions are steadily increasing and affect the pollution burden of the Arctic (Rahn et al., 1977; Shaw, 1982; Cahill, 2003), the northward transport into and across Siberia such as sampled by the YAK-AEROSIB flights in April needs further investigation.

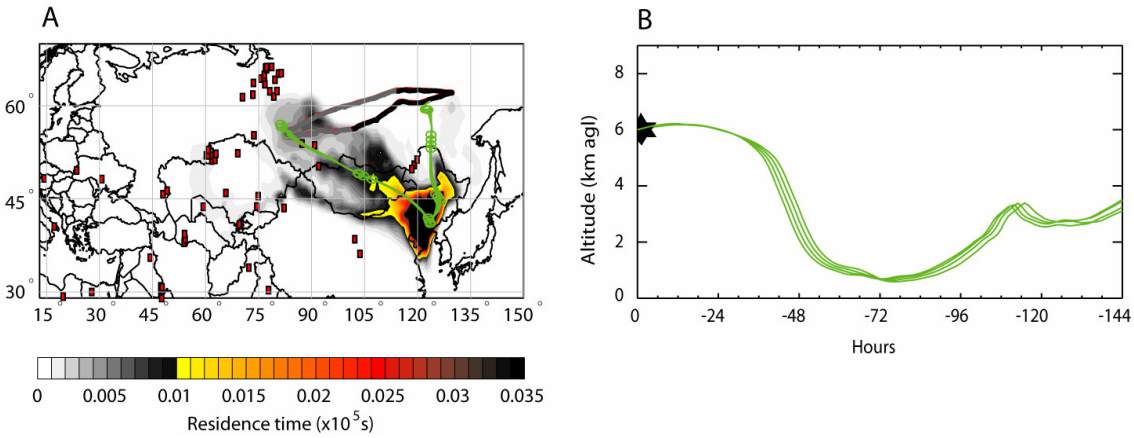

Figure 6.9. Footprint of the high CO concentrations (CO>220ppb) computed using the FLEXPART model. FLEXPART releases a large number of particles at the receptor (instrument) location and computes time-reversed transport. ECMWF reanalysis wind field is used. The footprint, or potential emission sensitivity (PES) is defined as the geographic distribution of the cumulative counts of the particles residence time. The colour scale represent the footprint in the lowest 1500 m, and therefore the sensitivity to emissions occurring in these areas. The green curves represent 3 typical high CO back-trajectories computed using the HYSPLIT model. In the right panel, the variation of altitude with time is plotted for these 3 back-trajectories.

6.9. Conclusion and future outlook

The YAK-AEROSIB project main achievement was to measure tropospheric CO_2, CO and O_3 in Siberia, where few CO_2 observations are available. This paper describes the first three campaigns carried out in April 2006, September 2006 and August 2007. These campaigns densely sampled the troposphere with permanent alternance of ascents and descents up to 7 km.

The ensemble of vertical profiles is appropriate to discriminate AGCM skills at modelling CO_2 concentrations at a scale intermediate between continental and synoptic scales, including the 'rectifier effect' issue. In a preliminary assessment, the LMDZ-INCA model was weakly sensitive to synoptic features but proved able to reproduce qualitatively the general CO_2 distribution. Notably, the "CO_2 BL" was rather correctly positioned in the vertical in the flight of 7 September 2006, but the model did not satisfactorily represent the vertical gradient in August. The seasonal variation sampled by our survey revealed a large boundary layer gradient in CO_2 (~20 ppm) between April

2006 and August the following year, whereas it was only ~8 ppm in the free troposphere. When de-trending this value for interannual increase the gradient is even larger.

At the synoptic scale, although well-mixed in the lower troposphere, the contribution of European pollutants to concentrations over Siberia can be disentangled from other sources using a Lagrangian modelling approach. European anthropogenic contributions (~10 ppb CO) was observed (according to the FLEXPART model diagnostic) immediately above the boundary layer. In a case this signal was found to be comparable to Central Asia fires' emissions. O_3 concentrations were high in this airmass, most likely due to the photochemistry in the fire plumes.

AGCM models transporting CO_2 fluxes and anthropogenic pollutants should be matched against such a dataset. Models must show their ability to give a good vertical representation of the CO_2 concentration field. Model-based source apportionment for CO and O_3 enhancements in the troposphere could also better separate the different pollution sources that affect the Siberian air shed, and potentially the Arctic downwind. New campaigns have been carried out in July 2008, including a new itinerary that sampled the Siberian Arctic coast. Analysis of this new data set will further inform us on atmospheric composition in this region.

6.10. Simulations LMDZ : résultats supplémentaires

La simulation présentée dans la section 6.7 est extraite d'une étude de comparaison entre les mesures et des simulations calculées par le modèle LMDZ. Une partie de ces résultats ont été présentés à l'EGU 2008 (Paris et al., 2008. The Siberian pathways: experimental insights into atmospheric transport across Eurasia, Geophys. Res. Abstracts, 10, EGU2008-A-04228). Le modèle LMDZ est exploité à une résolution de 3.75° par 2.5° sur 19 niveaux verticaux. Les champs de vents ECMWF sont nudgés dans la dynamique. Les émissions anthropiques d'EDGAR sont utilisées, et la combustion de biomasse n'est pas intégrée. Je montre ci-dessous des résultats complémentaires issus de la simulation de septembre 2006. La Figure 6.10 montre l'advection de CO2 fossile d'Europe et d'Asie vers la Sibérie. On constate ainsi que LMDZ simule ici une advection majoritairement dans la basse troposphère (<3 km), en ligne avec les résultats d'autres études de modélisation.

Un schéma de chimie simplifié permet également de calculer la distribution de CO (Fig. 6.11). On peut ainsi remarquer qu'une large partie centrale du vol est affectée par des concentrations importantes de CO correctement reproduites par le modèle, malgré la non-prise en compte des émissions de biomasse.

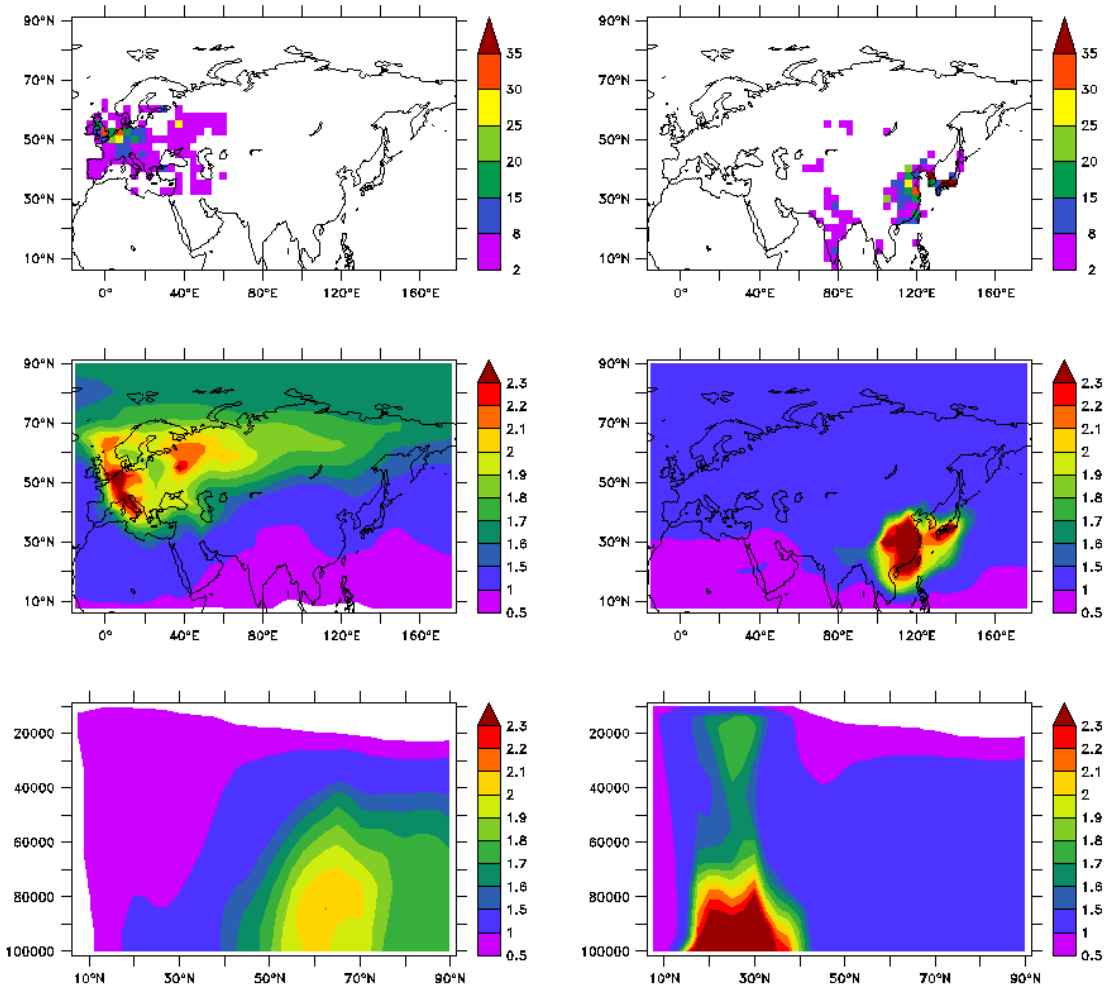

Figure 6.10. Advection du CO_2 anthropique en Sibérie. En haut, émissions de CO_2 selon EDGAR (10^9 kg m^{-2} s^{-1}). Milieu, colonne intégrée sur la troposphère et bas, coupe à 100°E (ppm). A gauche, les émissions européennes, à droite, les émissions asiatiques seulement.

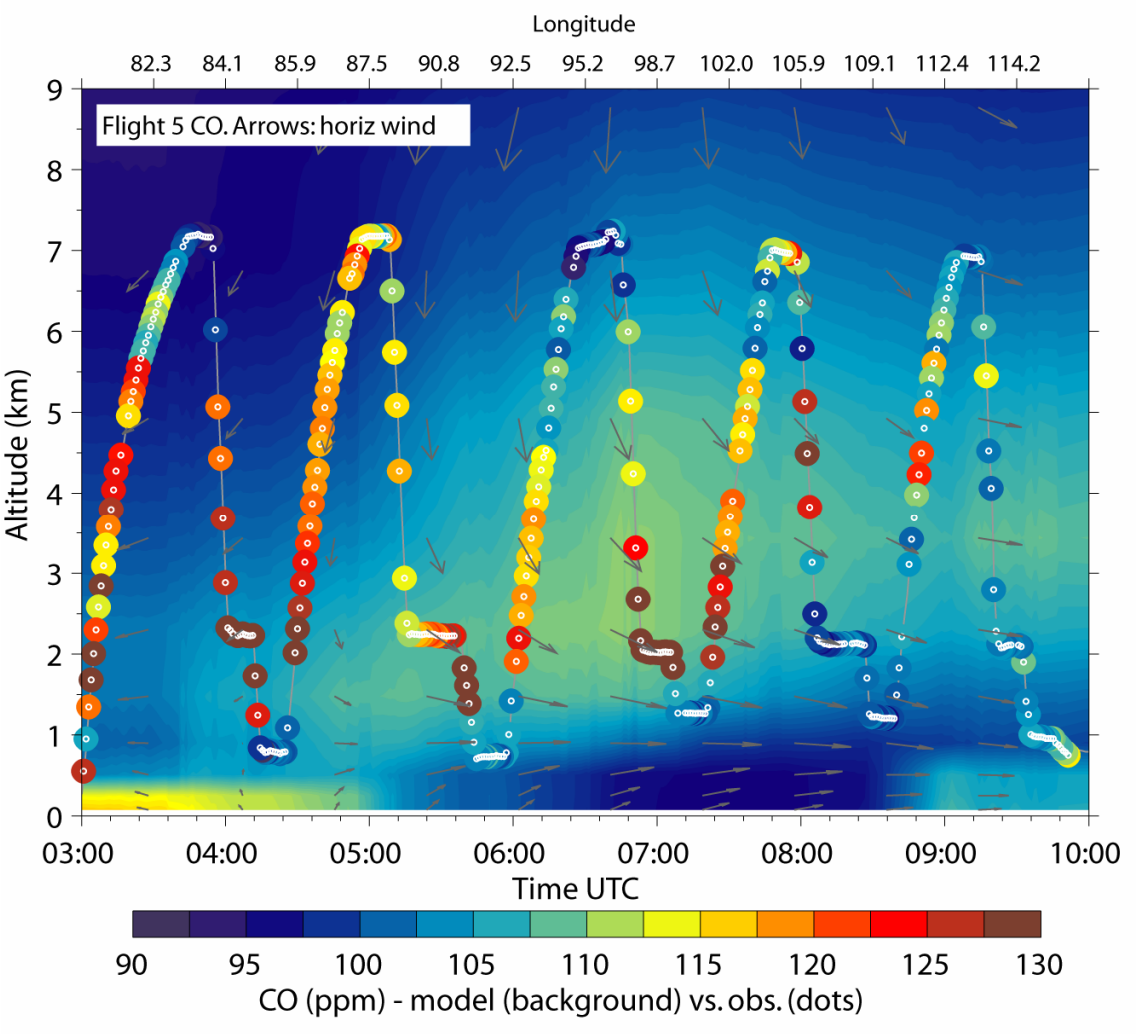

Figure 6.11. CO mesuré durant le vol 5 le 7 septembre 2006. La mesure in situ (points) est superpose sur les profiles de CO interpolés de la simulation LMDZ (couleur de fond). L'échelle de couleur est commune entre les mesures et la simulation (ppb).

Les simulations de CO_2 et de CO présentées ici reproduisent bien les observations. La correlation obtenue entre données et simulation sur le CO_2 est de $R^2 = 0.46$ et la pente de regression de 0.18 ± 0.01, ce qui dénote une forte sous-estimation de la variabilité, erreur attendue de la part d'un modèle global. La simulation de CO présente une correlation $R^2 = 0.08$ et une pente de 0.09 ± 0.01. Les simulations de CO sont mal correlée en été de par la présence de panaches fins ayant des concentrations de CO élevée. En avril (non montré) une simulation du vol 4 (14 avril) atteint une corrélation $R^2 = 0.45$ et une pente de 0.25 ± 0.02. Par ailleurs les émissions en Asie (notamment Russie et Chine) fournies par EDGAR sont largement sous-évaluées (p. ex. Streets et al., 2003 ; Ohara et al., 2007) ce qui contribue fortement à la sous estimation des panaches de pollution. Ceci est particulèrement visible dans la simulation du vol 2 (12 avril 2006 ; Fig. 6.12)

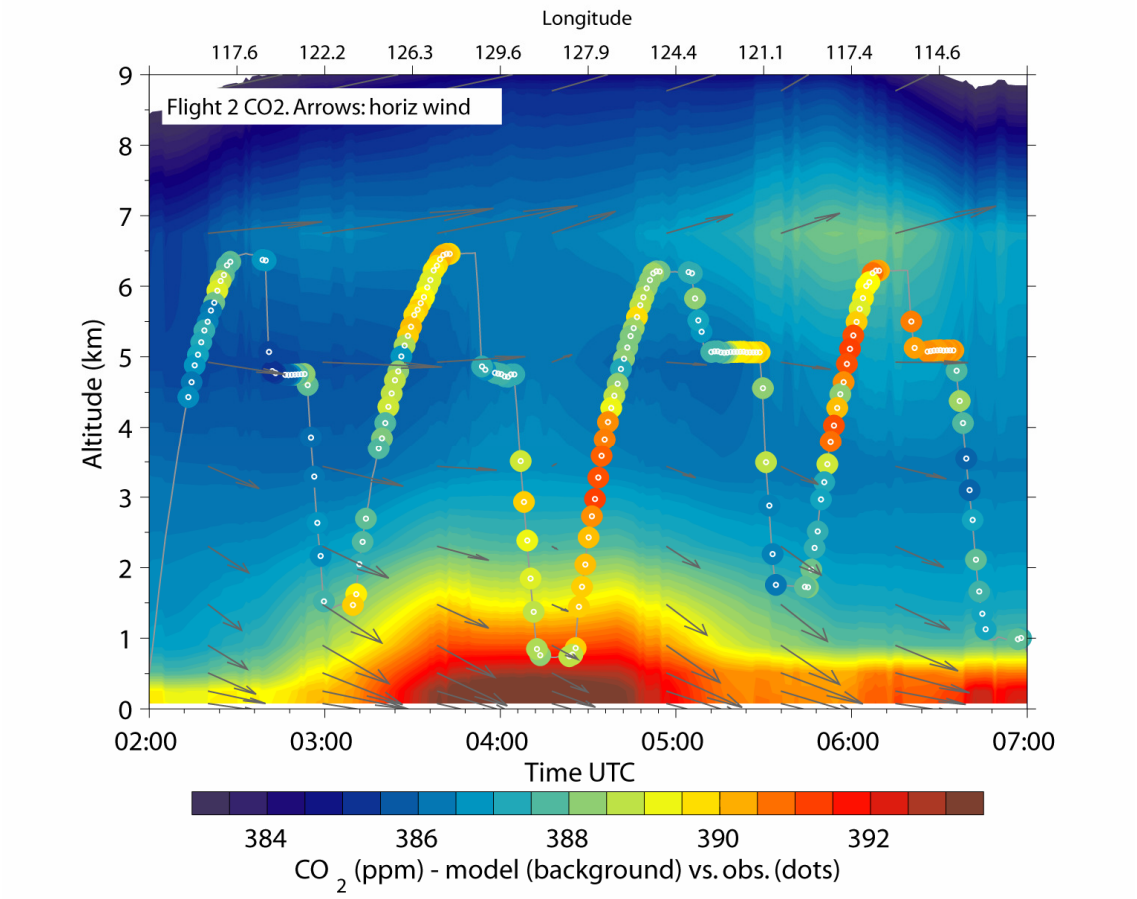

Figure 6.12. CO_2 mesuré durant le vol 2 le 12 avril 2006. La mesure in situ (points) est superpose sur les profiles de CO interpolés de la simulation LMDZ (couleur de fond). L'échelle de couleur est commune entre les mesures et la simulation (ppm).

Chapitre 7.
Conclusion et perspectives

Ce travail de thèse a été consacré à la mesure et à l'analyse de la composition atmosphérique en CO_2, CO et O_3 au dessus de la Sibérie afin d'en cerner la variabilité et les causes de variations, et d'évaluer l'utilité de telles mesures aéroportées pour une meilleure estimation de la contribution du transport atmosphérique aux concentrations régionales. L'apport de ces mesures est également illustré en relation avec la détermination du puits régional de CO_2 en Sibérie.

7.1. Réalisation des campagnes

Cinq campagnes aéroportées intensives ont eu lieu entre 2006 et 2008 dans le cadre du projet YAK-AEROSIB. J'ai pris progressivement en charge l'ensemble des aspects liés à la préparation, la gestion, la réalisation et la valorisation de ces campagnes.

J'ai décrit et analysé dans cette thèse les données obtenues lors des trois premières campagnes. Les deux campagnes de juillet 2008 ont été réalisées trop tardivement pour y être incluses. Les trois premières campagnes ont eu lieu en avril 2006, septembre 2006 et août 2007 (voir chapitre 2). Chacune de ces trois campagnes s'est déroulée selon des modalités similaires. Le plan de vol est fixé au préalable en accord avec les autorités russes. La séquence de campagne consiste en deux jours de vol, un jour de repos et un jour de vol. Le trajet consiste en une large boucle d'environ 7000 km : Novossibirsk-Myrni-Iakutsk-Bratsk-Novossibirsk. Durant les campagnes un maximum d'ascensions et descentes entre la surface et 7 km sont effectuées afin d'échantillonner au mieux la basse et moyenne troposphère. Durant chaque campagne sont ainsi réalisés environ 28 profils (sondages) verticaux.

Une partie importante de mon travail de thèse a été dédiée à l'organisation et à la participation aux campagnes de mesure sur le terrain. Ceci inclut d'une part une action en amont

assurant la disponibilité des instruments, et d'autre part une action spécifique à chaque campagne. Les actions en amont incluent l'obtention de diverses autorisations auprès des autorités russes pour l'exportation, le maintien sur le territoire et la possibilité d'utiliser les instruments sur un trajet spécifique qui doit lui aussi être justifié. Ces actions ont été menées à bien en lien avec l'Institut d'Optique Atmosphérique de Tomsk qui assurait l'interface avec les autorités russes. Les actions liées à chaque campagne incluent la gestion financière liée essentiellement à la location de l'avion, la logistique nécessaire à la participation des scientifiques français (entre 2 et 4 personnes pour chaque campagne), ainsi que le rassemblement des données traitées de CO_2, CO et O_3 en une base de données unique. J'ai également travaillé à rendre ces campagnes possibles par l'organisation de réunions de pilotage prévues dans le cadre du GDRE, par une coordination tenant compte des différences culturelles et par une gestion budgétaire du projet YAK-AEROSIB. Le budget total du projet est légèrement inférieur à 1m€. En tant qu'administrateur du projet j'ai également aidé à coordonner les rapports d'activité aux organismes soutenant ce programme (dont CNRS et INSU).

L'expertise acquise par l'équipe a été sollicitée pour participer aux campagnes aéroportées du programme POLARCAT (www.polarcat.no). J'ai établi en collaboration avec le partenaire russe et les membres de POLARCAT l'itinéraire spécifique de la quatrième campagne (voir chapitre 2) et coordonné la participation du LSCE à un projet ANR « POLARCAT ».

7.2. Traitement des données

J'ai testé et opéré l'instrument Condor (CO_2) durant deux campagnes parmi les cinq et assuré l'intégralité du traitement des données CO_2. J'ai développé à cette fin un logiciel d'analyse des mesures permettant d'assurer la qualité des données (voir Annexes). Un instrument NDIR CO_2 similaire ainsi que la chaîne complète de traitement des données ont été vérifiés par des comparaisons avec des mesures flacons réalisées par C. Gerbig (MPI-BGC, Jena) lors de la première campagne CarboEurope Regional Experiment (Dolman et al, 2006). Ces données ainsi traitées ont été utilisées dans une étude de modélisation régionale (Sarrat et al., 2007).

L'analyse des données m'a conduit à développer des routines de visualisation des données en trois dimensions, et en deux dimensions pour la comparaison mesures-modèles (voir notamment article présenté dans le chapitre 6). J'ai réutilisé ces routines pour une autre campagne aéroporté en Europe (Xueref et al., 2008, manuscrit en préparation).

7.3. Distribution du CO_2

Le CO_2 mesuré a montré une important variabilité, tant dans les gradients observés durant chaque campagne qu'entre ces campagnes (chapitres 3 et 4). En avril 2006, les concentrations de CO_2 étaient comprises entre 385-390 ppm, avec des panaches de pollution dans la troposphère libre

jusqu'à 392 ppm. Dans la troposphère libre, les valeurs estivales étaient comprises entre 375 et 380 ppm en septembre 2006 et entre 372 et 380 ppm en août 2007. Le gradient entre couche limite et troposphère libre était plus important en août 2007, avec des concentrations observées comprises entre 365 et 373 ppm (hors panaches de pollution locale) contre 372-378 ppm en septembre 2006. L'accentuation de ce gradient au mois d'août reflète l'influence de l'assimilation du CO_2 par la biosphère.

7.4. Distribution du CO et de l'O_3

Les concentrations de CO observées ont révélé l'impact de la pollution, particulièrement importante durant la campagne d'avril 2006 (chapitre 3), et des processus de combustion en général sur l'atmosphère sibérienne (chapitre 4). Les concentrations les plus élevées ont été relevées en avril 2006, avec des concentrations entre 160 et 200 ppb de CO. Certains panaches associés à une pollution anthropique dans la troposphère libre ont révélé des concentrations jusqu'à 220 ppb. Les concentrations typiquement observées en septembre 2006 et aout 2007 étaient d'environ 95-110 ppb. En août 2007, des panaches associés à des feux de forêts dans la basse troposphère ont été mesurés avec des concentrations comprises entre 200 et 300 ppb.

La mesure de la distribution de l'O_3 montre un gradient négatif vers la surface, en relation avec la localisation des sources (contribution stratosphérique et production photochimique in-situ) et des puits (déposition à la surface, et titration). Ce gradient est accentué en été, avec une accentuation au niveau de la couche limite. Les concentrations ainsi observées se situent entre 20 ppb environ pour la couche limite estivale et 70-85 ppb pour la partie haute de la trajectoire de l'avion (6-7 km) en général.

7.5. Transport atmosphérique à grande échelle en Sibérie

Avant les résultats des campagnes YAK-AEROSIB, premières campagnes intensives en Sibérie à mesurer CO_2, CO et O_3, l'atmosphère sibérienne était considérée comme une zone amont propre, l'air se chargeant en polluants durant la circulation zonale au dessus de la Chine. Quelques études de modélisation globale ont intégré la contribution européenne voyageant à travers la Sibérie (Liu et al., 2002, 2003) mais très peu de mesures ont permis de valider cette contribution amont (Pochanart et al., 2003). La prise en compte de ces contraintes observationnelles dans l'un des modèles d'un exercice d'intercomparaison (Kiley et al., 2003) semble réduire le biais systématique du CO simulé sous le vent de l'Asie du nord-est. De manière générale, très peu d'études expérimentales ont eu lieu en Sibérie (Akimoto, 2003). Les campagnes YAK-AEROSIB ont permis de documenter pour certaines périodes la variabilité de CO et O_3, traceurs utilisés dans les études de

modélisation, et d'expliquer cette variabilité par le transport atmosphérique en association avec des émissions anthropiques ou de combustion de biomasse.

Les mesures effectuées en avril 2006 ont mis en évidence l'impact sur la composition atmosphérique en altitude en Sibérie des émissions chinoises (chapitre 3 ; Paris et al., 2008). L'évènement observé pendant cette campagne était associé à un important passage frontal au dessus de la Chine du nord-est qui a provoqué un soulèvement rapide de la couche limite. Cette masse d'air polluée a été injectée dans la troposphère moyenne, d'où elle a pu être advectée vers la Sibérie en deux jours environ.

La conservation des pentes CO/CO_2 associée aux émissions fossiles dans les processus de transport synoptique à moyenne échelle, a été montrée pour l'événement de pollution Chinois d'avril 2006. Par contre, les pentes ne sont pas conservées en été lorsque la photosynthèse est active et décorrèle le CO_2 du CO. Palmer et al. (2004) ont proposé une méthode basée sur l'utilisation conjointe de mesures atmosphériques de CO et de CO2 comme base pour contraindre les émissions de CO_2 fossiles, mais la variabilité saisonnière du CO_2 et du CO en Sibérie montre la difficulté d'appliquer la méthode sans biais saisonnier.

Dans le chapitre 4, l'analyse des mesures de la campagne de septembre 2006 ont également montré le transport à grande échelle d'émissions de feux de biomasse au Kazakhstan, mélangées aux émissions anthropiques européennes pour augmenter les concentrations de CO de plusieurs dizaines de ppb au dessus de la Sibérie (à ~10000 km des émissions).

Cette interprétation des mesures a bénéficié d'une nouvelle méthode d'analyse des données basée sur la technique statistique descriptive du clustering. Cette technique, appliquée ici pour la première fois à des fonctions d'influence, permet d'associer les grandes caractéristiques des distributions de gaz trace observées à des régions d'origine.

7.6. CO_2 : contrainte sur le mélange vertical des modèles

Le mélange atmosphérique est souvent mal représenté dans les modèles globau (HTAP, 2007). La comparaison du CO_2 mesuré sur des campagnes représentatives de l'ensemble du continent Eurasien avec des résultats de modèles utilisés pour le calcul inverse des flux de CO_2 a montré l'apport important des nombreux profils verticaux que nus avons collectés pour contraindre le mélange vertical dans les modèles (chapitre 6). En effet le modèle global dont le mélange a été testé avec les données YAK-AEROSIB (LMDZ) a montré un biais de sous estimation du mélange vertical en été et de surestimation du mélange vertical en hiver. L'application systématique des campagnes en Sibérie pourrait amener à une réévaluation des flux de carbone régionaux, à l'instar de l'étude globale de Stephens et al. (2007) et Zhang et al. (2007).

7.7. Apport sur la formation des aérosols en troposphère propre

Les mesures effectuées lors des campagnes YAK-AEROSIB ainsi que les profils verticaux réguliers au dessus de la région de Novossibirsk ont été analysées dans le chapitre 5 et ont ainsi fournit un aperçu préliminaire du comportement des aérosols ultrafins dans cet environnement de troposphère libre propre éloignée des sources de pollution. Les données semblent confirmer l'hypothèse de Kulmala et al. (2006) selon laquelle une source importante de précurseurs de nucléation en troposphère libre continentale serait constituée par des espèces biogéniques insolubles injectées en altitude par la convection. Les mesures présentées ici étaient toutefois limitées à deux bandes de granulométrie (3–70 et 70–200 nm). Des mesures plus fines de la granulométrie sont nécessaires pour étayer fermement l'hypothèse de Kulmala et al.

7.8. Perspectives : quelles campagnes futures ?

Le succès des campagnes existantes, malgré l'absence de certains instruments initialement prévus et l'aspect fixe de l'itinéraire, appelle à la pérennisation de ces mesures afin d'augmenter la taille du jeu de données disponible et obtenir un aperçu de la variabilité interannuelle des caractéristiques observées. D'autre part l'organisation de campagnes répondant à des spécifications plus particulières semble s'imposer.

7.8.1. Observer les panaches de feux de biomasse

J'ai montré la contribution des feux de forêt à la concentration en CO et O_3 dans la troposphère sibérienne. Malheureusement l'observation de panaches de feux sibériens est très limitée dans le jeu de données que nous avons collecté. Les deux campagnes de juillet 2008 ont probablement échantillonné deux panaches, ce qui est peu étant donné l'importance des panaches observés par d'autres campagnes de mesures intégrées au programme POLARCAT. Il est essentiel de comprendre plus finement le comportement des panaches de feux de forêt, et notamment du transport de ces panaches. L'intégration de cette connaissance dans les modèles de circulation permettra de mieux comprendre l'impact global des feux de forêt sur la composition chimique de l'atmosphère.

A ce titre un objectif de futures campagnes basées sur l'ensemble actuel d'instruments à bord de l'Antonov-30 devrait s'attacher à échantillonner les panaches de feux de forêt durant le pic d'activité saisonnière (mai et août). Cela requiert une plus grande flexibilité du plan de vol afin de pouvoir adapter la stratégie d'échantillonnage aux circonstances météorologique et de danger de feux.

7.8.2. Suivre les anomalies de CO_2

Le projet YAK-AEROSIB est dédié à l'étude du cycle du carbone dans l'atmosphère sibérienne. A ce titre une première contribution a consisté à utiliser les gradients verticaux moyens pour contraindre les modèles atmosphériques. On peut concevoir que des campagnes YAK-AEROSIB dotées d'une plus grande flexibilité dans l'exécution et en mesure de maintenir une altitude correspondant à la couche limite permettraient un exercice de suivi de masse d'air, fournissant ainsi la base d'une expérience lagrangienne pour l'estimation directe des flux de CO_2 à partir de la concentration dans la colonne d'air. Ceci requiert en plus d'un plan de vol plus flexible la possibilité de voler plus longtemps dans la couche limite et plus près du sol.

7.8.3. Mesurer la nucléation d'aérosols

La mesure d'une granulométrie fine des aérosols, ainsi que de la concentration en précurseurs tels que SO_2 ou isoprène est particulièrement recommandée. En effet l'étude présentée dans le chapitre 5 ne reposait que sur deux canaux de tailles dans la batterie de diffusion, à savoir un cumul des particules en mode Aitken et nucléation, et en mode accumulation. Il est nécessaire pour confirmer l'hypothèse de nucléation à partir de composés insolubles, de mesurer la concentration de vapeurs organiques (Kulmala et al., 2006 ; O'Dowd et al., 2002) et d'aérosols dans des gammes de taille permettant de caractériser la nucléation (voir par exemple Young et al., 2007). Cet équipement coûteux pourrait apporter de nouveaux éléments sur la nucléation en troposphère continentale propre.

7.8.4. Améliorer l'assurance qualité et l'utilisation de traceurs

Avant d'être comparées aux modèles régionaux (Sarrat et al., 2007) les mesures in situ de la campagne CarboEurope, dans les Landes, ont été comparées aux mesures issues des prélèvements par flacons. Cette expérience parmi d'autres a montré l'importance de mesures flacons pour l'assurance qualité des mesures de CO_2. Il convient d'insister sur l'importance de pouvoir effectuer des prélèvements par flacon pour assurer la qualité des mesures, et étendre le panel d'espèces mesurées.

7.8.5. Contrainte des sources régionales de méthane

Les régions boréales comportent d'important puits potentiels de méthane, bien que l'amplitude et la localisation exacte de ces puits soient hautement incertaines. L'émanation de méthane dans les lacs et étangs boréaux pourrait émettre 24 ± 10 Tg CH_4 yr^{-1} (Walter et al., 2007). Les marais boréaux (dont le bassin de l'Ob, en Sibérie, est le plus important) émettent environ 30 Tg CH_4 yr^{-1} (Christensen et al., 1996) et pourraient dominer la variabilité interannuelle des concentrations atmosphériques de CH_4 (Bousquet et al., 2006). La décomposition bactérienne réactivée dans le pergélisol fondu pourrait participer à la mobilisation sous forme partiellement méthanique d'un stock d'environ 900 GtC (Zimov et al., 2006). On a aussi observé des émissions

importantes de méthane liées au réseau de gazoduc Sibérien (Bergamaschi et al., 1998). La mesure de ce composé est aussi nécessaire que celle du CO_2. Il sera alors possible de documenter la distribution de ce gaz à effet de serre dans la troposphère sibérienne et appliquer des méthodes d'analyse similaires à celles utilisées pour le CO_2. Un besoin de la part d'équipes de modélisation externes au projet YAK-AEROSIB a clairement été formulé. L'installation d'un instrument à bord de l'avion de recherche, telle qu'initialement incluse dans le cahier des charges du projet, permettrait une contribution importante à la connaissance des émissions de CH_4 dans une région au réseau de mesure très peu dense.

7.9. Perspectives : Modélisation des observations

7.9.1. Modélisation synoptique du soulèvement d'Avril 2006

Durant la thèse j'ai analysé le résultat de simulations pour le soulèvement de couche limite chinoise polluée observé durant la campagne d'avril 2006. Les simulations sont issues du modèle CHIMERE de transport et de chimie atmosphérique avec une maille de 50 km. Dans un premier temps j'ai constaté que d'une part ce modèle était capable de reproduire la phase (la localisation dans le temps et dans l'espace) de cet évènement de transport synoptique et d'autre part que les concentrations en CO simulées étaient faibles par rapport aux observations. En affinant l'inventaire de Streets et al. (2003) mis à jour pour 2006 à l'aide de profils temporels d'émissions en remplacement de l'inventaire EDGAR, les concentrations simulées sont beaucoup plus proche des observations.

Ce type d'analyse permet d'évaluer la capacité prédictive des modèles de transport régionaux à haute résolution en relation avec l'export des polluants continentaux. Il est généralement admis que les performances des modèles dans le transport des polluants diminuent avec l'altitude, dénotant entre autre l'incertitude associée avec les processus de mélange vertical. La simulation d'évènements de transport à l'échelle synoptique spécifiques reste un exercice difficile (en particulier pour les fronts), à cause de la sensibilité du modèle à la location et au timing de ces évènements. Il est envisageable d'utiliser le cas de soulèvement frontal de couche limite d'avril 2006 comme un test de la capacité de représentation du mélange vertical des modèles en ce qui concerne des situations synoptiques tels que les *warm conveyor belts*.

Dans la continuité des travaux sur les émissions anthropiques, j'ai également participé à l'analyse des inventaires d'émissions de CO_2 en Europe (Ciais et al., 2008, manuscrit soumis à Global Change Biology ; voir Annexe), permettant ainsi de dégager les incertitudes pertinentes pour les applications atmosphériques de ces inventaires.

L'utilisation de mesures en Sibérie permet de mieux contraindre les concentrations simulées par les modèles sous le vent de l'Asie du nord-est (Kiley et al., 2003). La question de l'export des polluants chinois a été largement explorée sur la base des données obtenues lors des campagnes

TRACE-P, mais ces études ont généralement échoué à déterminer les concentrations de polluants en amont de la région d'étude. Les profils de CO mesurés lors des campagnes YAK-AEROSIB constituent des conditions aux limites caractérisées sur la verticale pour des études intégrées de transport de la pollution en Asie du nord-est.

7.9.2. Contrainte du mélange vertical pour le CO_2

Dans le chapitre 6, j'ai montré que la représentation du mélange vertical (utilisant le CO_2 comme traceur) pouvait être évaluée à partir des profils moyens de chaque vol, fournissant ainsi de par l'étendue de la zone échantillonnée une mesure relativement insensible à l'erreur de représentation (c'est-à-dire l'erreur commise en comparant une mesure ponctuelle à une moyenne simulée sur un élément de grille). Stephens et al. (2007) ont montré qu'une sélection basée sur la représentation du gradient vertical parmi les modèles pouvait amener à une révision significative de la répartition géographique des flux de carbone. L'étude de Stephens et al. exploite des profils uniquement verticaux et réguliers dans le temps afin de départager les gradients verticaux simulés. J'envisage d'utiliser les campagnes YAK-AEROSIB afin de départager un ensemble de combinaisons de modèles de flux (optimisés ou non par rapport aux concentrations observées par le réseau de surface) et de transport atmosphérique (par exemple le groupe des modèles TRANSCOM ; www.purdue.edu/transcom) afin d'évaluer la capacité des modèles à représenter le mélange vertical, et de déconvoluer ce mélange vertical des anomalies de CO_2 liées aux puits et sources de surface.

7.9.3. Contribution de l'advection aux mesures de gaz trace

J'ai développé une application de la technique de clustering (une technique statistique classificatoire d'analyse exploratoire des données) pour l'interprétation d'un grand nombre de mesures obtenues lors de mesures atmosphériques. J'ai noté que cette technique n'est pas objective dans la mesure où sa formulation (nombre de clusters, métrique utilisée pour le calcul des distances à minimiser) avait un impact important sur la position des centroïdes résultants. L'application de cette technique à d'autres situations requiert en premier lieu une évaluation précise de ce biais. Une méthodologie indépendante d'une présélection de régions d'intérêt particulier est également souhaitable, par exemple en appliquant l'algorithme de clustering directement sur la matrice de temps de résidence.

Il sera possible d'appliquer à d'autres situations cette technique couplant fonction d'influence lagrangienne et clustering. Par exemple il est envisagé d'étudier les conditions météorologiques affectant les mesures réalisées au dessus de la forêt d'Orléans par l'équipe RAMCES du LSCE. Ceci permettra d'identifier plus rationnellement les mesures affectées par une advection de polluants de sources proches (région parisienne) ou continentales, car, comme l'ont montré Han et al. (2007) la dispersion lagrangienne est performante autant sur l'identification de sources ponctuelles qu'étendues.

Références bibliographiques

Akimoto, H. Global air quality and pollution, 2003. *Science*, **302** (5651), 1716-1719.

Akimoto, H., T. Ohara, J. Kurokawa, and N. Horii, 2006. Verification of energy consumption in China during 1996-2003 by using satellite observational data, *Atmos. Environ.*, **40**, 7663-7667.

Anderson, B.E. et al., 1996. Airborne observations of spatial and temporal variability of tropospheric carbon dioxide. *J. Geophys. Res.*, **101**(D1): 1985-1997.

Andreae, M. O. and P. Merlet, 2001. Emission of trace gases and aerosols from biomass burning, *Global Biogeochem. Cy.*, **15** (4), 955-966.

Andreae, M.O. et al., 1988: Vertical-Distribution of Dimethylsulfide, Sulfur-Dioxide, Aerosol Ions, and Radon over the Northeast Pacific-Ocean. *J. Atmos. Chem.*, **6**(1-2): 149-173.

Ankilov, A. et al., 2002a. Particle size dependent response of aerosol counters. *Atmos. Res.*, **62**, 209-237.

Ankilov, A., et al., 2002b. Intercomparison of number concentration measurements by various aerosol particle counters. *Atmos. Res.*, **62**, 177-207.

Appenzeller, C., Holton, J.R. and Rosenlof, K.H., 1996. Seasonal variation of mass transport across the tropopause. *J. Geophys. Res.*, **101**(D10): 15071-15078.

Arshinov M. Yu., B.D. Belan, Ph. Nedelec, J.-D. Paris, T. Machida, 2007. Spatial distribution of nanoparticles in the free troposphere over Siberia, in Nucleation and Atmospheric Physics, 17th International Conference on Nucleation and Atmospheric Aerosols, Galway, Ireland, 2007. C. D. O'Dowd and P. E. Wagner, eds. New York: Springer, p.819-823.

Arshinov, M. Y., and B. D. Belan, 2004. Vertical distribution of nanoparticles in the continental troposphere, *Atmospheric and Oceanic Optics*, **17**(7), 489-499.

Auvray, M. and Bey, I., 2005. Long-range transport to Europe: Seasonal variations and implications for the European ozone budget. *J. Geophys. Res.*, **110** (D11303).

Baker, D.F., Doney, S.C. and Schimel, D.S., 2006. Variational data assimilation for atmospheric CO_2. *Tellus*, **58B**(5): 359-365.

Bakwin, P.S. et al., 2003. Strategies for measurement of atmospheric column means of carbon dioxide from aircraft using discrete sampling. *J. Geophys. Res.*, **108**(D16).

Bakwin, P.S. et al., 2004. Regional carbon dioxide fluxes from mixing ratio data. *Tellus*, **56B**(4): 301-311.

Baldocchi, D. et al., 2001. FLUXNET: A new tool to study the temporal and spatial variability of ecosystem-scale carbon dioxide, water vapor, and energy flux densities. *B. Am. Meteorol. Soc.*, **82**(11): 2415-2434.

Baldocchi, D., F. M. Kelliher, T. A. Black, and P. Jarvis, 2000. Climate and vegetation controls on boreal zone energy exchange, *Global Change Biol.*, **6**, 69–83.

Banic, C.M., Isaac, G.A., Cho, H.R. and Iribarne, J.V., 1986. The Distribution of Pollutants near a Frontal Surface - a Comparison between Field Experiment and Modeling. *Water Air Soil Poll.*, **30**(1-2): 171-177.

Barkley, M.P. et al., 2007. Assessing the near surface sensitivity of SCIAMACHY atmospheric CO_2 retrieved using (FSI) WFM-DOAS. *Atmos. Chem. Phys.*, **7**(13): 3597-3619.

Bartalev, S. A., A. S. Belward, D. V. Erchov and A. S. Isaev, 2003. A new SPOT4-VEGETATION derived land cover map of Northern Eurasia. *Int. J. Remote Sensing*. **24** (9), 1977–1982.

Bashurova, V.S., Dreiling V., Hodger T.V., Jaenicke R., Koutsenogii K.P., Koutsenogii P.K., Kraemer M., Makarov V.I., Obolkin V.A., Potjomkin V.L. & Pusep A.Y., 1992. Measurements of Atmospheric Condensation Nuclei Size Distributions in Siberia. *J. Aerosol Sci.*, **23**, 191-199.

Beekmann, M., G. Ancellet, and G. Mégie, 1994. Climatology of tropospheric ozone in Southern Europe and its relation to potential vorticity. *J. Geophys. Res.* **99** (D6), 12841-12853.

Bergamaschi, P. et al., 1998. Isotope analysis based source identification for atmospheric CH4 and CO sampled across Russia using the Trans-Siberian railroad. *J. Geophys. Res.*, **103**(D7): 8227-8235.

Bergamaschi, P., R. Hein, M. Heimann, and P. J. Crutzen, 2000. Inverse modeling of the global CO cycle: 1. Inversion of CO mixing ratios, *J. Geophys. Res.*, **105**, 1909–1927.

Berkowitz, C.M., P.H. Daum, C.W. Spicer, and K.M. Busness, 1996. Synoptic patterns associated with the flux of excess ozone to the western North Atlantic. *J. Geophys. Res.* **101** (D22), 28923-28933.

Bertschi, I.T., Jaffe, D.A., Jaegle, L., Price, H.U. and Dennison, J.B., 2004. PHOBEA/ITCT 2002 airborne observations of transpacific transport of ozone, CO, volatile organic compounds, and aerosols to the northeast Pacific: Impacts of Asian anthropogenic and Siberian boreal fire emissions. *J. Geophys. Res.*, **109**(D23).

Bethan, S. et al., 1998. Chemical air mass differences near fronts. *J. Geophys. Res.*, **103**(D11): 13413-13434.

Bey, I., Jacob, D.J., Logan, J.A. and Yantosca, R.M., 2001. Asian chemical outflow to the Pacific in spring: Origins, pathways, and budgets. *J. Geophys. Res.*, **106**(D19): 23097-23113.

Boering, K.A. et al., 1996. Stratospheric mean ages and transport rates from observations of carbon dioxide and nitrous oxide. *Science*, **274**(5291): 1340-1343.

Bonan, G.B., 2008. Forests and climate change: Forcings, feedbacks, and the climate benefits of forests. *Science*, **320**(5882): 1444-1449.

Bonasoni, P., P. Cristofanelli, F. Calzolari, U. Bonafè, F. Evangelisti et al., 2004. Aerosol-ozone correlations during dust transport episodes, *Atmos. Chem. Phys.*, **4**, 1201-1215.

Bousquet, P. et al., 2000. Regional changes in carbon dioxide fluxes of land and oceans since 1980. *Science*, **290**(5495): 1342-1347.

Bousquet, P., et al., 2006. Contribution of anthropogenic and natural sources to atmospheric methane variability, *Nature*, **443**, 439– 443, doi:10.1038/nature05132.

Bousquet, P., Ciais, P., Peylin, P., Ramonet, M. and Monfray, P., 1999. Inverse modeling of annual atmospheric CO_2 sources and sinks 1. Method and control inversion. *J. Geophys. Res.*, **104**(D21): 26161-26178.

Buzorius, G., C. S. McNaughton, A. D. Clarke, D. S. Covert, B. Blomquist, K. Nielsen, and F. J. Brechtel (2004), Secondary aerosol formation in continental outflow conditions during ACE-Asia, *J. Geophys. Res.*, **109**, D24203, doi:10.1029/2004JD004749.

Cahill, C.F., 2003: Asian aerosol transport to Alaska during ACE-Asia. *J. Geophys. Res.*, **D108**.

Chameides, W.L. et al., 1992. Ozone Precursor Relationships in the Ambient Atmosphere. *J. Geophys. Res.*, **97**(D5): 6037-6055.

Chan, D., C.W. Yuen, K. Higuchi, A. Shashkov, J. Liu, J. Chen, and D. Worthy, 2004. On the CO_2 exchange between the atmosphere and the biosphere: the role of synoptic and mesoscale processes, *Tellus* **56B**, 194-212.

Chan, D., Ishizawa, M., Higuchi, K., Maksyutov, S. and Chen, J., 2008. Seasonal CO_2 rectifier effect and large-scale extratropical atmospheric transport. *J. Geophys. Res.*, **113**(D17309): doi:10.1029/2007JD009443.

Chapin, F.S. et al., 2005. Role of land-surface changes in Arctic summer warming. *Science*, **310**(5748): 657-660.

Charlson R.J., Langner J. & Rodhe H., 1990. Sulfate Aerosol and Climate. *Nature*, **348**, 22-22.

Chou, W.W. et al., 2002. Net fluxes of CO_2 in Amazonia derived from aircraft observations. *J. Geophys. Res.*, **107**(D22).

Christensen, T. R., I. C. Prentice, J. Kaplan, A. Haxeltine, and S. Sitch, 1996. Methane flux from northern wetlands and tundra: An ecosystem source modelling approach. *Tellus*, **48B**, 652–661.

Clarke, A.D., Eisele F., Kapustin V.N., Moore K., Tanner D., Mauldin L., Litchy M., Lienert B., Carroll M.A. & Albercook G., 1999. Nucleation in the equatorial free troposphere: Favorable environments during PEM-Tropics. *J. Geophys. Res.*, **104**, 5735-5744.

Clarke, A.D., Varner J.L., Eisele F., Mauldin R.L., Tanner D. & Litchy M., 1998. Particle production in the remote marine atmosphere: Cloud outflow and subsidence during ACE 1. *J. Geophys. Res.*, **103**, 16397-16409.

Cooper, O.R. et al., 2001. Trace gas signatures of the airstreams within North Atlantic cyclones: Case studies from the North Atlantic Regional Experiment (NARE '97) aircraft intensive. *J. Geophys. Res.*, **106**(D6): 5437-5456.

Cooper, O.R. et al., 2002. Trace gas composition of midlatitude cyclones over the western North Atlantic Ocean: A conceptual model. *J. Geophys. Res.*, **107**(D7-8).

Cotton, W.R. et al., 1995. Cloud venting - A review and some new global annual estimates. *Earth-Sci. Rev.*, **39**(3-4): 169-206.

Covert, D. S., V. N. Kapustin, P. K. Quinn, and T. S. Bates, 1992. New particle formation in the marine boundary layer, *J. Geophys. Res.*, **97** (18), 20581-29589.

Crutzen, P.J. and Fishman, J., 1977. Average Concentrations of Oh in Troposphere, and Budgets of CH4 CO H-2 + CH3CCL3. *Geophys. Res. Lett.*, **4**(8): 321-324.

Crutzen, P.J. et al., 1998. Trace gas measurements between Moscow and Vladivostok using the Trans-Siberian Railroad. *J. Atmos. Chem.*, **29**(2): 179-194.

Curtius, J., 2006. Nucleation of atmospheric aerosol particles. C. R. Physique, 7: 1027–1045.

Dal Maso, M. et al., 2008. Aerosol particle formation events at two Siberian stations inside the boreal forest. *Boreal Env. Res.*, **13**, 81-92.

Damoah, R. et al., 2004. Around the world in 17 days - hemispheric-scale transport of forest fire smoke from Russia in May 2003. *Atmos. Chem. Phys.*, **4**, 1311-1321.

de Reus M., Strom J., Curtius J., Pirjola L., Vignati E., Arnold F., Hansson H.C., Kulmala M., Lelieveld J. & Raes F., 2000. Aerosol production and growth in the upper free troposphere. *J. Geophys. Res.*, **105**, 24751-24762.

Delmas, R., Mégie, G. et Peuch, V.-H., 2005. Physique et chimie de l'atmosphère, Editions Belin, collection Echelles

Denning, A. S., I. Y. Fung, and D. A. Randall, 1995. Gradient of atmospheric CO_2 due to seasonal exchange with land biota. *Nature*, **376**, 240–243.

Denning, A.S., Takahashi, T. and Friedlingstein, P., 1999. Can a strong atmospheric CO_2 rectifier effect be reconciled with a "reasonable" carbon budget? *Tellus*, **51B**(2): 249-253

Dorling, S.R., Davies, T.D. and Pierce, C.E., 1992. Cluster-Analysis - a Technique for Estimating the Synoptic Meteorological Controls on Air and Precipitation Chemistry - Method and Applications. *Atmos. Environ.*, **26**(14): 2575-2581.

Draxler, R.R. and Hess, G.D., 1997. Description of the Hysplit 4 modeling system. NOAA Tech Memo ERL ARL-224, December, 24p.

Duce, R.A., Unni, C.K., Ray, B.J., Prospero, J.M. and Merrill, J.T., 1980. Long-Range Atmospheric Transport of Soil Dust from Asia to the Tropical North Pacific - Temporal Variability. *Science*, **209**(4464): 1522-1524.

Duncan, B.N. and Bey, I., 2004. A modeling study of the export pathways of pollution from Europe: Seasonal and interannual variations (1987-1997). *J. Geophys. Res.*, **109**(D8).

Duncan, B.N. et al., 2007. Global budget of CO, 1988-1997: Source estimates and validation with a global model. *J. Geophys. Res.*, **112**(D22): -.

Eckhardt, S. et al., 2003. The North Atlantic Oscillation controls air pollution transport to the Arctic. *Atmos. Chem. Phys.*, **3**, 1769-1778.

Eckhardt, S., A. Stohl, H. Wernli, P. James, C. Forster, and N. Spichtinger, 2004. A 15-year climatology of warm conveyor belts, *J. Clim.*, **17** (1), 218-237.

Edwards, D.P. et al., 2004. Observations of carbon monoxide and aerosols from the Terra satellite: Northern Hemisphere variability. *J. Geophys. Res.*, **109**(D24). doi:10.1029/2004JD004727

Eneroth, K., E. Kjellstrom, and K. Holmen, 2003. Interannual and seasonal variations in transport to a measuring site in western Siberia and their impact on the observed atmospheric CO2 mixing ratio, *J. Geophys. Res.*, **108**(D21).

Fan, S. et al., 1998. A large terrestrial carbon sink in North America implied by atmospheric and oceanic carbon dioxide data and models. *Science*, **282**(5388): 442-446.

Fehsenfeld, F.C. et al., 2006. International Consortium for Atmospheric Research on Transport and Transformation (ICARTT): North America to Europe - Overview of the 2004 summer field study. *J. Geophys. Res.*, **111**(D23).

Fishman, J. et al., 2008. Remote sensing of tropospheric pollution from space. *B. Am. Meteorol. Soc.*, **89**(6): 805-821.

Folberth, G., D. A. Hauglustaine, P. Ciais, and J. Lathière, 2005. On the role of atmospheric chemistry in the global CO_2 budget, *Geophys. Res. Lett.*, **32**, L08801, doi:10.1029/2004GL021812.

Forster, C., O. Cooper, A. Stohl, S. Eckhardt, P. James, et al., 2004: Lagrangian transport model forecasts and a transport climatology for the Intercontinental Transport and Chemical Transformation 2002 (ITCT 2k2) measurement campaign. *J. Geophys. Res.*, **109**, D07S92, doi:10.1029/2003JD003589.

Forster, C., Stohl, A. and Seibert, P., 2007. Parameterization of convective transport in a Lagrangian particle dispersion model and its evaluation. *J. Appl. Meteorol. Clim.*, **46**(4): 403-422.

Fromm, M.D. and Servranckx, R., 2003. Transport of forest fire smoke above the tropopause by supercell convection. *Geophys. Res. Lett.*, **30**(10).

Gamnitzer, U., U. Karstens, B. Kromer, R.E.M. Neubert, H.A.J. Meijer et al., 2006. Carbon monoxide: A quantitative tracer for fossil fuel CO_2?. *J. Geophys. Res.* **111** (D22), D22302, doi:10.1029/2005JD006966.

Garrett, T.J. and Verzella, L.L., 2008. An evolving history of arctic aerosols. *B. Am. Meteorol. Soc.*, **89**(3): 299-302.

Gerbig, C. et al., 2003a. Toward constraining regional-scale fluxes of CO_2 with atmospheric observations over a continent: 1. Observed spatial variability from airborne platforms. *J. Geophys. Res.*, **108**(D24).

Gerbig, C. et al., 2003b. Toward constraining regional-scale fluxes of CO_2 with atmospheric observations over a continent: 2. Analysis of COBRA data using a receptor-oriented framework. *J. Geophys. Res.*, **108**(D24).

Global Carbon Project (GCP), 2008. Carbon budget 2007. www.globalcarbonproject.org

Gloor, M., S.-M. Fan, S. Pacala, and J. Sarmiento, 2000. Optimal Sampling of the Atmosphere for Purpose of Inverse Modeling: A Model Study, *Global Biogeochem. Cy.*, **14**(1), 407–428.

Goldstein A.H., McKay M., Kurpius M.R., Schade G.W., Lee A., et al.., 2004. Forest thinning experiment confirms ozone deposition to forest canopy is dominated by reaction with biogenic VOCs. *Geophys. Res. Lett.*, **31**.

Goodale, C.L. et al., 2002. Forest carbon sinks in the Northern Hemisphere. *Ecol. Appl.*, **12**(3): 891-899.

Granier, C., Muller, J.F., Petron, G. and Brasseur, G., 1999. A three-dimensional study of the global CO budget. *Chemosphere - Global Change Science*, **1**(1-3): 255-261.

Gruber, N. et al., 2004. The Vulnerability of the Carbon Cycle in the 21st Century: An Assessment of Carbon-Climate-Human Interactions. In: C.B. Field and M.R. Raupach (Editors), *The global carbon cycle : integrating humans, climate, and the natural world*. Island Press, Washington, pp. 45-76.

Gruber, N., N. Bates, and C. Keeling, 2002. Interannual variability in the North Atlantic Ocean carbon sink. *Science*, **298**, 2374– 2378.

Gurney, K.R. et al., 2002. Towards robust regional estimates of CO_2 sources and sinks using atmospheric transport models. *Nature*, **415**(6872): 626-630.

Han, Y.J., Holsen, T.A., Hopke, P.K. and Yi, S.M., 2005. Comparison between back-trajectory based modeling and Lagrangian backward dispersion modeling for locating sources of reactive gaseous mercury. *Environ. Sci. Technol.*, **39**(10): 3887-3887.

Hauglustaine, D.A. et al., 2004. Interactive chemistry in the Laboratoire de Meteorologie Dynamique general circulation model: Description and background tropospheric chemistry evaluation. *J. Geophys. Res.*, **109**(D4).

Heald, C.L. et al., 2004 : Comparative inverse analysis of satellite (MOPITT) and aircraft (TRACE-P) observations to estimate Asian sources of carbon monoxide. *J. Geophys. Res.*, **109**(D23).

Heintzenberg J., Birmili W., Theiss D. & Kisilyakhov Y., 2008. The atmospheric aerosol over Siberia, as seen from the 300 m ZOTTO tower. *Tellus*, **60B**, 276-285.

Hemispheric Transport of Air Pollution (HTAP), 2007. Interim Report, United Nations Press, New York City, USA, 165 pp.

Hermann M., Heintzenberg J., Wiedensohler A., Zahn A., Heinrich G. & Brenninkmeijer C.A.M., 2003. Meridional distributions of aerosol particle number concentrations in the upper troposphere and lower stratosphere obtained by Civil Aircraft for Regular Investigation of the Atmosphere Based on an Instrument Container (CARIBIC) flights. *J. Geophys. Res.*, **108**.

Hess, P. G., and T. Vukicevic, 2003. Intercontinental transport, chemical transformations, and baroclinic systems, *J. Geophys. Res.*, **108**(D12).

Hiyama, T., M.A.S., R. Suzuki, J. Asanuma, M. Y. Mezrin, N. A. Bezrukova, T. Ohata, 2003. Aircraft observations of the atmospheric boundary layer over a heterogeneous surface in eastern Siberia, *Hydrol. Process.*, **17** (14), 2885-2911.

Holmes and A.J. Dolman, 2008: Greenhouse gas fluxes at a continental tundra site in NE Siberia and radiative forcing of advancing of the growing season. *Geophysical Research Abstracts*, **10**, EGU2008-A-06961, SRef-ID: 1607-7962/gra/EGU2008-A-06961

Holton, J.R. et al., 1995. Stratosphere-Troposphere Exchange. *Rev. Geophys.*, **33**(4): 403-439.

Hong, S.M., J.P. Candelone, C.C. Patterson & C.F. Boutron, 1994. Greenland Ice Evidence of Hemispheric Lead Pollution 2-Millennia Ago by Greek and Roman Civilizations. *Science* **265**(5180), 1841-1843.

Honrath, R.E. et al., 2004. Regional and hemispheric impacts of anthropogenic and biomass burning emissions on summertime CO and O_3 in the North Atlantic lower free troposphere. *J. Geophys. Res.*, **109**(D24).

Hoppel, W. A., G. M. Frick, J. Fitzgerald, and R. E. Larson, 1994. Marine boundary-layer measurements of new particle formation and the effects nonprecipitating clouds have on aerosol-size distribution, *J. Geophys. Res.*, **99**(D7), 14443-14459.

IPCC (Intergovernmental Panel on Climate Change), 2007. Climate change 2007: the physical Science basis: contribution of Working Group I to the Fourth Assessment Report of the Intergovernmental Panel on Climate Change. Cambridge University Press, Cambridge ; New York, viii, 996 p. pp.

Jacob, D.J. et al., 2003 : Transport and Chemical Evolution over the Pacific (TRACE-P) aircraft mission: Design, execution, and first results. *J. Geophys. Res.*, **108**(D20): 1-19.

Jacob, D.J., Logan, J.A. and Murti, P.P., 1999. Effect of rising Asian emissions on surface ozone in the United States. *Geophys. Res. Lett.*, **26**(14): 2175-2178.

Jacob, D.J., S.M. Fan, S.C. Wofsy, P.A. Spiro, P.S. Bakwin et al., 1992. Deposition of Ozone to Tundra. *J. Geophys. Res.* **97** (D15), 16473-16479.

Jaffe, D. et al., 1999. Transport of Asian air pollution to North America. *Geophys. Res. Lett.*, **26**(6): 711-714.

Jaffe, D. et al., 2004. Long-range transport of Siberian biomass burning emissions and impact on surface ozone in western North America. *Geophys. Res. Lett.*, **31**(16).

Jobson B.T., McKeen S.A., Parrish D.D., Fehsenfeld F.C., Blake D.R., Goldstein A.H., Schauffler S.M. & Elkins J.C., 1999. Trace gas mixing ratio variability versus lifetime in the troposphere and stratosphere: Observations. *J. Geophys. Res.*, **104**, 16091-16113.

Jung, M. et al., 2008. Diagnostic assessment of European gross primary production. *Global Change Biol.*, **14**: 1-16.

Kasibhatla, P., et al., 2002. Top-down estimate of a large source of atmospheric carbon monoxide associated with fuel combustion in Asia, *Geophys. Res. Lett.*, **29**(19), 1900, doi:10.1029/2002GL015581.

Kavouras, I.G., Mihalopoulos, N. and Stephanou, E.G., 1999. Secondary organic aerosol formation vs primary organic aerosol emission: In situ evidence for the chemical coupling between monoterpene acidic photooxidation products and new particle formation over forests. *Environ. Sci. Technol.*, **33**(7): 1028-1037.

Keyser, D., 1999. On the representation and diagnosis of frontal circulations in two and three dimensions, in *The Life Cycles of Extratropical Cyclones*, M. A. Shapiro and S. Grønås, Eds., Amer. Meteor. Soc., 239–264

Kiley, C. M., et al., 2003. An intercomparison and evaluation of aircraft-derived and simulated CO from seven chemical transport models during the TRACE-P experiment, *J. Geophys. Res.*, **108**(D21), 8819, doi:10.1029/2002JD003089.

Korhonen, P., M. Kulmala, A. Laaksonen, Y. Viisanen, R. McGraw, and J. H. Seinfeld, 1999. Ternary nucleation of H2SO4, NH3, and H2O in the atmosphere, *J. Geophys. Res.*, **104**(D21), 26349-26353.

Koutsenogii, P., 1997. Aerosol measurements in Siberia. *Atmos. Res.*, **44**, 167-173.

Koutsenogii, P.K., Bufetov N.S., Drozdova V.I., Golobkova V.L., Khodger T.V., Koutzenogii K.P., Makarov V.I., Obolkin V.A. & Potemkin V.L., 1993. Ion Composition of Atmospheric Aerosol near Lake Baikal. *Atmos. Environ.*, **27**, 1629-1633.

Krinner, G., N. Viovy, N. de Noblet-Ducoudre, J. Ogee, J. Polcher et al., 2005. A dynamic global vegetation model for studies of the coupled atmosphere-biosphere system, *Global Biogeochem. Cy.*, **19**, GB1015, doi:10.1029/2003GB00219

Kulmala, M. et al., 2004. Formation and growth rates of ultrafine atmospheric particles: a review of observations. *J. Aerosol Sci.*, **35**(2): 143-176.

Kulmala, M., A. Reissell, M. Sipila, B. Bonn, T. M. Ruuskanen, K. E. J. Lehtinen, V. M. Kerminen, and J. Strom, 2006b. Deep convective clouds as aerosol production engines: Role of insoluble organics, *J. Geophys. Res.*, **111** (D17) D17202,

Kulmala, M., Lehtinen, K.E.J. and Laaksonen, A., 2006a. Cluster activation theory as an explanation of the linear dependence between formation rate of 3nm particles and sulphuric acid concentration. *Atmos. Chem. Phys.*, **6**: 787-793.

Labonne, M., Breon, F.M. and Chevallier, F., 2007. Injection height of biomass burning aerosols as seen from a spaceborne lidar. *Geophys. Res. Lett.*, **34**(11).

Lamarque, J.F. et al., 2003. Identification of CO plumes from MOPITT data: Application to the August 2000 Idaho-Montana forest fires. *Geophys. Res. Lett.*, **30**(13).

Langenfelds R. L., R. J. Francey, B. C. Pak, L. P. Steele, J. Lloyd, C. M. Trudinger, and C. E. Allison, 2002. Interannual growth rate variations of atmospheric CO2 and its δ13C, H2, CH4, and CO between 1992 and 1999 linked to biomass burning, *Global Biogeochem. Cy.*, **16** (3), 1048, doi:10.1029/2001GB001466.

Lapina, K., Honrath, R.E., Owen, R.C., Martin, M.V. and Pfister, G., 2006. Evidence of significant large-scale impacts of boreal fires on ozone levels in the midlatitude Northern Hemisphere free troposphere. *Geophys. Res. Lett.*, **33**(10).

Larson, V.E. and Volkmer, H., 2008. An idealized model of the one-dimensional carbon dioxide rectifier effect. *Tellus*, **60B**(4): 525-536.

Lathiere J., Hauglustaine D.A., Friend A.D., De Noblet-Ducoudre N., Viovy N. & Folberth G.A., 2006: Impact of climate variability and land use changes on global biogenic volatile organic compound emissions. *Atmos. Chem. Phys.*, **6**, 2129-2146.

Lauvaux, T., M. Uliasz, C. Sarrat, F. Chevallier, P. Bousquet et al., 2008. Mesoscale inversion: First results from the CERES campaign with synthetic data. *Atmos. Chem. Phys.*, **8**: 3459–3471.

Law, K.S. and Stohl, A., 2007. Arctic air pollution: Origins and impacts. *Science*, **315**(5818): 1537-1540.

Law, R.M. et al., 1996. Variations in modeled atmospheric transport of carbon dioxide and the consequences for CO_2 inversions. *Global Biogeochem. Cy.*, **10**(4): 783-796.

Leaitch, W. R., and G. A. Isaac, 1991. Tropospheric Aerosol Size Distributions from 1982 to 1988 over Eastern North-America, *Atmos. Environ.*, **25A**(3-4), 601-619.

Le Treut, H., Li, Z.X. and Forichon, M., 1994. Sensitivity of the LMD General Circulation Model to greenhouse forcing associated with two different cloud water parameterizations. *J. Climate*, **7**(12): 1827–1841.

Lee, S.-H., J. M. Reeves, J. C. Wilson, D. E. Hunton, A. A. Viggiano, T. M. Miller, J. O. Ballenthin, and L. R. Lait, 2003. Particle formation by ion nucleation in the upper troposphere and lower stratosphere, *Science*, **301**, 1886-1889.

Lelieveld, J. et al., 2002. Global air pollution crossroads over the Mediterranean. *Science*, 298(5594): 794-799.

Lelieveld, J. et Dentener, F.J., 2000. What controls tropospheric ozone? *J. Geophys. Res.*, **105**(D3): 3531-3551.

Levin, I., et U. Karstens, 2007. Inferring high-resolution fossil fuel CO_2 records at continental sites from combined (CO_2)-C-14 and CO observations, *Tellus* **59B**, 245-250.

Levin, I., P. Ciais, R. Langenfelds, M. Schmidt, M. Ramonet et al., 2002. Three years of trace gas observations over the EuroSiberian domain derived from aircraft sampling - a concerted action, *Tellus* **54B**, 696-712.

Liang, J.Y. et al., 1998. Seasonal budgets of reactive nitrogen species and ozone over the United States, and export fluxes to the global atmosphere. *J. Geophys. Res.*, **103**(D11): 13435-13450.

Liang, Q., L. Jaegle, D. A. Jaffe, P. Weiss-Penzias, A. Heckman, and J. A. Snow, Long-range transport of Asian pollution to the northeast Pacific: Seasonal variations and transport pathways of carbon monoxide, *J. Geophys. Res.*, **109**(D23), 2004.

Lin C.Y., Wang Z., Chen W.N., Chang S.Y., Chou C.C.K., Sugimoto N. & Zhao X., 2007. Long-range transport of Asian dust and air pollutants to Taiwan: observed evidence and model simulation. *Atmos. Chem. Phys.*, **7**, 423-434.

Lin, J.C., C. Gerbig, S.C. Wofsy, A.E. Andrews, B.C. Daube et al., 2003. A near-field tool for simulating the upstream influence of atmospheric observations: The Stochastic Time-Inverted Lagrangian Transport (STILT) model. *J. Geophys. Res.* **108** (D16) doi:10.1029/2002JD003161.

Lin, J.C., et al., 2004. Measuring fluxes of trace gases at regional scales by Lagrangian observations: Application to the CO_2 Budget and Rectification Airborne (COBRA) study. *J. Geophys. Res.*, **109**(D15).

Liu, H., D. J. Jacob, I. Bey, R. M. Yantosca, B. N. Duncan, and G. W. Sachse, 2003. Transport pathways for Asian pollution outflow over the Pacific: Interannual and seasonal variations, *J. Geophys. Res.*, **108**(D20), 8786, doi:10.1029/2002JD003102.

Liu, H., D. J. Jacob, L. Y. Chan, S. J. Oltmans, I. Bey, et al., 2002. Sources of tropospheric ozone along the Asian Pacific Rim: An analysis of ozonesonde observations, *J. Geophys. Res.*, **107**(D21), 4573, doi:10.1029/2001JD002005.

Lloyd, J. et al., 2001. Vertical profiles, boundary layer budgets, and regional flux estimates for CO_2 and its C-13/C-12 ratio and for water vapor above a forest/bog mosaic in central Siberia. *Global Biogeochem. Cy.*, **15**(2): 267-284.

Lloyd, J. et al., 2007. An airborne regional carbon balance for Central Amazonia. *Biogeosciences*, **4**(5): 759-768.

Lloyd, J., R.L. Langenfelds, R.J. Francey, M. Gloor, N.M. Tchebakova et al., 2002. A trace-gas climatology above Zotino, central Siberia, *Tellus* **54B**, 749-767.

Machida, T., Nakazawa, T., Ishidoya, S., Maksyutov, S., Tohjima, Y.. 2001: Temporal and spatial variations of atmospheric CO2 mixing ratio over Siberia. Proceedings of the 6th International Carbon Dioxide Conference, 1–5 October 2001, Sendai, Japan. pp 15–18.

Maignan F., Breon F.M., Vermote E., Ciais P. & Viovy N., 2008: Mild winter and spring 2007 over western Europe led to a widespread early vegetation onset. *Geophys. Res. Lett.*, **35**.

Maksyutov, S. et al., 2003. Effect of recent observations on Asian CO_2 flux estimates by transport model inversions. *Tellus*, **55B**(2): 522-529.

Maksyutov, S., T. Machida, K. Shimoyama, C. Carouge, A. Peregon et al., 2006. Top-down approach to West Siberian regional carbon budget: combination of the CO_2 observations and inverse modelling, *Eos Trans. AGU*, **87**(52), Fall Meet. Suppl., Abstract GC21B-02

Malardel, S., 2005. Fondamentaux de météorologie. Cépaduès Editions, Toulouse, 708p.

Marenco, A., et al., 1998: Measurement of ozone and water vapor by Airbus in-service aircraft: The MOZAIC airborne program, An overview. *J. Geophys. Res.*, **103**, 25631-25642.

Mari, C., M.J. Evans, P.I. Palmer, D.J. Jacob, and G.W. Sachse, 2004. Export of Asian pollution during two cold front episodes of the TRACE-P experiment. *J. Geophys. Res.* **109** (D15), doi:10.1029/2003JD004307.

Mauzerall, D.L. et al., 1998. Photochemistry in biomass burning plumes and implications for tropospheric ozone over the tropical South Atlantic. *J. Geophys. Res.*, **103**(D7): 8401-8423.

Mazzoni, D. et al., 2007. A data-mining approach to associating MISR smoke plume heights with MODIS fire measurements. *Remote Sens. Environ.*, 107(1-2): 138-148.

McDonald, K.C., J.S. Kimball, E. Njoku, R. Zimmermann, and M. Zhao, 2004. Variability in Springtime Thaw in the Terrestrial High Latitudes: Monitoring a Major Control on the Biospheric Assimilation of Atmospheric CO_2 with Spaceborne Microwave Remote Sensing. *Earth Interactions*, **8**, 1–23.

McKeen, S.A. et al., 2002. Ozone production from Canadian wildfires during June and July of 1995. *J. Geophys. Res.*, **107**(D14).

McRae, D.J. et al., 2006. Variability of fire behavior, fire effects, and emissions in Scotch pine forests of Central Siberia. *Mitigation and Adaptation Strategies for Global Change*, **11**: 45-74.

Messager, C., M. Schmidt, M. Ramonet, P. Bousquet, P. Simmonds, et al., 2008. Ten years of CO_2, CH_4, CO and N_2O fluxes over Western Europe inferred from atmospheric measurements at Mace Head, Ireland. *Atmos. Chem. Phys. Discuss.* **8**, 1191-1237.

Methven, J. et al., 2006. Establishing Lagrangian connections between observations within air masses crossing the Atlantic during the International Consortium for Atmospheric Research on Transport and Transformation experiment. *J. Geophys. Res.*, **111**(D23).

Miller, C.E. et al., 2007. Precision requirements for space-based X-CO_2 data. *J. Geophys. Res.*, 112**(**D10).

Minikin A., Petzold A., Strom J., Krejci R., Seifert M., van Velthoven P., Schlager H. & Schumann U., 2003. Aircraft observations of the upper tropospheric fine particle aerosol in the Northern and Southern Hemispheres at midlatitudes. *Geophys. Res. Lett.*, **30**.

Moody, J.L. and Galloway, J.N., 1988. Quantifying the relationship between atmospheric transport and the chemical composition of precipitation on Bermuda. *Tellus*, **40B**(5): 463-479.

Moxim, W. J., H. Levy II, and P. S. Kasibhatla (1996), Simulated global tropospheric PAN: Its transport and impact on NOx, *J. Geophys. Res.*, **101**(D7), 12,621–12,638.

Myneni, R. B., F. G. Hall, P. J. Sellers, and A. L. Marshak, 1995. The interpretation of spectral vegetation indexes, *IEEE Trans. Geosci. Remote Sens.*, **33**, 481–486.

Nansen, F., 1890. The first crossing of Greenland. London, New-York: Longmans, Green&Co. Available online at http://www.archive.org/details/firstcrossingofg00nansiala.

Nakazawa, T., S. Sugawara, G. Inoue, T. Machida, S. Makshyutov, and H. Mukai, 1997. Aircraft measurements of the concentrations of CO_2, CH4, N2O, and CO and the carbon and oxygen isotopic ratios of CO_2 in the troposphere over Russia. *J. Geophys. Res.* **102** (D3), 3843-3859.

Nédélec P., et al., 2003. An improved infrared carbon monoxide analyser for routine measurements aboard commercial Airbus aircraft: technical validation and first scientific results of the MOZAIC III programme. *Atmos. Chem. Phys.*, **3**, 1551-1564.

Nédélec, P., et al., 2005. Extreme CO concentrations in the upper troposphere over northeast Asia in June 2003 from the in situ MOZAIC aircraft data. *Geophys. Res. Lett.*, **32**(14). L14807, doi:10.1029/2003JD004307.

Newell, R.E., and M.J. Evans, 2000. Seasonal changes in pollutant transport to the North Pacific: the relative importance of Asian and European sources.. *Geophys. Res. Lett.* **27** (16), 2509-2512.

Newell, R.E., V. Thouret, J.Y.N. Cho, P. Stoller, A. Marenco, and H.G. Smit, 1999. Ubiquity of quasi-horizontal layers in the troposphere, *Nature*, **398** (6725), 316-319.

Nicholls, M.E. et al., 2004. A multiple-scale simulation of variations in atmospheric carbon dioxide using a coupled biospherepheric model. *J. Geophys. Res.*, **109**(D18). D18117, doi:10.1029/2003JD004482

Nordenskiold, A. E., 1883. Nordenskiold on the Inland Ice of Greenland. *Science*, **2**(44): 732:738.

Novelli, P.C. et al., 2003. Reanalysis of tropospheric CO trends: Effects of the 1997-1998 wildfires. *J. Geophys. Res.*, **108**(D15).

Novelli, P.C., Masarie, K.A., Tans, P.P. and Lang, P.M., 1994. Recent Changes in Atmospheric Carbon-Monoxide. *Science*, **263**(5153): 1587-1590.

Nyeki S., Kalberer M., Lugauer M., Weingartner E., Petzold A., Schroder F., Colbeck I. & Baltensperger U., 1999. Condensation Nuclei (CN) and Ultrafine CN in the Free Troposphere to 12 km: A case study over the Jungfraujoch high-alpine research station. *Geophys. Res. Lett.*, **26**, 2195-2198.

Oberlander, E.A., C.A.M. Brenninkmeijer, P.J. Crutzen, N.F. Elansky, G.S. Golitsyn et al., 2002. Trace gas measurements along the Trans-Siberian railroad: The TROICA 5 expedition. *J. Geophys. Res.* **107** (D14), 4206, doi:10.1029/2001JD000953.

O'Dowd, C.D., Aalto, P., Hameri, K., Kulmala, M. and Hoffmann, T., 2002. Aerosol formation - Atmospheric particles from organic vapours. *Nature*, 416(6880): 497-498.

Ohara, T. et al., 2007. An Asian emission inventory of anthropogenic emission sources for the period 1980-2020. *Atmos. Chem. Phys.*, **7**(16): 4419-4444.

Olivier, J.G.J., J.A. Van Aardenne, F. Dentener, L. Ganzeveld, and J.A.H.W. Peters, 2005. Recent trends in global greenhouse gas emissions: regional trends and spatial distribution of key sources, in *Non-CO2 Greenhouse Gases (NCGG-4)*, edited by A.v. Amstel, Millpress, Rotterdam, pp. 325-330.

Owen, R. C., O. R. Cooper, A. Stohl, and R. E. Honrath, 2006. An analysis of the mechanisms of North American pollutant transport to the central North Atlantic lower free troposphere, *J. Geophys. Res.*, **111**(D23).

Palmer, P. I., D. J. Jacob, D. B. A. Jones, C. L. Heald, R. M. Yantosca, et al., 2003. Inverting for emissions of carbon monoxide from Asia using aircraft observations over the western Pacific, *J. Geophys. Res.*, **108**(D21), 8828, doi:10.1029/2003JD003397.

Palmer, P.I., P. Suntharalingam, D.B.A. Jones, D.J. Jacob, D.G. Streets et al., 2006. Using CO_2:CO correlations to improve inverse analyses of carbon fluxes. *J. Geophys. Res.* **111** (D12), doi:10.1029/2005JD006697.

Papayannis A., et al., 2007: Extraordinary dust event over Beijing, China, during April 2006: Lidar, Sun photometric, satellite observations and model validation. *Geophys. Res. Lett.*, **34**(7), L07806, doi:10.1029/2006GL029125.

Paris, J.-D. et al., 2008: The YAK-AEROSIB transcontinental aircraft campaigns: new insights on the transport of CO_2, CO and O_3 across Siberia. *Tellus*, **60B**, 551-568.

Perez-Landa, G. et al., 2007. Mesoscale circulations over complex terrain in the Valencia coastal region, Spain - Part 2: Modeling CO_2 transport using idealized surface fluxes. *Atmos. Chem. Phys.*, **7**(7): 1851-1868.

Pétron, G., C. Granier, B. Khattatov, J.F. Lamarque, V. Yudin, et al., 2002. Inverse modeling of carbon monoxide surface emissions using Climate Monitoring and Diagnostics Laboratory network observations. *J. Geophys. Res.* **107** (D24), 4761, doi:10.1029/2001JD001305.

Pétron, G., C. Granier, B. Khattotov, V. Yudin, J.-F. Lamarque, et al., 2004. Monthly CO surface sources inventory based on the 2000–2001 MOPITT satellite data, *Geophys. Res. Lett.*, **31**, L21107, doi:10.1029/2004GL020560.

Peylin, P. et al., 2005a. Daily CO_2 flux estimates over Europe from continuous atmospheric measurements: 1, inverse methodology. *Atmos. Chem. Phys.*, **5**: 3173-3186.

Peylin, P. et al., 2005b. Multiple constraints on regional CO_2 flux variations over land and oceans. *Global Biogeochem. Cy.*, **19**(1).

Peylin, P., Baker, D., Sarmiento, J., Ciais, P. and Bousquet, P., 2002. Influence of transport uncertainty on annual mean and seasonal inversions of atmospheric CO_2 data. *J. Geophys. Res.*, **107**(D19).

Pfister, G. G., et al., 2005. Quantifying CO emissions from the 2004 Alaskan wildfires using MOPITT CO data, *Geophys. Res. Lett.*, **32**, L11809, doi:10.1029/2005GL022995.

Pfister, G. G., et al., 2006. Ozone production from the 2004 North American boreal fires. *J. Geophys. Res.*, **111**(D24).

Pochanart, P., Akimoto, H., Kajii, Y., Potemkin, V.M. and Khodzher, T.V., 2003: Regional background ozone and carbon monoxide variations in remote Siberia/East Asia. *J. Geophys. Res.*, **108**(D1). doi:10.1029/2001JD001412

Potosnak, M.J. et al., 1999. Influence of biotic exchange and combustion sources on atmospheric CO2 concentrations in New England from observations at a forest flux tower. *J. Geophys. Res.*, **104**(D8): 9561-9569.

Purvis, R.M. et al., 2003. Rapid uplift of nonmethane hydrocarbons in a cold front over central Europe. *J. Geophys. Res.*, **108**(D7).

Rahn, K.A., Borys, R.D. and Shaw, G.E., 1977. Asian Source of Arctic Haze Bands. *Nature*, **268**(5622): 713-715.

Ramanathan, V. and Carmichael, G., 2008. Global and regional climate changes due to black carbon. *Nature Geosci.*, 1(4): 221-227.

Ramonet M., et al., 2002: Three years of aircraft-based trace gas measurements over the Fyodorovskoye southern taiga forest, 300 km north-west of Moscow. *Tellus*, **54B**, 713-734.

Randerson, J.T. et al., 2006. The impact of boreal forest fire on climate warming. *Science*, **314**(5802): 1130-1132.

Raupach, M.R., 1991. Vegetation-atmosphere interaction in homogeneous and heterogeneous terrain - some implications of mixed-layer dynamics. *Vegetatio*, **91**(1-2): 105-120.

Rayner, P.J. and Law, R.M., 1995. A comparison of modelled responses to prescribed CO2 sources. Tech. paper 36, CSIRO Div. of Atmos. Res.

Rayner, P.J. et al., 2008. Interannual variability of the global carbon cycle (1992-2005) inferred by inversion of atmospheric CO_2 and $\delta^{13}C(CO_2)$ measurements. *Global Biogeochem. Cy.*, **22**(3).

Rayner, P.J., Law, R.M., O'Brien, D.M., Butler, T.M. and Dilley, A.C., 2002. Global observations of the carbon budget - 3. Initial assessment of the impact of satellite orbit, scan geometry, and cloud on measuring CO_2 from space. *J. Geophys. Res.*, **107**(D21).

Real, E. et al., 2007. Processes influencing ozone levels in Alaskan forest fire plumes during long-range transport over the North Atlantic. *J. Geophys. Res.*, **112**(D10).

Reichle, H.G. et al., 1999. Space shuttle based global CO measurements during April and October 1994, MAPS instrument, data reduction, and data validation. *J. Geophys. Res.*, **104**(D17): 21443-21454.

Reichstein M., et al., 2007: Determinants of terrestrial ecosystem carbon balance inferred from European eddy covariance flux sites. *Geophys. Res. Lett.*, **34**.

Reichstein, M. et al., 2005. On the separation of net ecosystem exchange into assimilation and ecosystem respiration: review and improved algorithm. *Global Change Biol.*, **11**(9): 1424-1439.

Reischl G.P., Majerowicz A., Ankilow A., Eremenko S. & Mavliev R., 1991: Comparison of the Novosibirsk Automated Diffusion Battery with the Vienna Electro Mobility Spectrometer. *J. Aerosol Sci.*, **22**, 223-228.

Rivier, L. et al., 2006. Evaluation of SF_6, C_2Cl_4, and CO to approximate fossil fuel CO_2 in the Northern Hemisphere using a chemistry transport model. *J. Geophys. Res.*, **111**(D16). doi:10.1029/2005JD006725.

Röckmann, T., Brenninkmeijer, C.A.M., Hahn, M. and Elansky, N., 1999. CO mixing and isotope ratios across Russia; trans-Siberian railroad expedition TROICA 3, April 1997. *Chemosphere - Global Change Science*, **1**: 219-231.

Rosenfeld, D. et al., 2008. Flood or drought: How do aerosols affect precipitation? *Science*, **321**(5894): 1309-1313.

Sadourny, R. and Laval, K., 1984. January and July performance of the LMD general circulation model. In: A. Berger and C. Nicolis (Editors), *New Perspectives in Climate Modeling*. Elsevier Science, New York, pp. 173–198.

Santaren, D., Peylin, P., Viovy, N. and Ciais, P., 2007. Optimizing a process-based ecosystem model with eddy-covariance flux measurements: A pine forest in southern France. *Global Biogeochem. Cy.*, **21**(2).

Sarrat, C. et al., 2007. Atmospheric CO2 modeling at the regional scale: Application to the CarboEurope Regional Experiment. *J. Geophys. Res.*, **112**(D12).

Schmitgen, S. et al., 2004. Carbon dioxide uptake of a forested region in southwest France derived from airborne CO2 and CO measurements in a quasi-Lagrangian experiment. *J. Geophys. Res.*, **109**(D14).

Seibert, P., and A. Frank, 2004. Source-receptor matrix calculation with a Lagrangian particle dispersion model in backward mode. *Atmos. Chem. Phys.*, **4**, 51-63.

Seinfeld, J.H. and Pandis, S.N., 1998. Atmospheric chemistry and physics: from air pollution to climate change. Wiley, New York, 1326 p.

Shapiro, M.A., Hampel, T. and Krueger, A.J., 1987. The Arctic Tropopause Fold. *Mon. Weather Rev.*, **115**(2): 444-454.

Shaw G.E., 1982. Evidence for a Central Eurasian Source Area of Arctic Haze in Alaska. *Nature*, **299**, 815-818.

Shibistova O., et al., 2002: Seasonal and spatial variability in soil CO_2 efflux rates for a central Siberian Pinus sylvestris forest. *Tellus*, **54B**, 552-567.

Shvidenko, A., Schepaschenko, D., McCallum, I. and Nilsson, S., 2007: CD-ROM "Russian Forests and Forestry", International Institute for Applied Systems Analysis and the Russian Academy of Science, Laxenburg, Austria. http://www.iiasa.ac.at/Research/FOR/forest_cdrom/

Sirois, A. and Bottenheim, J.W., 1995. Use of Backward Trajectories to Interpret the 5-Year Record of Pan and O-3 Ambient Air Concentrations at Kejimkujik National-Park, Nova-Scotia. *J. Geophys. Res.*, **100**(D2): 2867-2881.

Smith N.V., Saatchi S.S. & Randerson J.T., 2004: Trends in high northern latitude soil freeze and thaw cycles from 1988 to 2002. *J. Geophys. Res.*, **109**.

Soja A.J., Cofer W.R., Shugart H.H., Sukhinin A.I., Stackhouse P.W., McRae D.J. & Conard S.G., 2004. Estimating fire emissions and disparities in boreal Siberia (1998-2002). *J. Geophys. Res.*, **109**.

Stephens, B.B. et al., 2007. Weak northern and strong tropical land carbon uptake from vertical profiles of atmospheric CO_2. *Science*, **316**(5832): 1732-1735.

Stohl A. and Eckhardt S., 2004: Intercontinental Transport of Air Pollution: An Introduction. Springer, Berlin.

Stohl A., Forster C., Frank A., Seibert P. & Wotawa G., 2005: Technical note: The Lagrangian particle dispersion model FLEXPART version 6.2. *Atmos. Chem. Phys.*, **5**, 2461-2474.

Stohl, A. & Law, K., 2006. Polar Study using Aircraft, Remote Sensing, Surface Measurements and Models, of Climate, Chemistry, Aerosols, and Transport (POLARCAT). IGACtivities Newsletter, **33**, pp. 16-32. Available online at http://www.igac.noaa.gov/newsletter/igac33/May_2006_IGAC_33.pdf

Stohl, A. & Thomson, D.J., 1999. A density correction for Lagrangian particle dispersion models. *Bound.-Lay. Meteorol.*, **90**(1): 155-167.

Stohl, A., 2001. A 1-year Lagrangian "climatology" of airstreams in the Northern Hemisphere troposphere and lowermost stratosphere. *J. Geophys. Res.*, **106**(D7): 7263-7279.

Stohl, A., 2006. Characteristics of atmospheric transport into the Arctic troposphere. *J. Geophys. Res.*, **111**(D11).

Stohl, A., C. Forster, A. Frank, P. Seibert, and G. Wotawa, 2005. Technical note: The Lagrangian particle dispersion model FLEXPART version 6.2, *Atmos. Chem. Phys.*, **5**, 2461-2474.

Stohl, A., C. Forster, H. Huntrieser, H. Mannstein, W.W. McMillan et al., 2007b. Aircraft measurements over Europe of an air pollution plume from Southeast Asia - aerosol and chemical characterization, *Atmos. Chem. Phys.*, **7**, 913-937.

Stohl, A., Eckhardt, S., Forster, C., James, P. and Spichtinger, N., 2002: On the pathways and timescales of intercontinental air pollution transport. *J. Geophys. Res.*, **107**(D23).

Stohl, A., M. Hittenberger, and G. Wotawa, 1998. Validation of the Lagrangian particle dispersion model FLEXPART against large-scale tracer experiment data, *Atmos. Environ.*, **32**(24), 4245-4264.

Stohl, A., T. Berg, J.F. Burkhart, A.M. Fjaeraa, C. et al., 2007a. Arctic smoke - record high air pollution levels in the European Arctic due to agricultural fires in Eastern Europe in spring 2006, *Atmos. Chem. Phys.*, **7**, 511-534.

Streets D.G., Gupta S., Waldhoff S.T., Wang M.Q., Bond T.C. & Bo Y.Y., 2001. Black carbon emissions in China. Atmospheric Environment, **35**, 4281-4296.

Streets, D.G., T.C. Bond, G.R. Carmichael, S.D. Fernandes, Q. Fu et al., 2003. An inventory of gaseous and primary aerosol emissions in Asia in the year 2000. *J. Geophys. Res.* **108** (D21), 8809, doi: 10.1029/2002JD003093.

Stull, R.B., 1988. An introduction to boundary layer meteorology. Atmospheric sciences library. Kluwer Academic Publishers, Dordrecht ; Boston, xii, 666 p.

Suntharalingam, P., D. J. Jacob, P. I. Palmer, J. A. Logan, R. M. Yantosca, et al., 2004. Improved quantification of Chinese carbon fluxes using CO_2/CO correlations in Asian outflow. *J. Geophys. Res.* **109** (D18), doi:10.1029/2003JD004362.

Takegawa, N. et al., 2004. Removal of NOx and NOy in Asian outflow plumes: Aircraft measurements over the western Pacific in January 2002. *J. Geophys. Res.*, **109**(D23).

Tans, P.P., Fung, I.Y. and Takahashi, T., 1990. Observational Constraints on the Global Atmospheric CO_2 Budget. *Science*, **247**(4949): 1431-1438.

Tarvainen V., Hakola H., Rinne J., Hellen H. & Haapanala S., 2007. Towards a comprehensive emission inventory of terpenoids from boreal ecosystems. *Tellus*, **59B**, 526-534.

Thornton, D.C., Bandy, A.R., Blomquist, B.W., Bradshaw, J.D. and Blake, D.R., 1997. Vertical transport of sulfur dioxide and dimethyl sulfide in deep convection and its role in new particle formation. *J. Geophys. Res.*, **102**(D23): 28501-28509.

Traub, M., H. Fischer, M. de Reus, R. Kormann, J. Heland, et al., 2003. Chemical characteristics assigned to trajectory clusters during the MINOS campaign, *Atmos. Chem. Phys.*, **3**, 459-468

Trentmann, J. et al., 2006. Modeling of biomass smoke injection into the lower stratosphere by a large forest fire (Part I): reference simulation. *Atmos. Chem. Phys.*, **6**: 5247-5260.

Tunved P., Hansson H.C., Kerminen V.M., Strom J., Dal Maso M., Lihavainen H., Viisanen Y., Aalto P.P., Komppula M. & Kulmala M., 2006. High natural aerosol loading over boreal forests. *Science*, **312**, 261-263.

Turnbull, J. C., Miller, J. B., Lehman, S. J., Tans, P. P., Sparks, R. J. et al., 2006. Comparison of $^{14}CO_2$, CO, and SF_6 as tracers for recently added fossil fuel CO_2 in the atmosphere and implications for biological CO_2 exchange. *Geophys. Res. Lett.* **33**, L01817, doi:10.1029/2005GL024213.

Turquety, S. et al., 2007. Inventory of boreal fire emissions for North America in 2004: Importance of peat burning and pyroconvective injection. *J. Geophys. Res.*, **112**(D12).

Twohy, C. H., et al., 2002. Deep convection as a source of new particles in the midlatitude upper troposphere, *J. Geophys. Res.*, **107**, doi:10.1029/2001JD000323.

Val Martin M., Honrath R.E., Owen R.C., Pfister G., Fialho P. & Barata F., 2006: Significant enhancements of nitrogen oxides, black carbon, and ozone in the North Atlantic lower free troposphere resulting from North American boreal wildfires. *J. Geophys. Res.*, **111**.

Van Aardenne, J.A., F. Dentener, J.G.J. Olivier and J.A.H.W. Peters, 2005. The EDGAR 3.2 Fast Track 2000 dataset (32FT2000). Available online at http://www.mnp.nl/edgar/model/v32ft2000edgar/docv32ft2000/

van der Molen, M. K., and A. J. Dolman, 2007. Regional carbon fluxes and the effect of topography on the variability of atmospheric CO_2. *J. Geophys. Res.* **112**, D01104, doi:10.1029/2006JD007649

van der Werf, G. R., J. T. Randerson, L. Giglio, J. G. Collatz, P. Kasibhatla, and A. F. Arellano, 2006. Interannual variability in global biomass burning emissions from 1997 to 2004, *Atmos. Chem. Phys.*, **6**, 3423–3441.

van der Werf, G.R. et al., 2004. Continental-scale partitioning of fire emissions during the 1997 to 2001 El Nino/La Nina period. *Science*, **303**(5654): 73-76.

Vartiainen E., Kulmala M., Ehn M., Hirsikko A., Junninen H., et al.., 2007. Ion and particle number concentrations and size distributions along the Trans-Siberian railroad. *Boreal Environ. Res.*, **12**, 375-396.

Vaughan, G., W.E. Garland, D.J. Dewey, and C. Gerbig, 2003. Aircraft measurements of a warm conveyor belt - A case study, *J. Atmos. Chem.*, **46** (2), 117-129.

Wada, A. et al., 2007. Influence of continental air mass transport on atmospheric CO_2 in the western North Pacific. *J. Geophys. Res.*, **112**(D7).

Walter, K.M., Smith, L.C. and Chapin, F.S., 2007. Methane bubbling from northern lakes: present and future contributions to the global methane budget. Philos T R Soc A, 365(1856): 1657-1676.

Wang, J.W., A.S. Denning, L.X. Lu, I.T. Baker, K.D. Corbin, and K.J. Davis, 2007, Observations and simulations of synoptic, regional, and local variations in atmospheric CO_2. *J. Geophys. Res.* **112** (D4), doi:10.1029/2006JD007410.

Weber, R. J., J. J. Marti, P. H. McMurry, F. L. Eisele, D. J. Tanner, and A. Jefferson, 1996. Measured atmospheric new particle formation rates: implications for nucleation mechanisms, *Chem. Eng. Commun.*, **151**, 53-64.

Wild, O., P. Pochanart, and H. Akimoto, 2004. Trans-Eurasian transport of ozone and its precursors. *J. Geophys. Res.* **109** (D11), doi:10.1029/2003JD004501.

Wilks, D.S., 2006. Statistical methods in the atmospheric sciences. Academic Press, Amsterdam, Boston, 627 pp.

Williams J., de Reus M., Krejci R., Fischer H. & Strom J., 2002. Application of the variability-size relationship to atmospheric aerosol studies: estimating aerosol lifetimes and ages. *Atmos. Chem. Phys.*, **2**, 133-145.

Wofsy, S.C. et al., 1993. Net Exchange of CO_2 in a Midlatitude Forest. *Science*, **260**(5112): 1314-1317.

Wotawa, G., Novelli, P.C., Trainer, M. and Granier, C., 2001. Inter-annual variability of summertime CO concentrations in the Northern Hemisphere explained by boreal forest fires in North America and Russia. *Geophys. Res. Lett.*, **28**(24): 4575-4578.

Yang, Z. et al., 2007. New constraints on Northern Hemisphere growing season net flux. *Geophys. Res. Lett.*, **34**(12).

Yi C., Davis K.J., Bakwin P.S., Denning A.S., Zhang N., Desai A., Lin J.C. & Gerbig C., 2004: Observed covariance between ecosystem carbon exchange and atmospheric boundary layer dynamics at a site in northern Wisconsin. *J. Geophys. Res.*, **109**, D08302, doi:10.1029/2003JD004164.

Yienger, J.J. et al., 2000. The episodic nature of air pollution transport from Asia to North America. *J. Geophys. Res.*, **105**(D22): 26931-26945.

Young L.H., Benson D.R., Montanaro W.M., Lee S.H., Pan L.L., et al.., 2007. Enhanced new particle formation observed in the northern midlatitude tropopause region. *J. Geophys. Res.*, **112**.

Yurganov, L.N. et al., 2005. Increased Northern Hemispheric carbon monoxide burden in the troposphere in 2002 and 2003 detected from the ground and from space. *Atmos. Chem. Phys.*, **5**: 563-573.

Zhou L.M., Tucker C.J., Kaufmann R.K., Slayback D., Shabanov N.V. & Myneni R.B., 2001: Variations in northern vegetation activity inferred from satellite data of vegetation index during 1981 to 1999. *J. Geophys. Res.*, **106**, 20069-20083.

Zimov, S. A., E. A. G. Schuur, and F. S. Chapin III, 2006. Permafrost and the global carbon budget. *Science*, **312**, 1612–1613.

Zuev, V. E., Belan, B. D., Kabanov, D. M., Kovalevskii, V. K., Luk'ianov et al., 1992. The Optik-E AN-30 laboratory-airplane for ecological studies. *Optika Atmosfery i Okeana*. **5** (10), 1012-1021.

Annexe 1
Moyens expérimentaux

1.1. Plateforme aéroportée

La plateforme aéroportée utilisée est un Antonov-30D de la compagnie Novossibirsk Avia basé à Novossibirsk (Fig. 1). Cet avion est un ancien avion de reconnaissance géographique utilisé régulièrement par l'équipe de l'Institut d'Optique Atmosphérique de Tomsk. La sonde de prélèvement atmosphérique est présentée dans la Figure 2. Les caractéristiques de l'avion sont résumées dans le tableau 1.

Figure 1. Vue de l'Antonov-30D utilisé pour les campagnes

Figure 2. Sonde de prélèvement

Table 1. Paramètres de l'Antonov-30D.

Paramètre	Valeur
Longueur de l'avion	24,3 m
Hauteur de l'avion	8,3 m
Plafond de vol	8100 m
Durée de vol (maximum)	8 h (+réserve)
Portée maximale	3400 km
Vitesse horizontale	300 km h^{-1}
Vitesse verticale pendant la montée	7.0 m s^{-1}
Vitesse verticale pendant la descente	3.5 m s^{-1}
Longueur de piste requise	1300 m
Équipage: Pilotes	7
Équipage: personnel scientifique	<10

1.2. Instrument CO_2

L'instrument CO_2 (Fig. 3 ; voir également la photographie Fig. 6 ci après) est basé sur un analyseur CO_2/H_2O LI-6262 (LI-COR, USA) largement modifié pour atteindre la précision et la stabilité requise en vol. La version commerciale de cet instrument est souvent utilisée pour les mesures à l'échelle de l'écosystème. La technique de mesure utilisée est l'absorption infrarouge non dispersive (NDIR, *non-dispersive infrared*). La fréquence d'acquisition du CONDOR est de 0.5 Hz. La précision requise pour de telles mesures est de 0.15 ppm. Les mesures sont basées sur la différence d'absorption du rayonnement infrarouge entre les deux cellules de l'instrument (Fig. 4). La cellule A (la cellule de référence) est remplie avec un gaz dont la teneur en CO_2 est mesurée à haute précision avant les campagnes, tandis que la cellule B (la cellule de l'échantillon) est utilisée pour le gaz à mesurer. La source est composée d'un filament de tungstène chauffé maintenu dans un vide poussé. Le rayonnement infra rouge (centré à 4.225 microns pour le CO_2) est transmis à travers les deux cellules, puis il est détecté par des semi-conducteurs au séléniure de plomb. Finalement, un système informatique intègre les deux mesures et permet de calculer la concentration de l'échantillon. Dans sa version commerciale, le LI-COR 6262 a une précision de 1 à 2 ppm avec des standards respectivement à 350 et 1000 ppm.

L'air extérieur pompé est déshydraté par une cartouche de perchlorate de magnésium avant d'être injecté dans la cellule échantillon.

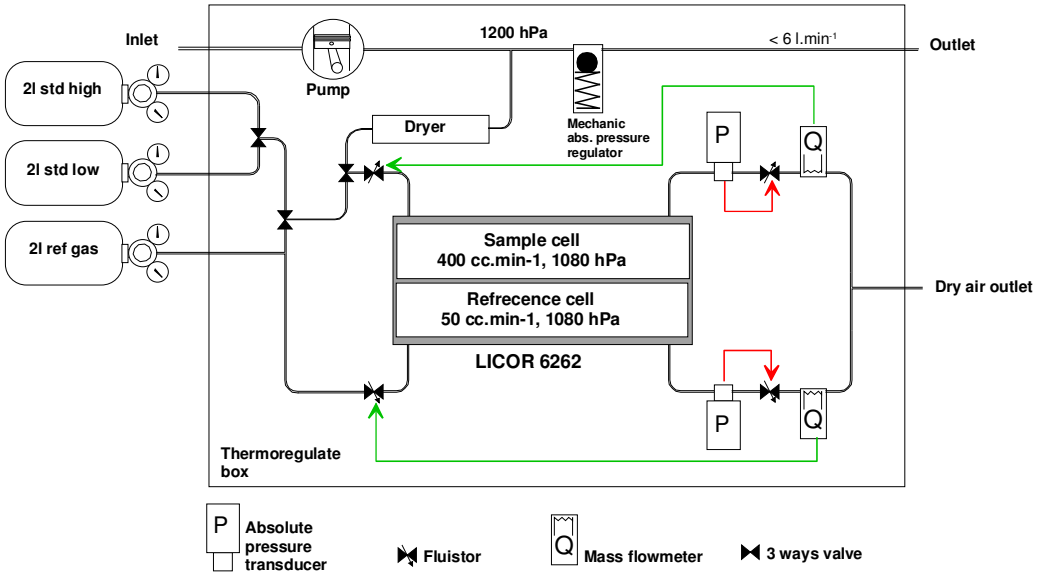

Figure 4. Schéma de fonctionnement de l'instrument CONDOR

Même en environnement pressurisé et climatisé, la température et la pression varient très rapidement. Pour remédier à ces problèmes, le CONDOR intègre un système de régulation actif de la température, du débit et de la pression. Des conditions de fonctionnement nominales sont stipulées pour chacune des deux cellules, par exemple une pression de 1080 ± 0.1 hPa, un débit pour la cellule de référence de 50 ± 0.2 cc min^{-1}, un débit pour la cellule échantillon de 400 ± 0.5 cc min^{-1} et enfin une température de 35 ± 0.6 °C.

Pour prendre en compte les dérives lentes du CONDOR liées aux paramètres physiques tels que la température ou la pression, un étalonnage s'effectue toutes les 30 minutes environ (avec un déclenchement automatique qui peut être également provoqué manuellement). Ceci consiste à faire passer pendant trois minutes le standard bas, puis trois minutes le standard haut dans la cellule échantillon. Les standards sont composés d'air synthétique avec des teneurs en CO_2 qui encadrent les concentrations atmosphériques. Les concentrations des bouteilles utilisées durant les campagnes YAK-AEROSIB sont données par la table 2 telles que mesurées en laboratoire avant les campagnes. Les valeurs des concentrations en CO_2 des standards utilisés ont été mesurées au laboratoire par rapport à l'échelle primaire internationale WMO maintenue par la NOAA.

Table 2. Bouteilles étalons CO_2 utilisées durant les campagnes YAK-AEROSIB

Type	Référence	Concentration ± écart type (ppm)
Low	CQB15919	370.60 ± 0.01
Zero	CQB15657	380.47 ± 0.01
High	CQB15939	409.76 ± 0.01

Le détecteur optique induit un bruit et une non-linéarité qui sont négligés par rapport à l'impact des variations dans l'écoulement des gaz et de performances des régulateurs.

On définit la sensibilité de la mesure (en mV ppm^{-1}) par l'équation suivante :

$$S = \frac{U_H\,[mV] - U_L\,[mV]}{C_H\,[ppm] - C_L\,[ppm]}$$

avec U la tension lue et C la concentration pour les gaz H (*high*) et L (*low*) Les valeurs de U_L et U_H sont calculées en prenant la moyenne des tensions de CO_2 sur tous les étalonnages. Elles peuvent également être calculées sur chaque calibration.

1.2.1. Traitement des données de l'instrument CO_2

Les deux séries d'étalonnage (*high* et *low*) comprenant la tension de lecture et les paramètres de maintenance permettent de calibrer le signal de mesure, augmentant l'exactitude d'un facteur 10 environ. Par ailleurs les bouteilles de référence peuvent être mesurées *a posteriori* en laboratoire, ce qui permet une correction des erreurs systématiques et de dérive sur des périodes de temps plus longues.

La série temporelle enregistrée par l'instrument se décompose en étalonnages *high* et *low* (~20% du temps) et en mesures d'air ambiant (signal utile ; ~80% du temps). Cette alternance permet de réaliser un premier encadrement des données. Dû au temps de montée de la régulation lors du changement d'admission du système, la valeur du standard *high* ou *low* doit être calculée sur une fenêtre d'environ 1 min sur les 3 min que dure la calibration, lorsque la pression est stabilisée après les oscillations provoquées par le changement de circuit.. Par ailleurs la stabilité n'est pas systématiquement acquise en fin de cycle et un contrôle manuel est donc nécessaire pour affecter cette fenêtre temporelle à la période ou les régulations sont les plus stables. On minimise ainsi la variance autour de la moyenne de référence. On peut ensuite obtenir la sensibilité instantanée et l'offset (erreur absolue) de l'instrument rapportés aux concentrations estimées des standards, au moment des 2 injections *high* et *low*.

La courbe temporelle d'étalonnage appliquée aux données in-situ est basée sur une interpolation des mesures individuelles d'étalonnage. Pour estimer la précision de cet étalonnage une mesure « cible » est utilisée, idéalement par l'injection d'un quatrième gaz standard mais en pratique en excluant un standard et en évaluant la capacité à le prédire par interpolation (approche type bootstrap).

Une fois les correspondances voltage-concentration définies finement pour l'ensemble de la mesure, on peut procéder au calcul final. Concrètement, le traitement des données du CONDOR requiert deux traitements logiciels consécutifs. Le premier logiciel, *Airjazz*, a été développé spécifiquement pour les instruments de type CONDOR. Ce logiciel permet de traiter, analyser et exporter les données brutes de mesure du CO_2 en obtenant un gain en précision d'un facteur 10 sur la concentration. Une deuxième couche logicielle, que j'ai réalisée avec Matlab, se superpose pour pouvoir prendre en compte le passage de zéros pour obtenir un gain supplémentaire en précision et filtrer de manière semi-automatique les mesures erronées. Ce fonctionnement est résumé dans le *flowchart* suivant

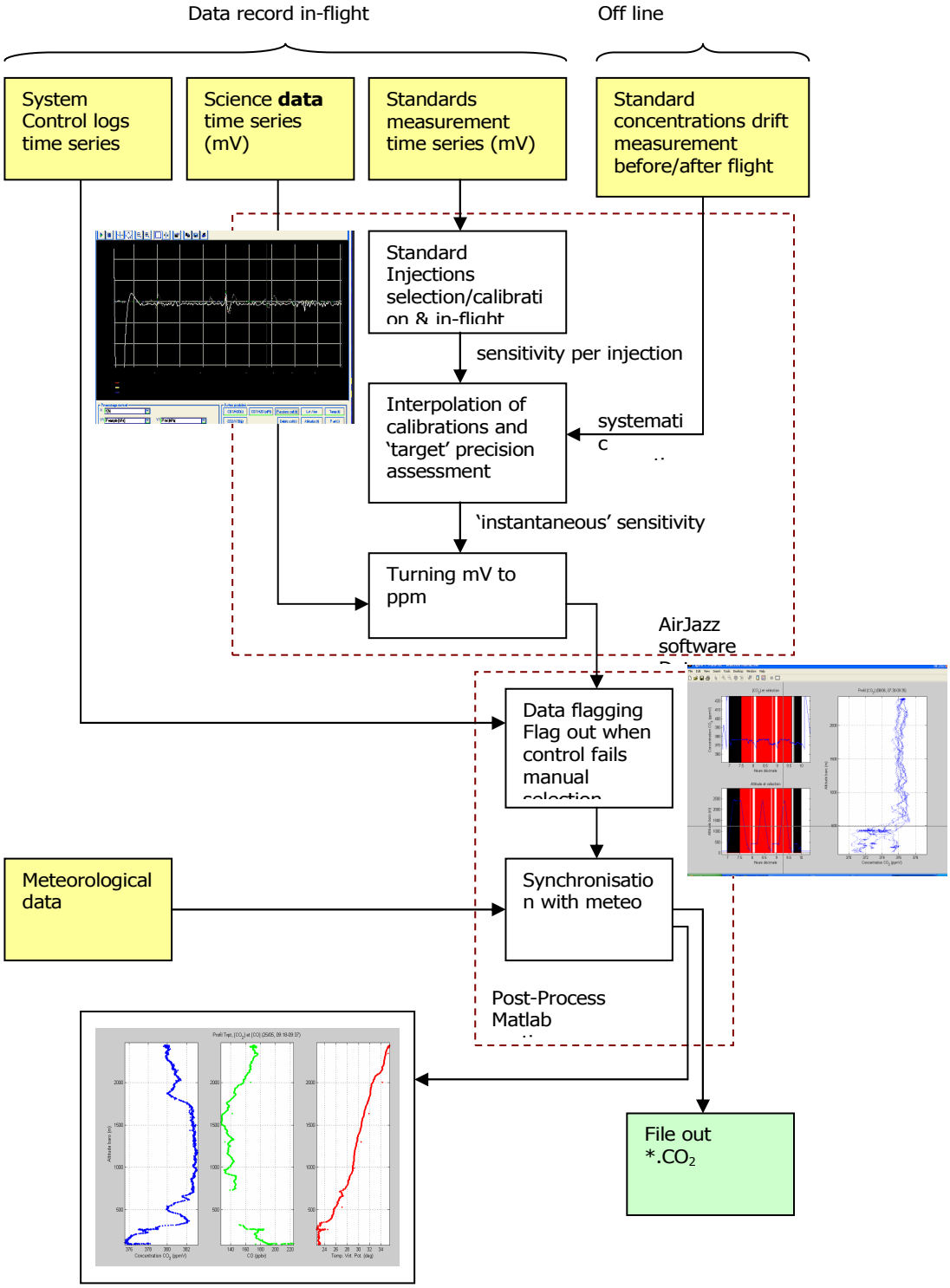

Figure 5. *Flowchart* du traitement de données

1.3. Instruments CO et O_3

Les instruments CO et O_3 sont des instruments entièrement automatisés similaires aux instruments utilisés par le programme MOZAIC (Measurement of OZone and water vapour by AIrbus in-service airCraft ; Marenco et al., 1998 ; Nédélec et al., 2003). Ils sont développés et opérés par le Laboratoire d'Aérologie partenaire du projet YAK-AEROSIB.

L'instrument dédié au CO (Fig. 6) est basé sur un modèle commercial (Model 48C, TEI Thermo Environment Instruments, USA) utilisant la technique de corrélation à filtre de gaz dans l'infrarouge. Le modèle 48CTL est reconnu par l'Agence de protection de l'environnement américaine (méthode référence EQSA-0486-060). Le Laboratoire d'Aérologie a amélioré la précision de l'instrument grâce aux modifications suivantes :

- ajout de calibrages en vol périodiques (toutes les 20 minutes) ;
- intégration de nouveaux détecteurs infrarouge, avec un refroidissement présentant de meilleures caractéristiques ;
- amélioration de la régulation thermique ;
- augmentation de la pression de fonctionnement et une régulation dans la cellule ;
- augmentation du débit ;
- ajout d'un piège à humidité et un filtre à ozone.

La précision réalisée sur une intégration de 30 secondes (déterminée comme correspondant au temps de réponse de l'instrument) est de 5 ppb ou 5% CO pour des concentrations particulièrement élevées, avec un seuil de détection de 10 ppb.

L'analyseur O_3 est également développé à partir d'un modèle commercial de Thermo Instruments (Model 49), un analyseur d'ozone à réponse rapide. Les modifications incluent un calibrage interne et une avionisation poussée. L'instrument est basé sur l'absorption UV, avec deux cellules séparées pour l'échantillon et un zéro. La précision atteinte est de 2 ppb ou 2% sur un temps d'intégration de 4 secondes. La pression et la température sont régulées. Les modifications apportées incluent une transformation électrique stabilisée de 27VDC (courant également fourni à l'instrument CO). Dans le cadre du projet YAK-AEROSIB, l'instrument ozone inclut un ordinateur dédié à l'acquisition de données et au contrôle de l'instrument. L'analyser d'ozone a été calibre en laboratoire selon une source de Thermo Instruments Model49PS, référencée NIST (*National Institute of Standards and Technology* américain). Un générateur d'O_3 couple à un module de calibrage est utilisé en laboratoire avant et après chaque campagne.

1.3.1. Caractéristiques générale des instruments

Un aperçu des caractéristiques instruments est synthétisé dans la table 3 ci-dessous.

Table 3. Caractéristiques des instruments utilisés.

Espèce mesurée	Technique	Frequence d'acquisition	Précision	Reference
CO_2	NDIR	2 s	0.15 ppm	Paris et al., 2008
CO	correlation filtre à gaz IR	1 s[a]	5 ppb/5%	Nedelec et al., 2003
O_3	absorption UV	4 s	2ppb/2%	Paris et al., 2008
Aerosols (conc)	Batterie de diffusion atmosphérique	1 min	~10%	p. ex. Reischl et al., 1991
Humidité relative	Sonde commerciale	1 s	7%	Zuev et al., 1992
Temperature	Honeywell	1 s	0.5°C	Zuev et al., 1992

[a]: une moyenne glissante sur 30 s est réalisée en amont.

Figure 6. Instruments CO_2 (gauche) et CO (droite)

1.4. Vol test en janvier 2006

Un vol test a eu lieu le 22 janvier 2006, durant lequel l'intégration des instruments ainsi que leur précision en vol a été testé. Ce vol test a consisté en un transit et un profil vertical à proximité de Novossibirsk pour un temps de vol total de 2h30. Durant ce vol test nous avons pu améliorer l'acquisition GPS et mettre en évidence une précision de l'instrument CO_2 dégradée par rapport aux spécifications initiales (Fig. 7) mais il n'a pas été possible de résoudre ce problème avant la première campagne.

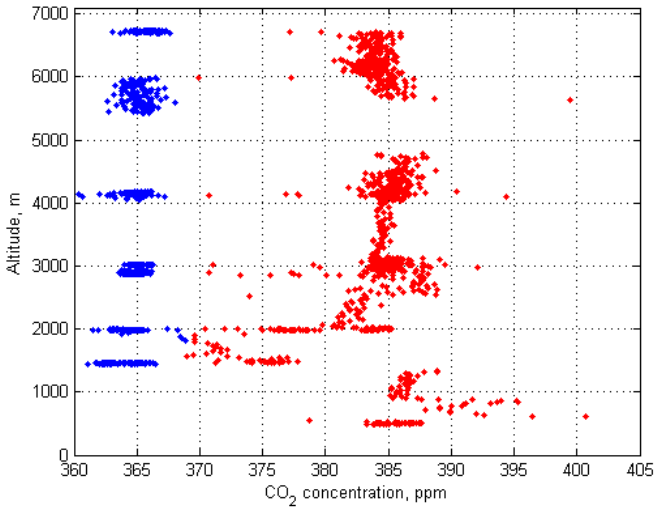

Figure 7. Profil de CO_2 le 22 janvier 2006. Passages de zéros en bleu, air ambiant en rouge.

Annexe 2
Données expérimentales

Cette section contient les données mesurées durant les trois premières campagnes. Le dioxyde de carbone est présenté en noir, le CO en rouge et l'ozone en bleu. L'altitude est indiquée en gris. La longitude est indiquée à intervalle de temps réguliers. Chaque figure est découpé en quatre panels où chaque correspond à un vol (voir chapitre 2).

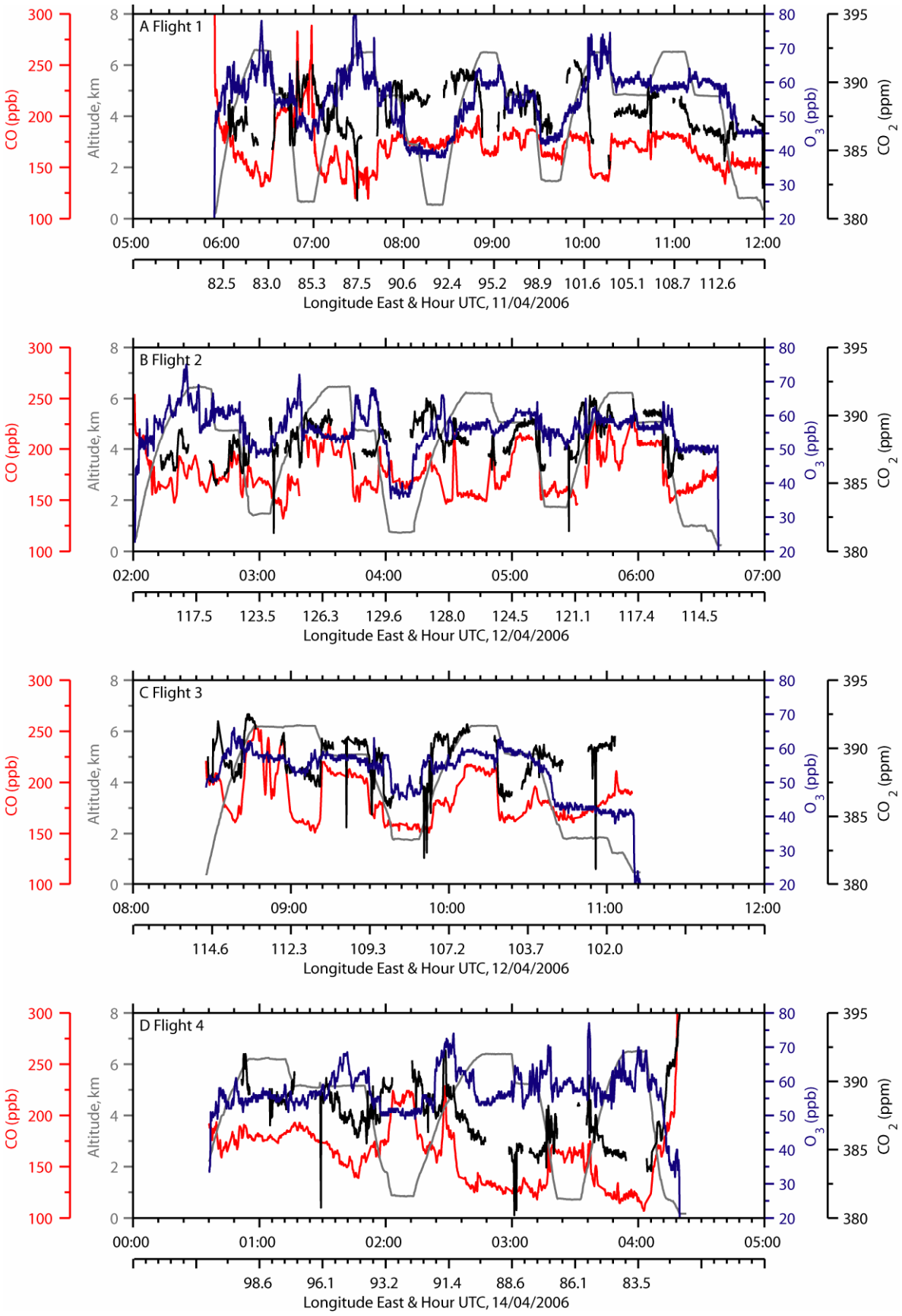

Figure 1. Mesures obtenues durant la campagne YAK-1

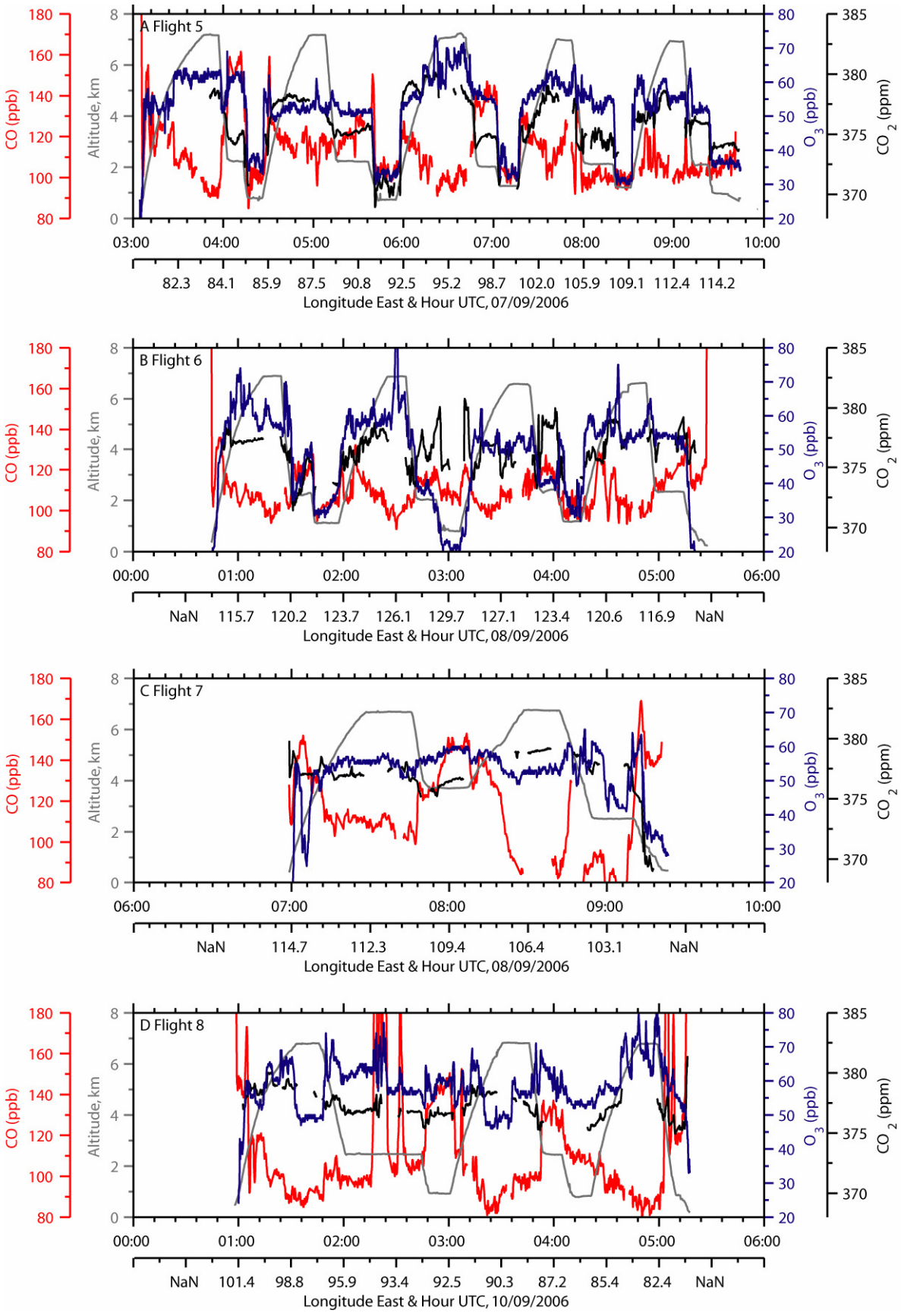

Figure 2. Mesures obtenues durant la campagne YAK-2

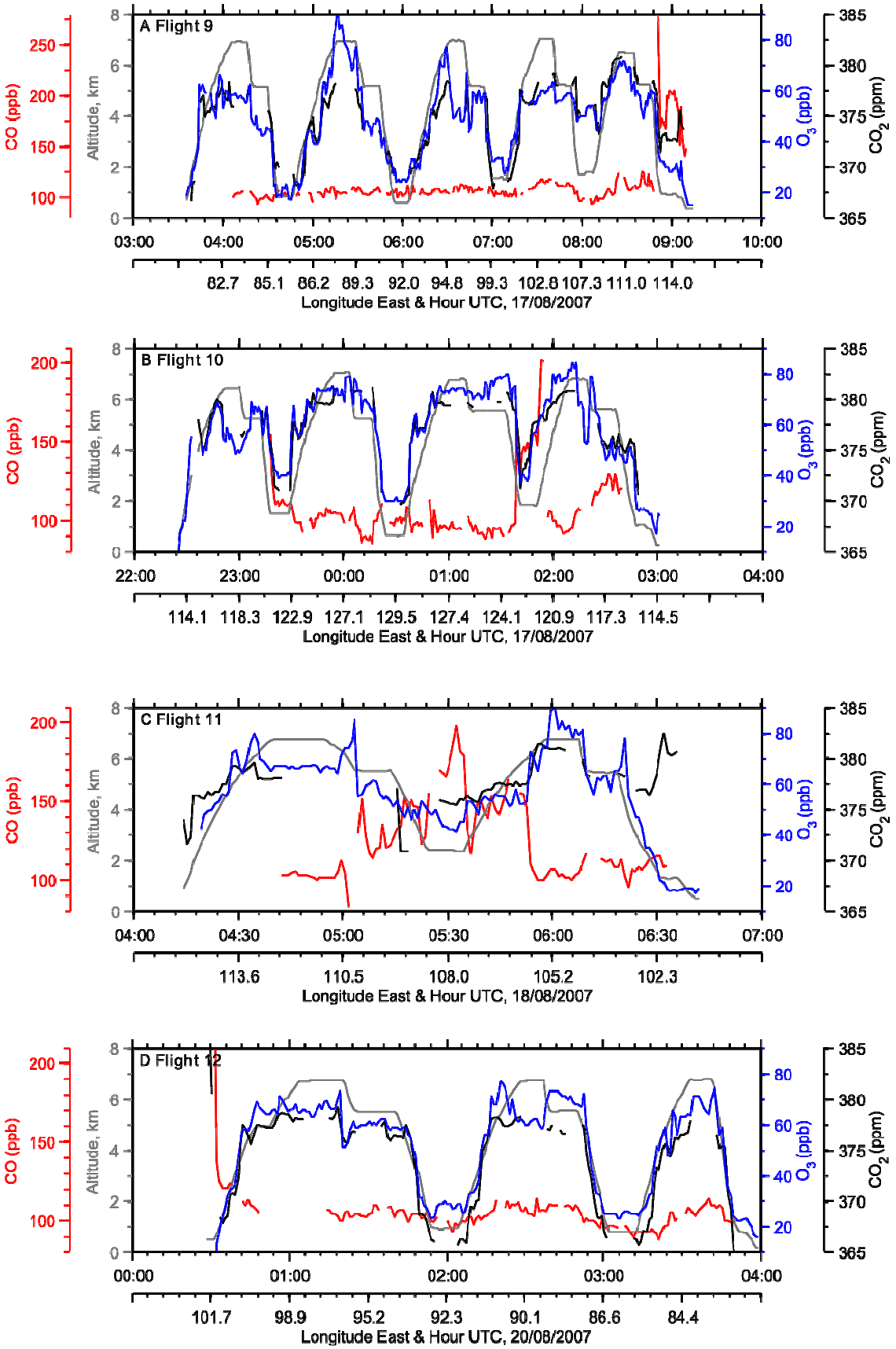

Figure 3. Mesures obtenues durant la campagne YAK-3

Annexe 3 : Article

The European carbon balance revisited. Part 4: fossil fuel emissions

P. Ciais[1*], J.D. Paris[1], G. Marland[2], P. Peylin[1], S. Piao[1], I. Levin[3], T. Pregger[4], Y. Scholz[4], R. Friedrich[4], S. Houwelling[5], D. Schulze[6], and members of the CARBOEUROPE Synthesis Team

[*] 1 Laboratoire des Sciences du Climat et de l'Environnement, Gif sur Yvette, France, 2 Carbon Dioxide Information Analysis Center, Oak Ridge National Laboratory, USA and International Institute for Applied Systems Analysis, Laxenburg, Austria, 3 Institut fuer Umweltphysik, Universitaet Heidelberg, Heidelberg, Germany, 4 Institute of Energy Economics and the Rational Use of Energy (IER), Stuttgart, Germany, 5 National Institute for Space Research, Utrecht, Netherlands, 6 Max Planck Institute for Biogeochemistry, Jena, Germany.

Abstract

We analyzed the magnitude, the trends and the uncertainties of fossil-fuel CO_2 emissions in EU-25, based on emission inventories from energy-use statistics. The stability of emissions during the past decade at EU-25 scale, masks decreasing trends in some regions, offset by increasing trends elsewhere. In the recent 4 years, the new Eastern EU-25 member states have experienced an increase in emissions, reversing after a decade-long decreasing trend. Mediterranean and Nordic countries have also experienced a strong acceleration in emissions. In Germany, France and UK, the stability of emissions is due to the decrease in the industry sector, offset by an increase in the transportation sector. When 5 different inventories models are compared, we have shown than the between-models uncertainty is as large as 19% of the mean for EU-25, and even bigger for individual countries. Accurate accounting for fossil CO_2 emissions depends on a clear understanding of system boundaries. We found that the largest source of errors between inventories is the use of distinct systems boundaries (e.g. counting or not bunker fuels, cement manufacturing, non-energy products). Once these inconsistencies are corrected, the between-models uncertainty can be reduced down to 7% at EU-25 scale. The uncertainty of emissions at smaller spatial scales than the country scale was analyzed by comparing two emission maps based upon economic and demographic activities. A number of spatial and temporal biases have been found among the two maps, indicating a significant increase in uncertainties when increasing the resolution at scales finer than ≈200 km. At 100 km resolution, for example, the uncertainty of regional emissions is estimated to be 60 g C m-2 y-1, up to 50% of the mean. The uncertainty on regional fossil-fuel CO_2 fluxes to the atmosphere could be reduced by making accurate 14C measurements in atmospheric CO_2, and by combining them with transport models. But transport models will have to be improved in parallel.

1.1. Introduction

Fossil-fuel CO2 emissions are derived from energy use and trade statistics using inventory models. Inventory models consider different sub-sectors of the economy such as the industry, the energy production and the transportation sectors, and their reliance on different fuel types, emission processes and emission factors. Compared to the variety of ecosystem models and their parameterizations (Tiktakk and van Grinsven, 1995), there are many fewer types of emission inventory models. Inventory models use as energy statistics as input, but they can differ by their degree of sophistication in the treatmemt of each sub-sector. Each European country report their sectorial emissions to the United Nations Framework Climate Change Convention (UNFCCC) secretariat in Bonn (UNFCCC, 1992, 2004) following the IPCC guidelines (IPCC, 2000, 2006), but the emission calculation methodologies and information content differ among countries. Then, there are global emission inventory analysis like CDIAC (Marland and Rotty, 1984 ; Marland et al. 2006 ; http://cdiac.esd.ornl.gov/trends/emis/tre_coun.htm), IEA (IEA 2007 ;

www.eia.doe.gov/oiaf/ieo/index.html) or EDGAR (Olivier et al. 2005). These global datasets use a methodology that may be less detailled than in the national reports, but they have the advantage of producing regularly updated annual emission estimates that can be consistently compared among countries. From these global datasets, recent trends in global and regional emissions (Raupach et al. 2007) can be assessed and assigned to economic driving forces. Finally, maps of the time varying emission can be obtained by disaggregation of country scale totals using geographically explicit demographic and enonomic activity data and information on the temporal variations in fossil fuel use (Andres et al. 1996 ; Brenkert et al. 1998 ; Streets et al. 2003 ; Ohara et al. 2007 ; Pregger et al. 2007).

A synthesis of fossil-fuel emissions in the EU-25, including their uncertainties and their spatial / temporal distribution, is complicated by the fact that these countries have a different reliance on fossil fuel vs. hydroelectric or nuclear sources to produce electricity, different car fleets and driving habits, as well as contrasted residential and industrial use of fossil fuels. The mix of fossil-fuel types for energy production is also very different among countries, ranging from gas-dominated (e.g. Netherlands) to coal-based (e.g. Poland), which has implication for average emission factors. Moreoer, for creating European emission maps, the data available for disagregation do not have the same level of details and accuracy in each region, which causes bias , e.g. when default values for one country are used to distribute emissions in another (Pregger et al. 2007).

At the EU-25 scale, fossil fuel emissions are the largest net source component of the European carbon balance, amounting to 1.01 Pg C y-1 during 2000-2004. This represents about ten times the absolute value of the European ecosystem carbon sink. When considered on a monthy basis, fossil-fuel CO2 emissions become however of similar magnitude as the seasonal Net Ecosystem Exchange (NEE). At the regional scale in densely populated and industrial regions, the fossil-fuel emissions dominate again over the NEE by several orders of magnitude, while the converse is true is rural areas. Given this interplay of emissions and natural sinks, it is particularly necessary over Europe to gain better understanding of regional details in fossil fuel emissions, for instance for applying the atmospheric approach to quantifying fluxes based on CO2 concentration measurements. When concentration measurements are inverted in an atmospheric transport model, even a small error in the magnitude and space-time distribution of the prescribed fossil emissions can impact the sought biospheric fluxes (Gurney et al. 2005; Peylin et al. 2008). It is also necessary in a synthesis of the EU-25 carbon balance to quantify the current uncertainties on fossil-fuel emission, and to consider these uncertainties in the context of space and time scales, so that they can eventually be compared with those of ecosystem fluxes.

There are now several datasets that provide estimates of these regional and national, anthropogenic emissions (see Methods section) so this paper looks briefly at the alternatives and their apparent differences. We look at the system boundaries for describing regional and national

emissions, the growth and distribution of emissions within the region, and the uncertainty in the emissions estimates. The goal is to gain understanding of the following questions :

- Although the total EU-25 emissions have remained globally stable over the past decade, are there significantly different regional and national trends ?
- Are there significant differences among the different fossil fuel emission datasets, and what is the systematic and random character of their uncertainties?
- How do these emission uncertainties increase from country-scale down to regional-scale in the disagregation process to create emission maps?

These questions are adressed in sequential order in the following sections 2-4. Section 5 looks at the possibiliblity to provide an independent verification of fossil fuel CO2 emissions using atmospheric concentration measurements and models.

1.2. Material and methods

1.2.1. Study area

In this assessment of the fossil CO_2 emissions in EU-24 (total area 4.4 10^6 km^2), our general definition of fossil fuel CO_2 emissions includes:

- All combustions (electricity generation, transportation sector, residential sector, and industry)
- Cement factory
- Other process emissions than cement, associated to chemical reactions emitting CO_2 from fossil carbon (Ammonia synthesis, Aluminum electrolysis, petrochemical)
- Non-energy use products manufactured from fossil fuel carbon
- Bunker fuels (i.e. fuels emitted for maritime or aircraft international transportation involving EU-25 countries)

Natural fossil CO_2 geological sources are not accounted for. Further, Europe was defined as the 25 member states of the European Union i.e. Austria, Belgium, Cyprus, Czech Republic, Denmark, Estonia, Finland, France, Germany, Greece, Hungary, Ireland, Italy, Latvia, Lithuania, Luxembourg, Malta, Netherlands, Poland, Portugal, Slovakia, Slovenia, Spain, Sweden and United Kingdom. The different fossil fuel CO_2 emission inventories that were used (§ 2.2) do not always include each of the five emission category above. This is summarized in Table 1.

1.2.2. Data sources

1.2.2.1 Country level fossil-fuel CO_2 emissions inventories

We used the fossil fuel and cement factory country emissions of the Carbon Dioxide Information and Analysis Center (CDIAC) (Marland et al. 2007; accessed from http://cdiac.esd.ornl.gov/trends/emis/tre_coun.htm) to analyze emission trends in each EU-25 country during the period 1992-2004. The CDIAC dataset allows trend analysis because it contains data are more up to date than UNFCCC national reports, uses the same system boundaries (definition) in each country, and applies the same methodology during the period of interest. We stopped our analysis in 2004, because no comprehensive data were available after that year in all EU-25 countries.

Fossil-fuel emissions data were grouped into six countries / groups of countries, with similar trends: 1) *Northern Europe* countries (Belgium, Luxembourg, Netherlands, Finland, Sweden, Denmark, and Austria), 2) *Mediterranean countries and Ireland* (Italy, Greece, Spain, and Portugal, Ireland), 3) the *new Eastern European EU-25 member states* since 2004 (Czech Republic, Estonia, Hungary, Lithuania, Latvia, Poland, Slovakia, Slovenia, Cyprus and Malta), 4) *Germany*, 5) *France*, and 6) *United-Kingdom*.

1.2.2.2 Emission country-level uncertainties

Uncertainties were estimated from the standard deviation of fossil-fuel CO_2 emissions among 4 inventories models, for 1990 and 2000. These inventory models are: 1) the CDIAC global dataset (Marland et al. 2007), 2) the GAINS model from IIASA (Höglund-Isaksen and Mechler, 2005 ; Klaasen et al. 2005; data from Lukewille et al. 2006), 3) the UNFCCC national communications (UNFCCC, 2007), and 4) the EDGARv3.2 FT2000 global dataset (Olivier et al., 2005, Van Aardenne et al., 2005). Different emission types accounted for by each model are summarized in Table 1.

Table 1. Summary of fossil-fuel CO_2 emissions inventories used in this study.

	Combustion of fuel in industry, electr gen., transportation, residential	Cement factory	Non ernergy use products (plastic, solvents)	Year	Reference
CDIAC	X			Each year 1990-2003	*Marland et al. 2007*
EDGAR v3.2	X	X	X	2000	*Olivier et al., 2005, Van Aardenne et al., 2005*
UNFCCC	X				*UNFCCC, 2007*
GAINS	X				*Höglund-Isaksen and Mechler, 2005; Klaasen et al. 2005*

1.2.2.3 Spatial and temporal distribution of emissions

Two independent methodologies were used to disaggregate the country-level fossil CO_2 emissions for year 2000, respectively by the Institute of Energy Economics and the Rational Use of Energy (IER) and by the CARBOEUROPE-IP Integration Component (CE). The difference between these two products provides hints on the uncertainty in disaggregated emission fields (discussed in section 4.1). The IER emission map (Pregger et al. 2007) is generated from country emission totals from the UNFCCC (United Nations Framework Convention on Climatic Change, 2004). These are disaggregated into finer scales using maps of activities such as road traffic (treated as line or area sources), large point sources, residential energy consumption, and temporal profiles of emissions for a number of sub-activities. In total, more than 300 different temporal profiles were used by Pregger et al. 2007 for allocating the temporal variability of emissions in each sub-sector. Some of these temporal profiles depend on temperature data, such as the seasonal fuel use by power plants. Other profiles relate to user behaviour such as traffic counts, holidays, and working times. The spatial resolution of the IER fossil fuel emission map is 0.5° x 0.5° and the temporal resolution is hourly. It is worth noting that the large IER database of activity maps, emission factors and temporal profiles is much more detailed for Germany than for other countries, where default values have been assumed in cases where specific information was not available. This more detailed treatment of finer scales over Germany creates a spatial bias compared with other countries.

The CE emission map is a simpler attempt to distribute temporally the EDGAR v3.2 emission map originally established at 1° x 1° spatial distribution (Van Ardenne et al., 2005). EDGAR v3.2 used population density and information on the location of some large point sources to distribute emissions spatially within countries. The temporal variability of emission of compounds related to CO_2, such as SO2 and CO, was used on hourly, daily and monthly scales provided by the EMEP database (Vestreng et al. 2005) to distribute emissions temporally. More details are provided in Peylin et al. (2008).

1.3. Emissions and trends in EU-25

Our analyses start with inventory data of CDIAC (§2.1) The EU-25 contributed 14% of global fossil CO_2 emissions during the 1992-2004 period (including emissions from the calcining of limestone to manufacture cement), that is an average source of 1.01 PgC yr-1 to the atmosphere (Marland et al. 2006. The EU-25 emissions stagnated during 1992-1999, (+0.03% yr-1 growth) at an average value of 0.99 PgC y-1, but they later increased during 2000-2004 (1.1% yr-1 growth). Yet, this recent acceleration in fossil CO2 emissions over the EU-25 is about three times lower than the acceleration of global emissions (Raupach et al. 2007).

This average trend in EU-25 emissions is composed of regionally different trends. In Figure 1, the fossil-fuel emissions are shown for six countries or groups of countries (see details in §2). Figure 2 shows the contribution of individual countries or groups of countries to the EU-25 total annual emission in the years 2000-2003 and to the emission trends over 2000-2003. In the group of *Northern Europe*, the emissions remained stable during the 1990s, but they fastly increased thereafter; by 3.8% y-1. In the group of *Mediterranean countries and Ireland*, there was a fast economic growth in the past decade. The GDP annual growth was 7.8% y-1, 3.8% y-1 and 3.8% y-1 in Ireland, Greece, and Spain, respectively (http://epp.eurostat.ec.europa.eu, accessed 13 June 2007). The emissions of this group increased almost linearly at a rate of 2.2 % y-1. This resulted in an overall multiplication by a factor of 1.2 since 1992. In the group *new Eastern, EU-25 member states*, emissions changes reflect the transition to market economies at the end of the 1990's (except for Cyprus and Malta). Emissions from that group decreased by 1.3% y-1 during 1992-1999, but this trend was reversed and emissions are now slightly increasing (0.4% yr-1 growth over 2000-2003). Although Ukraine and Belarus are not part of the EU-25, it is interesting to remark that their collective emissions declined at an even more pronounced rate (by 9.8% y-1) than in the new EU-25 Eastern European countries between 1992 and 1999, but that this trend was also reversed after 2000.

In Germany, the biggest European fossil fuel CO_2 emitter (Figure 3), emissions declined at a rate of 0.9 % y^{-1} after the reunification of the Federal Republic of Germany with the former Democratic Republic of Germany, and did not further decrease after 2000. In the UK, the fossil emissions show no significant trend (0.04 % y-1 growth over the period 1992-2003), with an increase in the transportation sector offsetting a decreasing trend in emissions associated with energy production. In France, the fossil emissions are on average lower than in the UK and Germany, because of the dominant share of nuclear power in electricity production (≈80%). But, French emissions increased by 1.5% yr-1 after 2000, with an increase in the transportation sector (+22% growth between 1990 and 2004) nearly offset by a decrease in the industry (-21.6% over the same period).

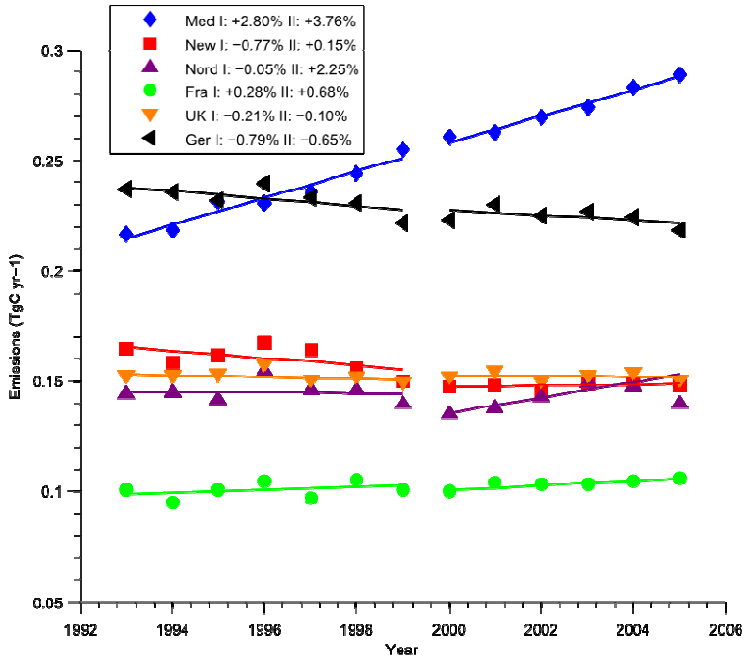

Figure 1. Trends in fossil-fuel CO_2 emissions for different groups / countries of EU-25 between 1990 and 2003. The group *Mediterranean countries and Ireland* includes Italy, Greece, Spain, and Portugal plus Ireland, which experienced fast economic growth in the past decade. The group *New EU-25 members* include Czech Republic, Estonia, Hungary, Lithuania, Latvia, Poland, Slovakia, Slovenia, Cyprus and Malta which (except Cyprus and Malta) underwent a transition from centrally planned to market economy after 1990, followed by fast economic growth after 2000. The group *Northern Europe* includes Belgium, Luxembourg, Netherlands, Finland, Sweden, Denmark, Austria.

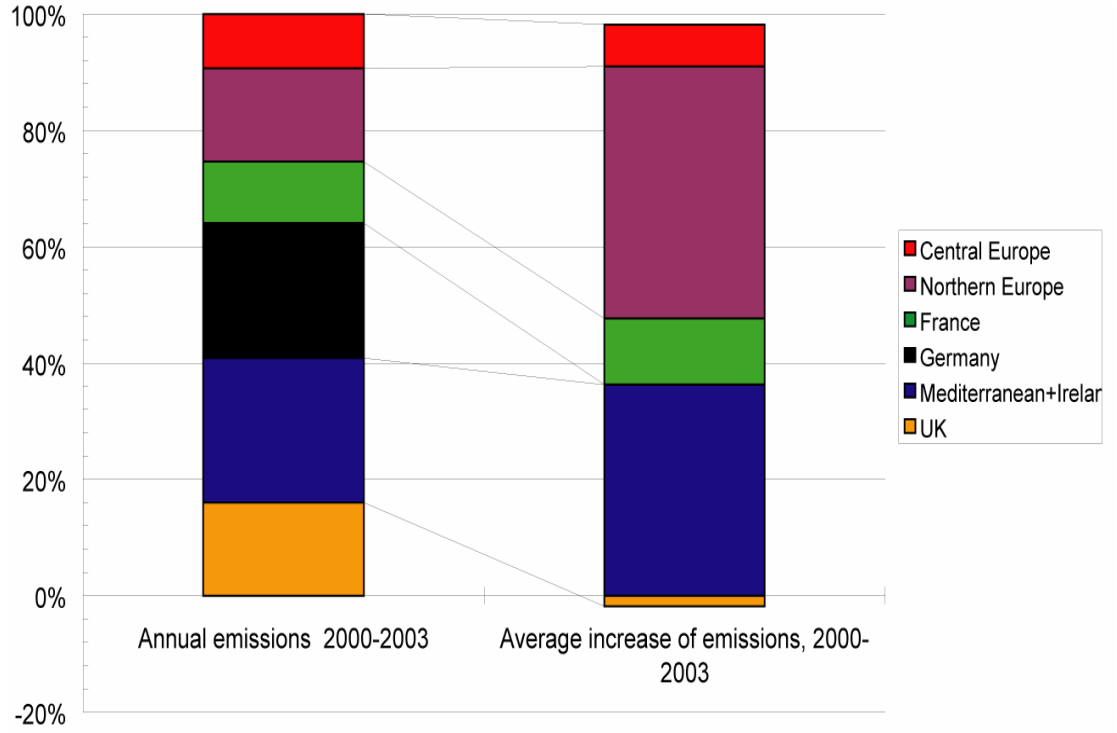

Figure 2. Relative contributions of different groups / countries to the total EU-25 fossil-fuel CO_2 emissions (left column) and to the growth rate of these emissions during 2000-2003. The negative growth rate for UK indicates that emissions have actually decreased over that period.

In Germany, the biggest European fossil fuel CO_2 emitter (Figure 3), emissions declined at a rate of 0.9 % y^{-1} after the reunification of the Federal Republic of Germany with the former Democratic Republic of Germany, and did not further decrease after 2000. In the UK, the fossil emissions show no significant trend (0.04 % y-1 growth over the period 1992-2003), with an increase in the transportation sector offsetting a decreasing trend in emissions associated with energy production. In France, the fossil emissions are on average lower than in the UK and Germany, because of the dominant share of nuclear power in electricity production (≈80%). But, French emissions increased by 1.5% yr-1 after 2000, with an increase in the transportation sector (+22% growth between 1990 and 2004) nearly offset by a decrease in the industry (-21.6% over the same period).

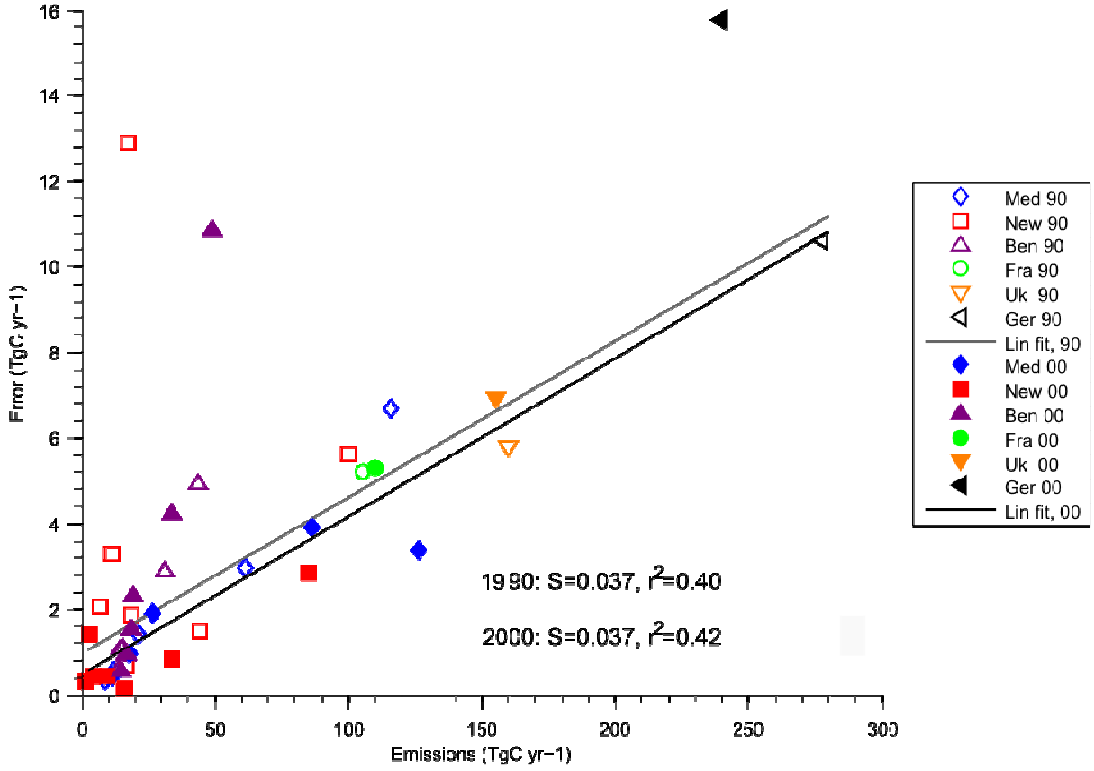

Figure 3. Uncertainty of CO_2 emissions indicated by the deviation between 4 different inventory models, as a function of mean emissions (average of the 4 different inventories). The groups / countries are colour coded with the same code as in Fig 1 and Fig 2.

1.4. Uncertainties in emissions

1.4.1. Uncertainties between different inventory datasets

Uncertainties in fossil fuel and cement emissions are particularly important to estimate in a synthesis of the European carbon balance. To gain understanding of this issue, we used 4 different inventories of national fossil-fuel related emissions (CDIAC, GAINS, UNFCCC, EDGARv3.2 ; see §2) as an initial indication of the 'between-model' emission uncertainty for the EU-25, and for different groups of countries. For our first comparison we simply accepted what the different data sets report as the national emissions total. The differences are seen to be rather large (Table 2), and while some of the differences are easily understood, others are more subtle and more difficult to resolve.

The emission uncertainties defined in that manner depend on differences in: 1) the underlying statistical datasets (e.g. different sources of energy data), 2) on the manipulation of input data, 3) on the assumed chemical composition of fuels; there is for example is a range of 20% in the carbon content between brown coal and anthracite when measured on a mass basis (Riediger, B., 1955), and 4) the system boundaries, e.g. the treatment of industrial processes such as cement

manufacture, fuels used in international commerce, flaring of natural gas at gas and oil fields, and fuels used for non-fuel products (asphalts, solvents, plastics, lubricants, solvents, and other products ; see Marland and Marland 2006).

Table 2. Emissions for a selection of EU-25 countries according to a suite of inventories. Values are given in TgC yr-1 Malta, Cyprus, Luxembourg and Slovenia are not represented.

	1990				2000			
	GAINS	UNFCCC	EDGAR	CDIAC	GAINS	UNFCCC	EDGAR ft	CDIAC
Germany	270.30	281.20	290.74	267.62	234.06	240.60	264.03	217.59
United Kingdom	155.31	160.76	167.57	155.38	156.40	149.86	163.76	151.81
Italy	117.98	118.53	121.53	106.34	126.16	126.43	132.15	116.82
France	104.09	107.63	111.17	98.92	112.26	110.90	120.71	96.66
Poland	98.64	108.17	100.00	94.87	85.29	90.74	86.65	82.13
Spain	60.49	62.13	64.85	57.81	86.38	83.92	91.55	76.96
Netherlands	43.32	43.32	50.14	38.13	48.77	46.32	66.21	37.96
Czech Republic	43.32	46.05	43.60		33.51	35.15	34.33	32.42
Belgium	29.97	32.43	34.06	27.46	33.79	33.79	41.14	27.91
Greece	20.71	22.89	22.07	19.71	26.43	28.34	30.25	24.64
Hungary	18.53	19.89	20.71	16.41	16.08	16.08	16.35	14.78
Lithuania	9.81	9.81	32.15		3.27	3.27	5.72	3.26
Austria	15.80	16.89	17.71	15.75	16.89	17.98	18.80	16.55
Finland	15.80	15.53	16.62	13.98	18.53	15.53	16.62	14.12
Slovak Republic	17.17	16.35	15.80		9.81	10.63	10.35	9.66
Sweden	14.44	15.26	16.08	13.50	19.07	14.44	16.89	12.68
Denmark	14.44	14.71	14.99	13.58	14.99	14.71	15.80	12.63
Portugal	11.99	11.72	12.81	11.55	18.26	17.17	19.07	16.29
Estonia	8.99	10.35	15.26		4.09	4.36	4.90	4.37
Ireland	8.45	8.99	8.99	8.36	11.72	12.26	11.44	11.34
Latvia	5.72	5.18	8.99		1.91	1.91	2.45	1.64

For the US, the 'between-model' emissions uncertainty calculated for the deviation among IEA (IEA, 2005), USEPA (USEPA, 2005) and CDIAC (Marland et al. 2006) inventories, as reported in the State Of the Carbon Cycle Report (SOCCR, 2008) is on the order of 2% of the mean in 1990, and of 4% in 2000, after an attempt was made to insure consistency of the system boundaries. This uncertainty is caused by systematic errors, and it must be kept in mind that if the three datasets have a common bias, the range of their result may not bracket the unknown truth.

The fact that inventory models often use common statistical input data of energy consumption and emission factors, or common treatment of some emission sectors (e.g. the IPCC treatment of the decay of durable products IPCC 1997, 2000) makes it further likely that they will have common biases. However, if a given inventory model and its input data do not change over time, the bias associated with this particular model's result will have very little inter-annual or long-term fluctuations, which enables an analysis of emission trends with a higher precision than the uncertainty across different emission models.

In order to illustrate this comparison for emissions from the EU-25, we compared CO_2 emissions among CDIAC, EDGAR, GAINS, and UNFCCC inventories (see §2) for 1990 and 2000. We take initially the total, national, reported emissions of CO_2. i.e. we have not tried to ensure consistency of the system boundaries. Figure 3 shows the uncertainty indicated by the standard deviation of the 4 estimates, as a function of average emissions. For year 2000, the total fossil CO_2 emission for EU-25 are : CDIAC 0.99, EDGAR 1.5, GAINS 1.36 and UNFCCC 1.10 Pg C y-1. The corresponding uncertainty of 19% (std. dev. = 0.23 Pg C y-1) is surprisingly large, compared to the uncertainty for the US calculated above. This reflects mostly a lack of consistency of the system boundaries, which is amplified in the EU-25 case by contrasting sectorial allocation of emissions in the different countries.

If we adjust the system boundaries of the 4 inventories reports so that they *consistently* do not include biofuels, marine bunker fuels, or oxidation of non-fuel hydrocarbons: then the corrected values are CDIAC 1.00, EDGAR 1.06, GAINS 1.09, and UNFCCC 1.10 Pg C y-1 (although the UNFCCC number still has non-fuel hydrocarbons in it), reducing the average uncertainty to 7%.

It is also seen in Figure 3 that emissions from each country / group of countries with a higher mean (e.g. Germany) are estimated with a larger absolute uncertainty by the 4 different inventories models. A linear regression to country data shown in Figure 3 (R2 = 0.5 for 1990; 0.7 for 2000) indicates an average 'between-model' uncertainty of 7% of the mean in 1990, and of 16% of the mean in 2000. The uncertainty apparently increased between 1990 and 2000 for Germany (+69%) and France, despite the fact than emissions decreased in Germany and remained stable in France between these two dates. A factor here is the re-unification of Germany, and the emissions value shown for 1990 is in fact the sum of the values for the former Federal Republic of Germany and German Democratic Republic. In the UK, the emission between-model uncertainty has increased between 1990 and 2000, while in the mean time the total emissions have decreased. In contrast, the between-model uncertainty has apparently been cut by a factor of 5 for the 10 new Eastern European member states between 1990 and 2000. This may reflect an improvement in the collection and processing of energy data. Together with the factor of 5 of reduction in uncertainty, the mean emissions of these new eastern European countries were reduced by 28% between 1990 and 2000. This suggests that the uncertainty reduction did not just reflect the reduction in activity, but also a convergence of emission coefficients and input data. A factor here, and in figures 1 and 3 generally, is the break up of the former Soviet Union, Yugoslavia, and Czechoslovakia; six of the ten countries in this group did not exist as independent states in 1990 and the emissions estimates for 1990 have been reconstructed from national energy data.

1.4.2. Uncertainties reduction through consistent system boundary definition

Figure 3 indicates that the apparent uncertainty in emissions estimates is on the order of up to 16% of the mean, and that this error is roughly proportional to the magnitude of emissions. This is a much larger discrepancy between inventory models for EU-25 than for the US (SOCCR 2008), but it still includes differences in the boundaries of the respective inventories. It is beyond the scope of this synthesis to compare the details of the 4 different inventory models. But a comparison for EU-25 between the two widely used datasets from CDIAC and EDGAR v3.2 for year 2000 was made. National totals reported by EDGAR v3.2 contain CO_2 emissions from the non-fuel use of fossil products, and from international bunker fuels, two quantities that are not reported by CDIAC (CDIAC includes these components in the global emission totals but not in the country estimates). Conversely, CDIAC reports CO_2 emission from cement production that is not included in EDGAR. Before any adjustment for these differences in system boundaries the ratio EDGAR/CDIAC emissions varies from 1.7 in the Netherlands, 1.2 in Germany and France, to 1 in the UK, with a mean ratio of 1.17 and a range of 0.94 to 1.77 for the EU-25 countries. This is illustrated in Figure 4. After subtracting cement emissions from CDIAC and bunker fuels plus non-fuel use emissions from EDGAR, the two dataset become more consistent, and the ratio of EDGAR/CDIAC closer to unity (1.07 for the EU-25 ; range 0.86 to 1.5), and the uncertainty indicated by the difference between both inventories has been reduced by a factor of two on average (Fig. 4). Still, even after adjustment, there are countries important by the magnitude of their emissions, like Netherlands and Belgium, for which the EDGAR emissions estimates remain significantly higher than those of CDIAC, by 30% and 20% respectively.

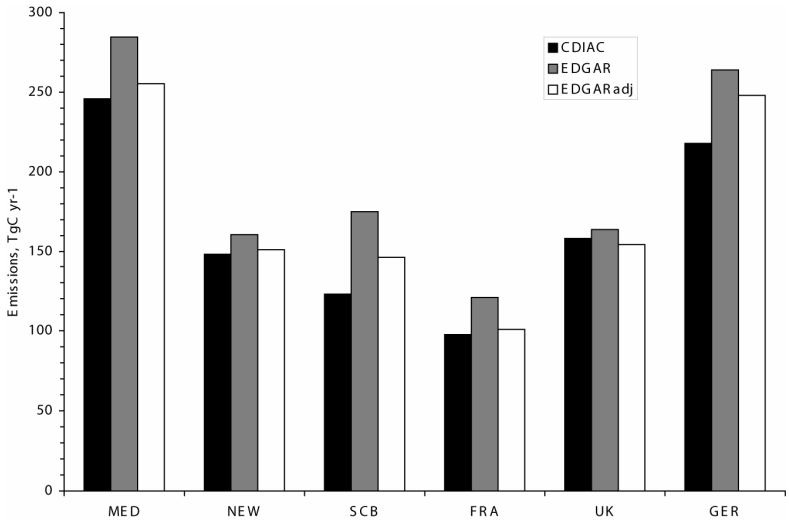

Figure 4. Example of systematic error in emissions for EU-25, indicated by differences between the CDIAC and EDGARv3.2 datasets. These uncertainties can be reduced when estimates of the same thing are compared. EDGAR-ADJ has removed bunker fuels and non-fuel products related emissions, which were not included in the CDIAC system boundary.

Marland et al. (1999) reported a systematic comparison of CO_2 emissions estimates from CDIAC and EDGAR for 1990. For the 19 countries that they identified as 'Western Europe', the mean difference between the two estimates was less than 3% when they established consistent systems boundaries. Rypdal and Winiwarter (2001) similarly concluded that the 2-sigma uncertainty for countries with "well developed energy statistics and inventories" can be as small as 2-4%, similar to the US 'between-models' emission uncertainty quoted above (SOCCR, 2008). Marland (2008) has recently reviewed the uncertainty of national emissions estimates and found that most analysts believe that the uncertainty for Western European countries, given common systems boundaries, is on the order of 5%. This is comparable to our mean difference of 7% for 2000 based on the 4 emissions inventories over the EU-25 countries after correction for inconsistencies (§3.2).

An alternative method to assess emission uncertainties consists of performing a full sensitivity analysis to all the input parameters of one inventory model. This method, which returns random uncertainties on emissions based upon the propagation of a priori uncertainty in each parameter, suggests a random error of 10% in a country with well-developed statistics, like Austria (Winiwarter, 2007). This random error on the total emission of Austria will be higher than 10% in case of positive correlation between parameters errors (e.g. errors in emission coefficients), which is a likely situation. Based on this and on the results above, we can speculate that relying on IPCC methodologies, which make management reports comparable, produces between-model uncertainties smaller than the 'true' random errors in emissions estimates. Hence, we recommend that both 'within model' uncertainties (obtained by varying internal parameters of each inventory model) must be assessed, to complete the information provided by 'between model' uncertainties (obtained from the spread of model results).

This analysis shows that redefining the system boundaries (improved *consistency*) is efficient to reduce between-model errors, and to quantify some elements of bias. However, for understanding of the carbon cycle, as emission data are combined with observations in the natural reservoirs (e.g. atmospheric concentrations), all types of anthropogenic sources need to be included, More narrow system boundaries will pay off for error reduction but at the possible expenses of limitation in accurate understanding of the carbon cycle. Thus, a broad and detailed system boundary is required for full carbon balance estimation, like the one undertaken in CARBOEUROPE-IP.

1.5. Uncertainties in the spatial and temporal distribution of emissions

With the need to obtain more detailed understanding of the carbon cycle, it becomes important to assess the uncertainty in the spatial distribution and temporal variability of emissions. Emissions inventories have traditionally been done at the scale of countries and years because this is the scale at which statistics on fuel consumption are generally maintained. In order to link the emissions with the measured atmospheric CO_2 concentration signals using atmospheric transport

models, the time-varying distribution of fossil emissions must be known ideally at the same spatial and temporal resolution as for the mesoscale transport models, typically 10 km and hourly (see for instance www.purdue.edu/eas/carbon/vulcan). We expect uncertainties on country, annual totals that are of few percent after carefully normalizing the system boundaries (see §3) to *increase* in the disaggregation process providing spatially-explicit emission maps. Our analysis in this section is focused on estimating how much the emission uncertainty increases when seeking emission estimates at finer scales.

1.5.1. Comparison between two emission flux

Figure 5 shows the differences between the IER and the CE emission maps, over two days in the winter, 1 month in the summer, and over a 12-month period for different locations along a North to South transect joining Berlin, Frankfurt, Paris, Milan, and Rome. This transect across five large European cities is plotted over the mean annual EDGARv3.2 emissions in Fig 5A. Both emission maps have been interpolated on the coarser CE 1° by 1° grid. The five cities considered have different traffic habits, residential energy use, and population densities. The upper row of plots in Fig. 5 compares the two emission maps for two consecutive days in January. A spatial bias is seen, with a hot spot of emissions in the IER map, at a distance of ≈600 km from Berlin (near Frankfurt), which is not present in the CE map. This source missing in CE, also clearly seen in the difference curve along the transect (Fig. 5D), likely reflects the finer original IER spatial resolution, the treatment of large point sources, and different projections impacting our 1° x 1° interpolation. The IER map likely contains a large point source in the grid point of discrepancy.

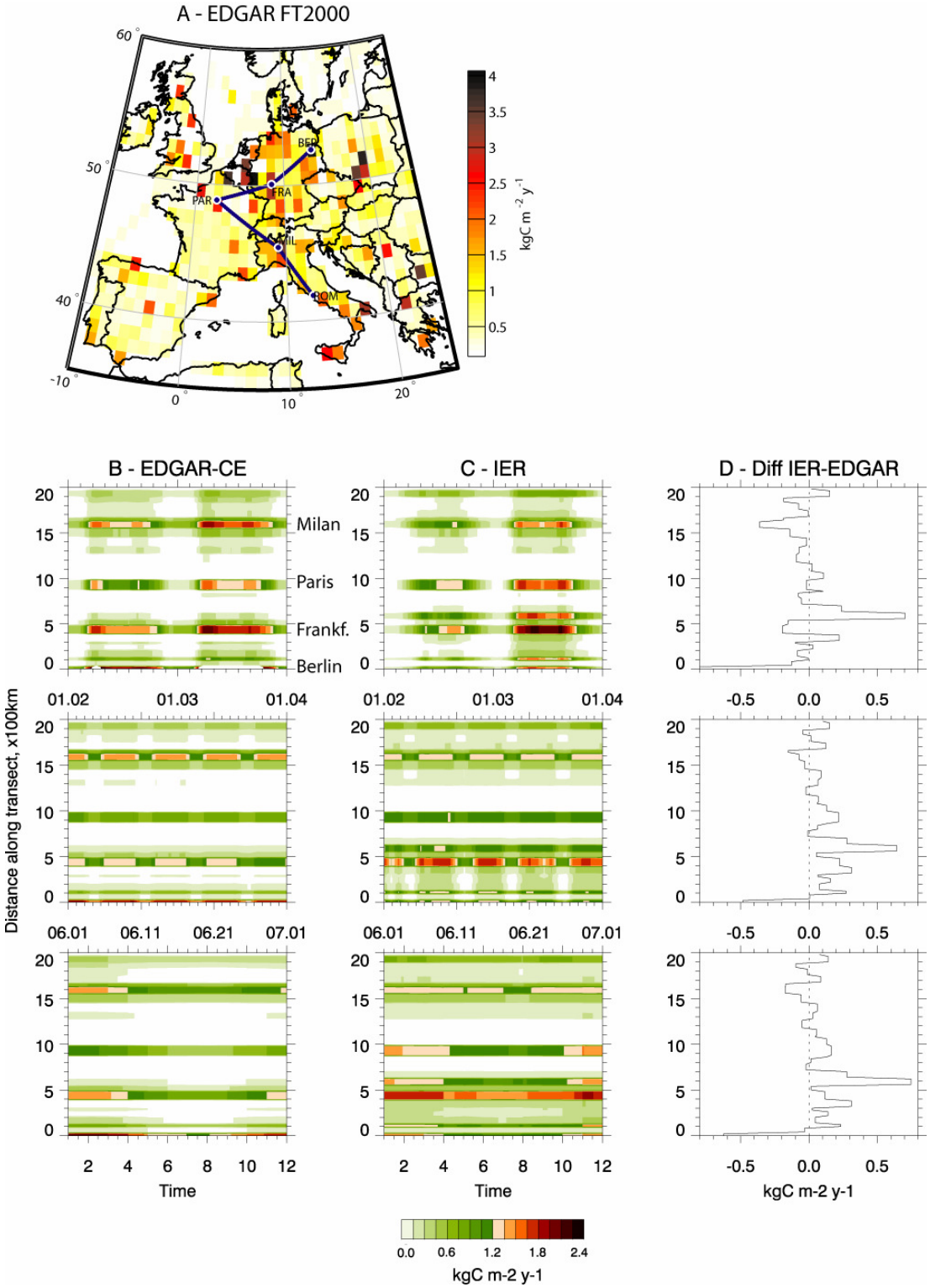

Figure 5. Spatial and temporal distribution of relative error between EDGAR and IER

Some temporal differences between IER and CE are also apparent in Fig 5. Both emission maps capture a larger emission peak during Jan 3 (a colder day) as compared to Jan 2. Rush hour traffic emission peaks in the morning and afternoon are more pronounced in CE, and the daytime

interval with higher emissions is longer in CE. This reflects the fact that more detailed temporal profiles based on car traffic data for Germany were used in IER.

The middle row of plots in Fig 5 compares the two emissions maps during four consecutive weeks in June. The same spatial bias in mean emissions along the Berlin-Rome transect are seen again, but the distribution of the spatial bias vs. distance to Berlin is different from the one seen on a diurnal time scale. This can be seen in the IER minus CE difference curve over Frankfurt, with a negative difference on a diurnal scale and a positive difference on a weekly scale (Fig. 5D top and middle plots). Finally, the bottom plots in Fig 5 compare the seasonal cycle of the two emissions maps. Both maps give larger emissions in winter than in summer everywhere along the chosen transect. A similar typical seasonal cycle was also inferred over the US by Blasing et al. (2005) from energy-use statistics in the different states. For Frankfurt and Paris, IER has a larger seasonal peak-to-peak amplitude of emissions than does CE (Fig 5, bottom row). The situation is opposite for Milan, where wintertime emissions are higher in CE than in IER. On an annual scale, this regional bias between IER and CE can also be seen in Fig 5D.

The magnitude of the spatial biases between IER and CE does not get reduced when averaging from diurnal to weekly to annual time scales. The regional sign of the biases is also similar across time scales, suggesting that beyond differences in temporal profiles, there must also exist spatial differences in the activity maps intervening in each product. The large difference between IER and CE emissions in Germany along the selected transect likely reflects the fact that IER is based on a more detailed set of demographic and economic activity data and parameters over Germany, which produces strong regional contrasts, while the IER and CE are more similar over other countries where default values are used by IER.

How does the uncertainty of emissions increases with decreasing spatial scales ? To answer this question, we calculated the RMS between the IER and CE maps for decreasing spatial aggregation (Fig. 6). Both maps were created starting with identical country emissions, implying an uncertainty of zero when at the country level. Fig. 6. shows that the uncertainty on emissions is kept small when going from country scale down to lengths scales of ≈ 200 km. For length scales smaller than 200 km, the uncertainty increases rapidly, reaching up 60 g C m-2 y-1 (roughly 25% of the mean annual emission flux density over EU-25).

The curves describing the uncertainty function of length scale also have temporal variations. Fig 6A shows that the uncertainty at small scales is larger in winter (DJF) than in spring and summer (SON), reflecting more wintertime differences in the temporal profiles used in the two maps (e.g. different residential heating or electricity production parameters). Fig 6B, comparing midnight and 0800AM emissions maps on February 1st and July 1st, respectively, further indicates that the uncertainty at small scales is always larger in the early morning (different traffic profile parameters) than in the night. The large uncertainty on regional emissions for scales finer than 200 km is a limit to derive accurate regional C budgets, which calls for specific methods to constrain emissions at these scales, as discussed in the following section.

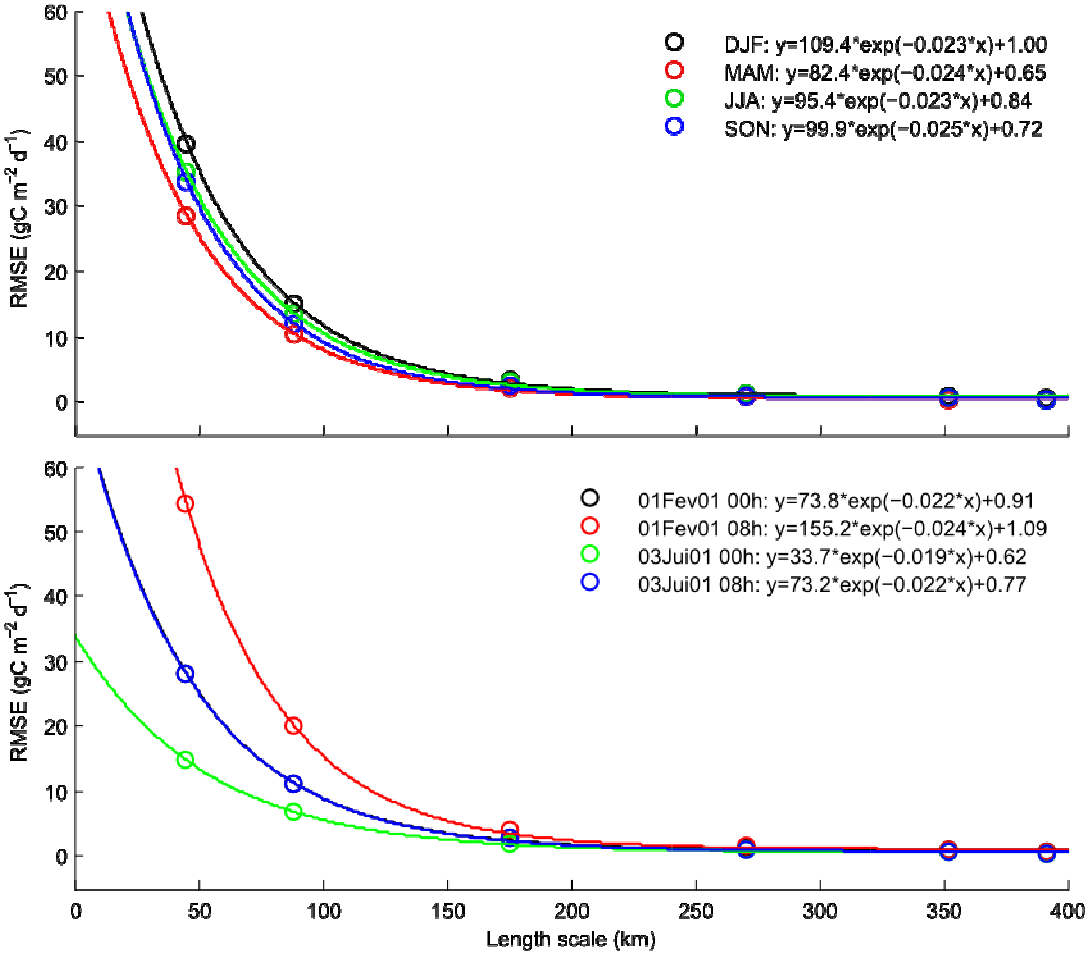

Figure 6. Uncertainty in emission as a function of spatial and temporal scale, obtained by the Root Mean Square Error (RMSE) between the IER and CE emission maps over the EU-25. The data originally gridded at 1° by 1° (≈ 100 km), are aggregated at coarser spatial resolution to calculate the RMSE.

1.6. Observational approach to derive fossil fuel CO_2 mixing ratios and emission constraints

The IER and CE fossil CO_2 flux maps were prescribed to 5 different mesoscale and global atmospheric transport models by Peylin et al. (2008). The differences found in modeled fossil-fuel CO_2 mixing ratio with different transport models with the same emission map are much larger (factor of 2-3) than the differences found with the same transport model but different emissions inventories. With the same model but different emissions inventories, mixing ratios differ by 20-50%, depending on station and season (Peylin et al. 2008). The transport models uncertainties are thus, still too large to place useful constraints of fossil fuel CO_2 mixing ratios, and from there, on fossil fuel emission maps, by inverse modelling. Improvements in model transport but also in the

emissions inventories are essential if we want to make progress in this field. Furthermore, high-resolution maps of emissions inventories are needed not only for the year 2000, for example as shown in Fig. 5, but also for subsequent years as emissions are changing not only due to economic changes in the different countries but also due to meteorological circumstances (e.g. temperature dependence of domestic heating).

"Monitoring" fossil-fuel CO_2 in the atmosphere is, in principle, possible via Radiocarbon ($^{14}CO_2$) observations. From a $^{14}CO_2$ measurement at a polluted sampling site, e.g. in the boundary layer on the continent, we can directly calculate the regional fossil-fuel CO_2 surplus if the undisturbed background $^{14}CO_2$ level is known (Levin et al., 2003). However, determining hourly fossil-fuel CO_2 from hourly $^{14}CO_2$ measurements at very high precision would be an expensive undertaking which so far has only been realised on a campaign basis (event sampling). In the frame of CarboEurope-IP the use of continuous carbon monoxide measurements to possibly serve as a proxy for fossil-fuel CO_2 has been extensively tested using data (Gamnitzer et al., 2006) and models (Rivier et al. 2005). These studies showed that CO is not a tracer which can be applied in a straight-forward way, as it has significant non-fossil fuel sources, is not conserved in the atmosphere (short-lived), and will need ongoing "calibration" with parallel precise $^{14}CO_2$ measurements.

A method has been proposed recently to derive hourly fossil fuel CO_2 mixing ratios from *combined* hourly CO and weekly integrated $^{14}CO_2$ measurements (Levin and Karstens, 2006b). This method has estimated uncertainties (on mixing ratios) between 15 and 40 % at European stations, with the errors increasing with decreasing fossil-fuel CO_2 mixing ratio. For further testing of this proposed method on an hourly time scale, typical diurnal cycles of ^{14}C-based fossil fuel CO_2 and CO measurements are required. An error on the fossil fuel CO_2 contribution of 15 – 40%, based on the Radiocarbon method has to be compared with the inventory uncertainty given in Fig. 6. It can be seen that for spatial scales finer than typically 150 km where bottom up emission maps differ by up to 50%, using carefully calibrated 14C atmospheric measurements would be competitive to reduce fossil CO_2 emission uncertainties.

1.7. Conclusions

We analyzed fossil-fuel CO_2 emissions over the EU-25. Fossil-fuel emissions is the single largest flux of the long-term carbon balance, and it is often considered as 'well know' from energy-use statistics. In contrast, larger research efforts are given to reduce uncertainty on ecosystem exchange. However, we have shown in this paper that uncertainty of fossil fuel emissions inventories is 19% when defined as the between-model std. dev. (5 inventory models). Most of this error is systematic, and when using *consistent* system boundaries (i.e. same sectors are compared), the between-model uncertainty reduces down to 7%. A higher degree of consistency of 2-3% between inventory models can be achieved for the US, where the sources of statistical data is more homogenous than in the 25 countries of EU-25. However, one must keep in mind *that all*

anthropogenic emissions related to fossil C use are eventually needed to quantify the imprint on the atmospheric CO_2 global growth rate and on climate change.

Inventories of CO_2 emissions (at the national and annual scale) can be improved with careful collection and reporting of data on energy use, but there are inherent uncertaities due to variations in fuel chemistry, uncertainty in measurement of the masses or volumes of fuel consumption, and the uncertainty introduced by survey methods that collect data from many but not all fuel users.

Emissions estimates at finer spatial and temporal scales, where primary data on fuel consuption are not routinely collected, will depend on the the quality of models that represent the principal fuel consuming processes. In constructing regional emission maps with geo-referenced information on economic and demographic activity, and on temporal profiles of emissions, additional uncertainties are introduced. We have shown by comparing two emission maps that the emission uncertainty increases for decreasing length scales, reaching up to 60% of the mean EU-25 flux density at scales < 150 km. Definitely, atmospheric radiocarbon measurements could help to constrain bottom-up fossil fuel emission maps.

An improved observational network is suggested for Europe in order to reliably determine high-resolution fossil fuel CO_2 mixing ratios based on observations. This requires continuous CO measurements and precise (≤ 2 ‰) e.g. weekly integrated $^{14}CO_2$ measurements at existing continuous CO_2 measurement sites (i.e. 10 ground level stations and 10 tower sites). In addition, monthly to two-monthly diurnal cycle studies with at least 12 samples per day are required at selected sites to test the proposed $^{14}CO_2$/CO method on the hourly time scale. (The total number of ^{14}C analyses for the European monitoring network would then sum up to weekly samples: 20 stations x 52 weeks = 1040 samples per year, and diurnal cycles: ca. 5 stations x 8/year x 12/day = 480 samples per year) Part of these measurements must be made by AMS technique (i.e. diurnal cycles) part should be made by conventional counting technique which is more precise and cheaper than AMS.

Besides using CO as a proxy for fossil fuel CO_2, other potential tracers such as SF_6, C_2Cl_4, C_2H_2 (Potosnak et al., 1999; Rivier et al., 2006), or other gases of purely anthropogenic origin should be tested for their applicability as respective tracers. This may be done at one or two selected urban sites where new instruments with the respective analytical capability could be set up an run quasi-continuously in parallel to CO_2, CO and $^{14}CO_2$ measurements.

In addition to constrain fossil CO_2 emissions, dedicated CO_2 flux measurements could be started over large cities. This will require high towers because of the heterogeneity of the source area. However, one has to consider that, even over big cities, still a large portion of the CO_2 flux measured will be due to biogenic emissions (advection and direct biogenic sources) so that these measurements will be difficult to evaluate for quantitative fossil fuel CO_2 flux estimates.

1.8. References

Andres, R. J., G. Marland, I. Fung, and E. Matthews (1996), A 1º by 1º distribution of carbon dioxide emissions from fossil fuel consumption and cement manufacture, 1950–1990, Global Biogeochem. Cycles, 10, 419– 429.

Brenkert, A. L. (1998), Carbon dioxide emission estimates from fossil-fuel burning, hydraulic cement production, and gas flaring for 1995 on a one degree grid cell basis. (available at http://cdiac.esd.ornl.gov/ndps/ndp058a.html)

Blasing, T.J., C.T. Broniak, and G. Marland, 2005: The annual cycle of fossil-fuel carbon dioxide emissions in the United States. Tellus B, 57(2), 107–115.

EIA, Energy Information Administration (2007) World Energy Outlook 2007. Office of Integrated Analysis and Forecasting US Department of Energy, Washington, DC 20585.

Gurney, K.R., Y.H. Chen, T. Maki, S.R. Kawa, A. Andrews, and Z. Zhu, 2005: Sensitivity of atmospheric CO_2 inversion to seasonal and interannual variations in fossil-fuel emissions. Journal of Geophysical Research, 110(D10), 10308, doi:10.1029/2004JD005373.

Klaasen, G., Berglund, C., and Wagner, F. (2005): The GAINS Model for Greenhouse Gases – Version 1.0: Carbon Dioxide (CO_2).- IIASA Interim Report IR-05-53, 97 pp. http://www.iiasa.ac.at/rains/gains/index.html

IEA (International Energy Agency), 2005: CO_2 Emissions from Fuel Combustion: 1971–2003. OECD/IEA, Paris, France, 556 pp.

IPCC, 2006: 2006 IPCC Guidelines for National Greenhouse Gas Inventories (5 Volumes). Published by the Institute for Global Environmental Strategies for the IPCC..

IPCC (2000): Good Practice Guidance and Uncertainty Management in National Greenhouse Gas Inventories. IPCC-TSU NGGIP, Japan.

Lükewille A., Wilson S., Pacyna J., Steenhuisen F., Panasiuk D., and Manø S. Inventory of Baseline 1990 and 2003 Emissions Final Report of the EVERGREEN EU funded project (2006)

Marland G, Rotty RM (1984) Carbon dioxide emissions from fossil fuels: a procedure for estimation and results for 1950-1982.Tellus Ser. B 36:232-261

Marland, G., Boden, T. A., and Andres, R. J.: Global, Regional, and National Fossil Fuel CO_2 Emissions. In Trends: A Compendium of Data on Global Change, U.s. department of energy, Carbon Dioxide Information Analysis Center, Oak Ridge National Laboratory, Oak Ridge, Tenn., U.S.A., 2006.

Marland E. and G. Marland (2003) The treatment of long-lived carbon-containing products in inventories of carbon dioxide emissions to the atmosphere, Env. Science and Policy 6: 139-152.

Marland, G., A. Brenkert, and J. Olivier, 1999. CO_2 emissions from fossil fuel burning: a comparison of ORNL and EDGAR estimates of national emissions, Environmental Science and Policy 2:265-274

Marland, G., 2006, Uncertainties in accounting for CO_2 from fossil fuels, Journal of Industrial Ecology

Olivier, J.G.J., and J.A.H.W. Peters, 2002.Uncertainties in global, regional, and national emissions inventories, pp. 525-540 in J. Van Ham, A.P.M. Baede, R. Guicherit, and J.F.G.M. Williams-Jacobse (eds.) Non-CO_2 greenhouse gases: scientific understanding, control options and policy aspects. Proceedings of the Third International Symposium, Maastricht, Netherlands, 21-21 January, 2002, ISBN 90-77017-70-4

Olivier, J.G.J., Van Aardenne, J.A., Dentener, F., Ganzeveld, L. and Peters, J.A.H.W. 2005. Recent trends in global greenhouse gas emissions: regional trends and spatial distribution of key sources. In: "Non-CO_2 Greenhouse Gases (NCGG-4)". A. van Amstel (coord.), page 325-330. Millpress, Rotterdam, ISBN 9059660439. Information available online at www.rivm.nl.

Ohara T., Akimoto, H., Kurokawa, J., Horii, N., Yamaji, K., Yan X. and Hayasaka T. (2007) An Asian emission inventory of anthropogenic emission sources for the period 1980–2020 Atmos. Chem. Phys. Discuss., 7, 6843–6902, 2007

Pregger, T., Scholz, Y., and Friedrich, R.: Documentation of the anthropogenic GHG emission data for Europe provided in the Frame of CarboEurope GHG and CarboEurope IP, Project report, Institut f¨ur Energiewirtschaft und Rationelle Energieanwendung, Universit¨at Stuttgart, Stuttgart, Germany, 2007.

Riediger, B., XI. Brennstoffe. In: Hütte, des Ingenieurs Taschenbuch, Theoretische Grundlagen (Editor: Akademischer Verein Hütte, e.V., Berlin), Verlag von Wilhelm Ernst & Sohn, Berlin 1955, 1668 pp.)

Rypdal, K., and W. Winiwarter, 2001. Uncertainties in greenhouse gas emissions inventories - evaluation, comparability, and implications. Environmental Science and Policy 4: 107-116.

Streets, D. G., et al. (2003), An inventory of gaseous and primary aerosol emissions in Asia in the year 2000, J. Geophys. Res., 108(D21), 8809, doi:10.1029/2002JD003093.

UNFCCC (1992) United Nations Framework Convention on Climate Change. UN, New York

UNFCCC (2004) United Nations Framework Convention on Climate Change (UNFCCC), S.: Greenhouse Gas Inventory Data, Tech. Rep. http://unfccc.int/ghg emissions data/items/3800.php, Bonn, Germany, 2004.

USEPA (U.S. Environmental Protection Agency), 2005: Inventory of U.S. Greenhouse Gas Emissions and Sinks: 1990–2003. EPA 430-R-05-003, EPA, Washington, DC.

Van Aardenne, J. A., Dentener, F. J., Olivier, J. G. J., Peters, J. A. H. W., and Ganzeveld, L. N.: The EDGAR 3.2 Fast track 2000 dataset (32FT2000), Tech. rep., Joint Research Centre (JRC), Ispra, Italy, available from http://www.mnp.nl/edgar/model/v32ft2000edgar, 2005.

Vestreng, V., Breivik, K., Adams, M.,Wagener, A., Goodwin, J., Rozovskkaya, O., and Pacyna, J. M.: Inventory Review 2005, Emission Data reported to LRTAP Convention and NEC Directive, Initial review of HMs and POPs, MSC-W 1/2005 ISSN 0804-2446, EMEP, 2005.

Winiwarter, W. (2007) National Greenhouse Gas Inventories: understanding uncertainties versus potential for improving reliability, Water Air Soil Pollut: Focus 7:443-450